TECHNISCHE UNIVERSITÄT MÜNCHEN

Ingenieurfakultät Bau Geo Umwelt

Lehrstuhl für Grundbau, Bodenmechanik, Felsmechanik und Tunnelbau

Long-Term Volume Change Behaviour of an Unsaturated Compacted Organic Soil under Oedometric Conditions

Iman Bagherpour

Vollständiger Abdruck der von der Ingenieurfakultät Bau Geo Umwelt der Technischen Universität München zur Erlangung des akademischen Grades eines

Doktor-Ingenieurs

genehmigten Dissertation.

Vorsitzender: Univ.-Prof. Dr.-Ing. Roberto Cudmani

Prüfer der Dissertation:

1. Univ.-Prof. Dr.-Ing. Norbert Vogt
2. Univ.-Prof. Dr.-Ing. Frank Rackwitz
   Technische Universität Berlin

Die Dissertation wurde am 14.03.2016 bei der Technischen Universität München eingereicht und durch die Ingenieurfakultät Bau Geo Umwelt am 29.07.2016 angenommen.

Abstract

The effects of time, stress, and matric suction on the volume change behaviour of an unsaturated compacted organic soil were studied by performing suction-controlled oedometer tests. The a,b,c isotache model which is known for saturated soft soils was adapted for unsaturated conditions. In addition, the patterns of isotaches for the soil structure and water phase were studied at constant values of net normal stress and matric suction. Furthermore, the suction-controlled oedometer tests were simulated using the adapted model and compared with the test results of overall volume and water volume changes.

Langfristiges Volumenänderungsverhalten eines ungesättigten verdichteten organischen Bodens unter oedometrischen Bedingungen

Kurzzusammenfassung

Die Einflüsse von Zeit, Spannung und Matrix-Saugspannung auf das Volumenänderungsverhalten eines ungesättigten verdichteten organischen Bodens wurden anhand von Kompressionsversuchen in Saugspannungs-kontrollierten Oedometerzellen untersucht. Das für gesättigte weiche Böden bekannte a,b,c Isotachen-Modell wurde für ungesättigte Bedingungen adaptiert. Außerdem wurden die Formen der Isotachen für die Bodenstruktur und die Wasserphase bei konstanten Werten für die Netto-Normalspannung und die Matrix-Saugspannung untersucht. Darüber hinaus wurden die in den Saugspannungs-kontrollierten Oedometerzellen durchgeführten Kompressionsversuche mit dem adaptierten Modell simuliert und mit den Versuchsergebnissen für die Gesamtvolumen- und Wasservolumenänderung verglichen.

Table of contents

List of Symbols

Latin Alphabet

Symbol	Unit	Description
a	-	Isotache parameter (saturated soils)
b	-	Isotache parameter (saturated soils)
c	-	Isotache parameter (saturated soils)
a_v^p, b_v^p, c_v^p	-	Isotache parameters for the soil structure of unsaturated soils at a constant net normal stress
a_w^p, b_w^p, c_w^p	-	Isotache parameters for the water phase (natural water mass change) of unsaturated soils at a constant net normal stress
$a_w^{(\mathrm{lin})^p}, b_w^{(\mathrm{lin})^p}, c_w^{(\mathrm{lin})^p}$	-	Isotache parameters for the water phase (linear water volume change) of unsaturated soils at a constant net normal stress
a_v^s, b_v^s, c_v^s	-	Isotache parameters for the soil structure of unsaturated soils at a constant matric suction
a_w^s, b_w^s, c_w^s	-	Isotache parameters for the water phase (natural water mass change) of unsaturated soils at a constant matric suction
$a_w^{(\mathrm{lin})^s}, b_w^{(\mathrm{lin})^s}, c_w^{(\mathrm{lin})^s}$	-	Isotache parameters for the water phase (linear water volume change) of unsaturated soils at a constant matric suction
C_C	-	Compression index
C_S	-	Swelling index
C_v	m^2/day	Coefficient of consolidation
C_α	-	Secondary compression index
e	-	Void ratio
e_0	-	Initial void ratio
e_a	-	Air ratio
e_w	-	Water ratio
G_s	-	Specific gravity of the soil particles
h	mm	Current height of the soil sample
h_0	mm	Initial height of the soil sample
H_{dr}	mm	Length of drainage path
h_s	mm	Height of solids in the soil element
h_v	mm	Height of voids in the soil element
h_{v_0}	mm	Initial height of voids in the soil element
m_d	g	Dry mass of the soil element
n	-	Porosity
n_0	-	Initial porosity
OCR_0	-	Over-consolidation ratio in a total natural strain coordinate for the isotache of initial intrinsic time (saturated soils)
OCR_{II}	-	Over-consolidation ratio in a total natural strain coordinate at the end of a loading step (saturated soils)

OCR_{vp}	-	Over-consolidation ratio in a visco-plastic natural strain coordinate (saturated soils)
OCR_{vp_0}	-	Over-consolidation ratio in a visco-plastic natural strain coordinate for the isotache of initial intrinsic time (saturated soils)
$OCR_{v\ \mathrm{II}}^{p}$	-	Over-consolidation ratio in an overall total natural strain coordinate at the end of a loading step when the net normal stress is constant
$OCR_{w\ \mathrm{II}}^{(\mathrm{lin})p}$	-	Over-consolidation ratio in a total linear water volume change coordinate at the end of a loading step when the net normal stress is constant
$OCR_{v\ \mathrm{II}}^{s}$	-	Over-consolidation ratio in an overall total natural strain coordinate at the end of a loading step when the matric suction is constant
$OCR_{w\ \mathrm{II}}^{(\mathrm{lin})s}$	-	Over-consolidation ratio in a total linear water volume change coordinate at the end of a loading step when the matric suction is constant
$OCR_{v\ vp\ \mathrm{I}}^{p}$	-	Over-consolidation ratio for the isotache I; in an overall visco-plastic natural strain coordinate at a constant net normal stress
$OCR_{w\ vp\ \mathrm{I}}^{p}$	-	Over-consolidation ratio for the isotache I; in a visco-plastic natural water mass change coordinate at a constant net normal stress
$OCR_{v\ vp\ \mathrm{I}}^{s}$	-	Over-consolidation ratio for the isotache I; in an overall visco-plastic natural strain coordinate at a constant matric suction
$OCR_{w\ vp\ \mathrm{I}}^{s}$	-	Over-consolidation ratio for the isotache I; in a visco-plastic natural water mass change coordinate at a constant matric suction
p	kPa	Net normal stress (σ – u_a)
p_0	kPa	Initial net normal stress when the matric suction is constant
p_g	kPa	Pre-consolidation stress at zero total strain (saturated soils)
$p_{g\ vp}$	kPa	Pre-consolidation stress at zero visco-plastic strain (saturated soils)
$p_{g_{vp(\mathrm{update})}}$	kPa	Updated pre-consolidation stress in a visco-plastic natural strain coordinate (saturated soils)
$p_{g\ v}^{s}$	kPa	Pre-consolidation net normal stress for the soil structure at zero overall total natural strain when the matric suction is constant
$p_{g\ w}^{s}$	kPa	Pre-consolidation net normal stress for the water phase at zero total natural water mass change when the matric suction is constant
$p_{g\ w}^{(\mathrm{lin})s}$	kPa	Pre-consolidation net normal stress for the water phase at zero total linear water volume change when the matric suction is constant
$p_{g\ v\ vp}^{s}$	kPa	Pre-consolidation net normal stress for the soil structure at zero overall visco-plastic natural strain when the matric suction is constant
$p_{g\ w\ vp}^{s}$	kPa	Pre-consolidation net normal stress for the water phase at zero visco-plastic natural water mass change when the matric suction is constant

$p^{s}_{g\ v\ vp(\mathrm{update})}$	kPa	Updated pre-consolidation net normal stress for the soil structure in an overall visco-plastic natural strain coordinate at a constant matric suction
$p^{s}_{g\ w\ vp(\mathrm{update})}$	kPa	Updated pre-consolidation net normal stress for the water phase in a visco-plastic natural water mass change coordinate at a constant matric suction
s	kPa	Matric suction ($u_a - u_w$)
s_0	kPa	Initial matric suction when the net normal stress is constant
s_0	kPa	Yield suction in the BBM
$s^{p}_{g\ v}$	kPa	Yield matric suction for the soil structure at zero overall total natural strain when the net normal stress is constant
$s^{p}_{g\ w}$	kPa	Yield matric suction for the water phase at zero total natural water mass change when the net normal stress is constant
$s^{(\mathrm{lin})p}_{g\ \ w}$	kPa	Yield matric suction for the water phase at zero total linear water volume change when the net normal stress is constant
$s^{p}_{g\ v\ vp}$	kPa	Yield matric suction for the soil structure at zero overall visco-plastic natural strain when the net normal stress is constant
$s^{p}_{g\ w\ vp}$	kPa	Yield matric suction for the water phase at zero visco-plastic natural water mass change when the net normal stress is constant
$s^{p}_{g\ v\ vp(\mathrm{update})}$	kPa	Updated yield matric suction for the soil structure in an overall visco-plastic natural strain coordinate at a constant net normal stress
$s^{p}_{g\ w\ vp(\mathrm{update})}$	kPa	Updated yield matric suction for the water phase in a visco-plastic natural water mass change coordinate at a constant net normal stress
S	mm	Settlement of the layer at time *t*
S_p	mm	Settlement of the layer when the excess pore-water pressure is zero (i.e., settlement of the layer at EOP)
S_r	-	Degree of saturation
Sr_0	-	Initial degree of saturation
t	day	Time
t_{90}	min	Time corresponding to 90% consolidation
T_v	-	Time factor
u_a	kPa	Pore-air pressure
U_{avg}	-	Average degree of consolidation
u_w	kPa	Pore-water pressure
v	-	Specific volume ($v = 1 + e$)
V_0	cm^3	Initial overall volume of the soil element
V_a	cm^3	Volume of air in the soil element
V_{current}	cm^3	Current overall volume of the soil element
$\overline{\mathrm{vd}}$, $\overline{\mathrm{vd}}^{p}_{v}$, $\overline{\mathrm{vd}}^{p}_{w}$, $\overline{\mathrm{vd}}^{s}_{v}$, $\overline{\mathrm{vd}}^{s}_{w}$	cm	Parameters which depend on the vertical distance between the isotaches

V_s	cm^3	Volume of solids in the soil element
V_v	cm^3	Volume of voids in the soil element
V_w	cm^3	Volume of water in the soil element
w	-	Water content
x, x_v^p, x_w^p, x_v^s, x_w^s	cm	Parameters which depend on the interval of isotaches
z	mm	Depth used for calculating the excess pore-water pressure (in Terzaghi – consolidation theory)

Greek Alphabet

Symbol	Unit	Description
$\Delta\varepsilon^H{}_{(b)}$	-	Change in total natural strain; for determining the isotache parameter b (saturated soils)
Δh	mm	Change in the height of the soil sample
Δt	day	Duration of creep (saturated soils)
Δt^p	day	Duration of creep at a constant net normal stress
Δt^s	day	Duration of creep at a constant matric suction
Δu or Δu_w	kPa	Excess pore-water pressure
Δu_0	kPa	Initial excess pore-water pressure (used in Terzaghi – consolidation theory)
ε^H	-	Total natural strain (saturated soils)
$\dot{\varepsilon}^H$	1/s	Total natural strain rate (saturated soils)
ε_e^H	-	Elastic part of the natural strain (saturated soils)
$\dot{\varepsilon}_e^H$	1/s	Elastic part of the natural strain rate (saturated soils)
ε_{vp}^H	-	Visco-plastic part of the natural strain (saturated soils)
$\dot{\varepsilon}_{vp}^H$	1/s	Visco-plastic part of the natural strain rate (saturated soils)
$\varepsilon^{(lin)}$	-	Total linear strain (saturated soils)
ε_v^H	-	Overall total natural strain
$\dot{\varepsilon}_v^H$	1/s	Rate of overall total natural strain
$\varepsilon_{v\ e}^H$	-	Elastic part of the overall natural strain
$\dot{\varepsilon}_{v\ e}^H$	1/s	Rate of elastic part of the overall natural strain
$\varepsilon_{v\ vp}^H$	-	Visco-plastic part of the overall natural strain
$\dot{\varepsilon}_{v\ vp}^H$	1/s	Rate of visco-plastic part of the overall natural strain
$\varepsilon_v^{(lin)}$	-	Overall total linear strain
ε_w^H	-	Total natural water mass change
$\dot{\varepsilon}_w^H$	1/s	Rate of total natural water mass change
$\varepsilon_{w\ e}^H$	-	Elastic part of the natural water mass change

$\dot{\varepsilon}^{H}_{w\,e}$	1/s	Rate of elastic part of the natural water mass change
$\varepsilon^{H}_{w\,vp}$	-	Visco-plastic part of the natural water mass change
$\dot{\varepsilon}^{H}_{w\,vp}$	1/s	Rate of visco-plastic part of the natural water mass change
$\varepsilon^{(\mathrm{lin})}_{w}$	-	Total linear water volume change
$\dot{\varepsilon}^{(\mathrm{lin})}_{w}$	1/s	Rate of total linear water volume change
$\varepsilon^{(\mathrm{lin})}_{w\quad e}$	-	Elastic part of the linear water volume change
$\dot{\varepsilon}^{(\mathrm{lin})}_{w\quad e}$	1/s	Rate of elastic part of the linear water volume change
$\varepsilon^{(\mathrm{lin})}_{w\quad vp}$	-	Visco-plastic part of the linear water volume change
$\dot{\varepsilon}^{(\mathrm{lin})}_{w\quad vp}$	1/s	Rate of visco-plastic part of the linear water volume change
$\varepsilon^{H\,p}_{v}$	-	Overall total natural strain at a constant net normal stress
$\varepsilon^{H\,p}_{v\;e}$	-	Elastic part of the overall natural strain at a constant net normal stress
$\varepsilon^{H\,p}_{v\;vp}$	-	Visco-plastic part of the overall natural strain at a constant net normal stress
$\dot{\varepsilon}^{H\,p}_{v\;vp}$	1/s	Visco-plastic part of the overall natural strain rate at a constant net normal stress
$\varepsilon^{(\mathrm{lin})\,p}_{v}$	-	Overall total linear strain at a constant net normal stress
$\varepsilon^{H\,p}_{w}$	-	Total natural water mass change at a constant net normal stress
$\varepsilon^{H\,p}_{w\,e}$	-	Elastic part of the natural water mass change at a constant net normal stress
$\varepsilon^{H\,p}_{w\,vp}$	-	Visco-plastic part of the natural water mass change at a constant net normal stress
$\dot{\varepsilon}^{H\,p}_{w\,vp}$	1/s	Visco-plastic part of the rate of natural water mass change at a constant net normal stress
$\varepsilon^{(\mathrm{lin})\,p}_{w}$	-	Total linear water volume change at a constant net normal stress
$\dot{\varepsilon}^{(\mathrm{lin})\,p}_{w\quad vp}$	1/s	Visco-plastic part of the rate of linear water volume change at a constant net normal stress
$\varepsilon^{H\,s}_{v}$	-	Overall total natural strain at a constant matric suction
$\varepsilon^{H\,s}_{v\;e}$	-	Elastic part of the overall natural strain at a constant matric suction
$\varepsilon^{H\,s}_{v\;vp}$	-	Visco-plastic part of the overall natural strain at a constant matric suction
$\dot{\varepsilon}^{H\,s}_{v\;vp}$	1/s	Visco-plastic part of the overall natural strain rate at a constant matric suction
$\varepsilon^{(\mathrm{lin})\,s}_{v}$	-	Overall total linear strain at a constant matric suction
$\varepsilon^{H\,s}_{w}$	-	Total natural water mass change at a constant matric suction
$\varepsilon^{H\,s}_{w\,e}$	-	Elastic part of the natural water mass change at a constant matric suction

$\varepsilon_{w\,vp}^{H\,s}$	-	Visco-plastic part of the natural water mass change at a constant matric suction
$\dot{\varepsilon}_{w\,vp}^{H\,s}$	1/s	Visco-plastic part of the rate of natural water mass change at a constant matric suction
$\varepsilon_{w}^{(\mathrm{lin})\,s}$	-	Total linear water volume change at a constant matric suction
$\dot{\varepsilon}_{w\quad vp}^{(\mathrm{lin})\,s}$	1/s	Visco-plastic part of the rate of linear water volume change at a constant matric suction
$\varepsilon_{a}^{(\mathrm{lin})}$	-	Total linear air volume change
ε^{m}	-	(Total) momentary strain
ε_{w}^{m}	-	(Total) momentary water volume change
κ	-	BBM stiffness parameter for changes in net mean stress of the elastic state of soil
λ or $\lambda(s)$	-	BBM stiffness parameter for changes in net mean stress of the virgin state of soil
ρ_d	g/cm^3	Dry density
ρ_s	g/cm^3	Density of soil solids
σ	kPa	Vertical total stress
$\acute{\sigma}_v$	kPa	Vertical effective stress (saturated soils)
$\acute{\sigma}_{v_0}$	kPa	Initial vertical effective stress (saturated soils)
τ	day	Intrinsic time (saturated soils)
τ_0	day	Initial intrinsic time (saturated soils)
τ_1	day	Reference intrinsic time (saturated soils)
$\tau_{v\,1}^{p}$	day	Reference intrinsic time for the soil structure at a constant net normal stress
$\tau_{w\,1}^{p}$	day	Reference intrinsic time for the water phase (natural water mass change) at a constant net normal stress
$\tau_{w\quad 1}^{(\mathrm{lin})\,p}$	day	Reference intrinsic time for the water phase (linear water volume change) at a constant net normal stress
$\tau_{v\,1}^{s}$	day	Reference intrinsic time for the soil structure at a constant matric suction
$\tau_{w\,1}^{s}$	day	Reference intrinsic time for the water phase (natural water mass change) at a constant matric suction
$\tau_{w\quad 1}^{(\mathrm{lin})\,s}$	day	Reference intrinsic time for the water phase (linear water volume change) at a constant matric suction
τ_{I}	day	Intrinsic time for the isotache I (saturated soils)
$\tau_{v\,\mathrm{I}}^{p}$	day	Intrinsic time for the isotache I of the soil structure at a constant net normal stress
$\tau_{w\,\mathrm{I}}^{p}$	day	Intrinsic time for the isotache I of the water phase (natural water mass change) at a constant net normal stress
$\tau_{v\,\mathrm{I}}^{s}$	day	Intrinsic time for the isotache I of the soil structure at a constant matric suction

$\tau^{s}_{w\,\mathrm{I}}$	day	Intrinsic time for the isotache I of the water phase (natural water mass change) at a constant matric suction
τ_{II}	day	Intrinsic time for the isotache II (saturated soils)
$\tau^{p}_{v\,\mathrm{II}}$	day	Intrinsic time for the isotache II of the soil structure at a constant net normal stress
$\tau^{p}_{w\,\mathrm{II}}$	day	Intrinsic time for the isotache II of the water phase (natural water mass change) at a constant net normal stress
$\tau^{(\mathrm{lin})\,p}_{w\quad\mathrm{II}}$	day	Intrinsic time for the isotache II of the water phase (linear water volume change) at a constant net normal stress
$\tau^{s}_{v\,\mathrm{II}}$	day	Intrinsic time for the isotache II of the soil structure at a constant matric suction
$\tau^{s}_{w\,\mathrm{II}}$	day	Intrinsic time for the isotache II of the water phase (natural water mass change) at a constant matric suction
$\tau^{(\mathrm{lin})\,s}_{w\quad\mathrm{II}}$	day	Intrinsic time for the isotache II of the water phase (linear water volume change) at a constant matric suction
ψ	kPa	Total suction

List of Abbreviations

Abbreviation	Description
ASTM	American Society for Testing and Materials
BBM	Barcelona basic model
DIN	Deutsches Institut für Normung (German institute for standardization)
EOP	End of primary consolidation
LIR	Load increment ratio
WP4	Water potential meter device (Dewpoint Hygrometer)

Chapter 1: Introduction

1.1 Overview

In this research, three conventional oedometer tests were performed on saturated soil samples at various Load Increment Ratios (LIR), and three suction-controlled oedometer tests were conducted on unsaturated soil samples. All six samples were prepared from a Sandy Organic Silt (OH) by using static compaction at the wet side of the Proctor optimum. At the beginning of each test, the water content and dry density of all samples were very similar.

Utilising the results of conventional oedometer tests, the sensitivity of isotache pattern to the LIR was examined. Based on all six tests, the effects of time, stress, and matric suction on the volume change behaviour of the compacted organic soil were studied under oedometric conditions.

The test results show that long-term volume change occurs both in the soil structure and in the water phase of an unsaturated compacted organic soil due to increasing the matric suction (s) or the net normal stress (p). The findings demonstrate that the secondary compression index (C_α) of a compacted organic soil in unsaturated conditions is not unique and is a function of time and net normal stress, similar to its saturated condition. Furthermore, C_α for this soil is a function of matric suction as well. Therefore, applying the classical method to study volume changes of unsaturated compacted organic soils using C_α (on a plot of void ratio versus logarithmic scale of time) leads to inaccurate results. This problem is solved by applying the isotache approach.

This research highlights that the volume change of an unsaturated compacted organic soil can also be predicted by the isotache approach used for saturated soils. The test results of overall volume and water volume changes indicate that at constant values of net normal stress (p) and matric suction (s), the patterns of isotaches exist for the investigated unsaturated compacted organic soil.

The a,b,c isotache model which is known for saturated soft soils was adapted for unsaturated conditions. In addition, the effects of matric suction on the volume change behaviour are discussed and the equations for selected parameters of the adapted a,b,c isotache model are suggested as a function of matric suction for the unsaturated compacted organic soil.

The suction-controlled oedometer tests were simulated using the adapted model and compared with the test results of overall volume and water volume changes. The comparison between the adapted a,b,c isotache model and the test results shows that the adapted model can simulate and predict the overall volume and water volume changes of this soil with high accuracy.

1.2 General Information

Civil engineering projects are also increasing in areas that are covered by organic soils. Despite spreading of these kinds of soils in large parts of the world and in large quantities, only few practical and theoretical studies have been done dealing with the volume change behaviour of compacted organic soils. The organic matter of these kinds of soils is mainly from plant origin.

Figure 1.1. Excavation of organic soil in a road construction project located approximately 35 km northeast of Munich, Germany.

Limsiri (2008) explains that the geotechnical properties of organic soils usually are not sufficient to bear the loads of heavy structures. These kinds of soils are problematic for construction and are typically removed from construction sites. Excavated organic soils are usually dumped if they cannot be used as topsoil in the course of building activities. For large amounts of these soils, transporting them is a difficult and expensive method to solve the problem. With the objective of protecting resources in the future, these soils can be reused as building materials as much as possible instead of being dumped. This alternative could be attractive, especially in areas where the price of coarse-grained soils as replacement material is high. Embankments, dikes, fills, and noise barriers along transportation lines are some examples of using organic soils for earth constructions.

Many construction projects have been carried out on organic soils and peats. For example, Samson (1985) reports that “For a length of 520 m, the autoroute [‘connecting Montreal to Quebec City’ (p. 308)] was constructed over a large peat deposit. On the right-of-way of the autoroute, the original thickness of the peat varied from 3.0 to 5.8 m” (p. 308).

Another example is Savidis, Rackwitz, and Schüßler (2008) who report on the construction of a federal road project south of Berlin which crosses “through a region of very soft peat soil with underlying organic silt, sand and boulder clay on a total length of about 140 m” (p. 2).

One of the considerable difficulties of constructing on (or with) organic soils is its high compressibility. Significant deformations due to secondary compression (i.e., creep) may continue for a long duration after construction. For example concerning geotechnical design of dikes on organic soils (e.g., for flood control), the maximum settlement should guarantee that the dike’s crown remains sufficiently above the design water level.

Sometimes there is an obligation to protect the archaeological heritage (Papadaki, 2013) or natural resources such as turf and peat by keeping the soil of these areas in its original location. For example

regarding the archaeological heritage, Papadaki (2013) explains that “in this effort, it is essential to understand what is happening underneath constructions (buildings, infrastructure, etc.) in order to assess the risk of destroying the remains” (p. 1). This could also be another motivation for this research.

Considering all explanations mentioned above, the ability to predict volume change characteristics as well as gaining a thorough understanding of the time and rate dependent behaviour of unsaturated compacted organic soils is imperative and has significant applications in geotechnical engineering. However, very little research based on experimental tests has been done so far in this area.

Usually soils used as construction materials are not saturated. Fredlund and Rahardjo (1986) explain that “In practice, many geotechnical problems involve unsaturated soils. The construction of earth-fill dams, highways, and . . . [many other construction projects] use unsaturated compacted soils” (p. 154). Ho, Fredlund, and Rahardjo (1992) point out that “Volume changes of the soil due to applied loads or environmental changes (i.e., rainfall and evaporation) are of interest to practising engineers” (p. 195).

1.3 Aim of Research

The classical method for calculating the secondary compression is through plotting void ratio versus the logarithmic scale of time – expecting a linear trend with the secondary compression index (C_α) as its gradient. However, the oedometer results of a compacted organic soil show that C_α is not unique and depends on time and stress.

The aim of this research was to study the long-term volume change behaviour of an unsaturated compacted organic soil. Den Haan (1994) described the a,b,c isotache model to overcome the large deformation problems of fully saturated soils such as peats, organic soils, and non-brittle soft clays. The model for saturated soils has a very consistent structure and is based on straightforward mathematical concepts. However, embankments and the foundations of most construction projects usually lie on unsaturated soil layers in which the a,b,c isotache model has not been applied prior to this research.

In order to achieve the objectives of this research, the following steps were taken:

- Three conventional oedometer tests were performed on saturated soil samples at various load increment ratios. The first aim of performing these tests was to compare the soil behaviour in saturated (matric suction = 0) and unsaturated conditions when the matric suction was kept constant and the net normal stress was increased. The second reason was to study the dependency of volume change behaviour on time and stress in the compacted organic soils, and the third purpose was to examine the sensitivity of isotache pattern to the Load Increment Ratio (LIR);
- Three suction-controlled oedometer tests were conducted on unsaturated soil samples and the effects of time, stress, and matric suction on the volume change behaviour were investigated;

- The a,b,c isotache model was adapted for unsaturated conditions based on the theory of overall volume and water volume changes of unsaturated soils (Fredlund & Morgenstern, 1976), and the isotache patterns were studied;
- The procedure to determine the adapted model parameters from suction-controlled oedometer tests on unsaturated soil samples was introduced;
- The equations for selected parameters of the adapted model were suggested as a function of matric suction (s) for an unsaturated compacted organic soil; and
- The suction-controlled oedometer tests were simulated using the adapted a,b,c isotache model and compared with the test results of overall volume and water volume changes.

Chapter 2: Literature Review

2.1 Literature Review on the Compressibility Behaviour of Saturated Soils

2.1.1 Introduction

In the literature of soil mechanics, creep is defined as the increasing of strain under a constant effective stress. When a one-dimensional constant stress is applied to a saturated soil sample, strain is theoretically ongoing but the rate of strain decreases with time. As shown in Figure 2.1, in this process, excess pore-water pressure approaches zero at the time corresponding to the end of primary (EOP) consolidation. In the classical method of calculating the secondary compression, this time is a boundary between the end of the primary consolidation and the beginning of the secondary compression (Casagrande, 1938 as cited in Holtz & Kovacs, 1981, p. 398, fig. 9.7). Raymond and Wahls (1976) and Mesri and Godlewski (1977) define the secondary compression index (C_α) as: $C_\alpha = \Delta e / \Delta \log t$ (as cited in Holtz & Kovacs, 1981, pp. 405-406).

A key assumption in the classical textbooks is that during the secondary compression phase, the plot of void ratio against the logarithmic scale of time is practically linear, and the overall graph is S-shaped. However, the oedometer results of a compacted organic soil do not show such properties and this will be discussed in *Sections 3.4* and *3.4.1*.

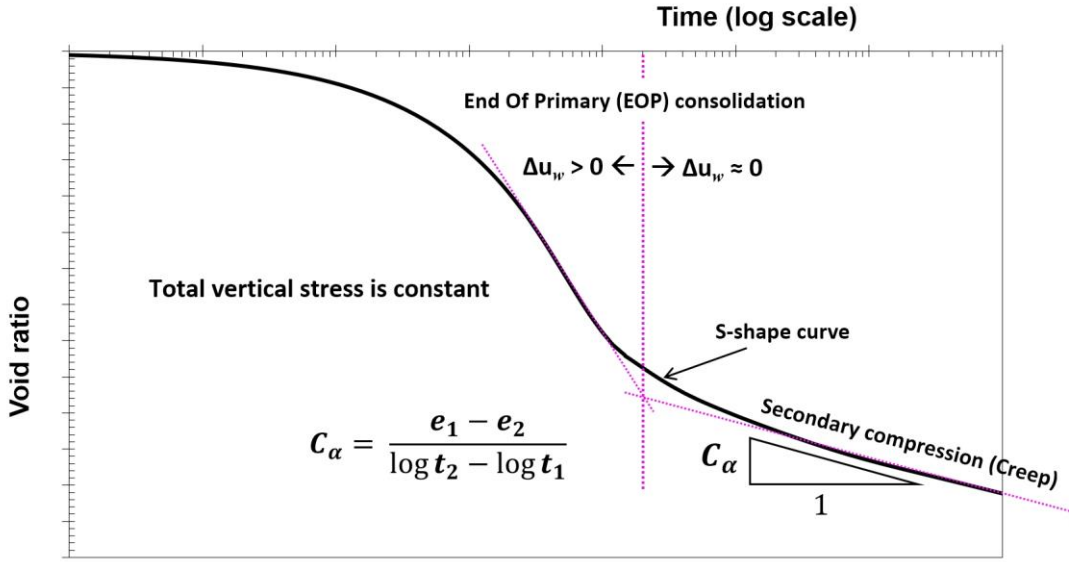

Figure 2.1. Classical method for calculating the secondary compression.

In practice, it is usually thought that the amount of primary consolidation is much higher than secondary compression and for this reason secondary compression attracts minor attention, whereas it will be presented in following chapters that the secondary compression is sometimes even more significant than the primary consolidation for a compacted organic soil. Settlement of organic soils is dominated by creep. In these kinds of soils, usually primary consolidation will finish quickly whereas secondary compression continues for a long duration after load application.

2.1.2 Strain

In this section, three kinds of strain for one-dimensional deformation will be explained, considering that in all calculations the strain is defined positive for compression of a soil sample.

2.1.2.1 Linear Strain

Linear strain ($\varepsilon^{(\mathrm{lin})}$) is defined as the change in height of the soil sample with respect to the initial height of the soil sample,

$$\varepsilon^{(\mathrm{lin})} = -\frac{\Delta h}{h_0} \tag{2.1}$$

where

Δh: Change in the height of the soil sample

h_0: Initial height of the soil sample

The minus sign in equation 2.1 is due to the convention in soil mechanics to take loss of height as being positive.

2.1.2.2 Momentary Strain

Momentary strain (ε^{m}) is defined as the change in the height of the soil sample with respect to the current height of the soil sample (Barends, 1992),

$$\varepsilon^{\mathrm{m}} = -\left(\frac{\Delta h}{h_0 - \Delta h}\right) \tag{2.2}$$

where ($h_0 - \Delta h$) is the current height of the soil sample (i.e., h).

In the following chapters, this definition in an adapted form is used to analyse the water volume change of unsaturated soils.

Momentary strain can also be expressed in terms of the linear strain ($\varepsilon^{(\mathrm{lin})}$) as follows:

$$\varepsilon^{m} = \frac{\varepsilon^{(\mathrm{lin})}}{1 - \varepsilon^{(\mathrm{lin})}}$$

2.1.2.3 Natural Strain

Den Haan and Kruse (2007) explain that the a,b,c isotache model works with the natural strain (ε^{H}) "to cope with the concavity of the stress [log] – strain curve which invariably develops at large strains" (p. 2114).

$$\varepsilon^{\mathrm{H}} = -\int_{h_0}^{h} \frac{dh}{h} = -\ln\left(\frac{h}{h_0}\right) = -\ln\left(\frac{h_0 - \Delta h}{h_0}\right) = -\ln\left(1 - \varepsilon^{(\mathrm{lin})}\right) \tag{2.3}$$

where h is the current height of the soil sample.

As Den Haan and Edil (1994) explain, "Natural strain is incrementally defined, whereas linear strain is a differential measure. Natural strain is sometimes named after Hencky, who was the first to employ it. It seems however to have first been introduced by Roentgen, 'of X-ray fame'" (p. 50).

Barends (1992) reports that the natural strain (ε^{H}) is the best strain parameter. Figure 2.2 shows that when strains are less than 10%, the difference between the three types of strains is not significant. Therefore, only for highly compressible soils, is using the natural strain important.

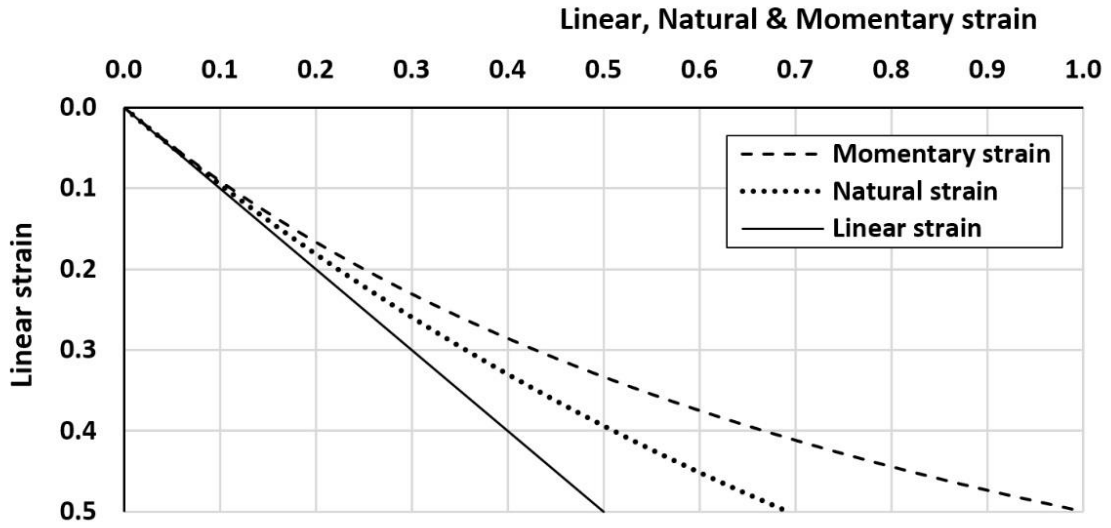

Figure 2.2. Three methods of strain measurement. Adapted and redrawn from Barends, 1992, p. 21, fig. 6.

Den Haan and Kruse (2007) presented in Figure 2.3, the results of a 24 hours compression of a peat sample. As is experimentally clear in this figure, the natural strain shows a good linear relationship between strain and stress.

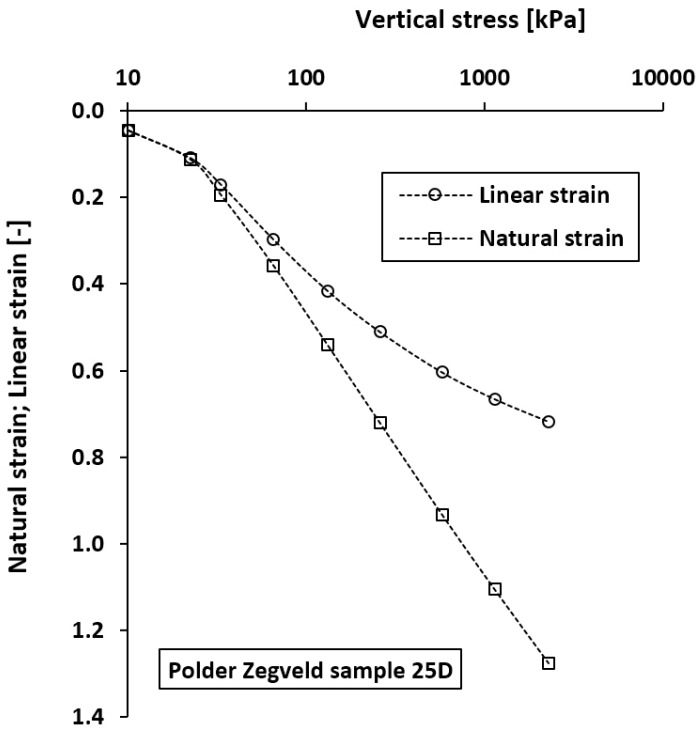

Figure 2.3. Comparison between the virgin 24 hours linear and natural strains of an oedometer test on a peat sample from Polder Zegveld. Adapted and redrawn from Den Haan & Kruse, 2007, p. 2114, fig. 17a.

In conventional analyses of settlement, researchers often use void ratio. Below, the relationships between void ratio and linear and natural strains are expressed for oedometric conditions.

$$e = \frac{V_v}{V_s} = \frac{h_v}{h_s}$$

$$\Delta e = e - e_0 = \frac{h_v}{h_s} - \frac{h_{v_0}}{h_s} = \frac{h_v - h_{v_0}}{h_s} = \frac{\Delta h}{h_s}$$

$$\frac{\Delta h}{h_0} = \frac{\Delta e \cdot h_s}{h_s + h_{v_0}} = \frac{\Delta e \cdot h_s}{h_s + e_0 \cdot h_s} = \frac{\Delta e}{1 + e_0} = \frac{e - e_0}{1 + e_0}$$

As already defined:

$$\varepsilon^{(\mathrm{lin})} = -\frac{\Delta h}{h_0} \qquad \text{Equation 2.1}$$

$$\varepsilon^{\mathrm{H}} = -\int_{h_0}^{h} \frac{dh}{h} = -\ln\left(\frac{h}{h_0}\right) = -\ln\left(\frac{h_0 - \Delta h}{h_0}\right) = -\ln\left(1 - \varepsilon^{(\mathrm{lin})}\right) \qquad \text{Equation 2.3}$$

Therefore:

$$\varepsilon^{(\mathrm{lin})} = -\left(\frac{e - e_0}{1 + e_0}\right) \tag{2.4}$$

$$\varepsilon^{\mathrm{H}} = -\ln\left(\frac{1 + e}{1 + e_0}\right) \tag{2.5}$$

and vice versa:

$$e = [(1 + e_0) \cdot \exp(-\varepsilon^{\mathrm{H}})] - 1 \tag{2.6}$$

The equations can be expressed also according to porosity (i.e., the volume of voids divided by the total volume):

$$e = \frac{n}{1 - n}$$

$$\varepsilon^{(\mathrm{lin})} = -\left(\frac{n - n_0}{1 - n}\right) \tag{2.7}$$

$$\varepsilon^{\mathrm{H}} = -\ln\left(\frac{1 - n_0}{1 - n}\right) \tag{2.8}$$

where

e: Current void ratio, e_0: Initial void ratio, Δe: Change in void ratio, n: Current porosity, n_0: Initial porosity, V_v : Current volume of voids, h_v: Current height of voids, h_{v_0}: Initial height of voids, V_s: Volume of solids, and h_s: Height of solids.

2.1.3 The "C_α/C_C Concept"

Mesri and Godlewski (1977) write that "for any one soil there is a unique relationship between $C_\alpha = \partial e/\partial \log t$ [i.e., secondary compression index] and $C_c = \partial e/\partial \log \bar{\sigma}$ [i.e., compression index] that holds true at all combinations of time, effective stress [i.e., $\bar{\sigma}$], and void ratio" (pp. 418-419). They report that "For a variety of natural soils the values of C_α/C_C are in the range of 0.025-0.10." They continue that "Depending on the shape of the void ratio-logarithm of effective stress curve, C_α may increase, decrease, or remain constant with time" (p. 428).

Mesri and Castro (1987) explain that "The C_α/C_C concept . . ., is a powerful tool for the analysis of secondary settlements and interpretation of data from load-controlled and deformation-controlled consolidation tests" (p. 244).

Mesri and Ajlouni (2007) report that "The magnitude of C_α/C_C appears to depend on the compressibility and deformability of the soil particles" (p. 856). Savidis et al. (2008) report the mean value of 0.075 for C_α/C_C obtained from oedometer tests on a saturated organic silt (p.6).

Rackwitz, Schüßler, Savidis, and Ney (2011) performed some oedometer tests on Gyttja soil (a type of organic soil and peat with high organic matter and water content), taken from the State of Brandenburg, Germany. Their test results indicate that the values of both the compression index (C_C) and the secondary compression index (C_α) increase with increasing amounts of organic content. They also report the mean values for C_α/C_C as 0.056 and 0.069 for the first loading and re-loading path, respectively (p. 101).

2.1.4 Hypotheses A and B

Degago, Grimstad, Jostad, Nordal, and Olsson (2011) explain that the time of End Of Primary (EOP) consolidation for a thin laboratory oedometer sample, which takes some minutes up to hours, is less than the time of EOP for a thick layer in the field, which takes some days up to several years. Ladd et al. (1977) introduced the hypotheses A and B (Figure 2.4) for describing the creep role in the primary consolidation phase (as cited in Degago et al., 2011). According to hypothesis A, strains at EOP are independent of the consolidation phase, whereas in the hypothesis B, strains at EOP increase with increasing the thickness of the soil sample. In other words, hypothesis A assumes that the relationship between the strain and the effective stress at EOP is independent of the thickness of a soil layer (Figures 2.4 & 2.5). This means that the corresponding strain of EOP in the hypothesis A in the laboratory and in situ is the same. In the hypothesis A, it is assumed that the strain at EOP is independent of the primary consolidation phase. On the other hand, in the hypothesis B, the strain of EOP increases as the thickness of the layer increases (Figures 2.4 & 2.6). Degago et al. (2011) continue that the isotache models can be classified as the hypothesis B (Figure 2.6).

It should be mentioned that both hypotheses are advocated by well-known researchers (see Degago et al., 2011, p. 898). Nash and Brown (2014) explain that the “recent reexaminations of the field and laboratory evidence by Degago (2011) and Degago et al. (2011) strongly support hypothesis B” (p. 2). Degago (2015) concluded that “there exist definitive data to demonstrate that hypothesis B agrees very well with the measured behaviour of cohesive soils.”

The a,b,c isotache model which has been chosen as the basis of this study, follows the hypothesis B.

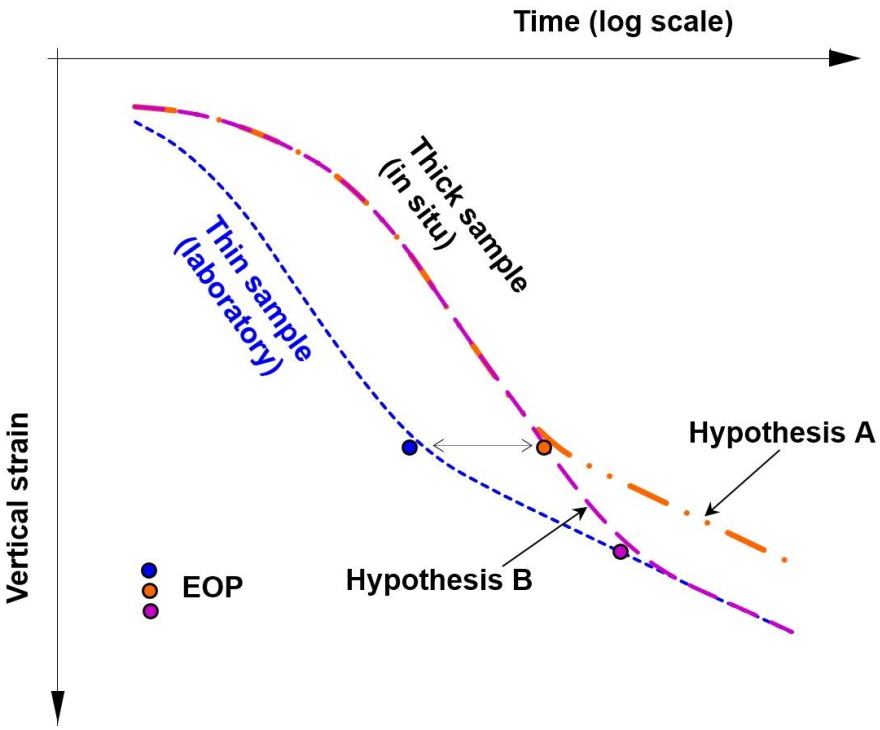

Figure 2.4. Description of the hypotheses A and B (after Ladd et al., 1977) for two samples with different thicknesses but with the same $\Delta\acute{\sigma}/\acute{\sigma}_{v_0}$. Adapted and redrawn from Degago, Grimstad, Jostad, Nordal, & Olsson, 2011, p. 898, fig. 1.

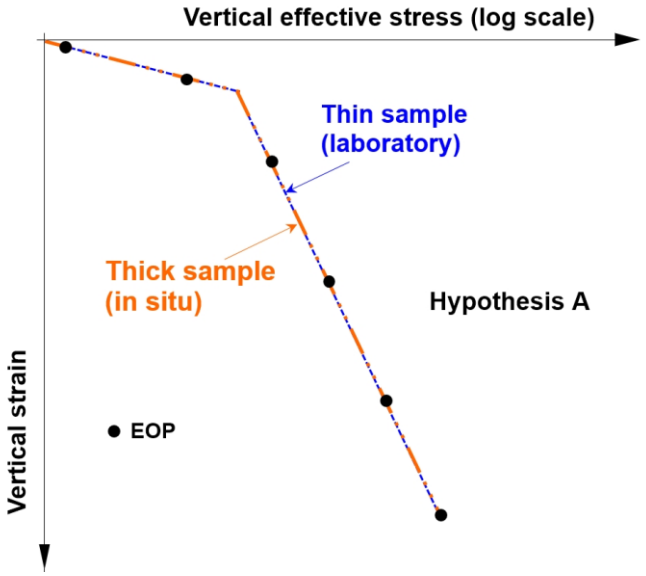

Figure 2.5. Description of the hypothesis A (after Ladd et al., 1977) for two samples with different thicknesses but with the same $\Delta\acute{\sigma}/\acute{\sigma}_{v_0}$. Adapted and redrawn from Degago, 2015.

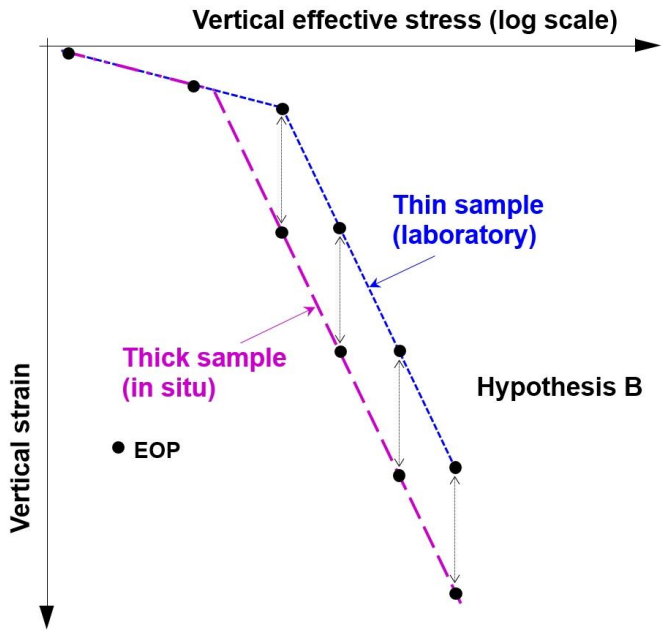

Figure 2.6. Description of the hypothesis B (after Ladd et al., 1977) for two samples with different thicknesses but with the same $\Delta\acute{\sigma}/\acute{\sigma}_{v_0}$. Adapted and redrawn from Degago, 2015.

2.1.5 The Isotache Approach

Buisman (1936, as cited in Vermeer & Neher, 1999) "was probably the first to propose a creep law for clay after observing that soft-soil settlements could not be fully explained by classical consolidation theory"(Vermeer & Neher, 1999, p. 250).

Šuklje (1957) was the first who introduced the isotache model as follows:

> "The position and slope of the consolidation curve in a given time must agree with the relationships between the speed [i.e., rate] of consolidation, the intergranular pressure [i.e., effective stress] and the porosity. These relationships are presented by a set of isotaches, derived from the consolidation curves of an oedometer test, carried out for various load increments . . ." (Šuklje, 1957, p. 200).

Bjerrum (1967) presents a "system of curves" which "exhibiting delayed consolidation" similar to the isotache concept (p. 98). He reports that:

> "The compressibility characteristics of a clay showing delayed consolidation cannot be described by a single curve in an e-log p diagram but require a system of lines or curves . . . . Each of these lines represents the equilibrium void ratio for different values of effective overburden pressure at a specific time of sustained loading. Consolidation tests have shown that the system of lines is approximately parallel . . ." (Bjerrum, 1967, p. 94).

Hobbs (1986) studied the compressibility behaviour of some peats with a system of isochrones similar to the isotache approach. He argues that "A uniform vertical spacing of the isochrones indicates a constant value of C_{sec} [i.e., coefficient of secondary compression] with time, and parallel ones indicate that C_{sec} does not vary with pressure" (p. 58).

Den Haan (1994) described the a,b,c isotache model for calculating the time-dependent strains to overcome the large deformation problems of fully saturated soils such as peats, organic soils, and non-brittle soft clays. He explains that the term isotache in the a,b,c isotache model "is copied" from Šuklje (1957). By using the a,b,c isotache model, the soil response can be modelled very well with a few parameters which can be simply determined from the conventional oedometer test (Den Haan, 1996). Krieg (2000) studied the viscous behaviour of some soils by using the isotache approach. Degago et al. (2011) indicated that "the isotache approach can capture the main characteristics of the time-dependent compressibility of clays during both the primary and secondary consolidation phases" (p. 897).

In the following sections, the a,b,c isotache model for saturated soils (Den Haan, 1994, 1996, 2008) is thoroughly described.

2.1.6 The a,b,c Isotache Model for Saturated Soils

2.1.6.1 Why the a,b,c Isotache Model?

In a personal communication with E. J. Den Haan on December 22, 2009, the question arose about the advantages of using the a,b,c isotache model compared to the classical theory of consolidation in soil mechanics. Den Haan's answer to this question was as follows:

"The classical consolidation theory breaks down when significant viscous effects are at play. Whereas the unique a,b,c relationship between effective stress, strain and creep strain rate holds independent of thickness, drainage conditions, duration and magnitude of loading. The natural strain formulation correctly describes compression up to large values. [The] a,b,c [isotache model] allows rigorous mathematical solution of the combined hydrodynamical and elasto-viscoplastic constitutive phenomena. The a,b,c parameters are easily determined and have reasonable correlations with the classical parameters. The drawback at present is that unloading is not properly accounted for. The behaviour during unloading and reloading appears to be difficult to cast in terms of isotaches."

In addition to his answer, it is worth mentioning that the classical method for calculating the secondary compression is through plotting void ratio versus the logarithmic scale of time. As it will be illustrated in *Sections 3.6.1* and *3.7.1*, the problem with this method is that the secondary compression index is not unique and is a function of time and vertical stress. In addition, the beginning time of creep in a non-S-shape plot cannot be defined (for more information, see *Sections 3.4* and *3.4.1*).

Den Haan and Van den Berg (2001) explain that during the settlement of low permeable soils with high creep potential, if the rate of creep is too high, the pore-water pressure might increase instead of decrease. In this situation, creep development produces a new consolidation phase and therefore the secondary compression index cannot be predicted with the classical method. This is another

advantage of using the a,b,c isotache model; such a phenomenon does not have any effect on the predicted results. In other words, the model can perfectly capture the effect of increasing the pore-water pressure on the creep evolution.

2.1.6.2 General Description of the a,b,c Isotache Model

As Taciroglu (1998) defines, “A constitutive model is the mathematical relationship which relates the stresses (loads) to the strains (displacements) in a medium. . . . The parameters (material constants) of a constitutive model should be measurable - directly or indirectly - via laboratory tests” (p. 1).

Figure 2.7 presents a sample calculation for determining the parameters a, b and c from the isotaches of a conventional oedometer test on a saturated compacted organic soil in the current study. Den Haan (1994) proposed that creep could be modelled in a semi-logarithmic stress-natural strain diagram by some parallel isotache lines, where each one represents a certain value of the creep rate. Each isotache can be drawn by joining natural strains under the various vertical stresses for an equal natural strain rate. Moving from upper to lower isotaches, the creep rate will decrease. The slope of isotaches in virgin creep tails is given by parameter b when the vertical axis is based on the total natural strain coordinate or by b-a if the vertical axis is based on the visco-plastic natural strain coordinate (see Figure 2.16).

As is presented in Figure 2.7, the vertical distance between the isotaches is $c \times x$. The parameter c also could be measured via the slope of each curve on a plot of the visco-plastic part of the natural strain (ε_{vp}^{H}) versus natural logarithm of the intrinsic time ($\ln \tau$) (see Figure 2.10b). The parameter c is identical in all loading steps and independent of the size and duration of the load increments. If parameter c is set to zero, creep will be totally deducted from the calculation of the model. Parameter x in Figure 2.7 is dependent on the interval of isotaches, which is illustrated in Figures 2.8 and 2.9. Some aspects of these figures such as intrinsic time will be explained later.

Den Haan (1996) explains that “The parameters a, b and c are related to the conventional parameters C_S, C_C and C_α respectively” (p. 2), where C_S: Swelling index, C_C: Compression index, and C_α: Secondary compression index. Den Haan (2008) also reports that “The isotaches are not sensitive to the size of the load increments” (p. 37).

Based on Figure 2.10b, on an isobar where vertical effective stress is constant, deformation increases with increasing intrinsic time. This can be expressed with the following equation:

$$\Delta\varepsilon_{vp}^{H} = \varepsilon_{vp_{\mathrm{II}}}^{H} - \varepsilon_{vp_{\mathrm{I}}}^{H} = c\,(\ln\tau_{\mathrm{II}} - \ln\tau_{\mathrm{I}}) = c\ \cdot \ln\frac{\tau_{\mathrm{II}}}{\tau_{\mathrm{I}}} \tag{2.9}$$

Therefore the visco-plastic part of the natural strain (i.e., creep) can be obtained via equation 2.9, which has been proposed by Den Haan (1994, 1996, 2008).

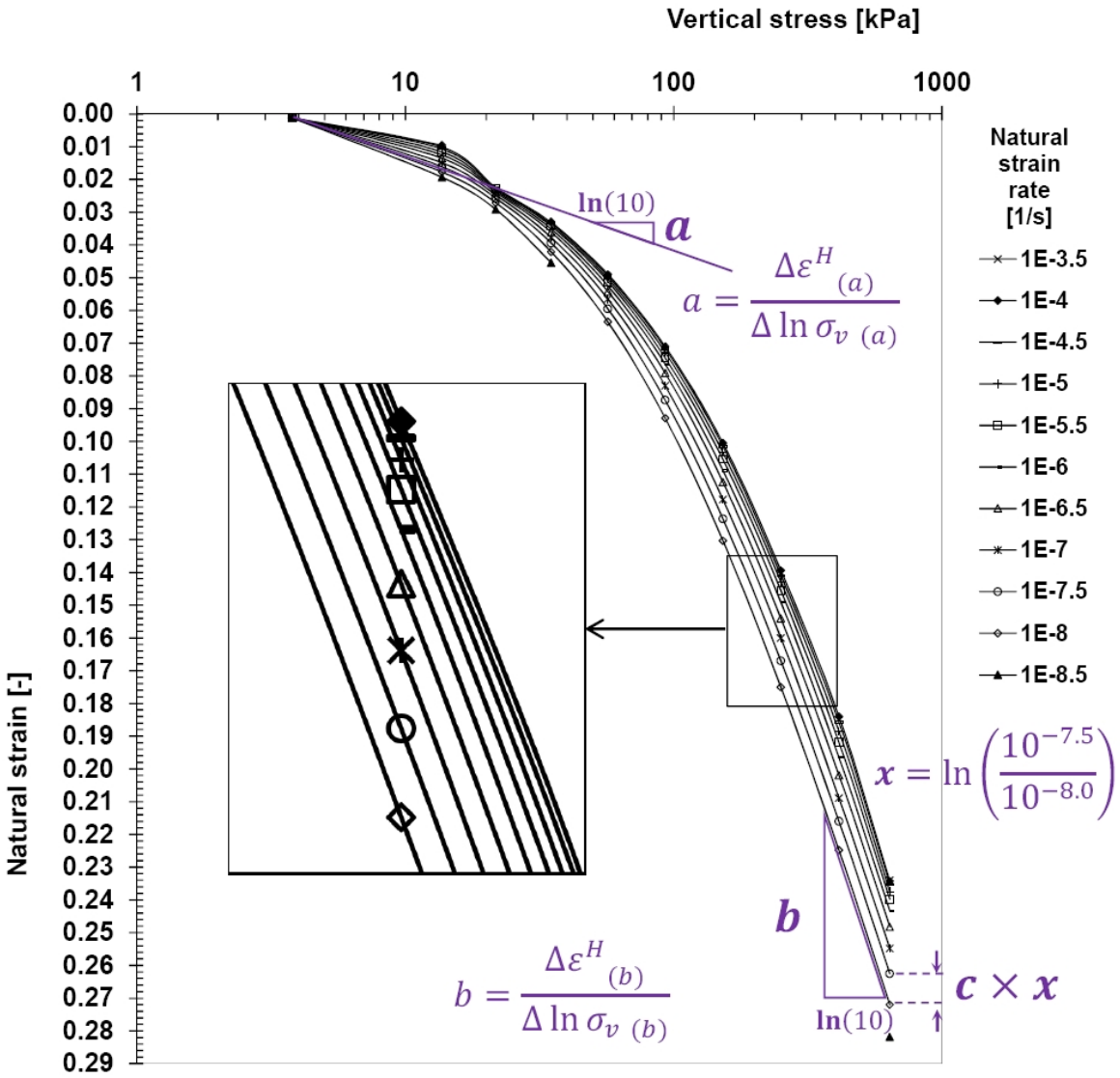

Figure 2.7. A sample calculation for determining the parameters a, b and c from the isotaches of the conventional oedometer test S2 (saturated compacted organic soil).

Den Haan (2008) described the a,b,c isotache model with the Maxwell element in Figure 2.11. The elastic part of the natural strain, which is produced by increasing the vertical effective stress during primary consolidation, is represented by a spring, and the visco-plastic part of the natural strain (i.e., creep) which is developed over time, is represented by a dashpot. According to this figure, total natural strain is equal to the elastic part plus the visco-plastic part of the natural strain (equation 2.10). In addition, total natural strain rate is equal to the elastic part plus the visco-plastic part of the natural strain rate (equation 2.11).

$$\varepsilon^H = \varepsilon_e^H + \varepsilon_{vp}^H \tag{2.10}$$

$$\dot{\varepsilon}^H = \dot{\varepsilon}_e^H + \dot{\varepsilon}_{vp}^H \tag{2.11}$$

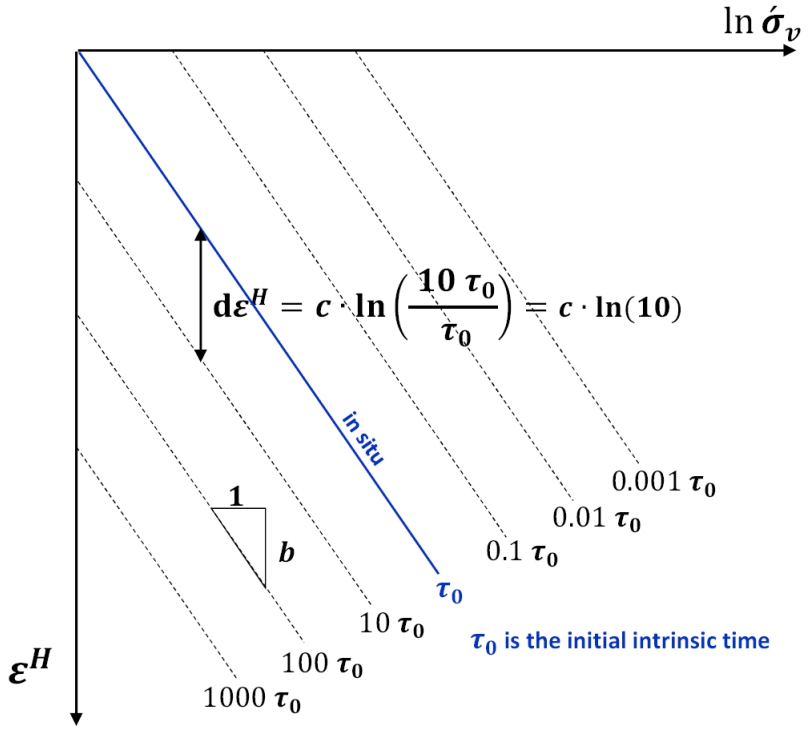

Figure 2.8. Vertical distance between the isotaches in an intrinsic form. Adapted and redrawn from Den Haan, 2008, p. 34, fig. 2a.

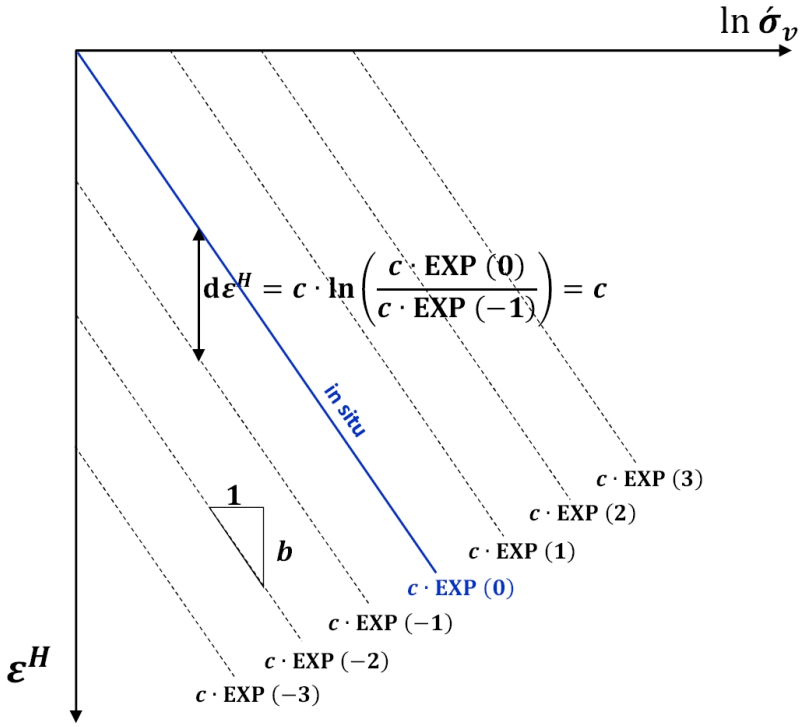

Figure 2.9. Vertical distance between the isotaches in an exponential form. Adapted and redrawn from Den Haan & Kamao, 2003, p. 204, fig. 1b.

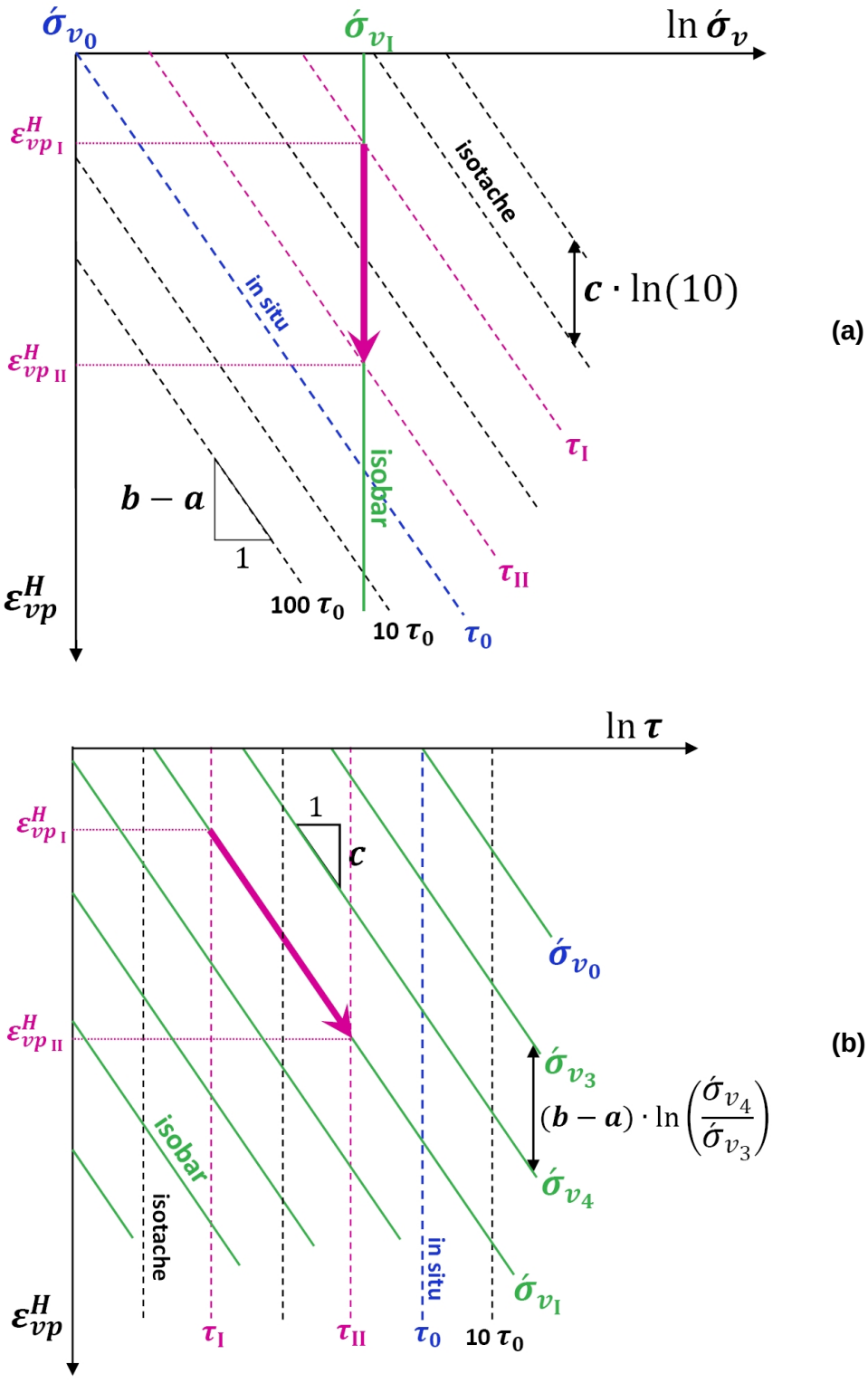

Figure 2.10. Creep isotaches and isobars. Adapted and redrawn from Sipkema, 2006, p. 23, fig. 4.7 & 4.8 and Den Haan, 1996, p. 3, fig. 1a & 1b.

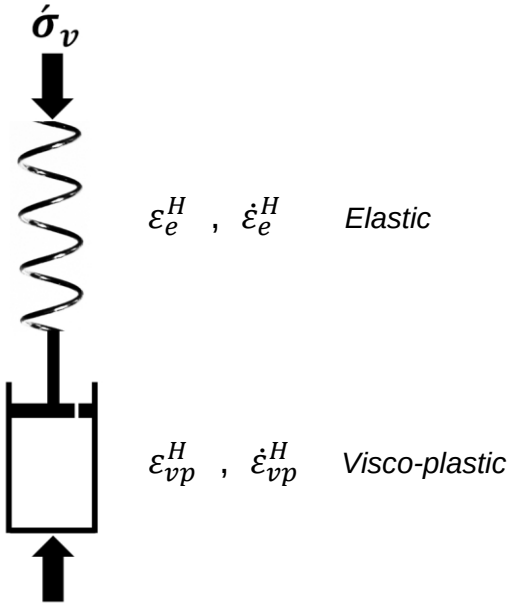

Figure 2.11. The isotache model represented as a Maxwell element. Adapted and redrawn from Den Haan, 2008, p. 34, fig. 1.

where

ε_e^H: Elastic part of the natural strain

$\dot{\varepsilon}_e^H$: Elastic part of the natural strain rate

ε^H: Total natural strain

ε_{vp}^H: Visco-plastic part of the natural strain

$\dot{\varepsilon}_{vp}^H$: Visco-plastic part of the natural strain rate

$\dot{\varepsilon}^H$: Total natural strain rate

Note:
In this research, *natural strain* (ε^H) without additional descriptions means *total natural strain* which is equal to the elastic part plus the visco-plastic part of the natural strain. Similarly, *natural strain rate* ($\dot{\varepsilon}^H$) without additional descriptions means *total natural strain rate* which is equal to the elastic part plus the visco-plastic part of the natural strain rate.

Den Haan and Kamao (2003) argue that the parameters a, b and c could be determined from incremental loading compression tests. Since it is not possible to separate elastic and visco-plastic strain of test results, they suggest that the isotaches be drawn using total strain and total strain rate. After dissipation of excess pore-water pressure, the total natural strain rate will be equal to visco-

plastic part of the natural strain rate and isotaches will afterwards have identical vertical distances. This concept can be expressed as follows:

According to equation 2.11 ($\dot{\varepsilon}^H = \dot{\varepsilon}_e^H + \dot{\varepsilon}_{vp}^H$) after end of consolidation,

$$\dot{\varepsilon}_e^H = 0 \rightarrow \dot{\varepsilon}^H = \dot{\varepsilon}_{vp}^H \tag{2.12}$$

This concept is applicable for drawing the 1-day reference isotache, which will be discussed later in *Section 2.1.6.9* to determine the model parameters.

2.1.6.3 Elastic Part of the Natural Strain

Den Haan (1996) explains that the elastic part of the natural strain develops along with the visco-plastic part of the natural strain, therefore, it is not possible to measure each one separately [in the laboratory or in the field].

Based on Figure 2.22,

$$\frac{a}{1} = \frac{\varepsilon_e^H - 0}{\ln \acute{\sigma}_v - \ln \acute{\sigma}_{v_0}}$$

Therefore the elastic part of the natural strain (ε_e^H) can be given by the following equation (Den Haan, 2008),

$$\varepsilon_e^H = a \cdot \ln\left(\frac{\acute{\sigma}_v}{\acute{\sigma}_{v_0}}\right) \tag{2.13}$$

Based on this equation, the elastic part of the natural strain increases linearly with $\ln\left(\acute{\sigma}_v/\acute{\sigma}_{v_0}\right)$.

In mathematics, we know that,

$$\frac{\mathrm{d}(\ln r)}{\mathrm{d}t} = \frac{1}{r} \cdot \frac{\mathrm{d}r}{\mathrm{d}t}$$

where r is an arbitrary parameter for change of variables, which can be defined here as:

$$r = \frac{\acute{\sigma}_v}{\acute{\sigma}_{v_0}}$$

so,

$$\frac{\partial \varepsilon_e^H}{\partial t} = a \frac{1}{\left(\frac{\acute{\sigma}_v}{\acute{\sigma}_{v_0}}\right)} \cdot \left[\frac{1}{\acute{\sigma}_{v_0}} \cdot \frac{\partial \acute{\sigma}_v}{\partial t}\right]$$

Therefore the elastic part of the natural strain rate ($\dot{\varepsilon}_e^H$) can be given by the following equation (Den Haan, 2008),

$$\frac{\partial \varepsilon_e^H}{\partial t} = \frac{a}{\acute{\sigma}_v} \cdot \frac{\partial \acute{\sigma}_v}{\partial t} \tag{2.14}$$

where

a: Isotache parameter, $\acute{\sigma}_v$: Desired vertical effective stress, $\acute{\sigma}_{v_0}$: Initial vertical effective stress, and t: Time.

Equation 2.14 shows that the elastic part of the natural strain rate has a relationship with the rate of vertical effective stress ($\partial \acute{\sigma}_v / \partial t$). After finishing the primary consolidation phase, the rate of vertical effective stress is zero and consequently: $\partial \varepsilon_e^H / \partial t = 0$. Therefore, according to $\dot{\varepsilon}^H = \dot{\varepsilon}_e^H + \dot{\varepsilon}_{vp}^H$, at the end of primary consolidation: $\dot{\varepsilon}^H = \dot{\varepsilon}_{vp}^H$.

Parameter “a” is always smaller than parameter b. Visschedijk and Trompille (2009) comment that “The parameter a is preferably determined from unloading curves, where creep rates are low” (p. 312).

2.1.6.4 Visco-plastic Part of the Natural Strain

In a,b,c isotache model, the visco-plastic part of the natural strain (i.e., creep) develops simultaneously with the elastic compression. In this model, the visco-plastic part of the natural strain is defined based on creep rate and intrinsic time; the latter will be discussed thoroughly in the following sections.

2.1.6.4.1 Intrinsic Time

One of the basic principles of the a,b,c isotache model is to use intrinsic time (τ), an alternative to the creep rate, instead of normal time. Den Haan (1994) suggests:

$$\tau = \frac{c}{\dot{\varepsilon}_{vp}^H} \tag{2.15}$$

where

c: Isotache parameter

$\dot{\varepsilon}_{vp}^H$: Visco-plastic part of the natural strain rate

According to this equation and Figure 2.12, immediately after applying a large stress to a soil, the rates of both elastic and creep strain are high, and therefore, intrinsic time is very small; thus,

larger stress → higher creep rate → smaller intrinsic time → isotache lies higher

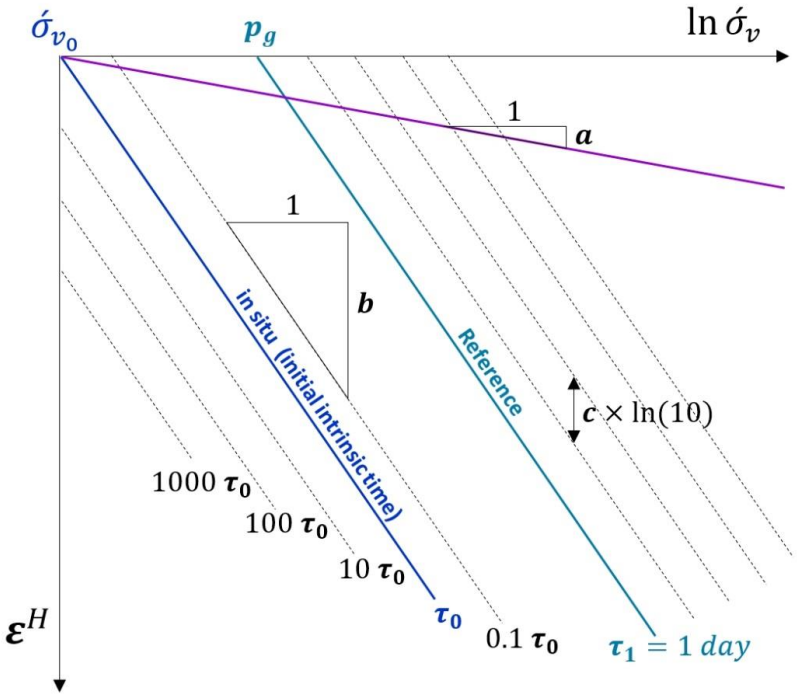

Figure 2.12. Structure of the a,b,c isotache model in a total natural strain coordinate system for saturated soils. Adapted and redrawn from Den Haan, 2008, p. 34, fig. 2a.

Parameter p_g in Figure 2.12 called pre-consolidation stress at zero total strain. Subscript g in p_g stands for "grensspanning" in Dutch (i.e., pre-consolidation stress).

Based on the theory of the model (Den Haan & Edil, 1994), creep strains are linear when plotted versus logarithm of the intrinsic times ($\ln \tau$) at constant vertical effective stress (see Figure 2.10b). Den Haan and Sellmeijer (2000) argue that creep in the a,b,c isotache model "is determined fully by vertical effective stress and intrinsic time, not time. The problem with time is that its origin is not well-defined . . ." (p. 10).

Time (t) that could be called normal time or clock time has a fixed origin and its value depends on the position of this origin, which is for example start of a loading step or beginning of a constructing process. Den Haan and Van den Berg (2001) explain that "intrinsic time is insensitive to changes in the origin of time, and remains related to creep isotaches" (p. 4). They continue that "Intrinsic time is the geological time necessary to attain the present degree of compression under the present vertical effective stress, if that stress was applied at the moment of formation of the soil" (p. 4). Figures 2.13 and 2.14 are presented here as a physical explanation of their somewhat complicated definition.

Assume that in Figure 2.13, τ belongs to an isotache that if extended backward, intersects the vertical axis at $e = \infty$. The intersection is the moment of soil formation, which means the void ratio was infinite before the settlement starts. Suppose that at this time, perhaps thousands of years ago, vertical effective stress was zero ($\acute{\sigma}_{v_0} = 0$) and the soil particles were suspended in water or air. Now consider the isotache with zero intrinsic time at the coordinates of ($\ln \acute{\sigma}_{v_A}, e = \infty$). For this isotache,

creep rate could be calculated as: $\dot{\varepsilon}_{vp}^{H} = c/\tau = c/0 = \infty$. This shows the highest rate of creep, which occurs in the beginning of the geological settlement. Therefore τ is the geological time necessary to attain the present degree of compression (e_0) at point A, under the present vertical effective stress ($\acute{\sigma}_{v_A}$), if $\acute{\sigma}_{v_A}$ would have been applied at the moment of formation of the soil. τ starts from $\tau = 0$ and continues up to τ.

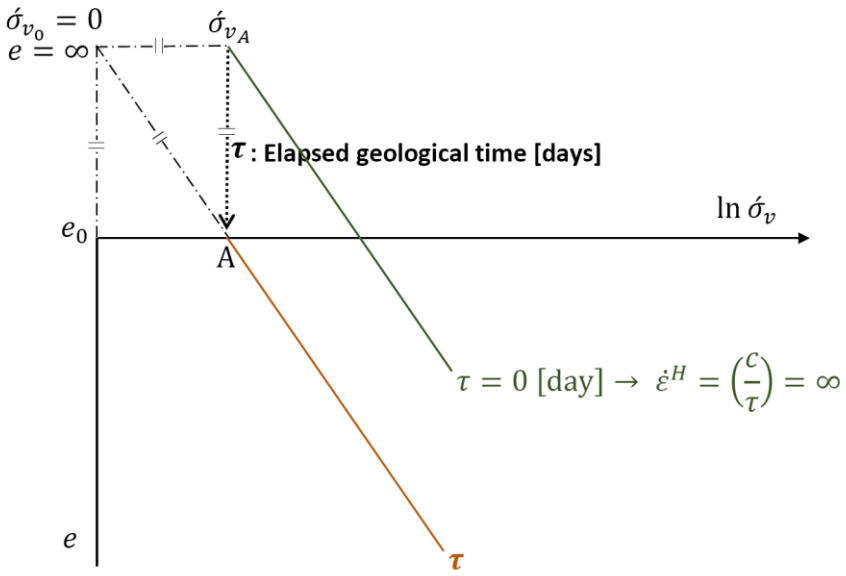

Figure 2.13. Physical concept of τ. Adapted and redrawn from Den Haan, 1996, p. 3, fig. 1a.

A similar argument could be given for τ_0. If in Figure 2.14, τ_0 extends backward, it will reach a point where $e = \infty$. Again, this position is the moment of soil formation, meaning the void ratio was infinite before the settlement starts. Similar to before, suppose that at this time vertical effective stress was zero ($\acute{\sigma}_v = 0$) and the soil particles were suspended in water or air. Considering the isotache with zero intrinsic time at the coordinates of ($\ln \acute{\sigma}_{v_0}$, $e = \infty$), again creep rate could be calculated as: $\dot{\varepsilon}_{vp}^{H} = c/\tau = c/0 = \infty$. This means that in the beginning of the geological settlement, the highest rate of creep occurs. Therefore τ_0 is the geological time necessary to attain the present degree of compression (e_0) under the present vertical effective stress ($\acute{\sigma}_{v_0}$), if that stress would have been applied at the moment of formation of the soil. τ_0 starts from $\tau = 0$ and continues up to τ_0.

Den Haan (1996) reports that “in a standard 24 h incremental loading test, τ is often approximately 1 day at the end of an increment” (p. 4). The natural strain rate at the end of 24 hours, as Den Haan and Edil (1994) explain, is about 10^{-7} (1/s) or slightly higher.

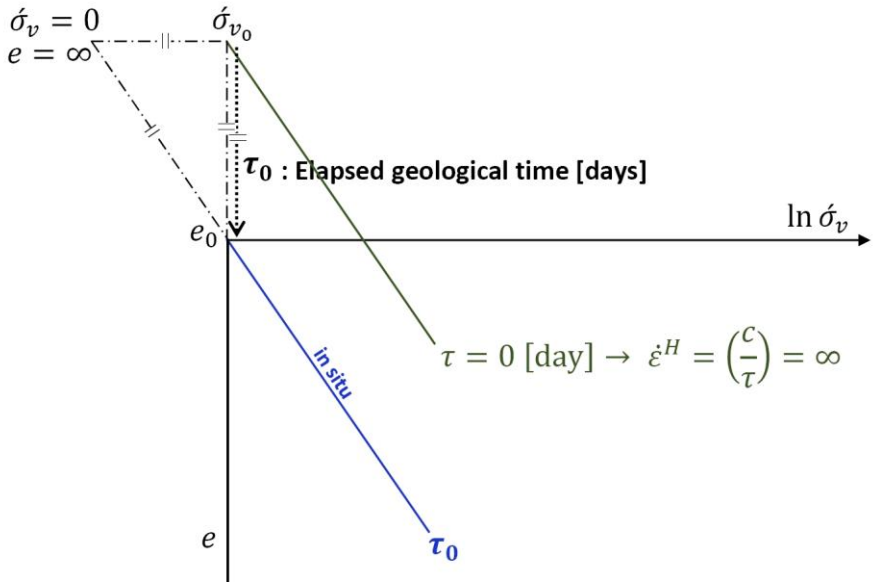

Figure 2.14. Physical concept of τ_0. Adapted and redrawn from Den Haan, 1996, p. 3, fig. 1a.

2.1.6.4.2 Isotache of Reference Intrinsic Time

As Den Haan (2008) explains, on a plot of the total natural strain (ε^H) versus the logarithmic scale of vertical effective stress ($\acute{\sigma}_v$), the abscissa (i.e., x-coordinate) of the intersection of the reference isotache (slope b) with a horizontal line originating from the initial condition ($\acute{\sigma}_v = \acute{\sigma}_{v_0}$, $\varepsilon^H = 0$) represents the pre-consolidation stress at zero total strain (p_g). This independent value belongs to the total natural strain coordinate and determines from laboratory tests. On the contrary, $p_{g\,vp}$, the pre-consolidation stress at zero visco-plastic strain, is dependent on p_g, parameters a, b and the initial vertical effective stress ($\acute{\sigma}_{v_0}$) (see equation 2.17 and Figure 2.16). In this study, all calculations for modelling of the creep were executed using the value of $p_{g\,vp}$. The related equations will be presented in the following sections.

Laboratories traditionally perform standard incremental oedometer test via 1-day steps. This is the first reason for choosing the reference intrinsic time equal to 1-day. The second reason is to simplify the model equations. Nevertheless, selecting a 1-day-value as the reference intrinsic time is not obligatory. Other time values are acceptable if their effect is considered correctly in the model equations. It is worth mentioning that the reference isotache should be always drawn parallel to the lowest isotache at the highest stress range.

2.1.6.4.3 Isotache of Initial Intrinsic Time

Calculation of settlement needs an initial condition. At the initial condition, strain is zero, vertical effective stress is $\acute{\sigma}_{v_0}$, and the intrinsic time is defined as initial intrinsic time (τ_0). Den Haan obtained an equation to calculate initial intrinsic time as follows (E. J. Den Haan, personal communication, July 14, 2014).

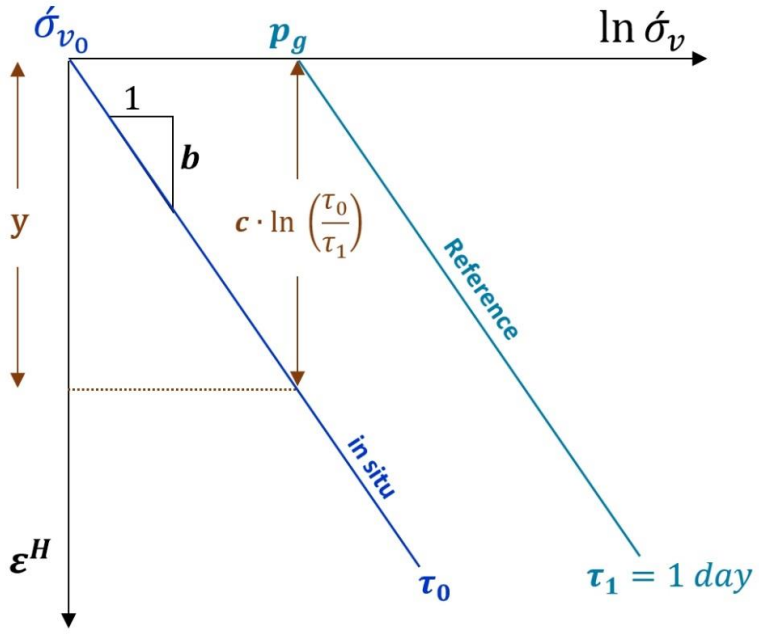

Figure 2.15. Relationship between the reference intrinsic time (τ_1) and the initial intrinsic time (τ_0) (E. J. Den Haan, personal communication, July 14, 2014).

As is shown in Figure 2.15, the vertical distance between the isotaches of *reference intrinsic time* (τ_1) and *initial intrinsic time* (τ_0) could be calculated through two different methods;

Via equation 2.9 by using parameter c,

$$y = c \cdot \ln\left(\frac{\tau_0}{\tau_1}\right)$$

As well as by using slope b (on the τ_0 line),

$$y = b \cdot \ln\left(\frac{p_g}{\acute{\sigma}_{v_0}}\right)$$

Since these two are equal, so

$$c \cdot \ln\left(\frac{\tau_0}{\tau_1}\right) = b \cdot \ln\left(\frac{p_g}{\acute{\sigma}_{v_0}}\right)$$

$$\left(\frac{\tau_0}{\tau_1}\right)^c = \left(\frac{p_g}{\acute{\sigma}_{v_0}}\right)^b$$

Therefore, as it has been presented by Den Haan (2008),

$$\tau_0 = \tau_1 \cdot \left(\frac{p_g}{\acute{\sigma}_{v_0}}\right)^{\left(\frac{b}{c}\right)} \tag{2.16}$$

where p_g is the pre-consolidation stress at zero total strain.

Based on the argument of Den Haan (2008) about the concept of initial intrinsic time, it can be concluded that creep in virgin condition under its self-weight during the "life time of the layer" is represented by the ordinate (i.e., y-coordinate) of the τ_0-isotache. It is worthwhile noting that the development of creep on τ_0-isotache is not due to external loads but the result of the increasing weight of soil as depth of layer increases. As Den Haan (2008) explains, the creep due to the weight of soil layer is called *autonomous settlement*. He reports, "the autonomous settlement of large parts of the Netherlands is in the order of 1 cm/year" (p. 36), although this includes the loss of peat solid material by oxidation.

2.1.6.5 Shifting from Total to Visco-Plastic Natural Strain

The results of laboratory tests are always according to the total strains and it is not possible to separate it into elastic and visco-plastic strains. However, the equations of the a,b,c isotache model works based on the separating elastic and visco-plastic part of the natural strains. Shifting from total to visco-plastic natural strains will be discussed in this section.

Den Haan (2008) described the effect of shifting from total to visco-plastic natural strain in Figure 2.16 by using the following equations. As is shown in this figure, the pre-consolidation stress at zero *total* strain is called p_g and the pre-consolidation stress at zero visco-plastic strain is called $p_{g\,vp}$. Consider the point M, which is the intersection of a line with slope "a" from the initial condition ($\acute{\sigma}_v = \acute{\sigma}_{v_0}$, $\varepsilon^H = 0$) and the 1-day reference isotache with slope b. The ordinate of M can be obtained through two different methods;

by using slope "a",

$$y = a \cdot \ln\left(\frac{p_{g\,vp}}{\acute{\sigma}_{v_0}}\right)$$

and also via slope b,

$$y = b \cdot \ln\left(\frac{p_{g\,vp}}{p_g}\right)$$

Since these two are equal, so

$$a \cdot \ln\left(\frac{p_{g_{vp}}}{\acute{\sigma}_{v_0}}\right) = b \cdot \ln\left(\frac{p_{g_{vp}}}{p_g}\right)$$

$$\left(\frac{p_{g_{vp}}}{\acute{\sigma}_{v_0}}\right)^a = \left(\frac{p_{g_{vp}}}{p_g}\right)^b$$

$$(p_{g_{vp}})^{b-a} = (p_g)^b \cdot (\acute{\sigma}_{v_0})^{-a}$$

$$p_{g_{vp}} = \left[(p_g)^b \cdot (\acute{\sigma}_{v_0})^{-a}\right]^{\left(\frac{1}{b-a}\right)} \tag{2.17}$$

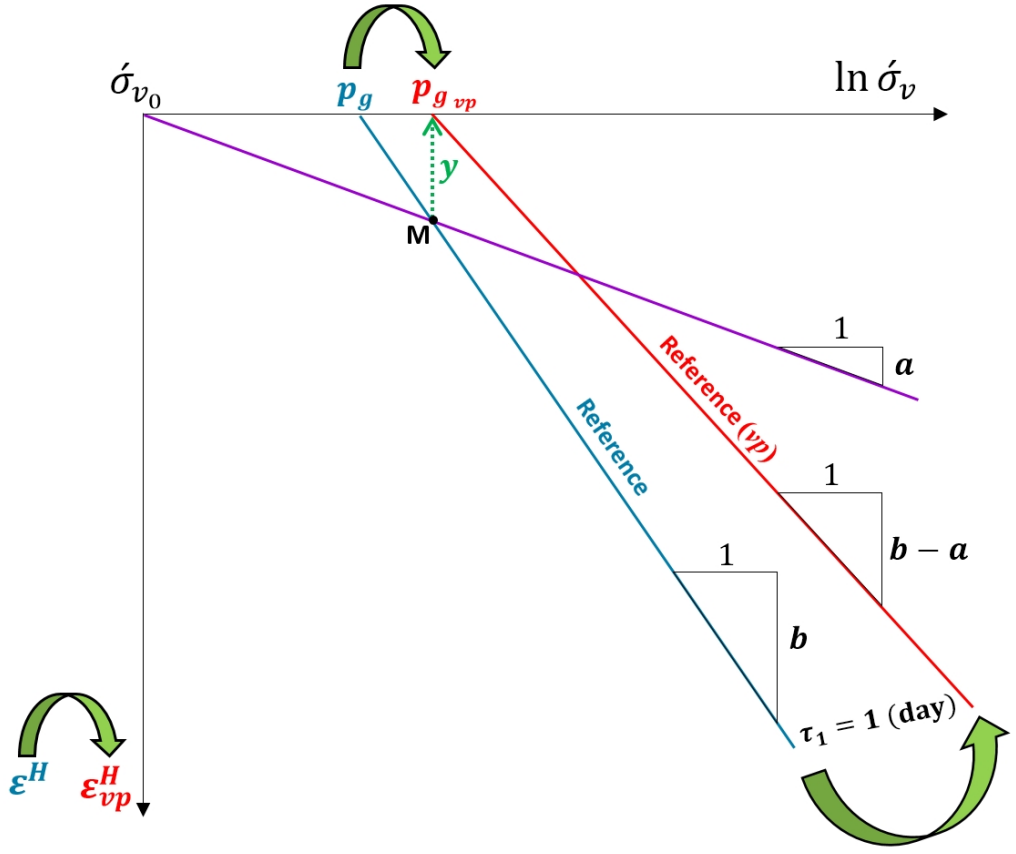

Figure 2.16. Rotation of the isotaches and increase of pre-consolidation stress by subtraction of elastic natural strains from total natural strains. Adapted and redrawn from Den Haan, 2008, p. 38, fig. 6.

Over-consolidation ratio in a *total* and *visco-plastic* natural strain coordinate for the isotache of initial intrinsic time (i.e., τ_0-isotache or in situ) can be defined, respectively as follows:

$$OCR_0 = \frac{p_g}{\acute{\sigma}_{v_0}} \quad \text{and} \quad OCR_{vp_0} = \frac{p_{g_{vp}}}{\acute{\sigma}_{v_0}} \tag{2.18}$$

Therefore, it can be concluded that (Den Haan, 2008),

$$OCR_0 = OCR_{vp_0}^{\left(\frac{b-a}{b}\right)} \tag{2.19}$$

With help of the equation 2.16, it could be obtained that

$$\tau_0 = \tau_1 \cdot \left(\frac{p_g}{\acute{\sigma}_{v_0}}\right)^{\left(\frac{b}{c}\right)} = \tau_1 \cdot OCR_0^{\left(\frac{b}{c}\right)}$$

Therefore (Den Haan, 2008),

$$\tau_0 = \tau_1 \cdot OCR_{vp_0}^{\left(\frac{b-a}{c}\right)} = \tau_1 \cdot \left(\frac{p_{g_{vp}}}{\acute{\sigma}_{v_0}}\right)^{\left(\frac{b-a}{c}\right)} \tag{2.20}$$

Figure 2.16 also presents a graphical method for finding the pre-consolidation stress at zero visco-plastic strain as follows:

- Construct the isotaches on a plot of the total natural strain (ε^H) versus the logarithmic scale of vertical effective stress ($\acute{\sigma}_v$),
- Draw a line from initial condition ($\acute{\sigma}_v = \acute{\sigma}_{v_0}$, $\varepsilon^H = 0$) under slope “a”,
- The intersection of this line and the 1-day reference isotache (slope b) at point M represents the pre-consolidation stress at zero visco-plastic strain on the horizontal axis ($p_{g_{vp}}$). This value belongs to the visco-plastic natural strain coordinate.

As shown above, the pre-consolidation stress at zero strain and the over-consolidation ratio for τ_0-isotache are able to transform from the total natural strains coordinate (p_g and OCR_0) to the visco-plastic natural strains coordinate ($p_{g_{vp}}$and OCR_{vp_0}), and vice versa.

2.1.6.6 Pre-Consolidation Stress

In soil mechanics, pre-consolidation stress is defined as the highest effective stress experienced by the soil in its stress history. In the a,b,c isotache model, pre-consolidation stress is a state dependent parameter and should be updated along with increasing the strain.

As is shown in Figure 2.17, assume that after increasing stress, the new value of visco-plastic natural strain on the 1-day reference isotache is $\varepsilon^H_{vp_{(\text{new})}}$. The relationship between $\varepsilon^H_{vp_{(\text{new})}}$, and the pre-

consolidation stress at zero visco-plastic strain ($p_{g_{vp}}$), and the updated pre-consolidation stress in a visco-plastic natural strain coordinate ($p_{g\ vp(\text{update})}$) can be expressed as:

$$\varepsilon^{H}_{vp_{(\text{new})}} = (b-a)\cdot \ln\left(\frac{p_{g_{vp}(\text{update})}}{p_{g_{vp}}}\right)$$

therefore,

$$p_{g_{vp}(\text{update})} = p_{g_{vp}} \cdot \text{EXP}\left(\frac{\varepsilon^{H}_{vp(\text{new})}}{b-a}\right) \tag{2.21}$$

This equation is essentially similar to the suggestion of Leoni, Karstunen and Vermeer (2008).

As is illustrated in Figure 2.17, $\varepsilon^{H}_{vp_{(\text{new})}}$ is the visco-plastic natural strain on the 1-day reference isotache at the end of the past step (or at the beginning of the new step).

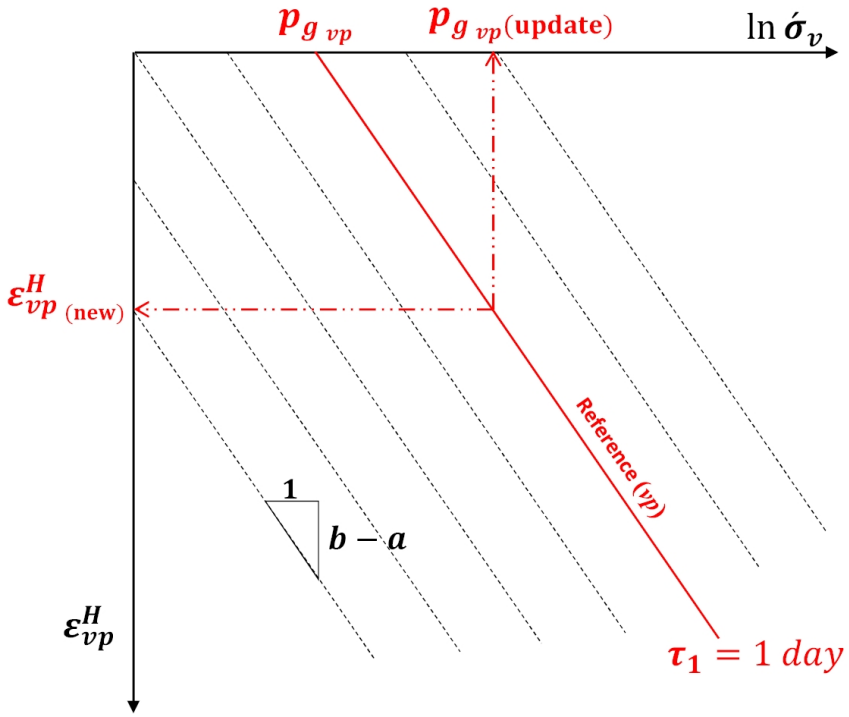

Figure 2.17. Updating pre-consolidation stress along with increasing strain in a visco-plastic natural strain coordinate.

2.1.6.7 Over-Consolidation Ratio (OCR)

In engineering practice, over-consolidation ratio (OCR) is defined as:

$$\text{OCR} = \frac{\text{Pre-consolidation stress}}{\text{Present effective stress}} \tag{2.22}$$

In the a,b,c isotache model, the 1-day reference isotache is defined similarly to the Normal Consolidation Line (NCL) which presents the virgin settlement of soils. The variations of over-consolidation ratio in a visco-plastic natural strain coordinate are illustrated in Figure 2.18, which is conceptually similar to the illustration of Leoni et al. (2008). This figure shows that higher isotaches have lower over-consolidation ratio and the value of OCR_{vp} for the 1-day reference line is equal to 1.

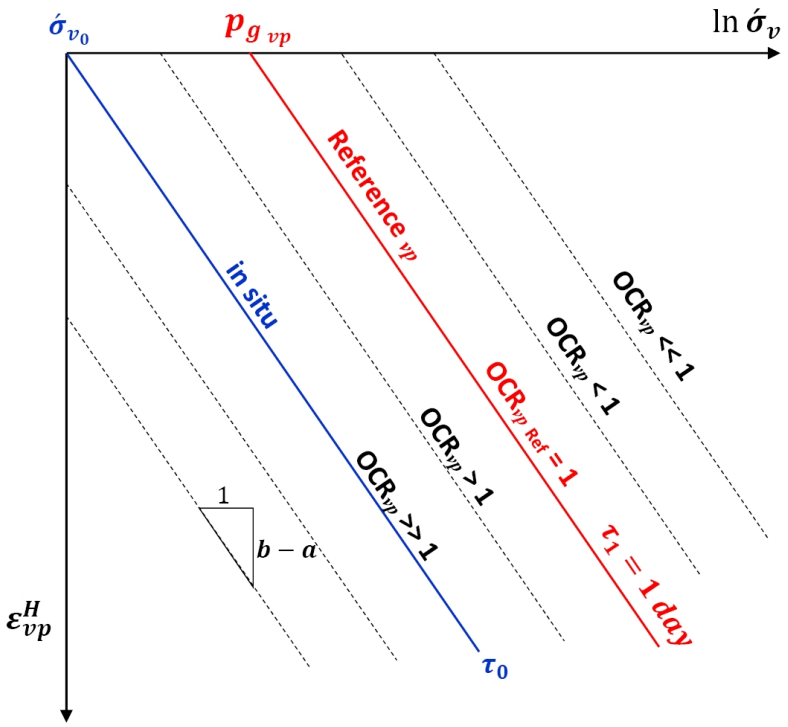

Figure 2.18. Consistency of OCR_{vp} for each isotache.

As Leoni et al. (2008) explain, “in a standard oedometer test with load doubled at each stage, at the end of primary consolidation OCR is between 0.5 and 1” (p. 216).

Figure 2.19 shows the variations of over-consolidation ratio in a visco-plastic natural strain coordinate for changes of strain or time at a constant vertical effective stress ($\acute{\sigma}_{v_x}$). The values of OCR_{vp} can be expressed for different isotaches as follows. Different colours are used to make it easy to distinguish each variable.

$$\mathbf{OCR}_{vp\ \mathrm{II}} = \frac{p_{g_{vp(\mathrm{update})_{\mathrm{II}}}}}{\acute{\sigma}_{v_x}} \ll 1$$

$$\mathbf{OCR}_{vp\ \mathrm{III}} = \frac{p_{g_{vp(\mathrm{update})_{\mathrm{III}}}}}{\acute{\sigma}_{v_x}} < 1$$

$$\mathrm{OCR}_{vp\ \mathrm{Ref}} = \frac{\acute{\sigma}_{v_x}}{\acute{\sigma}_{v_x}} = 1$$

$$\mathrm{OCR}_{vp\ \mathrm{IV}} = \frac{p_{g_{vp(\mathrm{update})_{\mathrm{IV}}}}}{\acute{\sigma}_{v_x}} > 1$$

$$\mathrm{OCR}_{vp\ 0} = \frac{p_{g_{vp(\mathrm{update})_0}}}{\acute{\sigma}_{v_x}} \gg 1$$

Figure 2.19 and the above equations indicate that the value of OCR_{vp} increases with increasing strain at a constant vertical effective stress during the creep phase. The parameters $p_{g_{vp(\mathrm{update})_{\mathrm{II\&III\&IV\&0}}}}$ are the updated pre-consolidation stresses which correspond to the different strains of $\varepsilon^{H}_{vp\ \mathrm{II\&III\&IV\&0}}$, respectively.

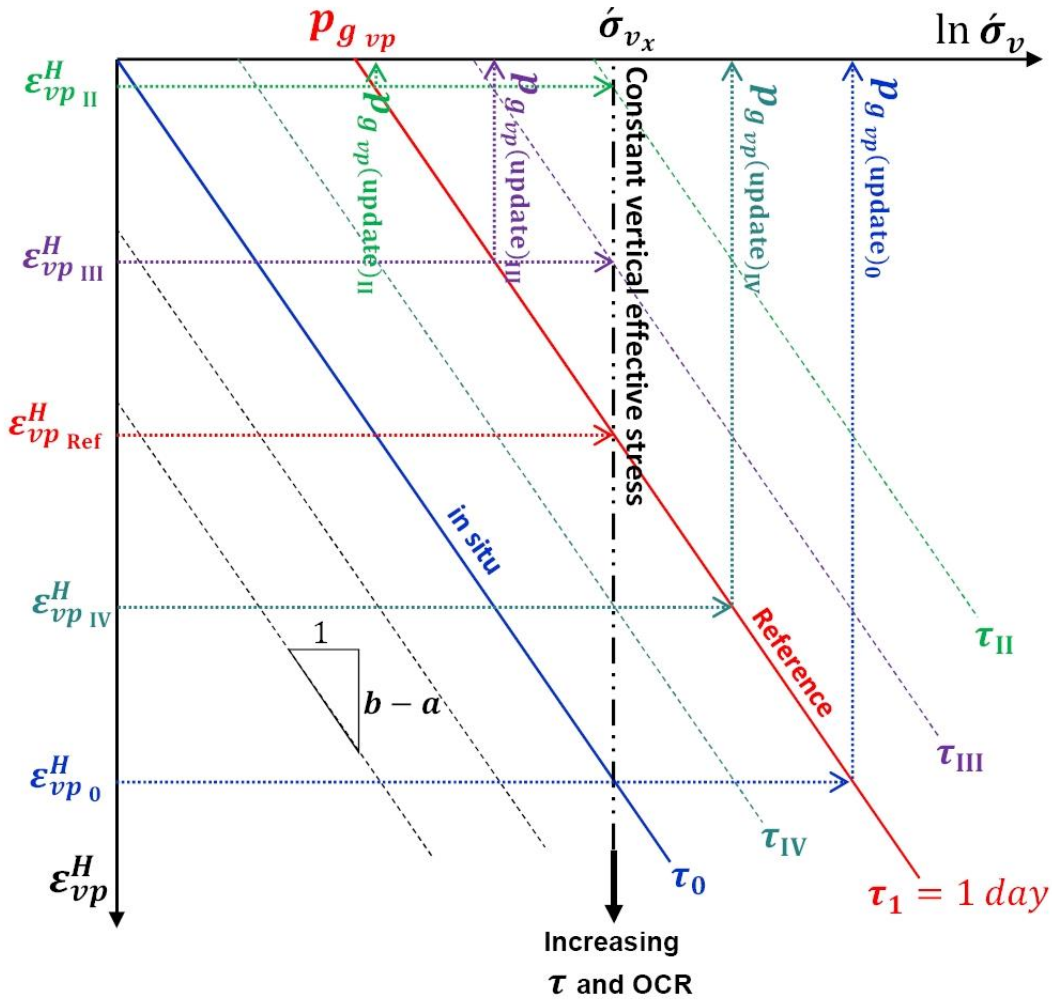

Figure 2.19. Calculation of the over-consolidation ratio in a visco-plastic natural strain coordinate for different isotaches at a constant vertical effective stress ($\acute{\sigma}_{v_x}$).

As shown in Figure 2.19, the $p_{g\ vp(\text{update})}$ exceeds the $\acute{\sigma}_{v_x}$ when the visco-plastic part of the natural strain exceeds the $\varepsilon^{H}_{vp\ \text{Ref}}$ (see equation 2.21 as well). In other words, it is possible that the updated pre-consolidation stress in a visco-plastic natural strain coordinate ($p_{g\ vp(\text{update})}$) exceeds the desired vertical effective stress ($\acute{\sigma}_{v_x}$) if the duration of the loading step is long enough; consequently the value of OCR_{vp} (i.e., $p_{g\ vp(\text{update})}/\acute{\sigma}_{v_x}$) exceeds 1.

Another situation is presented in Figure 2.20 which shows the variations of over-consolidation ratio in a visco-plastic natural strain coordinate at a constant visco-plastic natural strain.

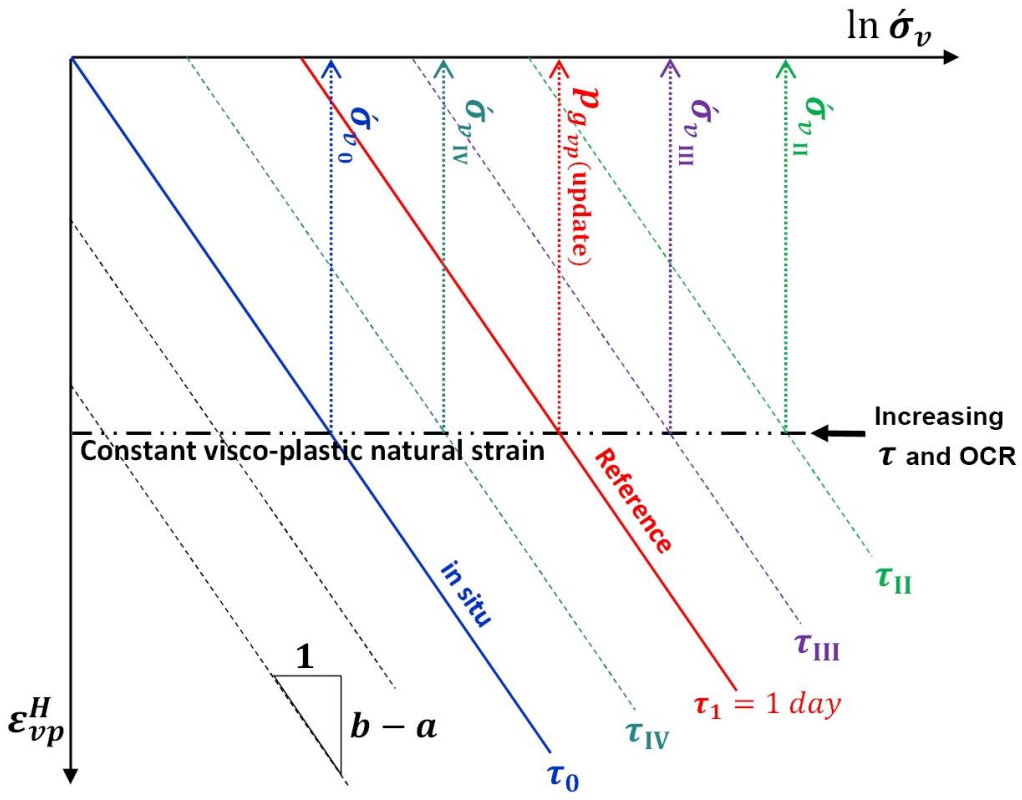

Figure 2.20. Calculation of the over-consolidation ratio in a visco-plastic natural strain coordinate for different isotaches at a constant visco-plastic natural strain.

The values of OCR_{vp} for changes of stress at a constant visco-plastic natural strain could be obtained for different isotaches as follows. Again, different colours are used to make it easy to distinguish each variable.

$$\text{OCR}_{vp\ \text{II}} = \frac{p_{g_{vp(\text{update})}}}{\acute{\sigma}_{v\ \text{II}}} \ll 1$$

$$\text{OCR}_{vp\ \text{III}} = \frac{p_{g_{vp(\text{update})}}}{\acute{\sigma}_{v\ \text{III}}} < 1$$

$$\mathbf{OCR}_{vp\ \mathbf{Ref}} = \frac{p_{g_{vp\,(\mathbf{update})}}}{p_{g_{vp\,(\mathbf{update})}}} = \mathbf{1}$$

$$\mathbf{OCR}_{vp\ \mathbf{IV}} = \frac{p_{g_{vp\,(\mathbf{update})}}}{\acute{\sigma}_{v\ \mathbf{IV}}} > \mathbf{1}$$

$$\mathbf{OCR}_{vp\ \mathbf{0}} = \frac{p_{g_{vp\,(\mathbf{update})}}}{\acute{\sigma}_{v\ \mathbf{0}}} \gg \mathbf{1}$$

Corresponding to the constant visco-plastic natural strain, $p_{g_{vp\,(\mathrm{update})}}$ is the updated pre-consolidation stress in a visco-plastic natural strain coordinate in Figure 2.20 and in the equations above. It can be concluded that by decreasing the vertical effective stress (from right to left) at a constant visco-plastic natural strain, the OCR_{vp} increases.

2.1.6.8 Implementation of the a,b,c Isotache Model

Considering $\acute{\sigma}_{v_A}$ as a loading stage in Figure 2.21, the ordinate of point N can be obtained through two different methods;

By using parameter c (see equation 2.9),

$$\varepsilon_{vp}^{H} = c \cdot \ln\left(\frac{\tau_1}{\tau_{\mathrm{I,A}}}\right)$$

as well as by using slope b-a (on the τ_1 isotache),

$$\varepsilon_{vp}^{H} = (b-a) \cdot \ln\left(\frac{\acute{\sigma}_{v_A}}{p_{g_{vp}}}\right)$$

Since these two are equal, so

$$c \cdot \ln\left(\frac{\tau_1}{\tau_{\mathrm{I,A}}}\right) = (b-a) \cdot \ln\left(\frac{\acute{\sigma}_{v_A}}{p_{g_{vp}}}\right)$$

$$\left(\frac{\tau_1}{\tau_{\mathrm{I,A}}}\right)^{c} = \left(\frac{\acute{\sigma}_{v_A}}{p_{g_{vp}}}\right)^{(b-a)}$$

$$\tau_{\mathrm{I,A}} = \tau_1 \cdot \left(\frac{p_{g_{vp}}}{\acute{\sigma}_{v_A}}\right)^{\left(\frac{b-a}{c}\right)}$$

In the above equation, $p_{g_{vp}}$ should be updated at each step by using equation 2.21 (see Figure 2.17).

$$\tau_{\mathrm{II,A}} = \tau_{\mathrm{I,A}} + \Delta t_{\mathrm{A}}$$

$$\varepsilon^{H}_{vp,\mathrm{A}} = c \cdot \ln\left(\frac{\tau_{\mathrm{II,A}}}{\tau_{\mathrm{I,A}}}\right)$$

where $\varepsilon^{H}_{vp,\mathrm{A}}$ is the visco-plastic (i.e., creep) part of the natural strain due to applying $\acute{\sigma}_{v_A}$ for a duration of Δt_A.

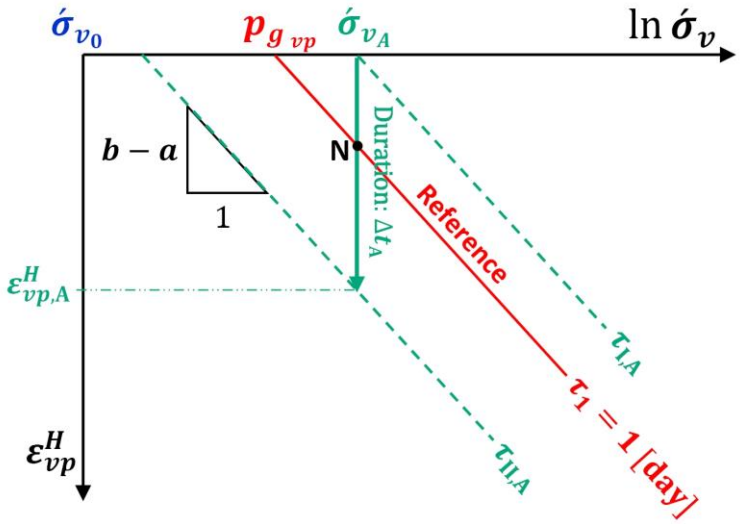

Figure 2.21. Creep calculation in the a,b,c isotache model.

Therefore based on the equations which were presented in previous sections (Den Haan, 1994, 1996, 2008; see also Leoni et al., 2008), the incremental form of the a,b,c isotache model for saturated soils, can be written as follows. In the equations, subscripts I and II denote the first and the last creep isotache in a step, respectively, and the subscript 1 stands for 1-day (see Figures 2.21 and 2.22). The reference intrinsic time is equal to one day ($\tau_1 = 1$ day) in all relevant calculations.

<u>Incremental Form of the a,b,c Isotache Model:</u>

$$p_{g_{vp}} = \left[(p_g)^b \cdot (\acute{\sigma}_{v_0})^{-a}\right]^{\left(\frac{1}{b-a}\right)} \qquad \text{Equation 2.17}$$

$$p_{g_{vp\,(\mathrm{update})_i}} = p_{g_{vp}} \cdot \mathrm{EXP}\left(\frac{\varepsilon^{H}_{vp_{i-1}}}{b-a}\right) \qquad (2.23)$$

$$OCR_{vp\ \mathrm{I}\ i} = \left(\frac{p_{g_{vp\,(\mathrm{update})_i}}}{\acute{\sigma}_{v\ i}}\right) \qquad (2.24)$$

$$\tau_{\mathrm{I}\ i} = \tau_1 \cdot OCR_{vp\ \mathrm{I}\ i}^{\left(\frac{b-a}{c}\right)} \qquad (2.25)$$

$$\tau_{\mathrm{II}\ i} = \tau_{\mathrm{I}\ i} + \Delta t_i \tag{2.26}$$

$$\varepsilon^H_{vp_i} = c \cdot \ln\left(\frac{\tau_{\mathrm{II}\ i}}{\tau_{\mathrm{I}\ i}}\right) \tag{2.27}$$

$$\varepsilon^H_{e\ i} = a \cdot \ln\left(\frac{\acute{\sigma}_{v\ i}}{\acute{\sigma}_{v_0}}\right) \tag{2.28}$$

$$\varepsilon^H_i = \varepsilon^H_{e\ i} + \sum_0^i \varepsilon^H_{vp_i} \tag{2.29}$$

$$\varepsilon^{(\mathrm{lin})}_i = 1 - \mathrm{EXP}\,(-\varepsilon^H_i) \tag{2.30}$$

where

a, b, c: Isotache parameters

$\varepsilon^H_{vp_i}$: Visco-plastic part of the natural strain (step i)

$\sum_0^i \varepsilon^H_{vp_i}$: All the visco-plastic parts of the natural strain accumulated up to the current step i

$\varepsilon^H_{e\ i}$: Elastic part of the natural strain (step i)

ε^H_i: Total natural strain (step i)

$\varepsilon^{(\mathrm{lin})}_i$: Total linear strain (step i)

p_g: Pre-consolidation stress at zero total strain

$p_{g_{vp}}$: Pre-consolidation stress at zero visco-plastic strain

$p_{g_{vp_{(\mathrm{update})_i}}}$: Updated pre-consolidation stress in a visco-plastic natural strain coordinate (step i)

$\acute{\sigma}_{v_0}$: Initial vertical effective stress

$\acute{\sigma}_{v\ i}$: Desired vertical effective stress (step i)

$OCR_{vp\ \mathrm{I}\ i}$: Over-consolidation ratio in a visco-plastic natural strain coordinate for the isotache I (step i)

Δt_i: Duration of creep (in days) for step i

$\tau_{\mathrm{I}\ i}$: Intrinsic time (in days) for the isotache I (step i)

$\tau_{\mathrm{II}\ i}$: Intrinsic time (in days) for the isotache II (step i)

τ_1: Reference intrinsic time (in days)

For the definition of intrinsic time, see equation 2.15.

The equations above have been used in *Section 5.4* for simulating the test results not only in the saturated conditions, but also with an adapted form in the unsaturated conditions.

Assuming two steps A and B in an oedometer test on a saturated soil sample and supposing a fast dissipation of excess pore-water pressure, Figure 2.22 illustrates the incremental form of the a,b,c isotache model. The elastic part of the natural strain is observed after applying the load in step A (upper plot), and then the load is maintained constant to determine the creep parameters (lower plot). In the visco-plastic phase, creep starts from an isotache with the intrinsic time of $\tau_{\mathrm{I,A}}$ and continues for a duration of Δt_{A} to reach a new isotache with the intrinsic time of $\tau_{\mathrm{II,A}}$. Following, the load of step B is applied and the new elastic part of the natural strain is observed once again (upper plot). In the visco-plastic part (lower plot), creep starts from an isotache with the intrinsic time of $\tau_{\mathrm{I,B}}$ and continues for a duration of Δt_{B} to reach a new isotache with the intrinsic time of $\tau_{\mathrm{II,B}}$.

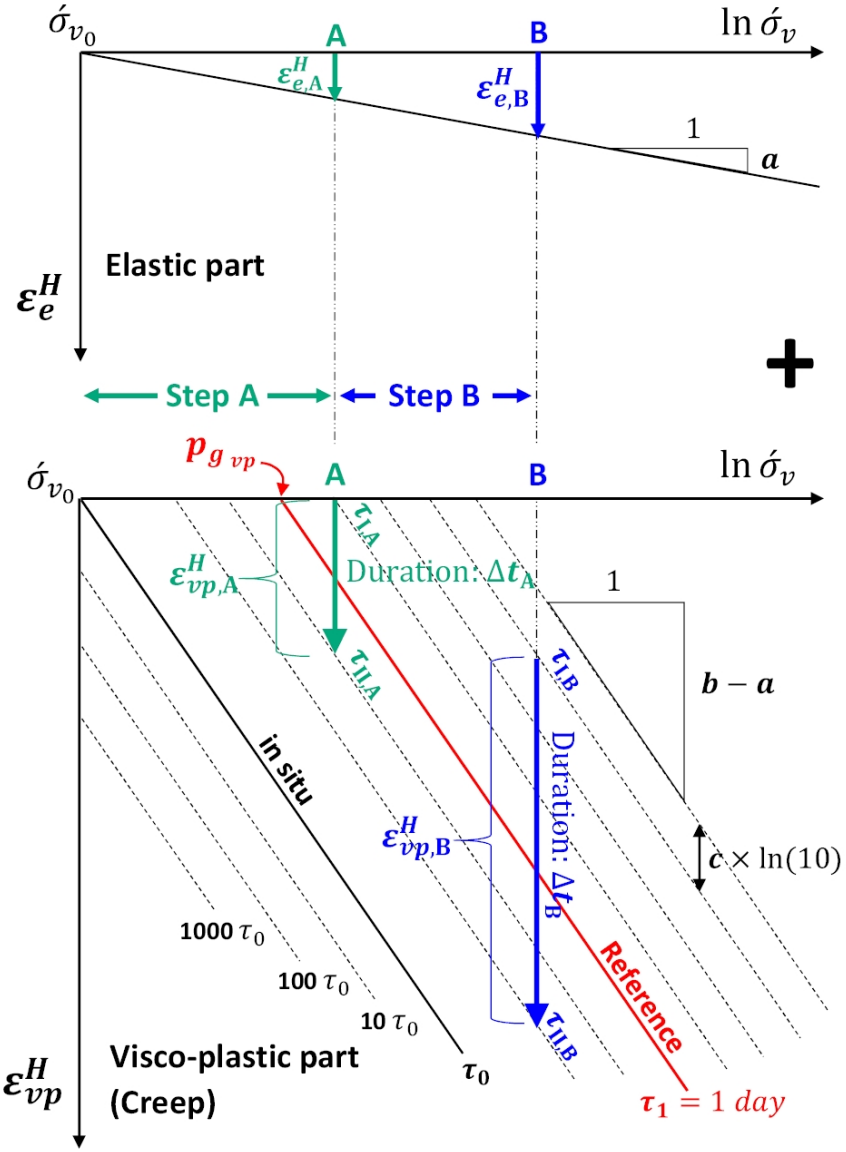

Figure 2.22. Illustration of the incremental form of the a,b,c isotache model.

As Figure 2.22 shows, the sum of the natural strains of these two steps is equal to $\varepsilon^{H}_{e,\mathrm{B}} + \varepsilon^{H}_{vp,\mathrm{A}} + \varepsilon^{H}_{vp,\mathrm{B}}$.

2.1.6.9 Determination of Parameters

Atkinson (2007) argues that "Some parameters are material parameters. They depend on the nature of the [soil] grains and are related to soil classification parameters. Other parameters are state dependent parameters; they are often related to the state by parameters which are themselves material parameters" (p. 270). According to his definition, the parameters a, b and c in the isotache model (for saturated soils) are the material parameters, since they are constant for all situations of a saturated soil, whereas $\acute{\sigma}_{v_0}$, p_g, OCR, and τ_0 are the state dependent parameters, which depend on the amount of soil compression.

"The position of the isotaches is also a material parameter. It is necessary to realize that this applies to the creep isotaches drawn with total strain" (E. J. Den Haan, personal communication, September 24, 2015).

Den Haan (1996, 2008) explains that all necessary parameters of the a,b,c isotache model can be achieved by conventional oedometer tests. He emphasises that the parameters are only reliable if the tests continue to the virginal stress range. The stress range for determining a reliable virginal value of parameter b should be chosen larger than the pre-consolidation stress at zero total strain (p_g) as much as possible. Den Haan (2008) also recommends that soft soil should "be loaded to at least 16 times the overburden stress" (p. 38). For parameter c, in addition to the latter prerequisite, a reliable value can be determined only from the large stress steps, which continue for a sufficient time in the creep phase. Den Haan and Sellmeijer (2000) also report that the c value changes a little in the virgin range of stress and it is preferred to choose an average. They explain that more straight, parallel, and equidistant isotaches can be found under higher stresses at a lower natural strain rate. According to Den Haan and Sellmeijer (2000), the reason that the isotaches at lower stresses are not straight, parallel, and equidistant is "stress reduction due to sampling" and breaking the contact of soil particles during an initial swelling before beginning the test in over-consolidated soils. This swelling produces a higher strain rate than in unchanged soil for a similar stress range. They report that this problem can also arise from sampling disturbance.

As seen in Figure 2.7, the isotaches with high natural strain rates (i.e., total natural strain isotaches) are not perfectly straight nor parallel. From the author's experience, this may be due to the time of completing the load application. This operation can be very fast for small loads, which normally consists of up to three or four separate weights, and will be slower when the amounts of weights increases and therefore the total load of a new step cannot be applied at once. This aspect is also mentioned in ASTM D2435/D2435M (2011), as follows: "Load application should be completed in a time corresponding to 0.01 times t_{100} or less. As an example, for soils where primary consolidation is completed in 3 min, the applied load should be stable in less than 2 s." However, adding loads so fast is very difficult when many weights must be applied at once. Therefore, the rate of load application cannot be kept constant during different steps and in fact, the shape of isotaches suffers

from this operational insufficiency. The same problem exists for suction-controlled oedometer tests, where the net normal stresses and suctions must be applied using manual regulators.

Procedure for determining model parameters from conventional oedometer tests on saturated soil samples:

1. Construct the isotaches on a plot of the total natural strain (ε^H) versus vertical effective stress (log scale) as shown in Figure 2.23. The unit of the natural strain rates should be chosen [1/s]. ASTM D4186 (2006) suggests calculating the rate of strain as follows:

$$\dot{\varepsilon}_n = \frac{\varepsilon_{(n+1)} - \varepsilon_{(n-1)}}{t_{(n+1)} - t_{(n-1)}} \tag{2.31}$$

where subscript (n+1) denotes the next recorded data and subscript (n–1) denotes the previously recorded data. Unlike ASTM D4186 (2006) which uses linear strain, here natural strain should be used for calculations. Before drawing the isotaches, the negative and zero values of strain rate should be removed from the data column of the spreadsheet.

2. Locate the position of 1-day reference isotache. For this aim, the natural strain rate should be formatted as 1×10^{-n}. An example is presented below to calculate the rate of natural strain for 1 day with proper format.

Assume that the c = 0.006, so

$$\tau = \frac{c}{\dot{\varepsilon}^H_{vp}} \rightarrow \dot{\varepsilon}^H_{vp} = \frac{0.006}{24 \times 60 \times 60} = 6.94 \times 10^{-8} \left(\frac{1}{s}\right)$$

$$6.94 \times 10^{-8} = 1 \times 10^{-n} \rightarrow -n = \log(6.94 \times 10^{-8}) = -7.16$$

Therefore the rate of natural strain for 1 day in the proper format will be: $\dot{\varepsilon}^H_{vp} = 1 \times 10^{-7.16}(1/s)$.

On the 1-day reference isotache, generally the primary consolidation is finished and $\dot{\varepsilon}^H_e = 0$, therefore according to $\dot{\varepsilon}^H = \dot{\varepsilon}^H_e + \dot{\varepsilon}^H_{vp}$, it can be concluded that $\dot{\varepsilon}^H = \dot{\varepsilon}^H_{vp}$.

Based on the experience of Watabe and Leroueil (2012), “the minimum strain rates obtained from laboratory tests are generally around $1 \times 10^{-9}(s^{-1})$” (p. 6).

3. Plot the 1-day reference isotache passing from the position that was found in the last step, parallel to the lowest isotache at the highest stress level. The parameter b is the slope of this line and can be calculated as:

$$b = \frac{\Delta \varepsilon^H{}_{(b)}}{\Delta \ln \sigma_{v\ (b)}} \tag{2.32}$$

4. The abscissa of the intersection of the 1-day reference isotache (slope b) with a horizontal line originating from the initial condition ($\acute{\sigma}_v = \acute{\sigma}_{v_0}$, $\varepsilon^H = 0$) represents the pre-consolidation stress at zero total strain (p_g).

5. Find the minimum slope of an uppermost isotache by visual inspection of the non-virgin part of the isotaches. The parameter "a", which is equal to this minimum slope, can be calculated as:

$$a = \frac{\Delta\varepsilon^H{}_{(a)}}{\Delta \ln \sigma_{v\ (a)}} \tag{2.33}$$

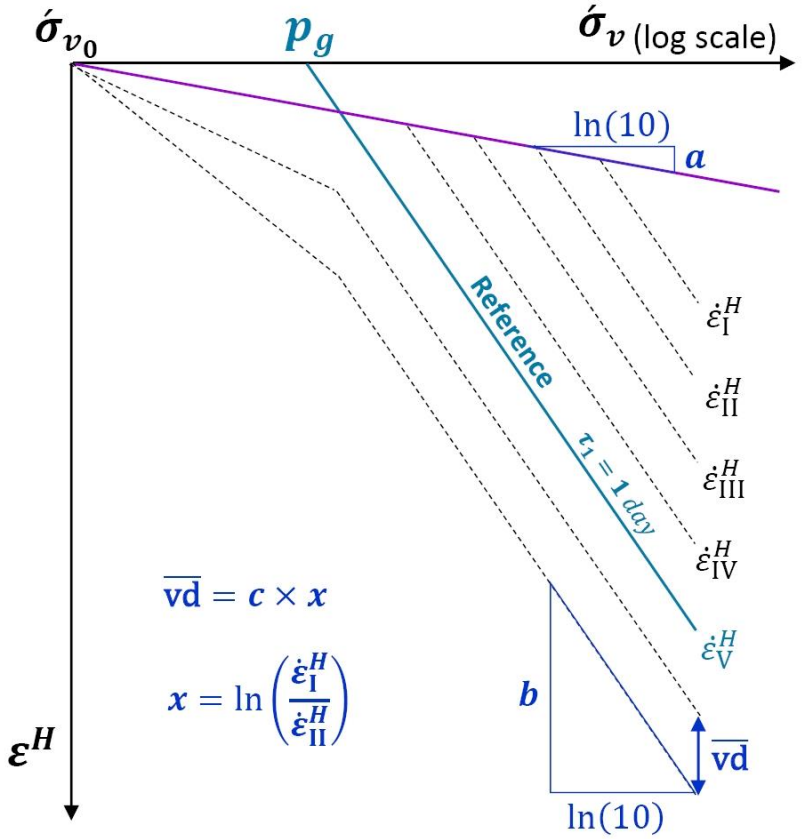

Figure 2.23. Determination of parameters (for saturated soils).

6. The parameter c can be calculated as:

$$c = \frac{\overline{\mathrm{vd}}}{x} \tag{2.34}$$

$$x = \ln\left(\frac{\dot{\varepsilon}^H_{\mathrm{I}}}{\dot{\varepsilon}^H_{\mathrm{II}}}\right) \tag{2.35}$$

Where: $\overline{vd}$ is an average of the vertical distance between the isotaches in a region where they lie more straight, parallel, and equidistant, at the highest stress level and lowest strain rate, and x is a parameter which depends on the interval of isotaches (for more information, see Figures 2.7, 2.8 and 2.9).

2.1.6.10 Values of c/b and a/b for saturated Conditions

Den Haan and Sellmeijer (2000) explain that the ratio a/b is approximately 0.1-0.2. In addition, Den Haan (1996) reports the ratio c/b in the range of 0.04-0.1. He explains that these values "agree quite well" with observed values of C_α/C_C by Mesri and Godlewski (1977) who had found a unique relationship between the secondary compression index (C_α) and the compression index (C_C).

Watabe and Leroueil (2012) report that when the rate of strain decreases, C_α/C_C may also decrease. In addition, Den Haan (1996) explains about difficulties of using the rule of C_α/C_C due to time and stress dependency of C_α and C_C. Compared to these parameters, Den Haan suggests using c and b parameters, which are "independent of stress and time" (p. 11) and are "constant in the virgin range" (p. 13). He explains that the constancy of c/b is greater than C_α/C_C.

2.1.6.11 Conclusion

As shown in this section, the a,b,c isotache model of Den Haan (1994, 1996, 2008) for saturated soils has a very consistent structure and is based on straightforward mathematical concepts. However, embankments and the foundations of most construction projects usually lie on unsaturated soil layers in which the a,b,c isotache model has not been applied prior to this research.

To study the overall volume and water volume changes of an unsaturated compacted organic soil, the a,b,c isotache model for saturated soils was adapted for unsaturated conditions in the following chapters without changing its mathematical concepts.

2.2 Literature Review on the Volume Change Behaviour of Unsaturated Soils

2.2.1 Introduction

Soils above the groundwater table are usually unsaturated. The pore-water pressures of unsaturated soils “are negative relative to atmospheric conditions” (Rahardjo & Fredlund, 1995, p. 750).

It is important to study the effects of matric suction on the characteristics of primary consolidation and secondary compression. Most research on secondary compression is related to saturated soils; only a few studies have focused on the dependency of creep on matric suction in unsaturated soils.

Jommi and Romero (2008) explain that environmental actions such as cyclic drying and wetting can create significant deformations on compacted soils. These hydraulic loads should be considered in addition to the external loads for the “analysis of the service life of earth constructions such as dams, embankments, [and] waste disposal facilities” (p. 617).

2.2.2 Compaction

Compaction is one of the most suitable methods for improving the geotechnical properties of organic soils. Compressibility and permeability of soil is reduced through compaction and the bearing capacity is increased. In civil engineering practice, dry densities of compacted soils normally compare with the results of the Proctor test on the same soil type in laboratory (ASTM D698-00a & ASTM D1557-12). It should be mentioned that during the compaction process, only amounts of voids, which are filled with air, will be decreased and the water content of soil does not change. By changing the amount of water, this process can be improved and dry density reaches its highest value with a specific moisture content. Of course, the maximum dry density achieved by compaction is a “state dependent parameter” and is related to many factors (see *Section 2.1.6.9* for the definition of state dependent parameters).

Lambe and Whitman (1969) explain that “for a given compactive effort and dry density, the soil tends to be more flocculated for compaction on the dry side as compared to compaction on the wet side” (p. 517).

Leroueil and Hight (2013) argue that two soil samples with the same dry density but on different sides of the compaction curve “have different particle arrangements and may exhibit different behaviours” (p. 43). They continue that “Experience has also shown that the air phase is continuous on the dry side of optimum whereas air is occluded on the wet side of optimum, i.e. the air is in the form of bubbles and so discontinuous” (p. 43). They report that on the dry side of optimum, the fabric is aggregated with large inter-aggregate pores, and air permeability is high, whereas on the wet side of optimum, the fabric is homogeneous with small pores, and air permeability is very low (p. 48). They also explain that “the saturated hydraulic conductivity of compacted soils is larger when the soil has been compacted on the dry side than on the wet side” (p. 50).

Fredlund, Rahardjo, and Fredlund (2012) explain that “Soils compacted above and below optimum water content conditions should be viewed as different soils” (p. 520).

Birle, Heyer, and Vogt (2008) performed an experimental study of the soil–water retention curve and the shrinkage behaviour of an unsaturated clay. In their investigations, they compacted clay samples statically and tested them by a chilled-mirror dewpoint hygrometer. Their test results show that the "soil–water retention curves in terms of gravimetric water content are independent of the initial dry density" in the investigated range but "are strongly influenced by the compaction water content at water contents above approximately 11–12.5%. In the high suction range at smaller water contents the soil–water retention curve is independent of the initial conditions." They also report that "the volumetric shrinkage strains of the compacted samples are independent of the initial dry density. . . . [but] the primary drying of the samples depends strongly on the compaction water content. . . . The rate of the volume change during the residual drying process was unaffected by the compaction water content" (p. 200).

Birle (2012) carried out experimental research to study the influence of the initial water content and dry density on the pore structure and the soil-water retention curve (SWRC) of a statically compacted clay. He reports, "The SWRC in terms of gravimetric water content is independent of the initial dry density in the high suction range (> 1500 kPa). . . . At suction pressures higher than 5.5 MPa the SWRC is even independent of the initial water content" (p. 151).

Based on oedometer test results, Honda, Iizuka, Ohno, Kawai, and Wang (2006) report that "The yield stress of saturated specimens only depends on the dry density. The dry density is affected by the water content at compaction, the compaction load, and the compaction method (e.g., static or dynamic)" (p. 844).

2.2.3 Stress State Variables and Constitutive Surfaces for Unsaturated Soils

To study the mechanical behaviour of unsaturated soils, at least two independent stress-state variables are needed. In the research area of unsaturated soils, it usually is conventional to use net normal stress ($\sigma - u_a$) and matric suction ($u_a - u_w$).

Fredlund and Rahardjo (1993) explain that the *soil structure constitutive surface* is a three-dimensional surface that relates net normal stress and matric suction to the overall volume change (Figure 2.24). With a similar definition, they explain that the *water phase constitutive surface* is a three-dimensional surface that relates net normal stress and matric suction to the water volume change of the soil sample.

Ho et al. (1992) explain that "The soil structure constitutive surface is a concave, warped surface when plotted on an arithmetic scale" (p. 195). For water phase, they report that "There is insufficient information in the literature to definitely define the form of the water phase constitutive surface" (p. 196).

Fredlund and Rahardjo (1993) point out that "an increase in matric suction causes a greater change in the volume of water in the soil than the overall volume change of the soil element." In addition, an increase in "net normal stress produces a greater change in the overall volume of the soil element than it produces for the change in water volume in the element" (p. 422).

Fredlund et al. (2012) explain that the overall volume change of an unsaturated soil sample in the one-dimensional consolidation is equal to the sum of the water volume change and the air volume change (p. 811). For one-dimensional consolidation under K_0 loading, they presented the following constitutive equations 2.36, 2.37 and 2.38, which were originally proposed by Fredlund and Morgenstern (1976),

$$\frac{dV_v}{V_0} = m_{1k}^s d(\sigma_y - u_a) + m_2^s d(u_a - u_w) \tag{2.36}$$

where

dV_v/V_0 : Overall volume change divided by the initial overall volume of the soil element

V_v : Volume of voids in the soil element

V_0 : Initial overall volume of the soil element

m_{1k}^s : Coefficient of overall volume change with respect to a change in net normal stress for K_0 loading

m_2^s : Coefficient of overall volume change with respect to a change in matric suction during K_0 loading

$d(\sigma_y - u_a)$: Change in net normal stress

$d(u_a - u_w)$: Change in matric suction

$$\frac{dV_w}{V_0} = m_{1k}^w d(\sigma_y - u_a) + m_2^w d(u_a - u_w) \tag{2.37}$$

where

dV_w/V_0 : Water volume change divided by the initial overall volume of the soil element

V_w : Volume of water in the soil element

m_{1k}^w : Coefficient of water volume change with respect to a change in net normal stress for K_0 loading

m_2^w : Coefficient of water volume change with respect to a change in matric suction during K_0 loading

Fredlund et al. (2012) explain that “The air phase constitutive relation is equal to the difference between the soil structure and the water phase constitutive equations. The air phase constitutive equation can also be expressed in a general form as a function of the stress state variables” (p. 811) as follows:

$$\frac{dV_a}{V_0} = m_{1k}^a d(\sigma_y - u_a) + m_2^a d(u_a - u_w) \tag{2.38}$$

where

dV_a/V_0 : Air volume change divided by the initial overall volume of the soil element

V_a : Volume of air in the soil element

m_{1k}^a : Coefficient of air volume change with respect to a change in net normal stress

m_2^a : Coefficient of air volume change with respect to a change in matric suction

Fredlund et al. (2012) assumed the soil solids to be incompressible and they presented the continuity requirement as following equations (pp. 811 & 796):

$$m_{1k}^s = m_{1k}^w + m_{1k}^a \tag{2.39}$$

$$m_2^s = m_2^w + m_2^a \tag{2.40}$$

$$\frac{dV_v}{V_0} = \frac{dV_w}{V_0} + \frac{dV_a}{V_0} \tag{2.41}$$

Based on the above relationships, if two constitutive equations for the volume changes are given, a third can also be calculated. Therefore, at least two constitutive equations are required to describe the volume change behaviour of unsaturated soils.

Based on an experimental study on a silty sand under K_0 loading conditions, Rahardjo and Fredlund (1995) explain that "The pore-water pressure dissipation during the consolidation test [i.e., increasing the total stress] was found to be faster than the pore-water pressure decrease during the increasing matric suction test". They also observed that "The water volume changes during the consolidation test were considerably smaller than the water volume changes during the increasing matric suction tests for the same increment of pressure change" (p. 749).

Curve 1 in Figure 2.24 schematically shows the results of a conventional oedometer test on a saturated soil sample. This curve can be simulated by using the classical a,b,c isotache model which was introduced in literature review of the a,b,c isotache model for saturated soils. Curves 2 and 3 schematically present the results of suction-controlled oedometer tests on an unsaturated soil sample for two conditions: at a constant net normal stress (Curve 2), and at a constant matric suction (Curve 3). Simulations of Curves 2 and 3 will be thoroughly explained in *Chapter 5* by using the adapted a,b,c isotache model.

Fredlund et al. (2012) explain that "The total stress increments are equal for isotropic loading in three directions (i.e., $d\sigma_x = d\sigma_y = d\sigma_z = d\sigma_3$). No shear stresses are developed in the soil mass under isotropic loading conditions" (p. 675). "Under isotropic loading conditions, the state variables are (i) net mean stress [which sometimes called mean net stress] $p = (\sigma_1+\sigma_2+\sigma_3)/3 - u_a$, (ii) soil suction $u_a - u_w$, and (iii) mean effective stress $p* = (\sigma_1+\sigma_2+\sigma_3)/3 - u_w$" (p. 694). They also explain that "A total stress increment of $d\sigma_y$ is applied in the vertical direction for K_0 loading, while the soil is not permitted to deform laterally (i.e., $d\varepsilon_x = d\varepsilon_z = 0$). The K_0 loading condition occurs during one-dimensional compression where deformation is only allowed in the vertical direction (i.e., $d\varepsilon_y$)" (p. 678).

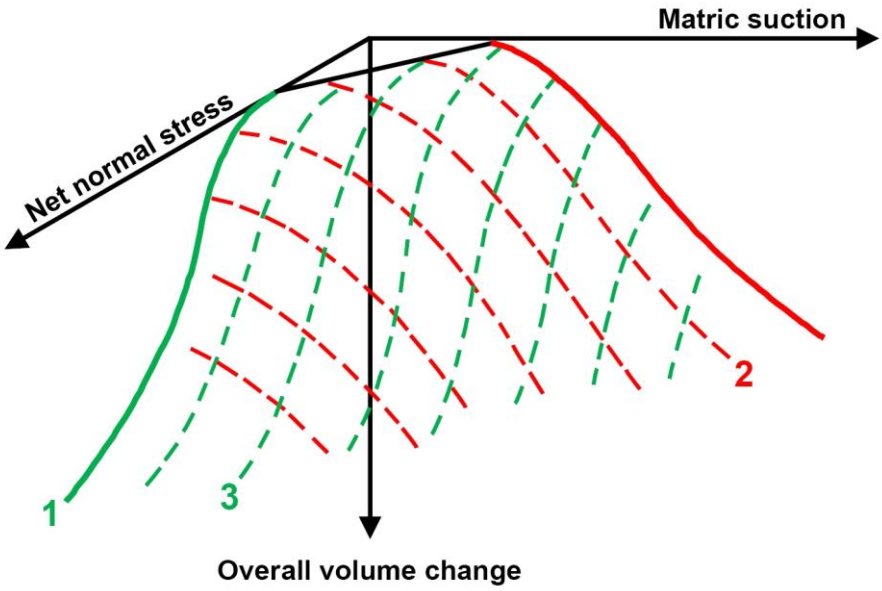

Figure 2.24. Three-dimensional constitutive surfaces of overall volume change with emphasis on three conditions. Adapted and redrawn from Fredlund & Rahardjo, 1993, p. 374, fig. 13.1.

2.2.4 An Introduction to Some Aspects of the Barcelona Basic Model

Alonso, Gens, and Josa (1990) at the Technical University of Catalunya proposed the Barcelona Basic Model (BBM), which is an elastic plastic strain hardening model that extends the modified Cam Clay model by adding the effect of suction. Although this model is not used in the current study, a summarised description is presented here because a majority of researchers have explained their model parameters based on the BBM. Figure 2.25 which is adapted and redrawn from Alonso, Pinyol, and Puzrin (2010) illustrates some aspects of this model. The BBM, which is based on the critical state theory, could be used in partially saturated soils with "moderate to low plasticity, such as sandy clays, clayey sands and silts, and granular soils" (Alonso, Gens, & Josa, 1990, p. 428).

The BBM has two yield surfaces for isotropic stress conditions, which are called loading-collapse (LC) and suction-increase (SI). As shown in Figure 2.25c, the loading collapse (i.e., LC or yield curve) can be determined by connecting all yield points on a suction versus net mean stress plot. At a constant suction, on a plot of specific volume ($v = 1 + e$) versus natural logarithm of net mean stress (ln p), $\lambda(s)$ and κ are two stiffness parameters for changes in net mean stress of the virgin and the elastic states of soil respectively, as shown in Figure 2.25b. In this model, $\lambda(s)$ decreases with increasing suction, whereas κ remains constant (i.e., κ is independent of suction). Furthermore, the pre-consolidation (i.e., yield) stress increases with increasing suction (Figure 2.25b).

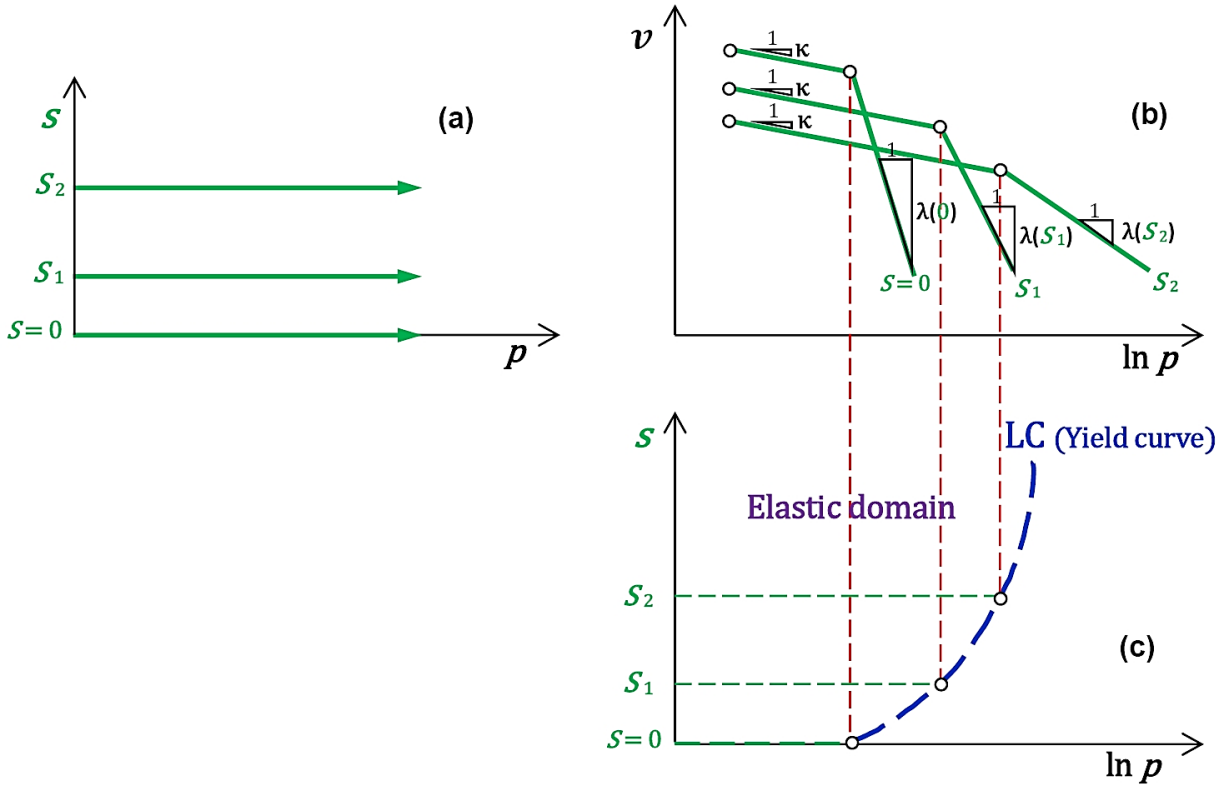

Figure 2.25. Some aspects of the Barcelona Basic Model: (a) Stress paths for isotropic loading at constant suctions; (b) compression curves; (c) yielding points and LC yield envelope. Adapted and redrawn from Alonso, Pinyol, & Puzrin, 2010, p. 98, fig. 3.14.

Yield due to increasing suction is an important aspect in the theory of unsaturated soils. Alonso et al. (1990) defined the yield suction (s_0) as the "maximum past suction ever experienced by the soil and bounds the transition from the elastic state to the virgin range when suction is increased" (p. 411). This is similar to the definition of the pre-consolidation stress in saturated soils. Figure 2.26 presents their definition, which parameter v on the vertical axis denotes specific volume and parameter s on the horizontal axis is matric suction.

Rahardjo and Fredlund (1996) explain that "Significant water volume changes occur when a soil is subjected to a matric suction value greater than the maximum past matric suction that the soil has ever experienced (e.g., increasing matric suction test)" (p. 353).

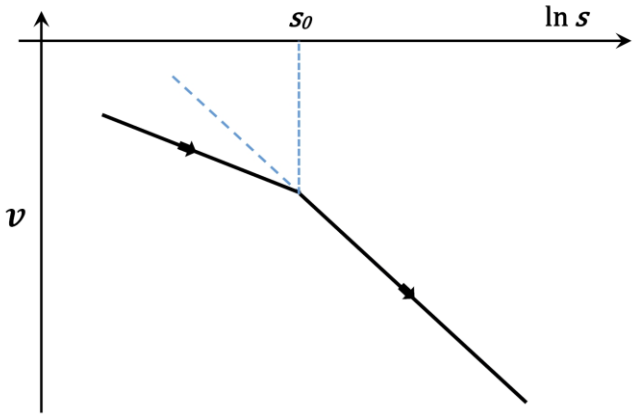

Figure 2.26. Definition of the yield suction (s_0) in the Barcelona Basic Model. Adapted and redrawn from Alonso, Gens, & Josa, 1990, p. 411, fig. 5.

2.2.5 The Effects of Suction on the Volume Change Behaviour

Qin, Ye, Chen, Chen, and Cui (2015) observed that in a highly compacted bentonite, the rate of strain "has less influence on the plastic compression index" and they concluded that "the 'isotache' concept can be used into the unsaturated soil" (p. 88). They report that the "virgin compression index" of a highly compacted bentonite decreases with increasing suction whereas yield stress increases with increasing suction. In addition, they found that the yield stress (at a constant suction) increases with increasing strain rate.

Based on a series of suction-controlled high-pressure oedometer tests on an unsaturated GMZ01 bentonite, Ye et al. (2014) defined an "incremental compression index" $C_c^* = \Delta e/\Delta \log \sigma_v$ where Δe is the change in void ratio for only one stress increment of $\Delta\sigma_v$. This was due to difficulty of finding a constant compression index. They emphasise that the incremental compression index (C_c^*) is not equal to the compression index (C_C), which generally can be obtained from the virgin compression curve (p. 107). They found that the value of the both incremental compression index (C_c^*) and the secondary compression index (C_α) depends on the applied vertical stress and total suction. According to their observations, the slopes of e versus log time curves decrease as time increases, which demonstrates "that C_α of GMZ01 bentonite samples is time-dependent" and is not unique (p. 106). They report that C_c^* and C_α "follow similar relationships with vertical stress and [total] suction" (p. 109). In other words, both of these parameters increase as the vertical stress increases and both decrease as total suction increases. They also point out that "the concept of constant ratio C_α/C_C [(Mesri & Godlewski, 1977)] can also be applied to unsaturated GMZ01 bentonite" (p. 109). In addition, they report "that the value of C_α/C_c^* of GMZ01 bentonite depends on the degree of saturation" (p. 108), and C_α/C_c^* decreases with increasing [total] suction. They suggest the following equation as a "viscoplastic suction dependent constitutive model" for GMZ01 bentonite (p.109):

$$C_\alpha/C_c^* = 0.0435 - 0.0051 \times \ln s \qquad R^2 = 0.935 \qquad (2.42)$$

where s is the value of [total] suction in [MPa].

Although total suction is denoted by s in this equation, it is conventionally denoted by ψ in the literature of unsaturated soil mechanics (Fredlund & Rahardjo, 1993; Murray & Sivakumar, 2010) and is defined as the sum of the matric suction and the osmotic suction (Total suction = Matric suction + Osmotic suction). The matric suction, which is often called s, is equal to the difference between the pore air pressure and pore water pressure (u_a-u_w), whereas the osmotic suction is "the result of chemical imbalance between the pore water in the soil volume under consideration and an external source of water" (Murray and Sivakumar, 2010, p. 10).

Fredlund and Rahardjo (1993) argue that "osmotic suction is related to the salt content in the pore-water which is present in both saturated and unsaturated soils." They continue that "For most geotechnical problems involving unsaturated soils, matric suction changes can be substituted for total suction changes, and vice versa". They explain that in geotechnical practice "Osmotic suction changes are generally less significant" and is "not necessary to take . . . [it] into account" (p. 63).

Based on a series of matric suction controlled tests on a loamy soil and a sandy clay which were compacted at different bulk densities and water contents, Cui, Défossez, Cui, and Richard (2010) reported that the slope of the unloading phase (C_S) is almost independent of matric suction, whereas the pre-consolidation stress increases with increasing matric suction. This agrees with most of the available test results in the literature (e.g., Alonso et al., 1990). Their test results also show that "the compression index (C_C) was constant or changed little with matric suctions for the two soils at different initial densities" (p. 337). Regarding the variation of C_C with the water content of the soil, they explain that "The data in the literature are contradictory" (p. 344). Based on their literature reviews, they distinguished two features: "one group of soils exhibiting compression indexes that decrease with matric suction. This feature has been reported for all soil textures" (clays soils, loess soils, and sandy soils as cited in Cui et al., 2010). "The compression index of a second group of soils increased with matric suction" which has been reported for loess soil and for sandy soils (as cited in Cui et al., 2010). They concluded that their "results tend to agree with the second group" (p. 344).

Based on a series of suction control triaxial creep tests on a clay soil, Lai, Wang, Ye, and Cui (2014) reported that both the strain and strain rate depend on stress and suction. They observed that the axial strain rate decreased with increasing matric suction.

Nowamooz, Mrad, Abdallah, and Masrouri (2009) performed some oedometer tests on a natural swelling soil by applying different suctions using the osmotic technique. They observed that due to increasing suction, pre-consolidation stress increases while the virgin compression index ($\lambda(s)$) decreases (see Figure 2.25b for the definition of $\lambda(s)$).

The results of experimental research by Rampino, Mancuso, and Vinale (2000) on a silty sand under unsaturated conditions are shown in Table 2.1. This table presents the average values of the soil parameters for the isotropic stress state condition. Figures 2.27 and 2.28 also illustrate the data from Table 2.1. The definition of BBM parameters (λ and κ) can be found in Figure 2.25b. Rampino et al. (2000) reported that "The influence of suction on all the soil parameters is always fitted using an exponential law" (p. 762). They found that due to increasing matric suction, the yield stress increases (Figure 2.28). The parameter κ exhibits a smaller decrease compared to λ, given an equal increase

in suction (see Table 2.1 & Figure 2.27). They concluded that “In the investigated suction range, compressibility decreases and the over-consolidation pressure increases, with the largest amount of change concentrated in the 0–100 kPa suction range” (p. 761). In other words, the greatest change in the parameters occurred when suction increases from 0 to 100 kPa. Figure 2.27 indicates that parameters λ and κ decrease with a higher gradient up to the suction of 100 kPa, and then continue to decrease with a lower gradient. A very interesting aspect of Figure 2.27b is that the value of κ again increases beyond a suction value of 200 kPa.

Table 2.1

Average Parameters of a Silty Sand for the Isotropic Stress State Condition

Suction, s [kPa]	Yield stress, $(p - u_a)_0$ [kPa]	λ	κ
0	35	0.022	0.0056
100	136	0.016	0.00517
200	159	0.015	0.00507
300	162	0.0148	0.00511

Note. Adapted from Rampino, Mancuso, & Vinale, 2000, p. 758, table 5.

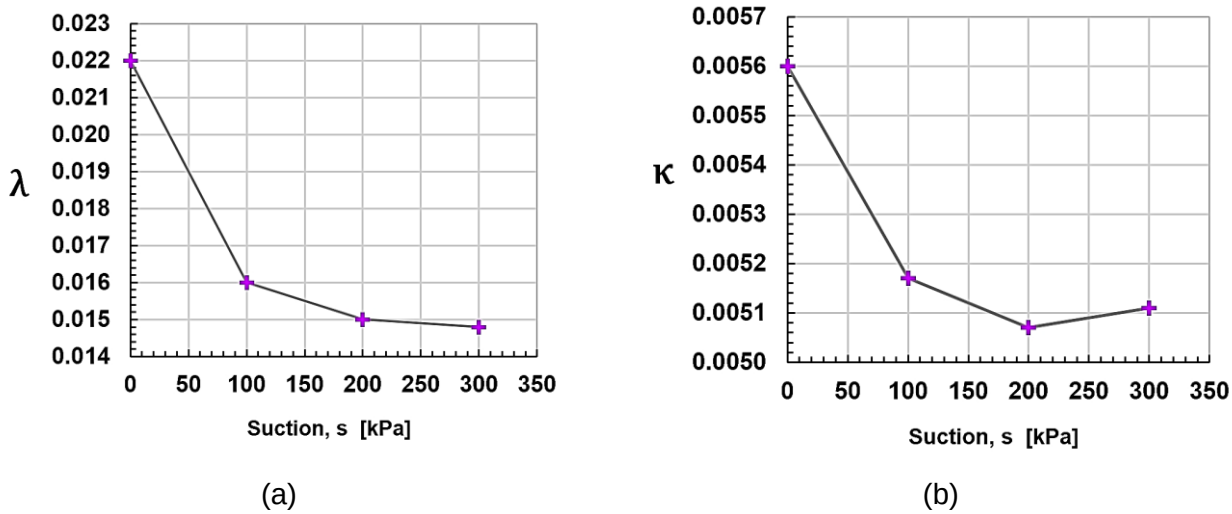

(a) (b)

Figure 2.27. Influence of suction on the model parameters λ and κ according to the data in Table 2.1. Adapted and redrawn from Rampino, Mancuso, & Vinale, 2000, p. 758, fig. 15.

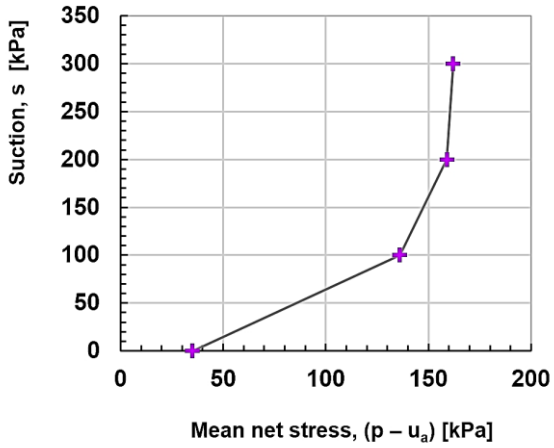

Figure 2.28. The loading-collapse yield curve on a plot of suction versus ($p - u_a$), according to the data in Table 2.1. Adapted and redrawn from Rampino, Mancuso, & Vinale, 2000, p. 758, fig. 16.

Koliji (2008) performed some conventional and suction-controlled oedometer tests on reconstituted (i.e., remoulded) samples of a clay with low plasticity (CL). Figure 2.29 shows the results of his oedometer tests on the saturated and unsaturated specimens. As seen in this figure, the tangential compressibility index (i.e., the slope of the normal consolidation part of the oedometer curve) increases significantly when the condition of soil samples changes from saturated to unsaturated. This behaviour contrasts with the results from other studies, which show the slope of virgin compression curve decreasing with increasing matric suction. On the other hand, Koliji (2008) observed the increase of pre-consolidation stress with increasing suction, which agrees with most experimental results available in the literature.

Chen, Fredlund, and Gan (1999) performed eight triaxial tests consisting of one saturated and seven unsaturated specimens of a (remoulded) compacted, low-plasticity loess. They observed that for the isotropic compression tests, the slope of volumetric strain versus net mean stress (log scale) for the saturated specimen is 1.66 times larger than for the unsaturated soil specimen with a soil suction of 50 kPa. They also found that increasing the suction beyond 50 kPa has no significant effect on the compressibility of unsaturated specimens. Based on their test results for the water phase in the isotropic compression tests, when suction increases from 0 to 50 kPa, the slope of water volume change versus net mean stress decreases significantly.

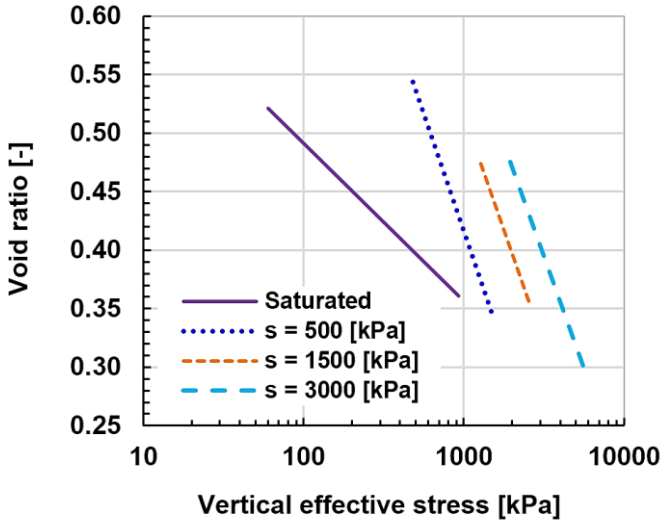

Figure 2.29. Comparison of the tangential compressibility index of a reconstituted clay with low plasticity (CL) at different suction levels of the oedometer tests. Adapted and redrawn from Koliji, 2008, p. 134, fig. 4.43(b).

Kayadelen (2008) conducted six unsaturated consolidation tests on a low plasticity clay (CL) which were statically compacted under optimum conditions. They observed that all the compressive indexes decrease nonlinearly with increasing matric suction, whereas the yield stress increases nonlinearly with increasing matric suction. These findings agree with most of the available test results in the literature. Kayadelen (2008) proposed the following exponential relationships as a function of the matric suction:

$$C_t = 0.1182e^{-0.0033s} \qquad R^2 = 0.98 \qquad (2.43)$$

$$D_t = 0.0227e^{-0.0016s} \qquad R^2 = 0.95 \qquad (2.44)$$

$$Yield\ stress = -0.0016s^2 + 1.5667s + 76.432 \qquad R^2 = 0.97 \qquad (2.45)$$

where

C_t : Slope of void ratio (e [-]) versus logarithmic scale of net vertical stress ($(\sigma_v - u_a)$ [kPa])

D_t : Slope of water content (w [-]) versus logarithmic scale of net vertical stress ($(\sigma_v - u_a)$ [kPa])

s : Matric suction [kPa]

Lloret and Alonso (1980) argue that “Deformation behaviour of unsaturated soil under field conditions depends mainly on existing (initial) conditions and the wetting and loading history of the soil. Suction increase (drying) or decrease (wetting) does not lead necessarily to shrinkage and swelling behaviour of the soil; the soil can experience a complex volume change reaction depending on the intensity of the applied external load” (p. 449).

Based on oedometer test results, Honda et al. (2006) report that “When the degree of saturation of a specimen is high, an increase in the suction leads to the compression of the structure of the soil skeleton, because the action of suction is similar to that of effective stress for saturated soil.” They continue that “When the degree of saturation of a specimen is low, however, an increase in suction leads to an increase in the stiffness of the soil skeleton without compression, while a decrease in suction leads to the compression of the structure of the soil skeleton due to a decrease in stiffness.” They also report that “Although the amount of suction applied to the specimens is 100 to 150 kPa . . ., the yield stress is higher (200 to 500 kPa) than that in the saturated state. It is interesting to note that the increments in yield stress are larger than the suction applied to the specimens” (p. 845).

Chapter 3: Laboratory Tests and Results

3.1 Introduction

This chapter describes the material properties, experimental program, test apparatus and methods for saturated and unsaturated conditions. In addition, the parameters used to study the volume change behaviour are introduced. The experimental results are presented and then the volume change behaviour of the soil structure (i.e., the overall volume) and the water phase are thoroughly analysed. At the end of this chapter, the dependency of volume change behaviour on time, stress and matric suction is discussed.

3.2 Soil Properties

The soil tested in this research is taken from approximately 35 km northeast of Munich, Germany. Table 3.1 summarises the properties of the organic soil used in all laboratory tests in this research. The water content of soil in its natural condition was about 87.6% (Birle, 2011). To determine the percentage of organic matter in each particle size, in addition to the routine sieve and hydrometer analysis of the natural soil, another analysis was performed on the soil that was left over after high-temperature heating. The grain size of organic particles can be better distinguished by comparing the percentage of grain size in the natural condition (consists of the organic and mineral particles) with the percentage of the remaining soil after high-temperature heating (i.e., ash which consists of only the mineral particles). According to the grain size distribution of the ash (Figure 3.1), the percentage of gravel (greater than 4.75 mm) is 1.5%, sand (greater than 0.075 mm and smaller than 4.75 mm) is 17.0%, silt (greater than 0.002 mm and smaller than 0.075 mm) is 80.5%, and the percentage of clay (smaller than 0.002 mm) is 1.0%.

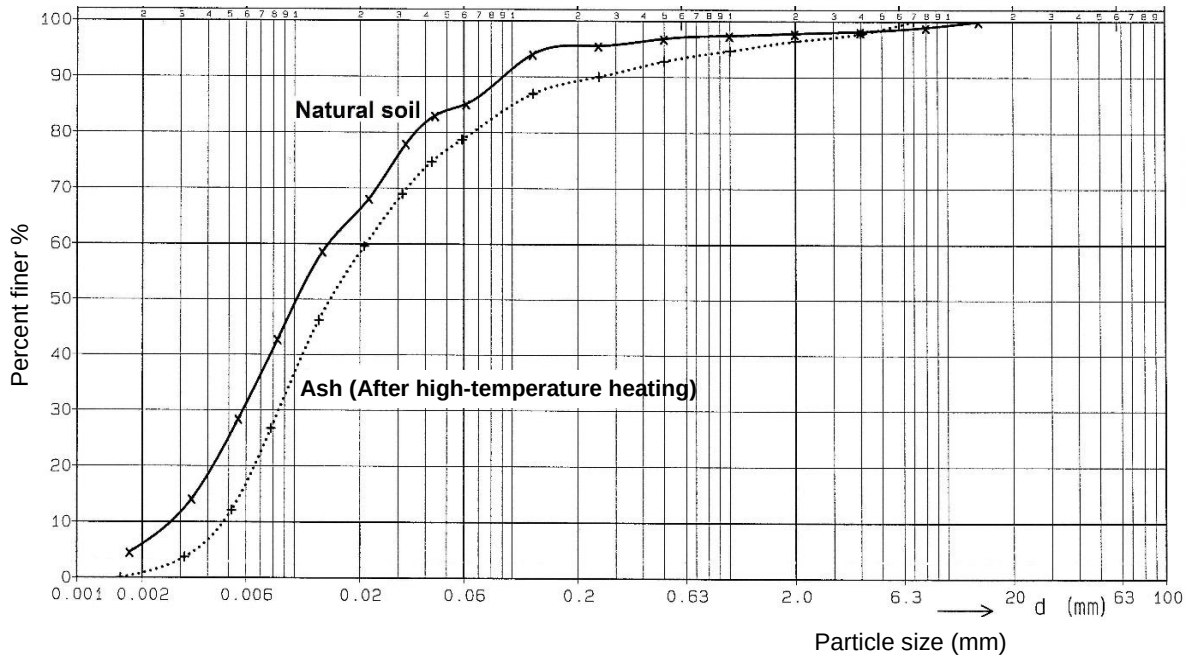

Figure 3.1. Comparison between the particle-size distribution of the natural soil and the soil remaining after high-temperature heating (i.e., ash).

According to ASTM D 2974 (2000), “The substance remaining after ignition is the ash. The ash content is expressed as a percentage of the mass of the oven-dried sample. . . . Organic matter is determined by subtracting percent ash content from one hundred.” This can be expressed as follows:

Ash content % = (Mass of ash × 100) / (Oven dried test sample at 105 °C)

Organic matter % = 100 – (Ash content %)

For determination of organic content, according to ASTM D 2974 (2000), several samples are dried (at least 16 hours in a conventional oven at 105 °C), then weighed, and heated at a high temperature oven. The temperature of the high temperature oven should be gradually increased up to 440 °C. Heating should be continued until the soil sample is completely transformed to ash and no further decrease in mass is observed (for more information, see Figure A.4, *Appendix A*). For the soil which was sieved finer than 4 mm, the amount of organic matter is 27%.

Landva and La Rochelle (1983) report that increasing organic content increases soil porosity. In addition, they point out that “the permeability of peat decreases very considerably with decreasing void ratio” (p. 159).

Table 3.1

Properties of the Organic Soil Used in All Laboratory Tests in This Research

Property	Value
Group symbol[1]	OH
Group name[1] Sandy Organic Silt	
Particle-size distribution[1] of the ash	
Gravel (> 4.75 mm)	1.5%
Sand (4.75 mm - 0.075 mm)	17.0%
Silt (0.075 mm - 0.002 mm)	80.5%
Clay (< 0.002 mm)	1%
Organic matter[2]	27%
Density of soil solids (ρ_s)[2]	2.214 g/cm^3
Liquid limit (LL)	116%
Plastic limit (PL)	72%
Natural water content	87.6%

Note. [1] According to the Unified Soil Classification System,

[2] For the soil finer than 4 mm.

Density of soil solids (ρ_s) finer than 4 mm is 2.214 g/cm^3. The following equation, which is proposed by Savidis et al. (2008) for organic silt/clay indicates the value of solid density (ρ_s) is in good agreement with the value of organic matter,

$$y = 2.75e^{-0.009x} \quad \text{Savidis et al. (2008)} \quad (3.1)$$

where y is solid density (g/cm^3) and x is organic content (%).

The liquid and plastic limits of the original specimen without oven drying are LL = 116% and PL = 72%, respectively (for more information, see Figure A.5, *Appendix A*). Based on ASTM D 2487 (2006), the soil is classified via Unified Soil Classification System as Sandy Organic Silt (OH).

Organic soils are very sensitive to drying. Decreasing the water content should only be performed via air-drying, and not by oven drying, to reach required water content. Based on the author's experience, completely air-drying and then adding the desired water content is not acceptable, since this process changes the properties of the organic soil significantly. To determine the water content, a maximum temperature of 60 ^{o}C was used in order to "reduce decomposition" in organic soils (ASTM D2216, 2010).

3.3 Sample Preparation

To prepare the soil samples, the soil was sieved finer than 4 mm at a 73.3% water content. It is not possible to pass this kind of soil through a finer mesh size due to high adhesion at this water content.

Only distilled water was used for sample preparation as well as the saturation of the soil samples. In addition, for suction-controlled oedometer tests, the distilled water was deaerated using a vacuum pump prior to the tests.

The process of sample preparation for organic soils is time consuming. This is due to the high expansion amount of the specimen after releasing the static load. To overcome this expansion, many trial and error steps are required to reach the target thickness of the soil sample. In this method, the soil sample is compressed a little bit more than the target value and then is released. This procedure finishes with the thickness of the soil sample matching the desired value.

Figure A.6 in *Appendix A* shows the mould used for static compaction of the soil samples. It consists of a cylinder with a 7 cm internal diameter and a piston, which is inserted into the cylinder. After putting soil into this cylinder, the piston is pressed until a desired thickness for the soil sample is achieved. All samples were prepared at a thickness of 2 cm and a diameter of 7 cm. In all the conventional oedometer tests and suction-controlled oedometer tests, silicone grease was used to reduce the friction effects between the soil sample and the inner part of the ring.

All six samples in this research were precisely prepared from the same soil type by using static compaction at the wet side of the Proctor optimum. Figure 3.2 shows the Proctor curve of the soil (by the method of decreasing water content) as well as the initial condition of the oedometer samples

(for more information, see Birle, 2011). At the beginning of each test, the water content and dry density of all samples were very similar to the following values:

$w_{\ initial} = 73.3\%$

$\rho_{d\ initial} = 0.774\ \left[\frac{g}{cm^3}\right]$

→ $S_{r\ initial} = 87.4\%$

Initial dry density of the soil samples was calculated with the initial thickness of the soil samples (before starting the tests) and the mass of the dried soil samples (after finishing the tests).

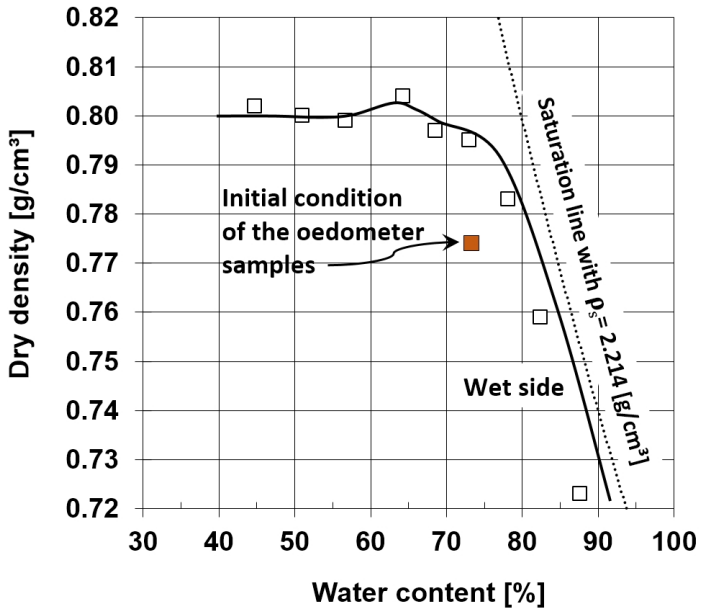

Figure 3.2. Proctor curve of the soil. Adapted and redrawn from Birle, 2011, p. 46, fig. 6.4.

An average saturated permeability value for the soil samples, which were prepared by static compaction at similar water contents and dry densities, is about 5×10^{-9} m/s (Birle, 2011, p. 174, Table 8.1).

When performing both conventional oedometer and suction-controlled oedometer tests, deformation of the soil samples was measured using digital gauges with 0.001 mm accuracy. Deformations were recorded every second at the beginning of each step of the tests. Therefore, the curves can be plotted with higher accuracy when the strain rate is maximum. Before and after the tests, the thickness of samples was precisely measured by considering the average of at least four different points, using a digital Vernier calliper (with a 0.001 mm accuracy). All tests were performed in a room with a central air conditioning system, at a constant temperature of 20.5 $\pm$ 1 °C.

3.4 Conventional Oedometer Tests on Saturated Soil Samples

Three conventional oedometer tests S1, S2 and S3 (see Figures A.7 & A.8, *Appendix A*) were carried out on saturated soil samples according to ASTM D2435/D2435M (2011). This standard has many overlaps with the DIN 18135:2012-04 (2012). Prior to tests, porous discs were saturated using a vacuum desiccator, which was partially filled with distilled water.

The first aim of performing these tests was to compare the soil behaviour in saturated (matric suction = 0) and unsaturated conditions when the matric suction was kept constant and the net normal stress was increased. The second reason was to study the dependency of volume change behaviour on time and stress in the compacted organic soils, and the third purpose was to examine the sensitivity of isotache pattern to the Load Increment Ratio (LIR).

ASTM 2435/D2435M (2011) defined the *Load Increment Ratio* (LIR) as:

$$\text{LIR} = \frac{\text{Change in total axial stress}}{\text{Current total axial stress}} \tag{3.2}$$

For example, if the total axial stress on the soil sample in the current step is 50 kN/m² and the following step is 100 kN/m², the calculated LIR is 1.

Three oedometer tests were conducted in a manner that each test had a constant LIR for almost all loading steps. For this aim, LIR for Tests S1, S2 and S3 was chosen 1.0, 0.65, and 0.3, respectively. Figures 3.3, 3.4 and 3.5 present the continuous settlement from the oedometer tests on saturated soil samples.

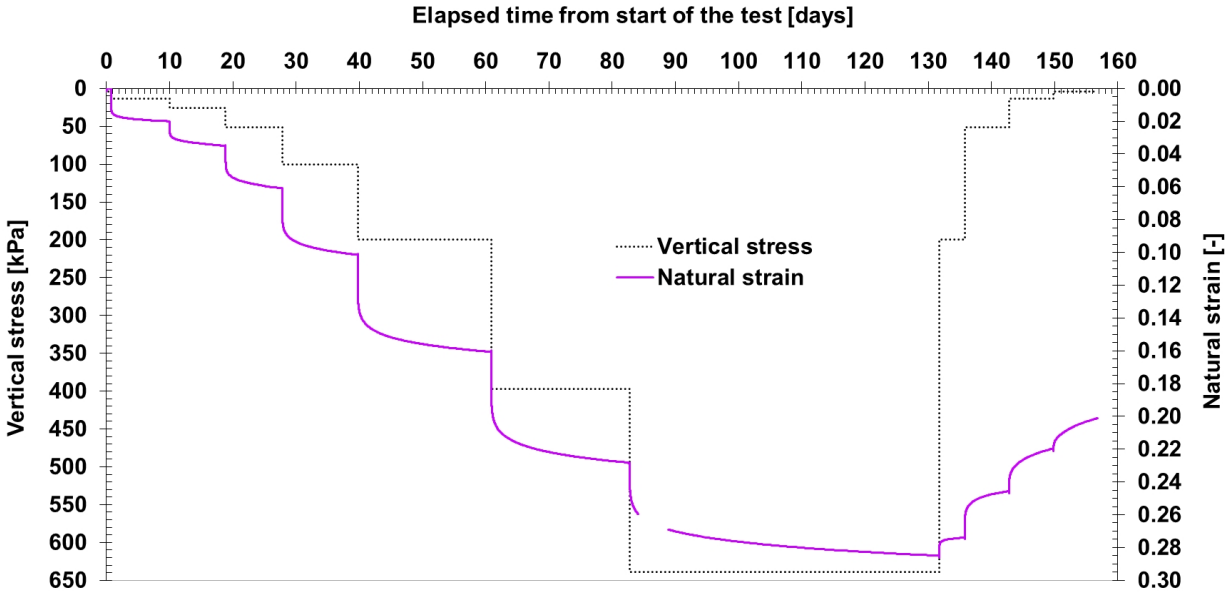

Figure 3.3. The natural strains and the vertical stresses during the oedometer test S1 (LIR = 1.0) on the saturated soil sample.

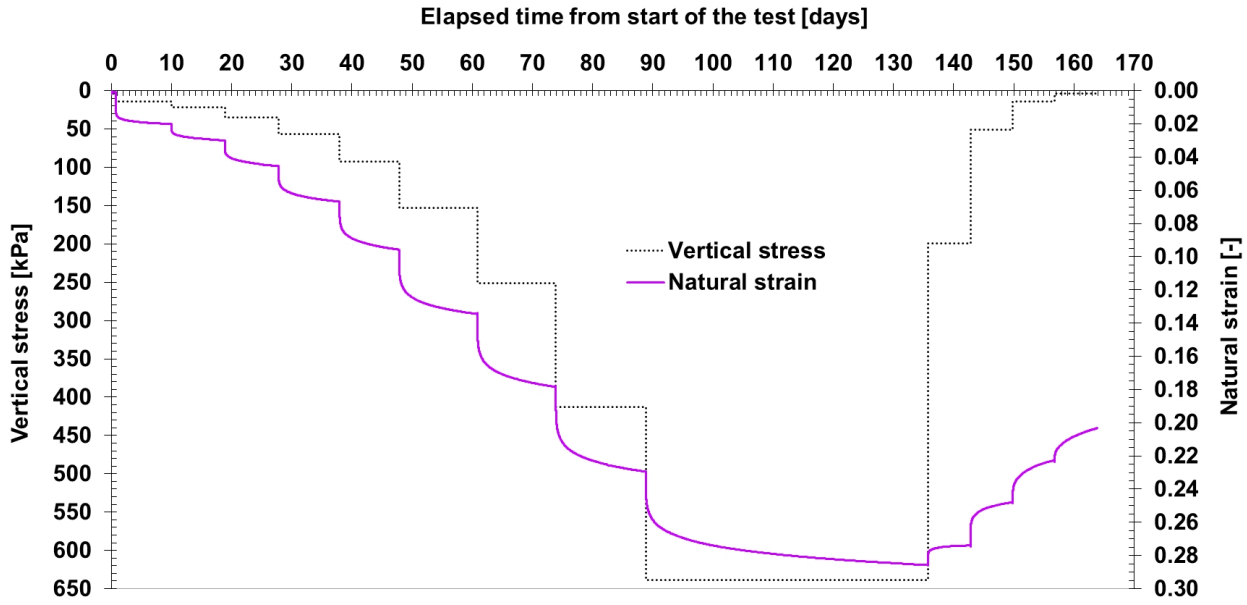

Figure 3.4. The natural strains and the vertical stresses during the oedometer test S2 (LIR = 0.65) on the saturated soil sample.

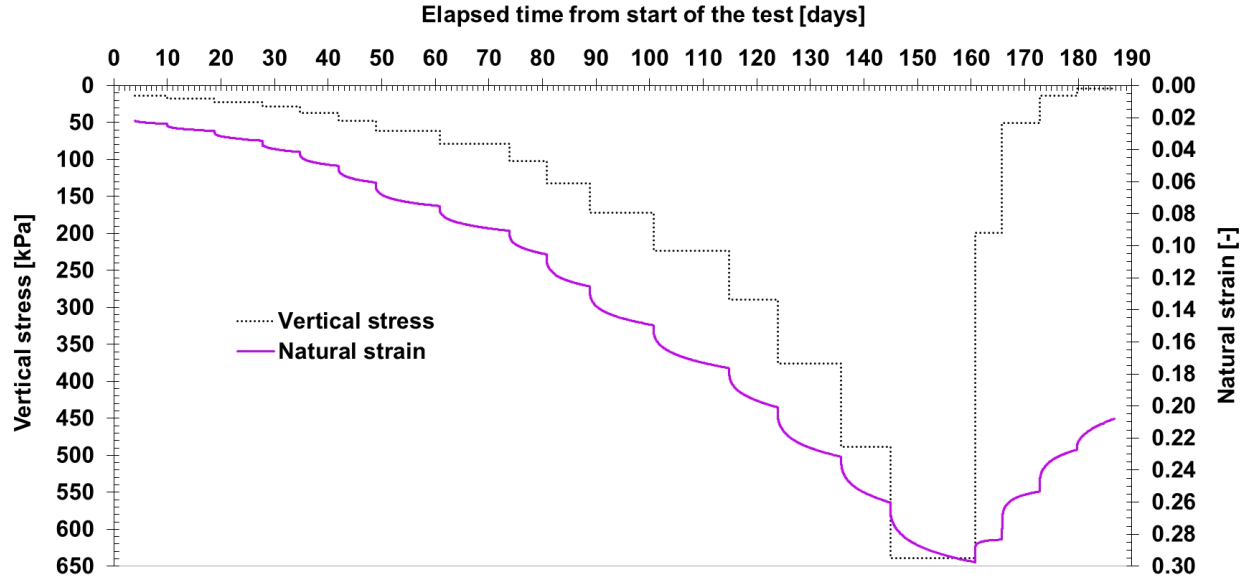

Figure 3.5. The natural strains and the vertical stresses during the oedometer test S3 (LIR = 0.3) on the saturated soil sample.

Colleselli, Cortellazzo, and Cola (2000) after applying different LIRs (i.e., LIR = 1, 3 & 19) in some special oedometer tests on peaty soils, reported that "The secondary coefficient [C_α] is quite similar for all the tests, so it is probably independent of the LIR imposed" (p.230). On the other hand, Hobbs (1986) argues that "The magnitude of the load increment ratio, $\Delta p/p$, has a profound effect on the shape of the consolidation curve, on the slope of the secondary tail immediately following the end of the primary stage and on the pore water pressure (Barden 1969; Berry & Vickers 1975). As a general

rule load increment ratios exceeding unity tend to produce . . . [S-shape curves]. These are known as Terzaghi curves." Hobbs (1986) explains that "with low values of the load increment ratio . . . there is no reversal of slope at or near the end of the primary stage" (pp. 47-48).

Based on creep oedometer tests performed on clays, Kim and Leroueil (2001) concluded that "Secondary consolidation dominates the general behaviour for small stress increments, with strain – log t curves showing no inflection point. For larger stresses, however, primary consolidation dominates and the curves show the classical 'S' shape, still with a large viscous component" (p. 492).

Den Haan and Edil (1994) demonstrated that the classical S-shape of isobars occurs for the high LIR steps only when the OCR is low (p. 58).

However, as seen in Figures 3.6, 3.7 and 3.8, the isobars in the current study are not S-shaped; the secondary compression index (C_α) continues to increase for the long duration of the test, even in low OCRs. As shown in Figure 3.6, even the isobars of Test S1 (LIR = 1) do not represent a classical S-shape in the low OCR steps. A maximum LIR value of 1 was chosen in this research, but the S-shape isobars might be observed with higher values of LIR.

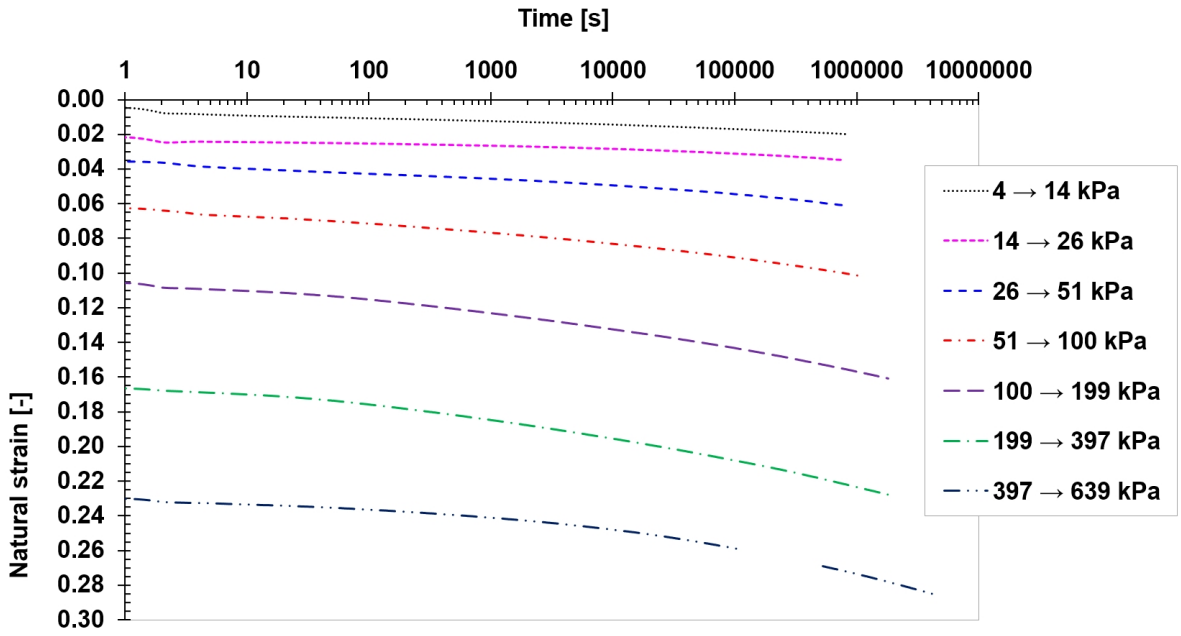

Figure 3.6. Loading isobars of the oedometer test S1 (LIR = 1.0) on the saturated soil sample.

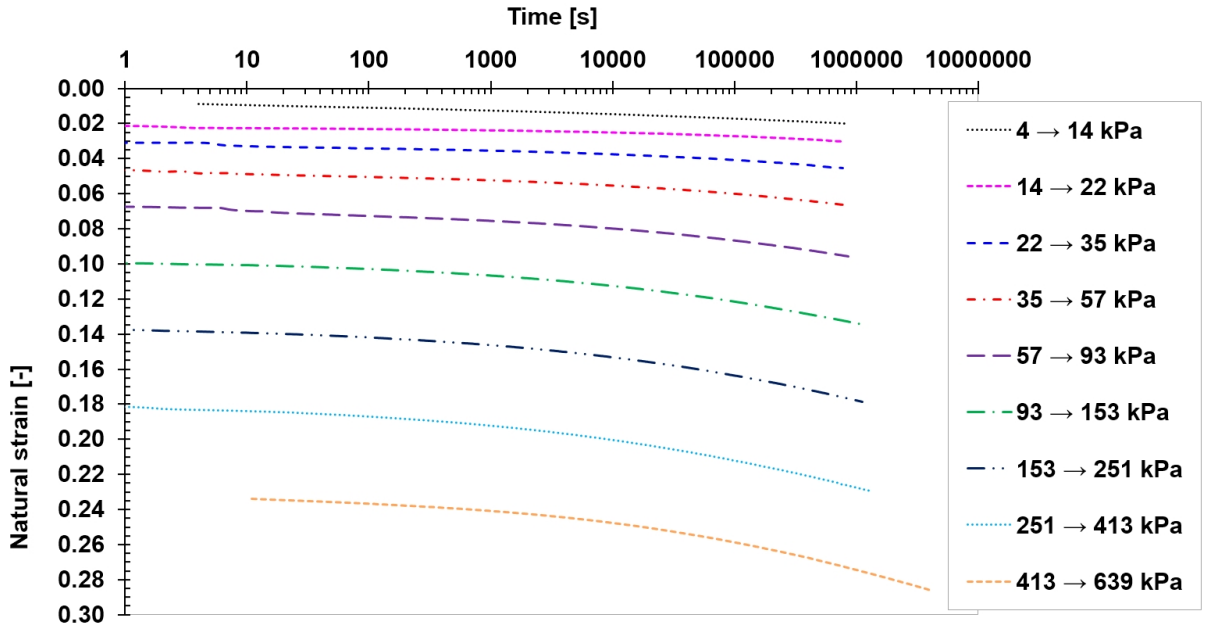

Figure 3.7. Loading isobars of the oedometer test S2 (LIR = 0.65) on the saturated soil sample.

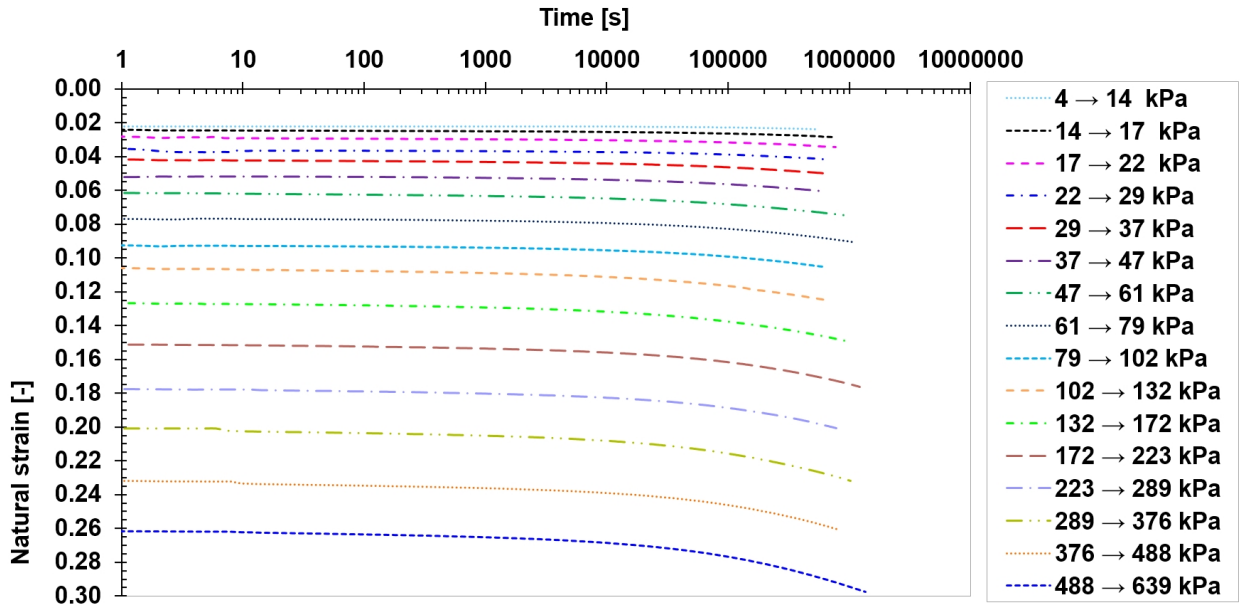

Figure 3.8. Loading isobars of the oedometer test S3 (LIR = 0.3) on the saturated soil sample.

Samson (1985) studied the postconstruction settlement of an expressway built on peat by precompression. They report that:

> "Postconstruction settlement resulting from secondary compression would normally be expected to continue on a linear relationship versus logarithm of time for many years, and until it ceases. Contrary to this expectation, at a time varying between $5\frac{1}{2}$ and 8 years after surcharging, the settlement -

log-time plots became steeper, with correspondingly larger coefficients of secondary compression . . . . The C_α values for this second linear segment of the settlement plots range from 0.028 to 0.073 and are on the average 2.4 times larger than those of the first linear segment" (Samson, 1985, p. 310).

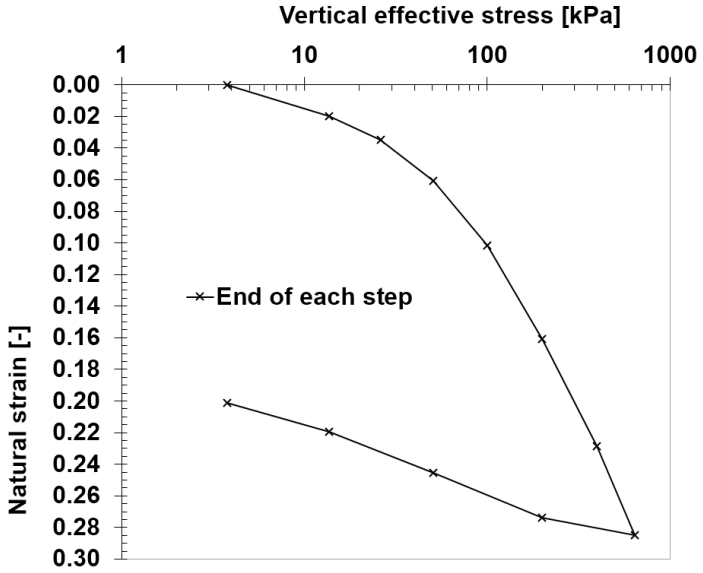

Figure 3.9. Variation of natural strain with vertical effective stress at the end of each step of the oedometer test S1 (LIR = 1.0) on the saturated soil sample.

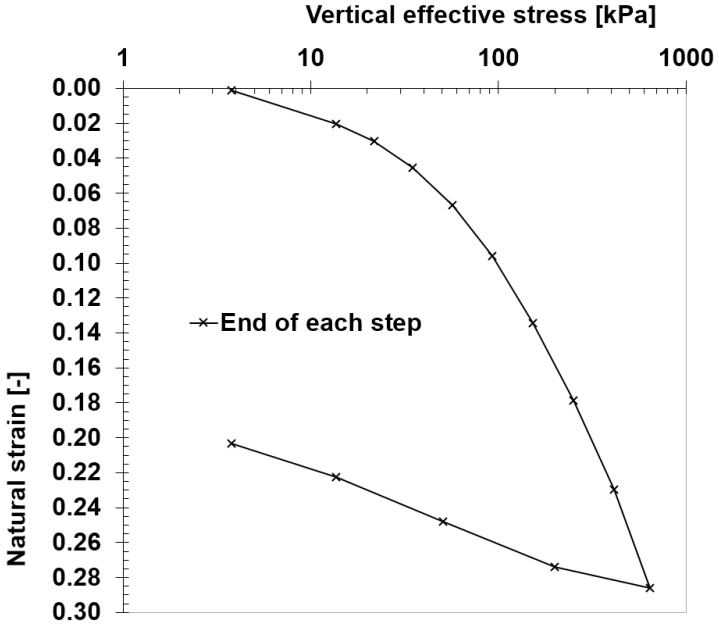

Figure 3.10. Variation of natural strain with vertical effective stress at the end of each step of the oedometer test S2 (LIR = 0.65) on the saturated soil sample.

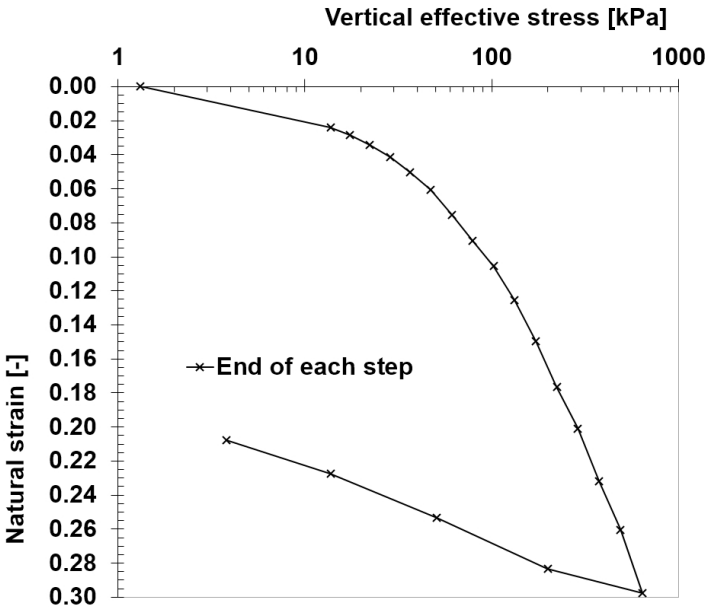

Figure 3.11. Variation of natural strain with vertical effective stress at the end of each step of the oedometer test S3 (LIR = 0.3) on the saturated soil sample.

3.4.1 Estimation of the Coefficient of Consolidation

The coefficient of consolidation (C_v) is a parameter that is used for predicting the rate of consolidation. Several procedures have been proposed based on graphical methods for estimating C_v. In this section, as an example, C_v for a step of Test S2 is obtained and compared using two recommended methods.

One well-known graphical method in classical textbooks for calculating C_v is the Logarithm-of-Time method by Casagrande (as cited in Knappett & Craig, 2012). In this method, EOP should be obtained by drawing gauge readings in the oedometer test against the logarithmic scale of time. However, these plots for the compacted organic soil of this study do not show an S-shape even after a long period of time. Consequently, EOP could not be determined (see Figures 3.6, 3.7 and 3.8). Therefore, the Logarithm-of-Time method is not suitable for this research.

Based on the oedometer tests on Gyttja soil taken from the State of Brandenburg, Germany, Rackwitz et al. (2011) observed that the value of the coefficient of consolidation (C_v) is almost independent of the amount of organic content (p. 102).

3.4.1.1 Square-Root-of-Time Method

Knappett and Craig (2012) explain that in the Square-Root-of-Time method (Taylor, 1948) deformation should be plotted versus the square root of time in minutes. They point out that C_v can be obtained via this method by shorter oedometer tests compared to Logarithm-of-Time method.

This method is recommended by Den Haan (1996) for determining the permeability in each test step as well as obtaining EOP. Shown in Figure 3.12, for applying the Square-Root-of-Time method, points B and C should be chosen on the horizontal axis in a manner that $\overline{\mathrm{AC}} = 1.15 \times \overline{\mathrm{AB}}$. If the linear portion of the curve is continued back, the intersection with the vertical axis (point D) represents the point where degree of consolidation is equal to zero. The intersection of $\overline{\mathrm{DC}}$ and the curve (point E) represents the 90% degree of consolidation. Thus, the corresponding value on the horizontal axis, $\sqrt{t_{90}}$, could be determined. The coefficient of consolidation is given by:

$$C_V = \frac{0.848(H_{dr})^2}{t_{90}} \qquad \text{Taylor (1948)} \qquad (3.3)$$

where H_{dr} is the length of drainage path. For the oedometer apparatus of this research, which have two porous disks on both sides, H_{dr} is equal to half the thickness of the sample (in each step).

Figure 3.12 shows determination of C_v by Square-Root-of-Time method for a step under vertical stress of 639 kPa in Test S2. The parameter C_v thus is obtained as follows:

Sample thickness at the beginning of current step = 15.918 [mm]

Sample thickness at the end of current step = 15.050 [mm]

The average of the sample thickness at current step = (15.918+15.050) / 2 = 15.484 [mm]

$$H_{dr} = \frac{15.484}{2} = 7.742\ [\mathrm{mm}]$$

From Figure 3.12: $\sqrt{t_{90}} = 1.6 \rightarrow t_{90} = 2.56\ [\mathrm{min}]$

$$C_V = \frac{0.848(H_{dr})^2}{t_{90}} = \frac{0.848(7.742)^2}{2.56} = 19.85\ \left[\frac{\mathrm{mm}^2}{\mathrm{min}}\right] = 0.0286\ \left[\frac{\mathrm{m}^2}{\mathrm{day}}\right]$$

Mesri and Castro (1987) report that “a common procedure for performing the incremental loading consolidation test is to maintain each pressure increment for 24 hrs. For most soft clays, standard specimen sizes, and drainage boundary conditions, the primary consolidation stage is completed in several hours and some secondary compression is included in the 24-hr pressure increment duration” (p. 234).

Based on Figure 3.12, the time corresponding to EOP is about **3.7 min**, which indicates a fast consolidation process of this soil.

Colleselli et al. (2000) argue that “The Taylor method can be applied in each case, whereas the Casagrande method cannot be used when primary consolidation is not clearly identified . . ., and in the load range lower than pre-consolidation pressure. The determination of EOP on the basis of pore pressure dissipation is theoretically correct, but in some tests the dissipation was so fast that the measurements were probably not reliable” (p. 233).

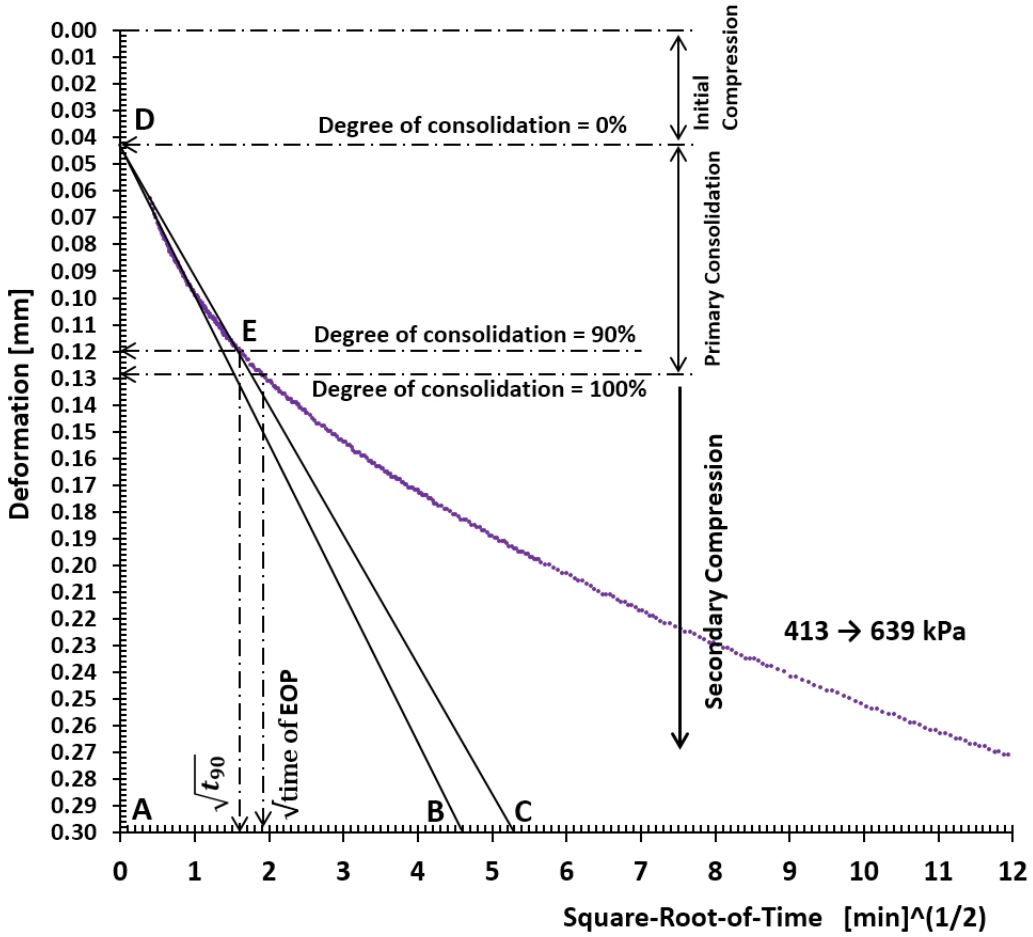

Figure 3.12. Determination of the coefficient of consolidation by Square-Root-of-Time method (Taylor, 1948 as cited in Knappett & Craig, 2012) for a step under vertical stress of 639 kPa in Test S2.

Wesley (2010) discusses about the "common mistaken interpretation" of the Square-Root-of-Time plot. With help of an example, the writer argues that an incorrect slope selection in the linear part of the curve may cause a wrong estimation in C_v "by a factor of nearly 40." The writer continues that "this practice occurs because of an expectation that all soils should conform to 'normal' behavior. Geotechnical engineers expect a straight line and laboratory technicians will obligingly provide one whether it exists or not! The proper interpretation in such cases should simply be that no straight line exists . . ." (Wesley, 2010, p. 72). As Wesley (2010) explains, the shape of Square-Root-of-Time curve depends on the drainage condition. When comparing a thick sample (say for example 1 m) with a thin sample (which in laboratories is conventionally about 2 cm), the Square-Root-of-Time plot of the thick sample is more linear at the beginning of a test. The writer argues that the soil layers in the field usually are thick and dissipation of the excess pore-water pressure takes much more time compared in the laboratory. "The absence of primary consolidation in the laboratory test is therefore not an indication that there will not be primary consolidation in the field. Similarly, the presence of a large proportion of secondary . . . [compression] in the oedometer test does not necessarily indicate that [only] secondary . . . [compression] will be important in the field" (Wesley, 2010, p. 71).

In order to calculate the time required to reach 100% primary consolidation of a saturated layer in the field under the same stress increment of the oedometer test, Das and Sobhan (2014) proposed the following equation:

$$T_v = \frac{C_v \cdot t_{(\text{lab})}}{{H_{dr}}^2{}_{(\text{lab})}} = \frac{C_v \cdot t_{(\text{field})}}{{H_{dr}}^2{}_{(\text{field})}}$$

or

$$t_{(\text{field})} = t_{(\text{lab})} \cdot \frac{{H_{dr}}^2{}_{(\text{field})}}{{H_{dr}}^2{}_{(\text{lab})}} \tag{3.4}$$

where T_v is time factor (for more information, see *Section 3.4.2*).

For the aforementioned soil sample with a 15.484 mm thickness under a stress increment of 413 to 639 kPa in an oedometer cell with two porous disks on *both sides*, the time required for 100% primary consolidation is 3.7 min as calculated by the Square-Root-of-Time method. For example, by using equation 3.4, the time required to reach 100% primary consolidation of a 2-m-thick layer of this saturated soil in the field, which is drained only on *one side* under the same stress increment, can be obtained as:

$$t_{(\text{field})} = 3.7 \cdot \frac{(2000)^2}{\left(\frac{15.484}{2}\right)^2} = 246919\,\text{min} \approx 171\,\text{days}$$

3.4.1.2 The Improved Rectangular Hyperbola Method

Sridharan and Prakash (1985) introduced the improved rectangular hyperbola method for situations when conventional methods such as the Logarithm-of-Time or the Square-Root-of-Time methods could not be used. They recommend the following procedure for obtaining the coefficient of consolidation (see Figure 3.13):

1. Obtain the values of time (t) and their respective deformations (Δh) “preferably at equal intervals of time” from the oedometer test.
2. Plot $(\text{t}/\Delta\text{h})$ versus t.
3. Identify a straight section in the curve, which has a slope of m, and draw it backward to intersect the $(\text{t}/\Delta\text{h})$ axis at point D. Bowles (1997) recommends that “If the $(\text{t}/\Delta\text{h})$ versus t curve exhibits more than one straight line part, use the first linear part for these computations” (p. 68).
4. Let the ordinate of point D be d.
5. Compute the coefficient of consolidation by the following equation:

$$C_V = \frac{0.2972 \text{ m } (H_{dr})^2}{\text{d}}$$ Sridharan and Prakash (1985) (3.5)

where H_{dr} is the length of drainage path as it was explained for the Square-Root-of-Time method.

Figure 3.13 illustrates the determination of C_v by the Improved Rectangular Hyperbola method for a step under vertical stress of 639 kPa in Test S2. The parameter C_v is calculated as follows:

$$C_V = \frac{0.2972 \times 6.14 \times (7.742)^2}{6} = 18.23 \left[\frac{\text{mm}^2}{\text{min}}\right] = 0.0263 \left[\frac{\text{m}^2}{\text{day}}\right]$$

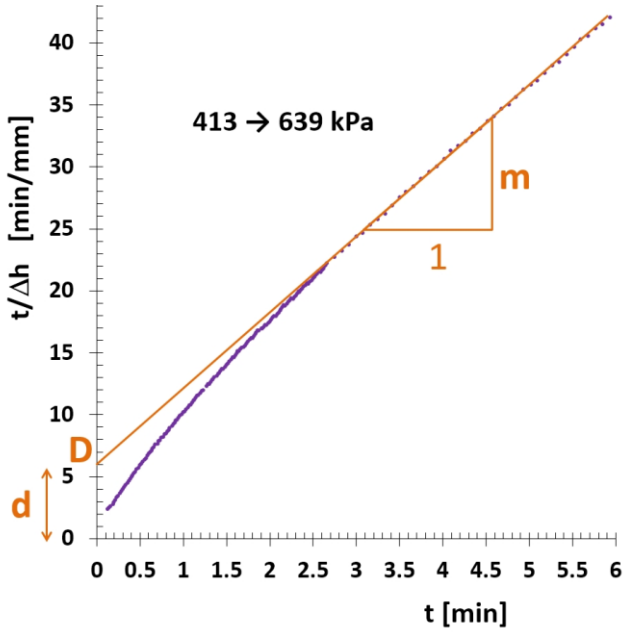

Figure 3.13. Determination of the coefficient of consolidation by the Improved Rectangular Hyperbola method (Sridharan & Prakash, 1985) for a step under vertical stress of 639 kPa in Test S2.

Comparing the result of the Square-Root-of-Time method and the Improved Rectangular Hyperbola method confirmed that both methods would be able to estimate C_v for this compacted organic soil with a reasonable accuracy. The above test results show that, after application of load, primary consolidation finishes quickly whereas secondary compression continues for a very long period of time.

3.4.2 Terzaghi – Consolidation Theory

Dissipation of the excess pore-water pressure of a thick layer in situ takes a much longer period of time compared to a laboratory sample (Wesley, 2010). Therefore, calculating the time of EOP, the amount of pore-water pressure, and the degree of consolidation during the primary consolidation phase would be important in geotechnical practice. One possibility is to use the well-known Terzaghi's one-dimensional consolidation theory. The excess pore-water pressure (Δu) as a function of depth (z) and time (t) can be calculated using the following equation (with some adaptions from Terzaghi, Peck, & Mesri, 1996, p. 228),

$$\Delta u(z,t) = \Delta\sigma_v \sum_{m=0}^{m=\infty} \left[\frac{2}{M} sin\left(\frac{M \cdot z}{H_{dr}}\right)\right] exp(-M^2 \cdot T_v) \tag{3.6}$$

where

$M = \pi(2m+1)/2$

$\Delta\sigma_v$: Vertical stress increment, which is equal to the initial excess pore-water pressure (Δu_0)

T_v : Time factor, which can be obtained as:

$$T_v = \frac{C_v \cdot t}{{H_{dr}}^2}$$

C_v : Coefficient of consolidation

As mentioned in *Section 3.4.1.1*, H_{dr} is the length of drainage path. For the oedometer apparatus of this research, which have two porous disks on both sides, H_{dr} is equal to half the sample thickness.

Verruijt (2001, p. 105) wrote a BASIC computer program for the analytical solution of equation 3.6. The program calculates the amount of excess pore-water pressure (Δu) as a function of depth (z) for a specific time (t). The script of this program has been adapted for Visual Basic for Applications (VBA), and is shown in *Appendix B* (Script 1). As an example, the following input values, which belong to a step under vertical stress of 639 kPa in Test S2, are used in Script 1 (*Appendix B*) to calculate the excess pore-water pressure (Δu) as a function of depth (z) for some specific times (t).

Drainage length (based on the calculation in *Section 3.4.1.1*): $H_{dr} = 0.007742$ [m]

Coefficient of consolidation (as the average of two calculated values): $C_v = 0.027$ [m^2/day]

"The curve representing the distribution of excess pore-water pressure with depth at any time is known as an isochrone" (Terzaghi et al., 1996, p. 112). Figure 3.14 presents the isochrones from the analytical solution of the primary consolidation (Script 1, *Appendix B*) for a step under vertical stress of 639 kPa in Test S2. In this figure, $\Delta u(z,t)$ is the excess pore-water pressure as a function of depth

(z) and time (t), and Δu_0 is the initial excess pore-water pressure which is equal to the vertical stress increment ($\Delta\sigma_v$).

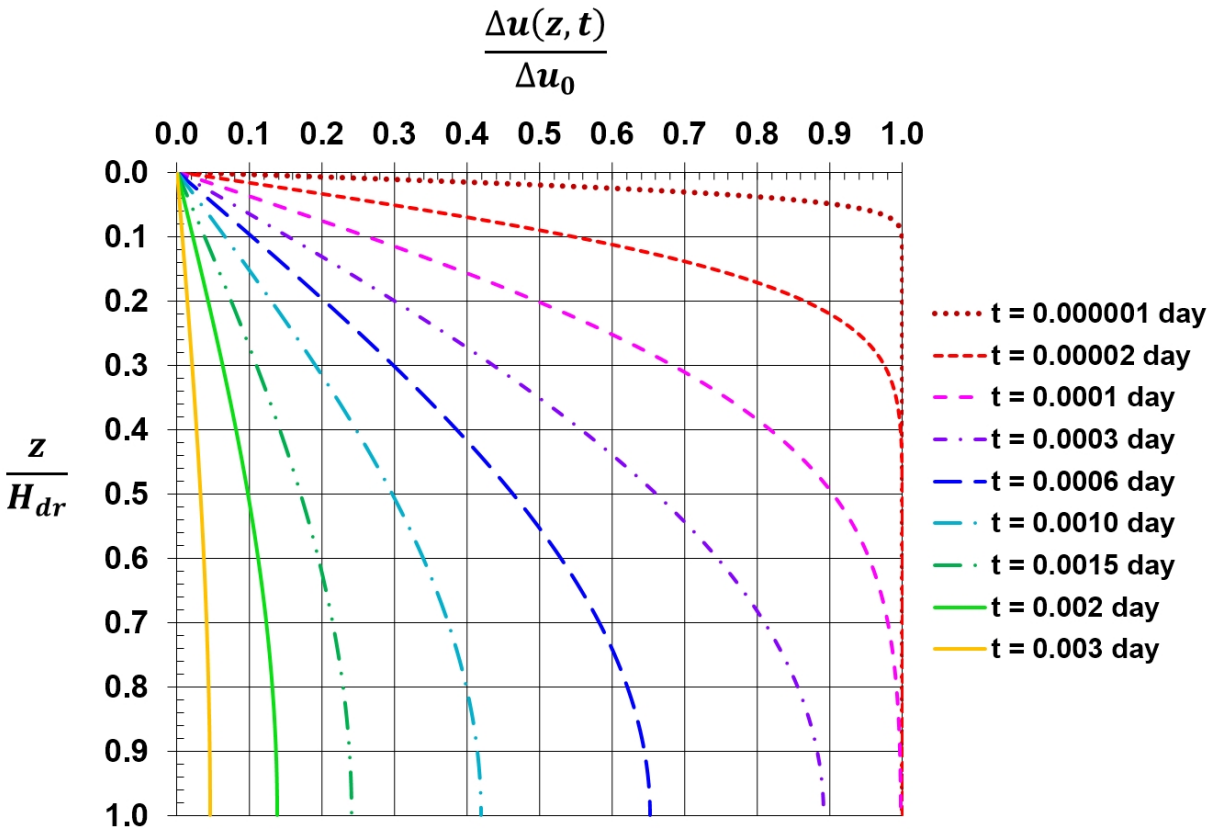

Figure 3.14. Isochrones from the analytical solution of the primary consolidation (Script 1, *Appendix B*) for a step under vertical stress of 639 kPa in Test S2.

The average degree of consolidation of a layer is defined as (Terzaghi et al., 1996, p. 228):

$$\mathrm{U_{avg}} = \frac{S}{S_p} \tag{3.7}$$

where

S: Settlement of the layer at time *t*

S_p: Settlement of the layer when the excess pore-water pressure is zero. In other words, this is the settlement of the layer at EOP.

The average degree of consolidation could also be derived as the following form (Terzaghi et al., 1996, p. 228):

$$\mathrm{U_{avg}} = 1 - \sum_{m=0}^{m=\infty} \frac{2}{M^2} exp(-M^2 \cdot T_v) \tag{3.8}$$

where the definitions of the variables of this equation are similar to the variables of equation 3.6.

Verruijt (2001, p. 108) wrote another BASIC computer program for the analytical solution of equation 3.8. The program calculates the average degree of consolidation ($\mathrm{U_{avg}}$) as a function of time (t). The script of this program has also been adapted for Visual Basic for Applications (VBA), and is presented in *Appendix B* (Script 2). As an example, the following input values, which belong to a step under vertical stress of 639 kPa in Test S2, are used in Script 2 (*Appendix B*) to calculate the average degree of consolidation versus time in the primary consolidation phase.

Drainage length (based on the calculation in *Section 3.4.1.1*): $H_{dr} = 0.007742$ [m]

Coefficient of consolidation (as the average of two calculated values): $C_v = 0.027$ [$\mathrm{m^2/day}$]

Figure 3.15 presents the average degree of consolidation versus time from the analytical solution of equation 3.8 (Script 2, *Appendix B*) for a step under vertical stress of 639 kPa in Test S2.

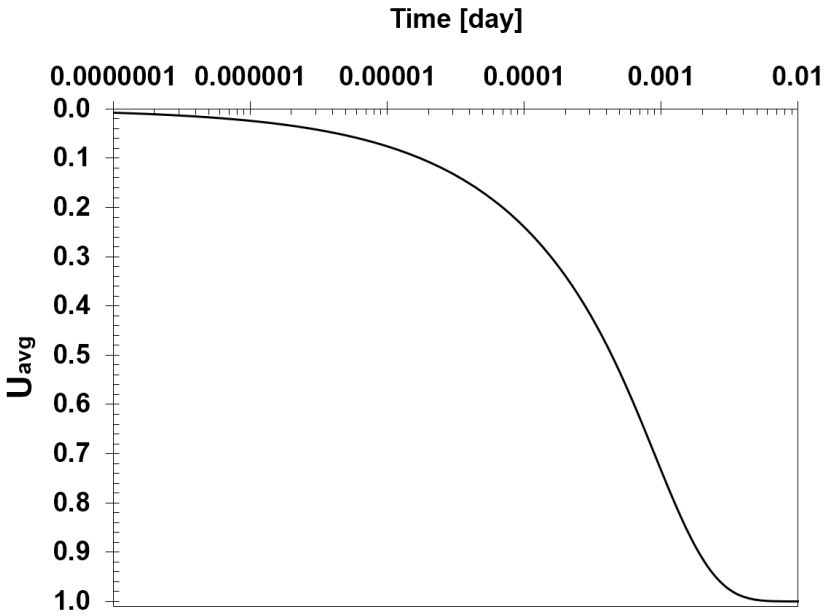

Figure 3.15. The average degree of consolidation versus time from the analytical solution of equation 3.8 (Script 2, *Appendix B*) for a step under vertical stress of 639 kPa in Test S2.

Settlement in the primary consolidation phase versus time can be calculated by simultaneously using equation 3.7 and the analytical solution of equation 3.8. An example result of this is shown in Figure 3.16 for a step under vertical stress of 639 kPa in Test S2. In this calculation, settlement of the soil sample at EOP was estimated from Figure 3.12 as $S_p = 0.129$ mm.

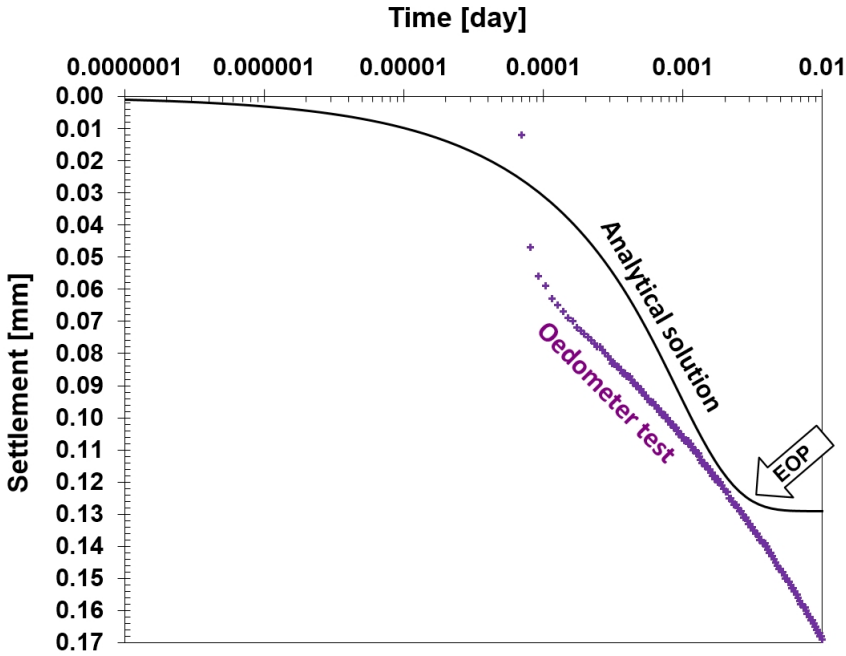

Figure 3.16. Comparison between the measured settlement and the analytical solution of equation 3.8 (by simultaneously using equation 3.7) in the primary consolidation phase for a step under vertical stress of 639 kPa in Test S2.

3.5 Laboratory Testing on Unsaturated Soil Samples

3.5.1 Introduction

There is very limited experimental data about the settlement modelling of unsaturated compacted organic soils in the literature. Kayadelen (2008) explains that, although the theories of unsaturated soils have been developed during the past decades, only little experimental tests have been done on the behaviour of unsaturated soils. The reason is due to the time consuming, complicated, and expensive laboratory equipment in testing of unsaturated soils.

In this research, the overall volume and water volume changes of the unsaturated compacted organic soil is studied under different values of matric suctions.

3.5.2 Suction-Controlled Oedometer Test Programs and Methods

The volume change behaviour of unsaturated soil samples was studied by three suction-controlled oedometer tests. These tests were performed using two fully software-controlled apparatus, which were designed by Birle (2011) for his doctoral research at Zentrum Geotechnik, Technische Universität München. These apparatus are shown in Figure 3.17. Figure C.1, in *Appendix C*, also

introduces the different components of these apparatus. In addition, Figures C.2 and C.3 show the calibration of the suction-controlled oedometers.

In this study, the overall volume and water volume changes were monitored during testing. To increase the accuracy of water volume measurement during the long duration tests, an additional standpipe was added to each suction-controlled oedometer apparatus as a benchmark (for more information, see *Appendix D*).

The apparatus can control both u_a and u_w by using the axis-translation technique. The testing program was conducted using a procedure similar to Birle (2011) in most parts. The exact procedure is described in detail in sections below.

Figure 3.17. The suction-controlled oedometers that were used in this study (Zentrum Geotechnik, Technische Universität München).

Figures 3.18 and 3.19 show two oedometer cells, which were used in this study. Birle (2011) reports that both these cells are, in principle, similar to the suction-controlled oedometer cells developed by the Universitat Politècnica de Catalunya (UPC-cell), which is described in detail in Romero (1999).

In this research, the effects of increasing matric suction and net normal stress were studied separately. In other words, the first part of the suction-controlled oedometer tests were conducted by increasing matric suction at a constant net normal stress, while for the second part of the tests, the net normal stress was increased, as the matric suction was kept constant.

Figure 3.18. TUM-cell (Cell 2) which was built by the Zentrum Geotechnik, Technische Universität München.

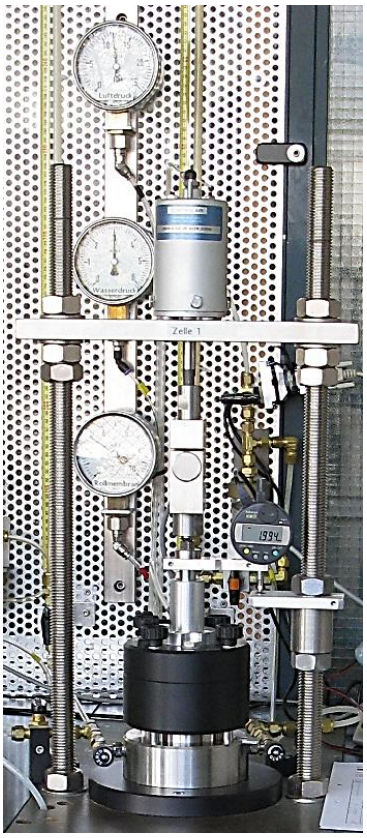

Figure 3.19. Wille-cell (Cell 1) built by *Wille Geotechnik* in collaboration with Prof. Schanz (as cited in Birle, 2011).

Figure 3.20 shows the stress paths that were used for oedometer tests in this research. In Test U1, the matric suction was increased incrementally (over 43 days) up to 891 kPa at a constant net normal stress of 15 kPa. Then the net normal stress was increased incrementally up to 637 kPa at a constant matric suction of 891 kPa. In Test U2, the matric suction was increased incrementally up to 290 kPa at a constant net normal stress of 5 kPa. Then the net normal stress was increased incrementally up to 496 kPa at a constant matric suction of 290 kPa. In Test U3, the matric suction was increased incrementally up to 92 kPa at a constant net normal stress of 15 kPa. Then the net normal stress was increased incrementally up to 499 kPa at a constant matric suction of 92 kPa. As previously mentioned in this chapter, three conventional oedometer tests (S1, S2 and S3) were carried out on saturated soil samples by applying a maximum vertical stress of 639 kPa. Tests S1, S2 and S3 were conducted at different “Load Increment Ratios” of 1.0, 0.65, and 0.3, respectively.

Duration of each test was U1: 177 days, U2: 62 days, and U3: 159 days, S1: 157 days, S2: 164 days and S3: 187 days.

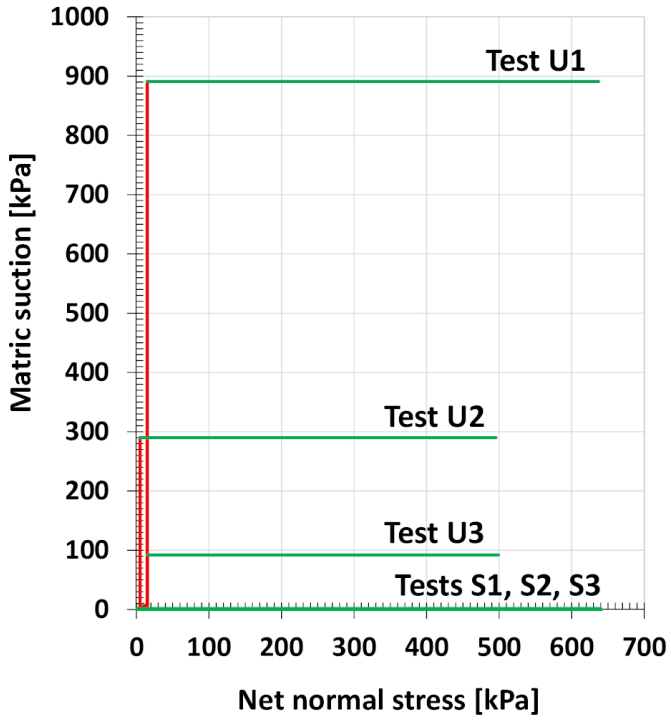

Figure 3.20. The stress paths that were used for oedometer tests in this research. Tests U1, U2 and U3 were performed by the suction-controlled oedometers on unsaturated soil samples. Tests S1, S2 and S3 were conducted by the conventional oedometers on saturated soil samples.

3.5.2.1 High Air Entry Disk

As Fredlund and Rahardjo (1993, p. 81) describe, “A high air entry disk has small pores of relatively uniform size” which separates air and water in unsaturated soil testing. When this ceramic disk is saturated with water, the “air cannot pass through the disk due to the ability of the contractile skin to resist the flow of air.” The matric suction of the soil sample, which is located on the high air entry disk, is calculated by subtracting the air pressure value above the high air entry disk from the water pressure below this ceramic disk (i.e., $u_a - u_w$). “The maximum matric suction that can be maintained across the surface of the disk is called its air entry value.” Ceramic disks with smaller pore size have higher air entry values. The ceramic disk acts as a boundary between the soil sample and the devices for measuring the pore-water pressure. Water in the saturated ceramic disk, connects the pore-water of the soil sample to the measuring devices for pore-water pressure. Air cannot pass through the ceramic disk into the measuring devices as long as the applied matric suction is less than the air entry value (see also Figure 3.21).

The maximum matric suctions applied in this study were 891, 290 and 92 kPa for Tests U1, U2 and U3, respectively. For Test U1 a 1500 kPa, and for Tests U2 and U3 a 500 kPa high air entry disk were used. The air pressure is applied to the upper part of the soil sample and the water pressure is applied to the underside of the high air entry disk.

Immediately before each test, the permeability of the saturated high air entry disk was measured. This was carried out by setting up the oedometer cell without the soil sample and increasing the water

pressure more than the air pressure to enforce the water flow through the ceramic disk. Afterwards the soil sample must be placed on top of the saturated high air entry disk (see Figures 3.22 and 3.23) and then the cell should be closed as fast as possible to prevent exposing the soil sample and ceramic disk to air.

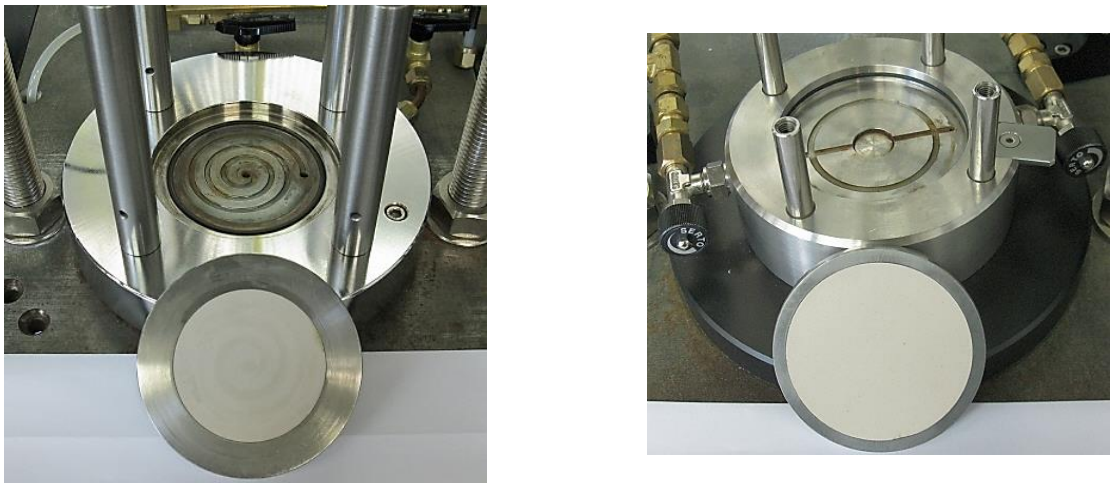

(a) (b)

Figure 3.21. The high air entry disks and the lower part (base) of (a) Cell 2 and (b) Cell 1, which are connected to the water pressure and the flushing system of the suction-controlled oedometers (Zentrum Geotechnik, Technische Universität München).

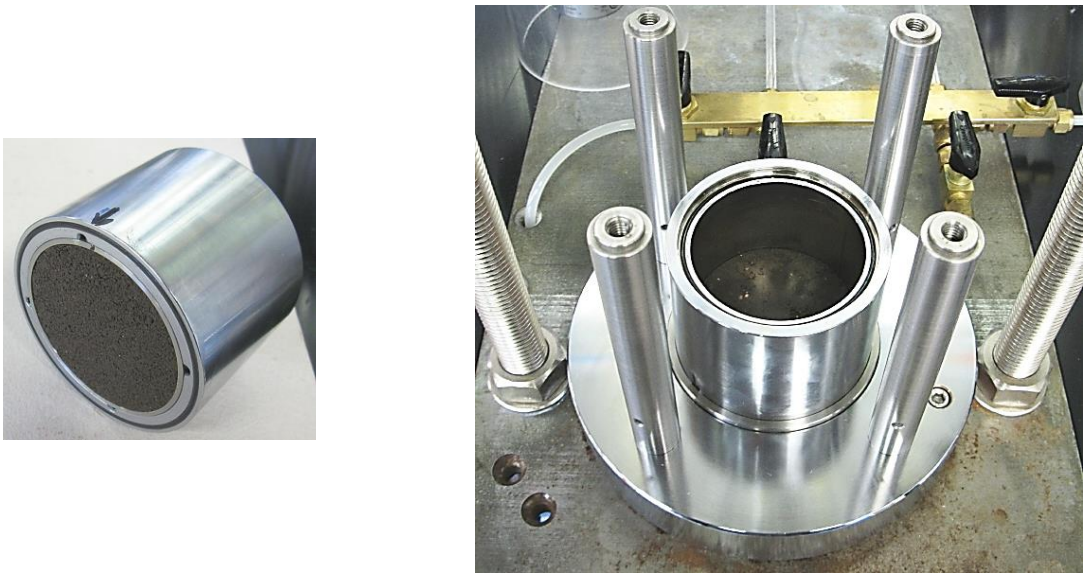

(a) (b)

Figure 3.22. Prior to starting the suction-controlled oedometer test; Cell 2. (a) Inserting the ring and the soil sample into the lower part of the cell, and (b) placing the soil sample on top of the saturated high air entry disk (Zentrum Geotechnik, Technische Universität München).

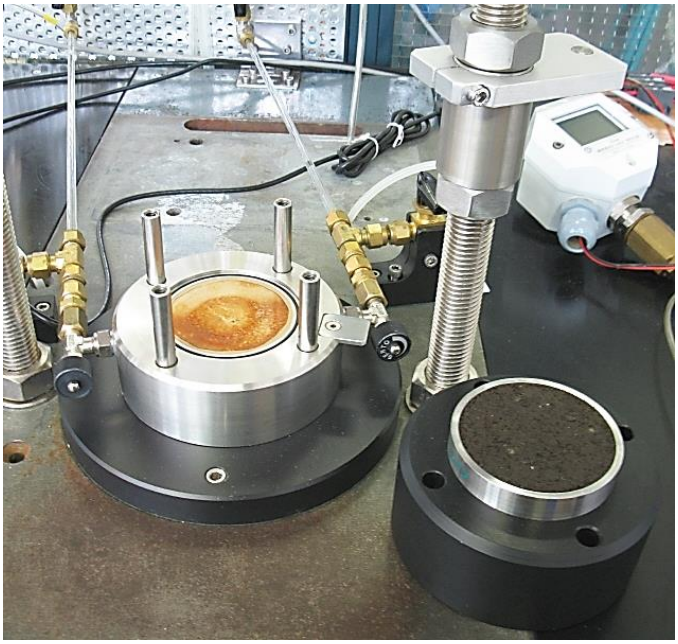

Figure 3.23. Prior to placing the soil sample on top of the saturated high air entry disk. Suction-controlled oedometer cell 1 (Zentrum Geotechnik, Technische Universität München).

3.5.2.2 Axis-Translation Technique

As Fredlund and Rahardjo (1993) explain, during an unsaturated test, if the water pressure approaches -1 atm (i.e., about -101 kPa), the water starts to cavitate and the occluded air bubbles accumulate below the high air entry disk, which creates errors in measurement of the pore-water pressure. The water level in the standpipes would also be affected by the occluded air bubbles accumulating below the high air entry disk. This problem can be solved by using the axis-translation technique.

Therefore, in this study the axis-translation technique (Hilf, 1956 as cited in Fredlund & Rahardjo, 1993) has been used for controlling the matric suction in the suction-controlled oedometer tests.

Rahardjo and Fredlund (1995) explain this technique as follows:

> "Direct measurements of pore-water pressures are limited to negative 101 kPa. The axis-translation technique (Hilf 1956) can be used to measure or to control pore-water pressures lower than negative 101 kPa. Using this method, both the pore-air and pore-water pressures are translated by an equal amount to positive pressures. The matric suction, (u_a - u_w), is not affected by this translation process, which allows the pore-water pressures to be measured or controlled in the positive pressure range. The technique performs well as long as the matric suction does not exceed the air entry value of the air entry disks" (p. 755).

For unsaturated testing using the axis-translation technique, Fredlund and Rahardjo (1993) recommend a system for flushing the air bubbles that accumulate below the ceramic disk.

In the current study, a fully software-controlled flushing system, as shown in Figure 3.24, was used to flush the air bubbles from below the high air entry disk. Flushing was conducted by applying a water pressure (higher than the pore-water pressure) to the water compartment (below the ceramic disk) to force air bubbles out of the water pressure system. The intervals between the flushing periods were related to the value of matric suction and varied from 4 up to 12 hours. A higher matric suction requires a shorter interval between flushing periods. A suitable flushing system guaranteed a permanent link between the water in saturated ceramic disk and the measuring devices of the pore-water pressure and water volume changes.

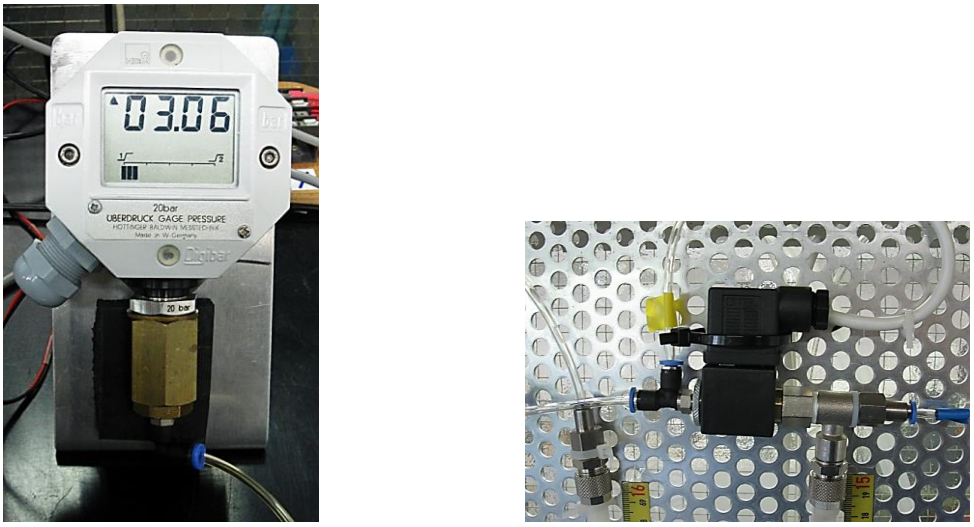

(a) (b)

Figure 3.24. Two components of the flushing system which are fully controlled by software in the suction-controlled oedometer apparatus. (a) Digital manometer and (b) electromechanical valve (Zentrum Geotechnik, Technische Universität München).

In this study, at the start of tests ($w_{\text{initial}} = 73.3\%$ & $\rho_{d\,\text{initial}} = 0.774\ \text{g}/cm^3$), the matric suction of the soil samples was about 26.5 kPa, based on the soil-water retention curve (Figure 3.25). At the beginning of suction-controlled oedometer tests, the soil sample was placed on top of the saturated high air entry disk and the cell was quickly closed. For example at the beginning of Test U3, the cell air pressure (u_a) increased to 316 kPa and the water pressure (u_w) increased to 308 kPa, which means the matric suction ($u_a - u_w$) applied to the soil sample was 8 kPa. Therefore, the soil sample which initially had 26.5 kPa matric suction sucked the water from the standpipes to reach the equilibrium at 8 kPa. As a result, the water volume of the soil sample increased in this step. After completing the equalisation of matric suction, the next step was applied. At the next step, without changing the water pressure, the cell air pressure was increased to 320 kPa, which resulted in an applied matric suction of 12 kPa (for more information, see Figure 3.61).

Equalisation of the matric suction is completed, when no more water flow either in or out of the soil sample is recorded. The equalisation time depends on the permeability and thickness of the specimen as well as the air entry value of the ceramic disk, and the value of matric suction. In this study, the maximum equalisation time for a change in matric suction was 23 days for Test U1 using a ceramic disk with the air entry value of 1500 kPa.

The change of net normal stress also needs an equalisation time for completing the settlement or the swelling. In this study, the maximum equalisation time for a change of net normal stress was also 23 days for Tests U1 and U3 using a ceramic disk with the air entry values of 1500 and 500 kPa, respectively.

Birle (2011) determined the drying path of the soil-water retention curve for the same soil type used in this research. Figure 3.25 shows his data in terms of water content (*w*). As shown in this figure, he used the axis translation technique for suction values smaller than 500 kPa, and WP4 device (water potential meter) for suction values greater than 500 kPa.

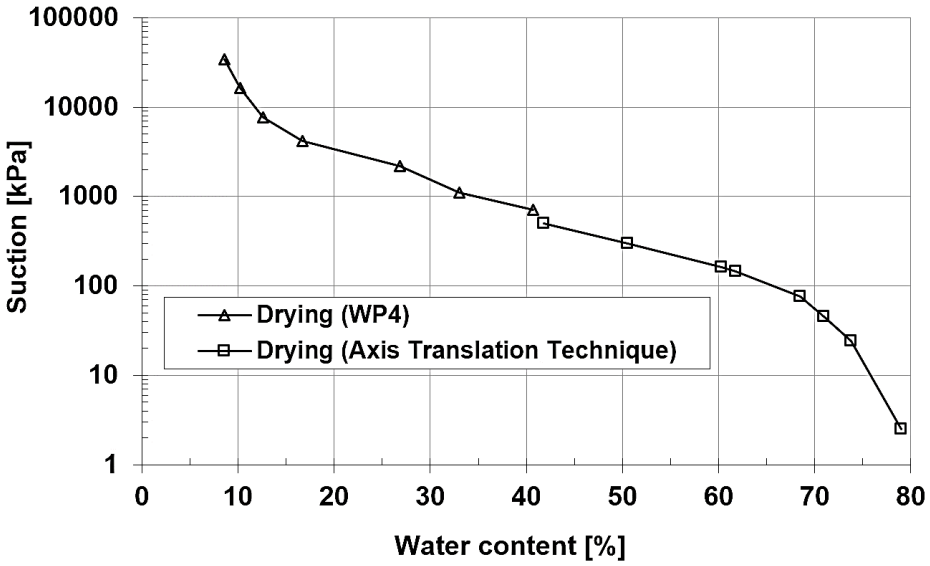

Figure 3.25. Drying path of the soil-water retention curve in terms of water content. Data from Birle, 2011, p. 115, fig. 6.76.

3.5.3 Definition of the Parameters Used for the Study of the Volume Change Behaviour of Unsaturated Soils

Figure 3.26 presents a conceptual description of the fundamental difference between the terms *total* and *overall* in this study. The term *total* denotes the sum of the elastic part and the visco-plastic part of the strain or strain rate (Den Haan, 2008), whereas the term *overall* (which sometimes also has been called *total* in the literature) denotes the sum of the volume of the air, water and solids (see also *Section 2.2.3*). The water and the soil solids are assumed to be incompressible in this research.

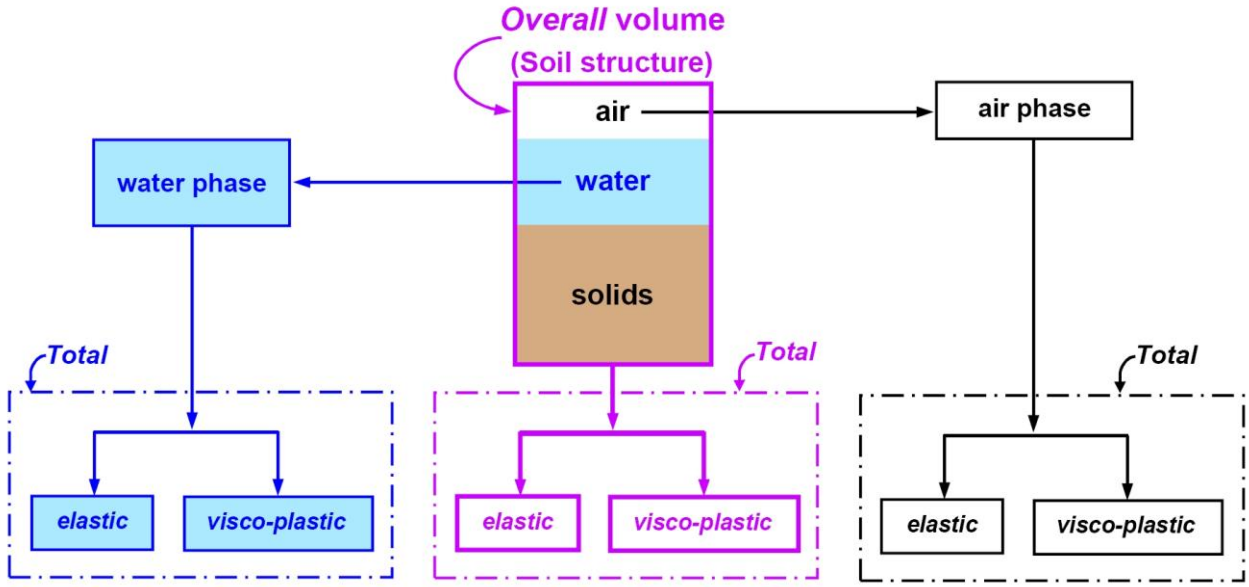

Figure 3.26. Conceptual description of the fundamental difference between the *total* and the *overall* in this study.

In this study, the following colours are used to make it easy to distinguish each variable in the figures and formulas of unsaturated soils:

Red: constant net normal stress,

Green: constant matric suction,

Purple: soil structure (i.e., overall volume), and

Blue: water phase.

3.5.3.1 Definition of the Linear Volumetric Parameters

For one-dimensional consolidation under K_0 loading, equation 2.41 is stated again here (for more information, see *Section 2.2.3*):

$$\frac{dV_v}{V_0} = \frac{dV_w}{V_0} + \frac{dV_a}{V_0}$$: (Fredlund, Rahardjo, & Fredlund, 2012)

This equation can be expressed in the following form:

$$\varepsilon_v^{(\mathrm{lin})} = \varepsilon_w^{(\mathrm{lin})} + \varepsilon_a^{(\mathrm{lin})} \qquad (3.9)$$

$$\varepsilon_v^{(\mathrm{lin})} = -\frac{dV_v}{V_0} \tag{3.10}$$

$$\varepsilon_w^{(\mathrm{lin})} = -\frac{dV_w}{V_0} \tag{3.11}$$

$$\varepsilon_a^{(\mathrm{lin})} = -\frac{dV_a}{V_0} \tag{3.12}$$

where

$\varepsilon_v^{(\mathrm{lin})}$: Overall total linear strain

$\varepsilon_w^{(\mathrm{lin})}$: Total linear water volume change

$\varepsilon_a^{(\mathrm{lin})}$: Total linear air volume change

V_0: Initial overall volume of the soil element

In the current study, the water phase isotaches of the unsaturated soil were drawn by using two different formulas; equation 3.11 for a linear water volume change (in Tests U1, U2 & U3) and equation 3.24 for a natural water mass change (in Test U3). For more information, see *Sections 3.5.3.3* and *4.3.3*.

Similar to the theory of the a,b,c isotache model, the *total* linear water volume change (equation 3.11) is equal to the *elastic* part ($\varepsilon_w^{(\mathrm{lin})}{}_e$) plus the *visco-plastic* part ($\varepsilon_w^{(\mathrm{lin})}{}_{vp}$) of the linear water volume change:

$$\varepsilon_w^{(\mathrm{lin})} = \varepsilon_w^{(\mathrm{lin})}{}_e + \varepsilon_w^{(\mathrm{lin})}{}_{vp} \tag{3.13}$$

Moreover, the rate of *total* linear water volume change ($\dot{\varepsilon}_w^{(\mathrm{lin})}$) is equal to the rate of *elastic* part ($\dot{\varepsilon}_w^{(\mathrm{lin})}{}_e$) plus the rate of *visco-plastic* part ($\dot{\varepsilon}_w^{(\mathrm{lin})}{}_{vp}$) of the linear water volume change:

$$\dot{\varepsilon}_w^{(\mathrm{lin})} = \dot{\varepsilon}_w^{(\mathrm{lin})}{}_e + \dot{\varepsilon}_w^{(\mathrm{lin})}{}_{vp} \tag{3.14}$$

In this study, the linear water volume change ($\varepsilon_w^{(\mathrm{lin})}$) without additional descriptions means the *total* linear water volume change. Similarly, the rate of linear water volume change ($\dot{\varepsilon}_w^{(\mathrm{lin})}$) without additional descriptions means the rate of *total* linear water volume change.

3.5.3.2 Definition of the Overall Natural Strain

Based on equation 3.10 for K_0 loading condition:

$$\varepsilon_v^{(\mathrm{lin})} = -\frac{dV_v}{V_0} = -\frac{d(A.h_v)}{A.h_0} = -\frac{dh_v}{h_0}$$

which is equivalent to the definition of the linear strain ($\varepsilon^{\mathrm{lin}}$) in *Section 2.1.2.1* (see equation 2.1). Therefore, similar to equation 2.5 in *Section 2.1.2.3,* the *overall total natural strain* for the K_0 loading condition can be obtained as:

$$\varepsilon_v^H = -\ln\left(\frac{1+e}{1+e_0}\right) \tag{3.15}$$

and, similar to equation 2.3:

$$\varepsilon_v^H = -\ln\left(1-\varepsilon_v^{(\mathrm{lin})}\right)$$

and vice versa:

$$\varepsilon_v^{(\mathrm{lin})} = 1-\exp(-\varepsilon_v^H) \tag{3.16}$$

where

e: Current void ratio

e_0: Initial void ratio

$\varepsilon_v^{(\mathrm{lin})}$: Overall total linear strain

Similar to the theory of the a,b,c isotache model, the overall *total* natural strain (ε_v^H) is equal to the *elastic* part ($\varepsilon_{v\ e}^H$) plus the *visco-plastic* part ($\varepsilon_{v\ vp}^H$) of the overall natural strain:

$$\varepsilon_v^H = \varepsilon_{v\ e}^H + \varepsilon_{v\ vp}^H \tag{3.17}$$

In addition, the rate of overall *total* natural strain ($\dot{\varepsilon}_v^H$) is equal to the rate of *elastic* part ($\dot{\varepsilon}_{v\ e}^H$) plus the rate of *visco-plastic* part ($\dot{\varepsilon}_{v\ vp}^H$) of the overall natural strain:

$$\dot{\varepsilon}_v^H = \dot{\varepsilon}_{v\ e}^H + \dot{\varepsilon}_{v\ vp}^H \tag{3.18}$$

In this research, the overall natural strain (ε_v^H) without additional descriptions means the overall *total* natural strain. Similarly the rate of overall natural strain ($\dot{\varepsilon}_v^H$) without additional descriptions means the rate of overall *total* natural strain.

The idealised pattern of the adapted a,b,c isotache model for the overall total natural strain of unsaturated soils is proposed in Figure 3.27. Various parameters on this figure will be thoroughly explained in the next chapter.

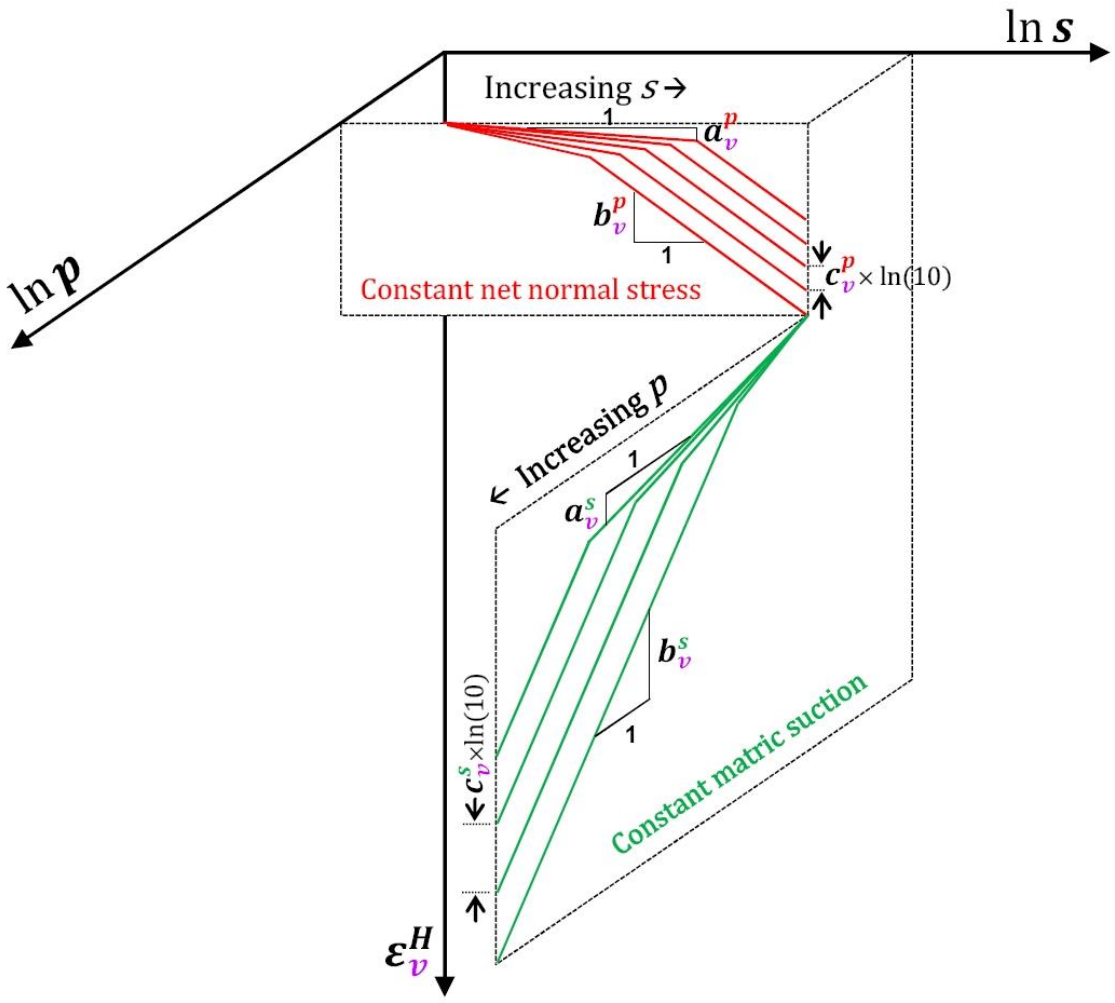

Figure 3.27. Idealised pattern of the adapted a,b,c isotache model for the overall total natural strain of unsaturated soils.

3.5.3.3 Definition of the Natural Water Mass Change

In soil mechanics, the water ratio (e_w) and the air ratio (e_a) of a soil sample are defined as follows:

$$e_w = \frac{V_w}{V_s} \tag{3.19}$$

$$e_a = \frac{V_a}{V_s} \tag{3.20}$$

and,

$$e = e_w + e_a \quad or \quad \frac{V_v}{V_s} = \frac{V_w}{V_s} + \frac{V_a}{V_s} \tag{3.21}$$

where

V_v: Volume of voids

V_s: Volume of solids

V_w: Volume of water

V_a: Volume of air

In addition, the relationships between the degree of saturation (Sr) and the water ratio and void ratio are as follows:

$$Sr = \frac{e_w}{e} \tag{3.22}$$

$$e_w = Sr.e = w.G_s \tag{3.23}$$

where w is the water content, and G_s is the specific gravity of the soil particles.

Toll (1988, as cited in Toll, 1995) introduced a conceptual model by using an "equivalent void ratio" (i.e., e_w) for unsaturated soils. He explains that when a soil is fully saturated, e_w is equal to the void ratio (e) (p. 807). Jommi and Della Vecchia (2010) write "In fact, a useful normalized variable to describe the evolution of water content is the water ratio, e_w, defined as the ratio between the volume of water in the pore space and the volume of solid particles . . ." (p. 364). Honda et al. (2006) point out that "The equivalent void ratio [e_w] tends to approach the void ratio with the progress of compression" (p. 844). This could be explained as an increase in the degree of saturation due to compression.

In order to define an equation for *natural water mass change* (ε_w^H), equation 3.15 for the overall natural strain of the soil structure (under the K_0 loading condition) is modified by changing the void ratio to the water ratio as follows:

$$\varepsilon_w^H = -\ln\left(\frac{1+e_w}{1+e_{w_0}}\right) \tag{3.24}$$

and vice versa:

$$e_w = \left[\left(1+e_{w_0}\right)\cdot \exp(-\varepsilon_w^H)\right] - 1 \tag{3.25}$$

where

ε_w^H : Total natural water mass change

e_w: Current water ratio

e_{w_0}: Initial water ratio

By combining the equations 3.15 and 3.25, the relationship between ε_v^H, ε_w^H and Sr can be obtained as:

$$\varepsilon_v^H = -\ln\left(\frac{Sr_0 \cdot \left[Sr - 1 + \left(1 + e_{w_0}\right) \cdot \exp(-\varepsilon_w^H)\right]}{Sr \cdot \left(Sr_0 + e_{w_0}\right)}\right) \tag{3.26}$$

where Sr_0 is the initial degree of saturation.

When the soil is fully saturated, the total natural water mass change (ε_w^H) is equal to the overall total natural strain (ε_v^H).

In contrast to the simple relationship between e, e_w and Sr (i.e., $e = e_w/Sr$), equation 3.26 represents a complicated relationship between ε_v^H, ε_w^H and Sr.

To determine the relationship between ε_w^H and $\varepsilon_w^{(\mathrm{lin})}$ the following calculations are performed:

$$dV_w = V_w - V_{w_0} = \frac{m_w - m_{w_0}}{\rho_w} = \frac{m_d(w - w_0)}{\rho_w} = \frac{m_d(w \cdot G_s - w_0 \cdot G_s)}{\rho_w \cdot G_s} = \frac{m_d\left(e_w - e_{w_0}\right)}{\rho_s}$$

Then,

$$\varepsilon_w^{(\mathrm{lin})} = -\frac{dV_w}{V_0} = -\frac{m_d\left(e_w - e_{w_0}\right)}{\rho_s \cdot V_0} \tag{3.27}$$

By substituting equation 3.25 into equation 3.27, the relationship between ε_w^H and $\varepsilon_w^{(\mathrm{lin})}$ is derived as:

$$\varepsilon_w^{(\mathrm{lin})} = \frac{m_d \cdot (1 + e_{w_0}) \cdot [1 - \exp(-\varepsilon_w^H)]}{\rho_s \cdot V_0} \tag{3.28}$$

and vice versa:

$$\varepsilon_w^H = -\ln\left(1 - \left[\frac{\rho_s \cdot V_0}{m_d \cdot (1 + e_{w_0})}\right] \cdot \varepsilon_w^{(\mathrm{lin})}\right) \tag{3.29}$$

where

m_d: Dry mass of the soil element

ρ_s: Density of soil solids

V_0: Initial overall volume of the soil element

Figure 3.28 compares the linear water volume change ($\varepsilon_w^{(\mathrm{lin})}$) and the natural water mass change (ε_w^H) based on equation 3.29 by using the parameters of Test U3 (i.e., ρ_s, V_0, m_d, e_{w_0}). This figure shows that when the amount of water volume change is high, the difference between the linear water volume change and the natural water mass change is significant.

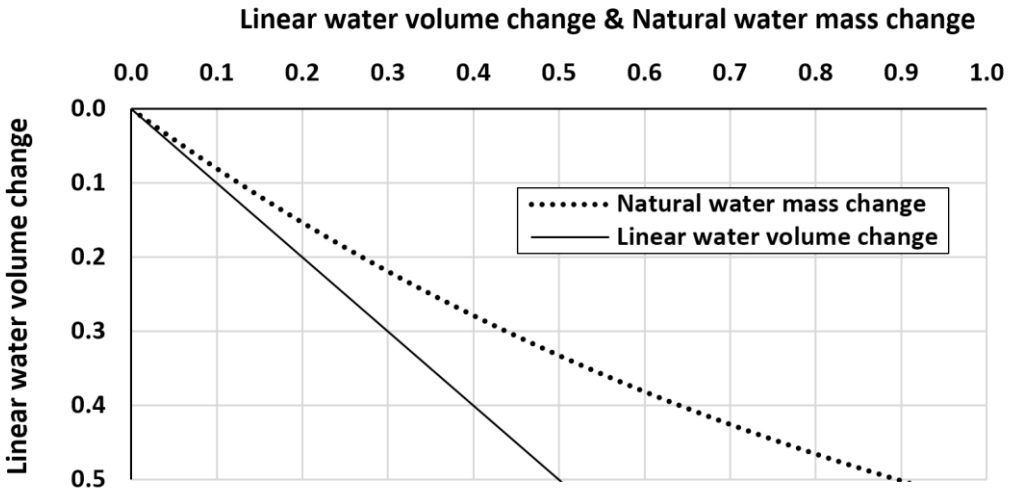

Figure 3.28. Comparison between the linear water volume change ($\varepsilon_w^{(\mathrm{lin})}$) and the natural water mass change (ε_w^H) by using the parameters of Test U3.

Here again similar to the theory of the a,b,c isotache model, the *total* natural water mass change (ε_w^H) is equal to the *elastic* part ($\varepsilon_{w_e}^H$) plus the *visco-plastic* part ($\varepsilon_{w_{vp}}^H$) of the natural water mass change:

$$\varepsilon_w^H = \varepsilon_{w_e}^H + \varepsilon_{w_{vp}}^H \tag{3.30}$$

Furthermore, the rate of *total* natural water mass change ($\dot{\varepsilon}_w^H$) is equal to the rate of *elastic* part ($\dot{\varepsilon}_{w_e}^H$) plus the rate of *visco-plastic* part ($\dot{\varepsilon}_{w_{vp}}^H$) of the natural water mass change:

$$\dot{\varepsilon}_w^H = \dot{\varepsilon}_{w_e}^H + \dot{\varepsilon}_{w_{vp}}^H \tag{3.31}$$

In this research, the natural water mass change (ε_w^H) without additional descriptions means the *total* natural water mass change. Similarly, the rate of natural water mass change ($\dot{\varepsilon}_w^H$) without additional descriptions means the rate of *total* natural water mass change.

Similar to the theory presented in *Section 2.2.3*, only *overall natural strain* and *natural water mass change* are sufficient to describe the volume change behaviour of an unsaturated soil. The required information for the air phase can also be obtained from the soil structure (i.e., the overall volume) and water phase. Equation 3.9 ($\varepsilon_v^{(\mathrm{lin})} = \varepsilon_w^{(\mathrm{lin})} + \varepsilon_a^{(\mathrm{lin})}$) cannot be used for “natural” values; in other words: $\varepsilon_v^H \neq \varepsilon_w^H + \varepsilon_a^H$. Therefore, the “natural” values should be converted to the “linear” values before using them in equation 3.9. This can be done using equation 3.16 for the soil structure and equation 3.28 for the water phase.

The idealised pattern of the adapted a,b,c isotache model for the total natural water mass change of unsaturated soils is proposed in Figure 3.29. Various parameters on this figure will be thoroughly explained in the next chapter.

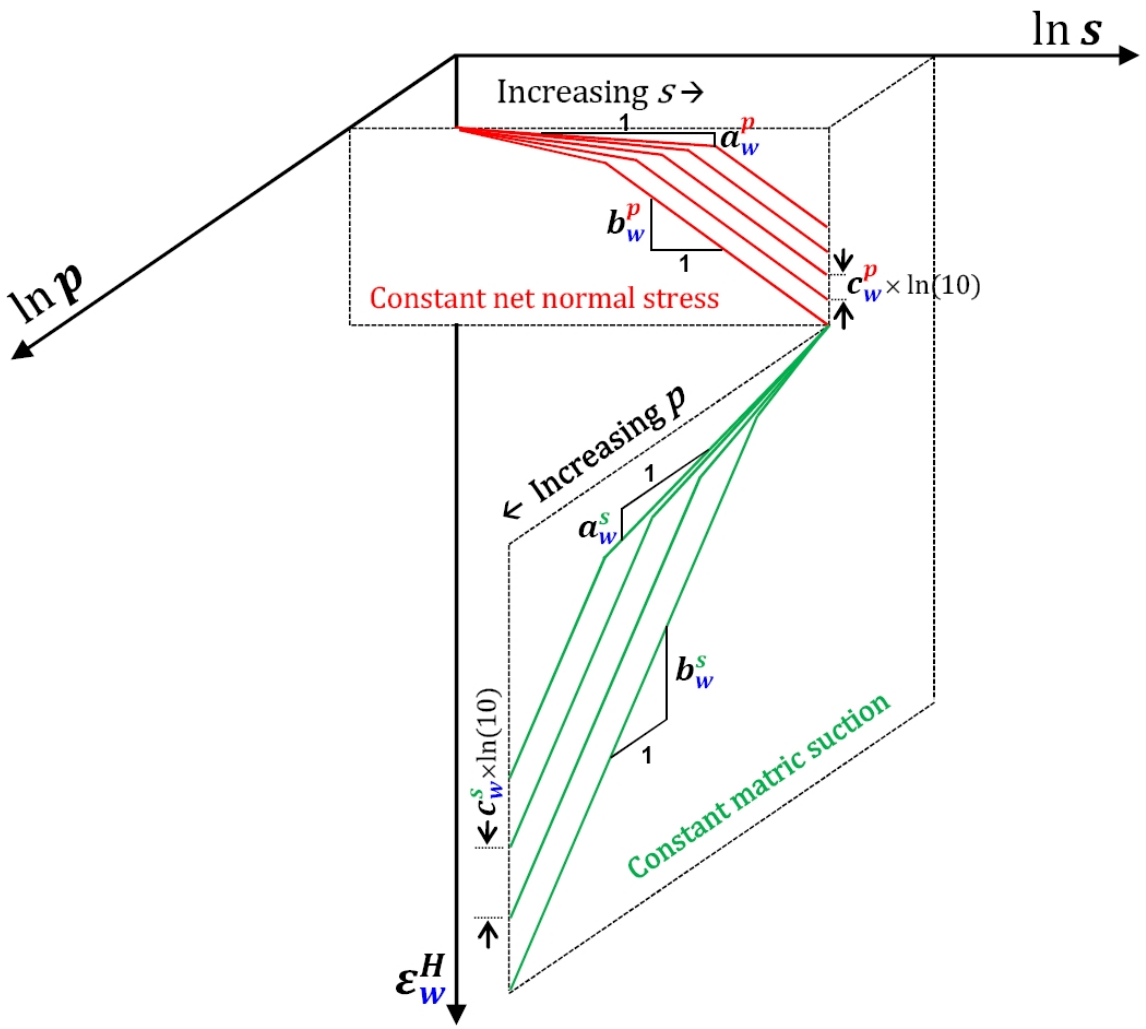

Figure 3.29. Idealised pattern of the adapted a,b,c isotache model for the total natural water mass change of unsaturated soils.

3.5.3.4 Definition of the Momentary Water Volume Change

The momentary water volume change (ε_w^m) could be defined similarly to what was introduced in *Section 2.1.2.2* for the definition of the momentary strain (equation 2.2). Thus, ε_w^m is defined as the water volume change divided by the current overall volume of the soil element:

$$\varepsilon_w^m = -\frac{\Delta V_w}{V_{\text{current}}} \tag{3.32}$$

This equation depends on the overall volume change of the soil sample because it represents the change in water volume (ΔV_w) at the same time that the overall volume of the soil sample (V_{current}) is changing. Therefore, the momentary water volume change (ε_w^m) is not suitable for studying the water phase via the isotache approach.

A necessary condition for a parameter to be used for studying the water phase of unsaturated soils via the isotache approach is that it be independent of the overall volume change of the soil sample. This study recommends using the "natural water mass change" (ε_w^H), especially when the water volume change is high.

3.5.4 Suction-Controlled Oedometer Test Results of Unsaturated Soil Samples

Romero, Della Vecchia, and Jommi (2011) argue that "the hydraulic state can be affected by adding or removing water, hence filling or emptying a given pore volume, or by changing the volume of the pores. As a way to tackle this conflict, Tarantino (2009) introduced the concept of *hydraulic* wetting related to a process which increases water volume, in contrast to the term *mechanical* wetting, associated with an increase in the degree of saturation due to a decrease of void ratio" (p. 315).

Considering the concept of hydraulic and mechanical wetting, in this research, long-term volume change behaviour of the unsaturated compacted organic soil was studied in terms of the overall natural strain (ε_v^H) and natural water mass change (ε_w^H), void ratio (e) and water ratio (e_w), linear ($\varepsilon_w^{(\mathrm{lin})}$) and momentary ($\varepsilon_w^m$) water volume change, as well as in terms of the degree of saturation (Sr).

3.5.4.1 Test U1

In Test U1, the matric suction was increased incrementally (over 43 days) up to 891 kPa at a constant net normal stress of 15 kPa. Then the net normal stress was increased incrementally up to 637 kPa at a constant matric suction of 891 kPa. The duration of this test was 177 days. Figure 3.30 presents the continuous monitoring of the natural water mass change (ε_w^H) and the overall natural strain (ε_v^H) for the suction-controlled oedometer test U1 on the unsaturated soil sample.

Figure 3.31 shows the continuous monitoring of the water ratio (e_w) and the void ratio (e) for the suction-controlled oedometer test U1 on the unsaturated soil sample. For each point on the curves, the degree of saturation can be obtained by: $Sr = e_w/e$. In this figure, as well as in Figures 3.44 and 3.57 for Tests U2 and U3, the curve of water ratio is always located below the curve of void ratio. By increasing degree of saturation (e.g., through decreasing matric suction or increasing net normal stress) the distance between the two curves decreases. This can also be observed in Figures 3.37 and 3.40 for Test U1, Figures 3.50 and 3.53 for Test U2, and Figures 3.63 and 3.66 for Test U3. The two curves coincide if a soil is fully saturated. As long as the change in e_w is equal to the change in e, the value of Sr remains constant. More information about the variations in the degree of saturation can be found in Figures 3.33, 3.46 and 3.59 for Tests U1, U2 and U3, respectively.

In contrast to the simple relationship between e, e_w and Sr (i.e., $e = e_w/Sr$), the relationship between ε_v^H, ε_w^H and Sr is complicated (see equation 3.26).

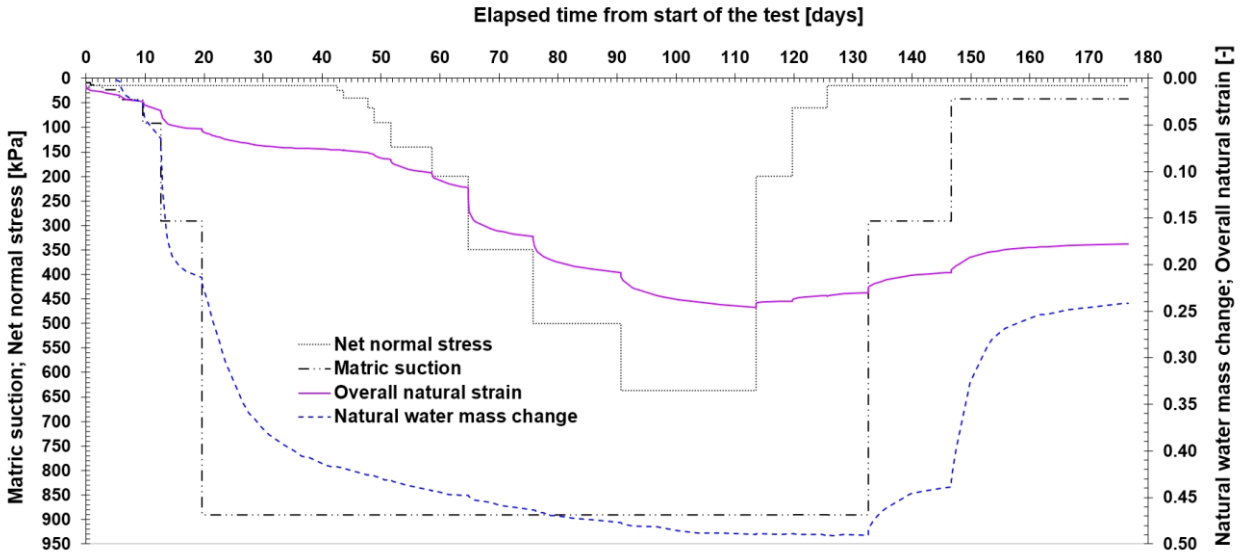

Figure 3.30. Continuous monitoring of the natural water mass change (ε_w^H) and the overall natural strain (ε_v^H) for the suction-controlled oedometer test U1 (unsaturated soil sample).

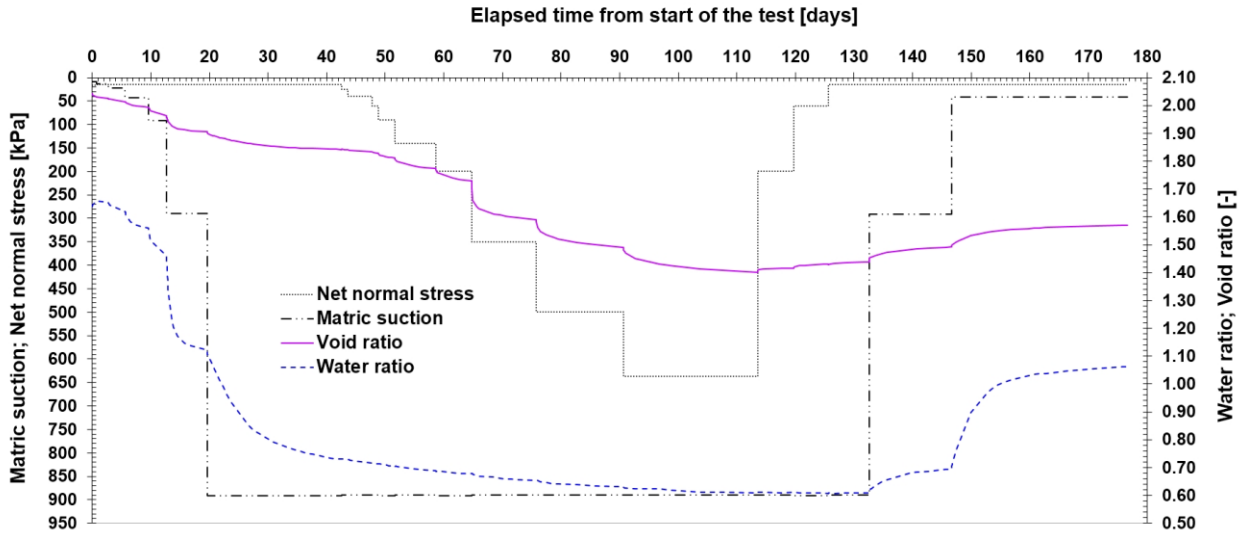

Figure 3.31. Continuous monitoring of the water ratio (e_w) and the void ratio (e) for the suction-controlled oedometer test U1 (unsaturated soil sample).

Figure 3.32 shows the continuous monitoring of the linear ($\varepsilon_w^{(\mathrm{lin})}$) and the momentary ($\varepsilon_w^m$) water volume change of the unsaturated soil sample in the suction-controlled oedometer test U1. As can be seen in this figure as well as in Figures 3.45 and 3.58 for Tests U2 and U3, when the overall volume is decreasing, the value of the momentary water volume change is greater than the value of the linear water volume change, because: $\mathrm{V_{current}} \leq \mathrm{V_0}$. Therefore, the volume changes in each step due to the applied net normal stress or matric suction can be much better distinguished for the momentary water volume change.

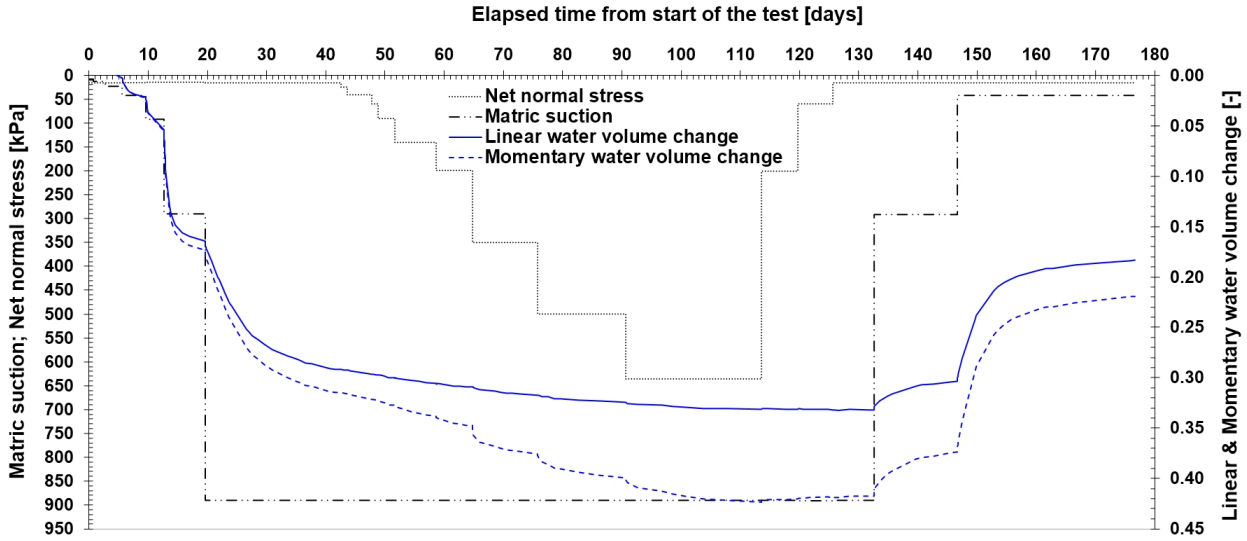

Figure 3.32. Continuous monitoring of the linear ($\varepsilon_w^{(\mathrm{lin})}$) and the momentary ($\varepsilon_w^m$) water volume change for the suction-controlled oedometer test U1 (unsaturated soil sample).

Figure 3.33 presents the continuous monitoring of the degree of saturation for the suction-controlled oedometer test U1 on the unsaturated soil sample. This figure, along with Figures 3.46 and 3.59 (for Tests U2 and U3), shows that the degree of saturation increases with increasing net normal stress due to the compression of the soil structure (i.e., reducing voids). These figures also indicate that the degree of saturation increases with decreasing matric suction due to the increasing water content of the soil sample.

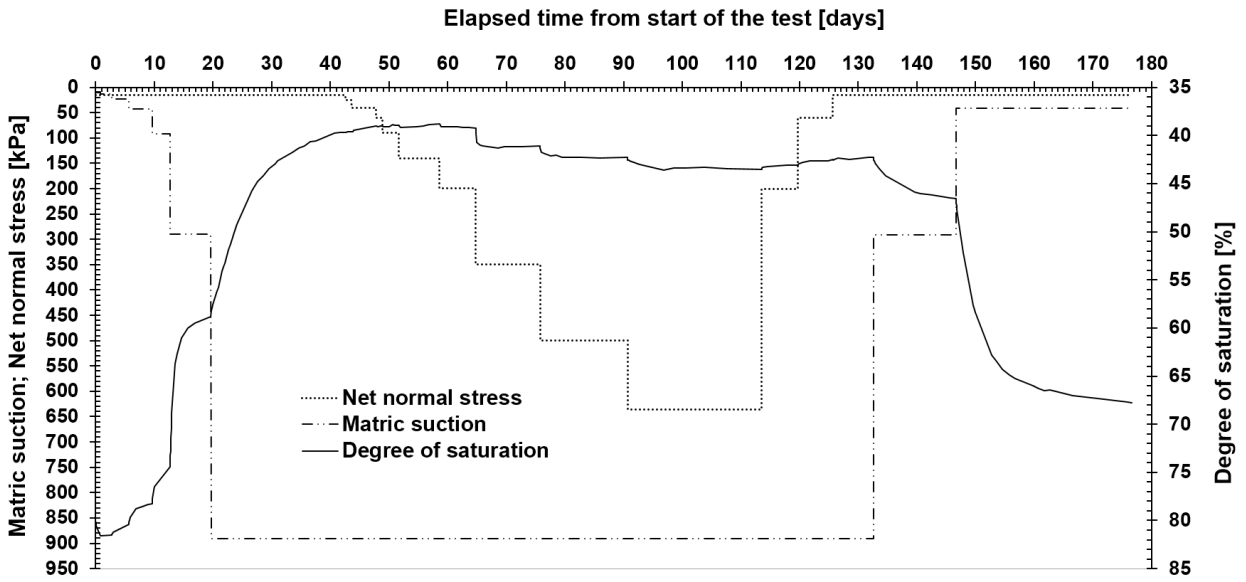

Figure 3.33. Continuous monitoring of the degree of saturation for the suction-controlled oedometer test U1 (unsaturated soil sample).

Isobars of the suction-controlled oedometer test U1 for the soil structure, and the water phase are plotted in Figures 3.34 and 3.35.

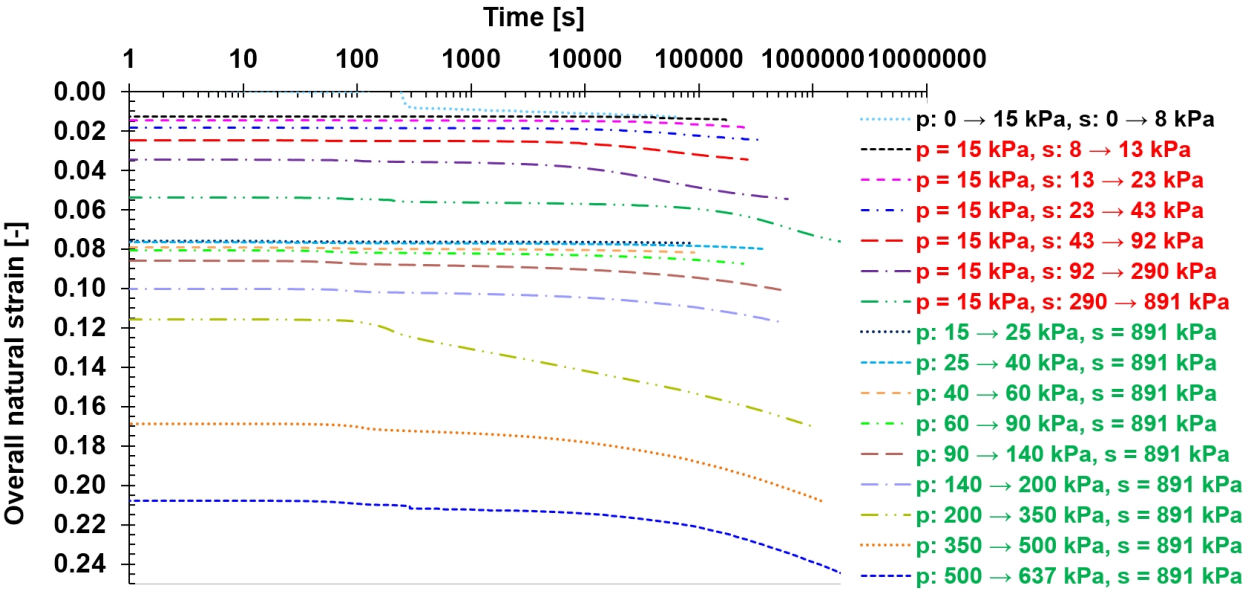

Figure 3.34. Isobars of the soil structure for the suction-controlled oedometer test U1 (unsaturated soil sample).

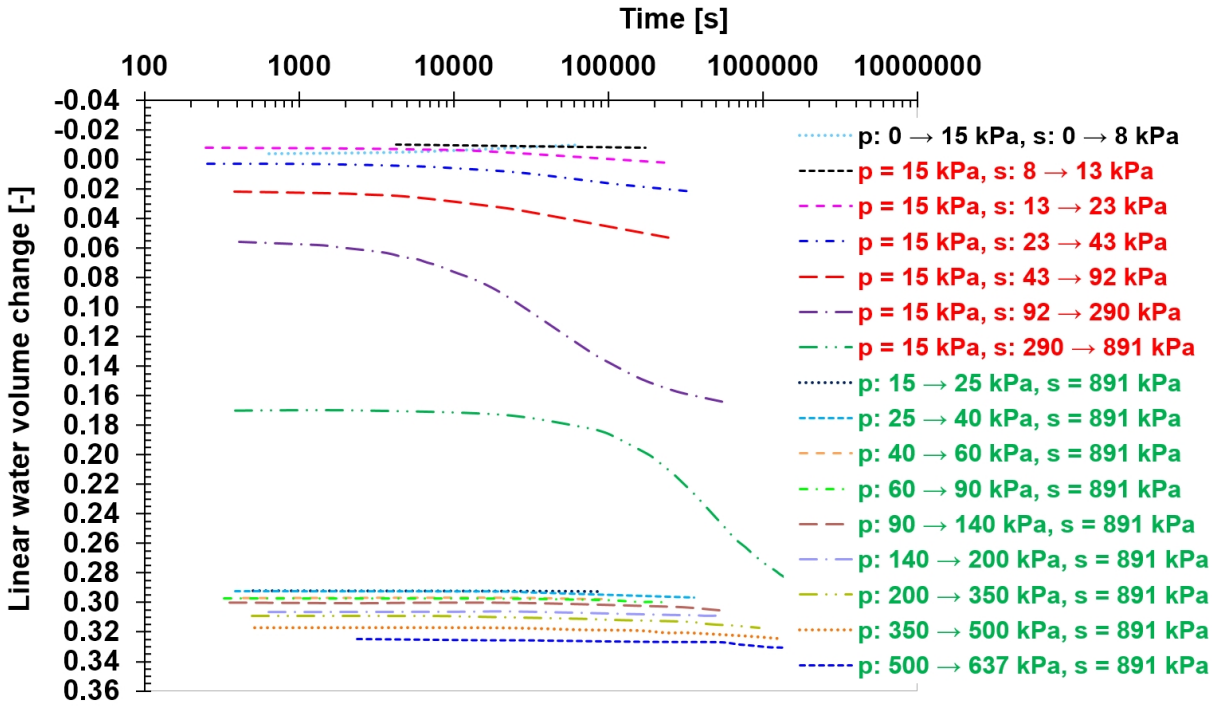

Figure 3.35. Isobars of the water phase for the suction-controlled oedometer test U1 (unsaturated soil sample).

Figure 3.36 shows the variations of the natural water mass change (ε_w^H) and the overall natural strain (ε_v^H) with matric suction, at a constant net normal stress of 15 kPa for the end of each step of the suction-controlled oedometer test U1. As can be seen in Figure 3.36 (as well as in Figures 3.49 and 3.62 for Tests U2 and U3), at a constant net normal stress when the applied matric suction is greater than the yield value, the slope of the natural water mass change curve is significantly steeper than the slope of the overall natural strain curve. Therefore, parameter b for the water phase is much larger than b for the soil structure at a constant net normal stress.

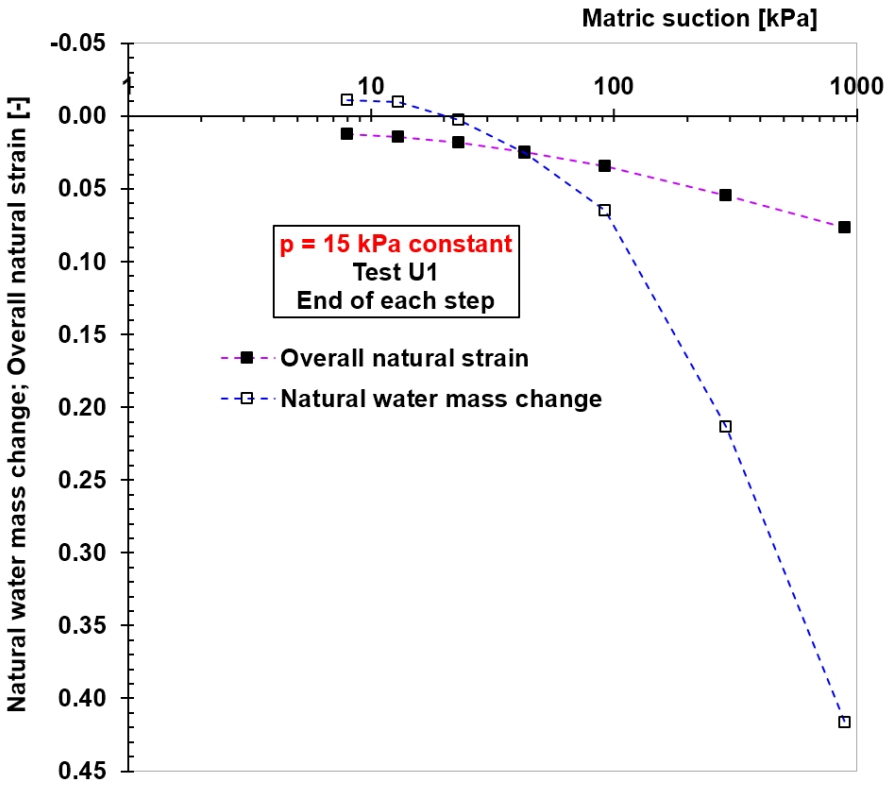

Figure 3.36. Variations of the natural water mass change (ε_w^H) and the overall natural strain (ε_v^H) with matric suction, at a constant net normal stress (*p*) for the suction-controlled oedometer test U1 (unsaturated soil sample).

Figure 3.37 presents the variations of the water ratio (e_w) and the void ratio (e) with matric suction, at a constant net normal stress of 15 kPa for the end of each step of the suction-controlled oedometer test U1. As can be seen in Figure 3.37 (as well as in Figures 3.50 and 3.63 for Tests U2 and U3), at a constant net normal stress when the applied matric suction is greater than the yield value, the slope of the water ratio curve is significantly steeper than the slope of the void ratio curve. Therefore, the air ratio ($e_a = e - e_w$, i.e., the vertical distance between two curves) increases with increasing matric suction. For each point on the curves, the degree of saturation can be obtained by: $Sr = e_w/e$.

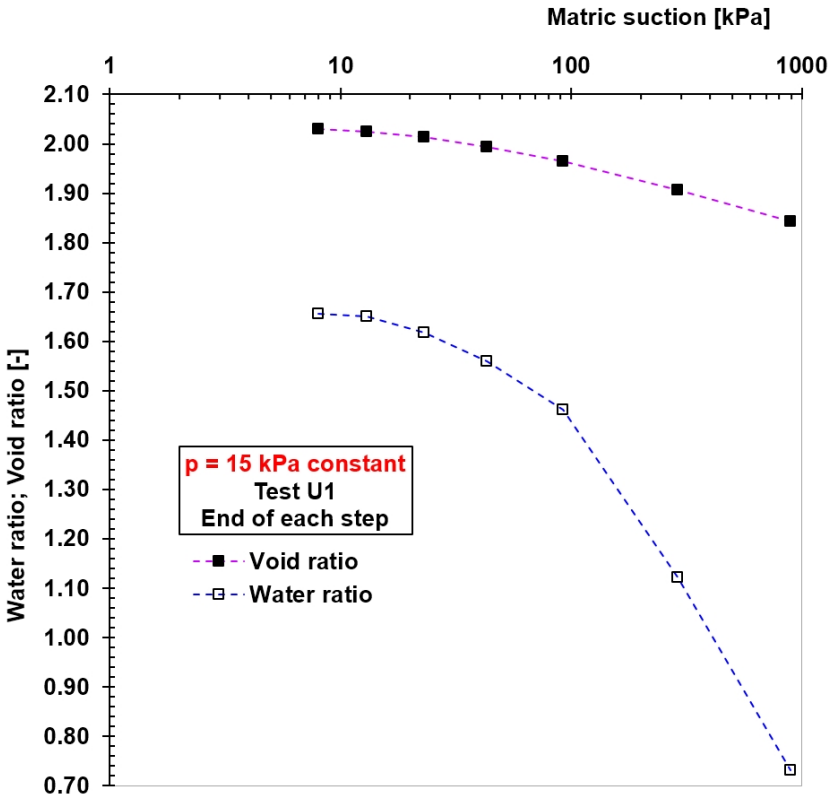

Figure 3.37. Variations of the water ratio (e_w) and the void ratio (e) with matric suction, at a constant net normal stress (p) for the suction-controlled oedometer test U1 (unsaturated soil sample).

Figure 3.38 shows the variations of the linear ($\varepsilon_w^{(\mathrm{lin})}$) and the momentary ($\varepsilon_w^m$) water volume change with matric suction, at a constant net normal stress of 15 kPa for the end of each step of the suction-controlled oedometer test U1. As can be seen in Figure 3.38 (as well as in Figures 3.51 and 3.64 for Tests U2 and U3), so long as the overall volume change of the soil sample is small, the difference between the linear and momentary water volume change is not significant.

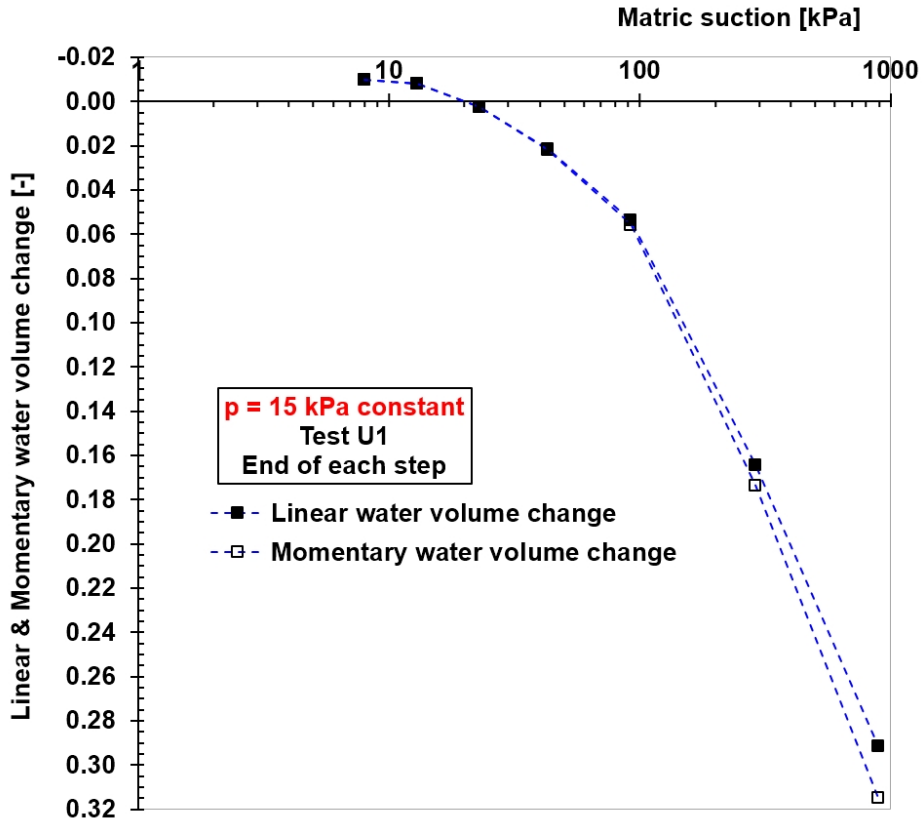

Figure 3.38. Variations of the linear ($\varepsilon_w^{(\mathrm{lin})}$) and the momentary ($\varepsilon_w^m$) water volume change with matric suction, at a constant net normal stress (p) for the suction-controlled oedometer test U1 (unsaturated soil sample).

Figure 3.39 presents the variations of the natural water mass change (ε_w^H) and the overall natural strain (ε_v^H) with net normal stress, at a constant matric suction of 891 kPa for the end of each step of the suction-controlled oedometer test U1. As can be seen in Figure 3.39 (as well as in Figures 3.52 and 3.65 for Tests U2 and U3), at a constant matric suction when the applied net normal stress is greater than the pre-consolidation value, the slope of the overall natural strain curve is significantly steeper than the slope of the natural water mass change curve. Therefore, parameter b for the soil structure is much larger than b for the water phase at a constant matric suction.

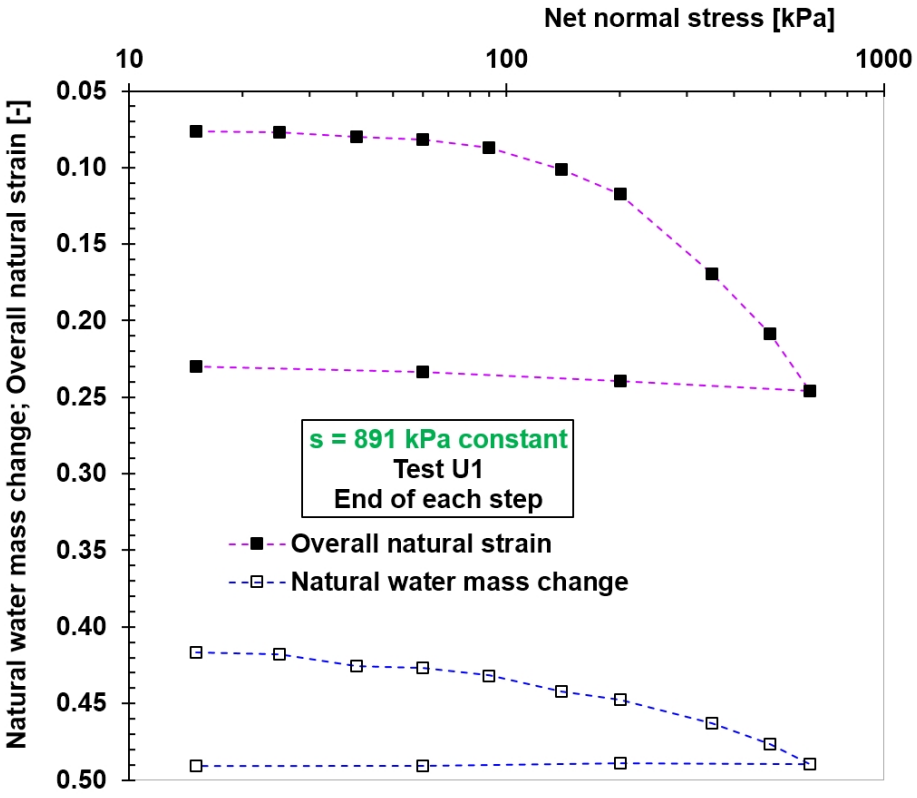

Figure 3.39. Variations of the natural water mass change (ε_w^H) and the overall natural strain (ε_v^H) with net normal stress, at a constant matric suction (s) for the suction-controlled oedometer test U1 (unsaturated soil sample).

Figure 3.40 shows the variations of the water ratio (e_w) and the void ratio (e) with net normal stress, at a constant matric suction of 891 kPa for the end of each step of the suction-controlled oedometer test U1. As can be seen in Figure 3.40 (as well as in Figures 3.53 and 3.66 for Tests U2 and U3), at a constant matric suction when the applied net normal stress is greater than the pre-consolidation value, the slope of the void ratio curve is significantly steeper than the slope of the water ratio curve. Therefore, the air ratio ($e_a = e - e_w$, i.e., the vertical distance between two curves) decreases with increasing net normal stress. For each point on the curves, the degree of saturation can be obtained by: $Sr = e_w/e$.

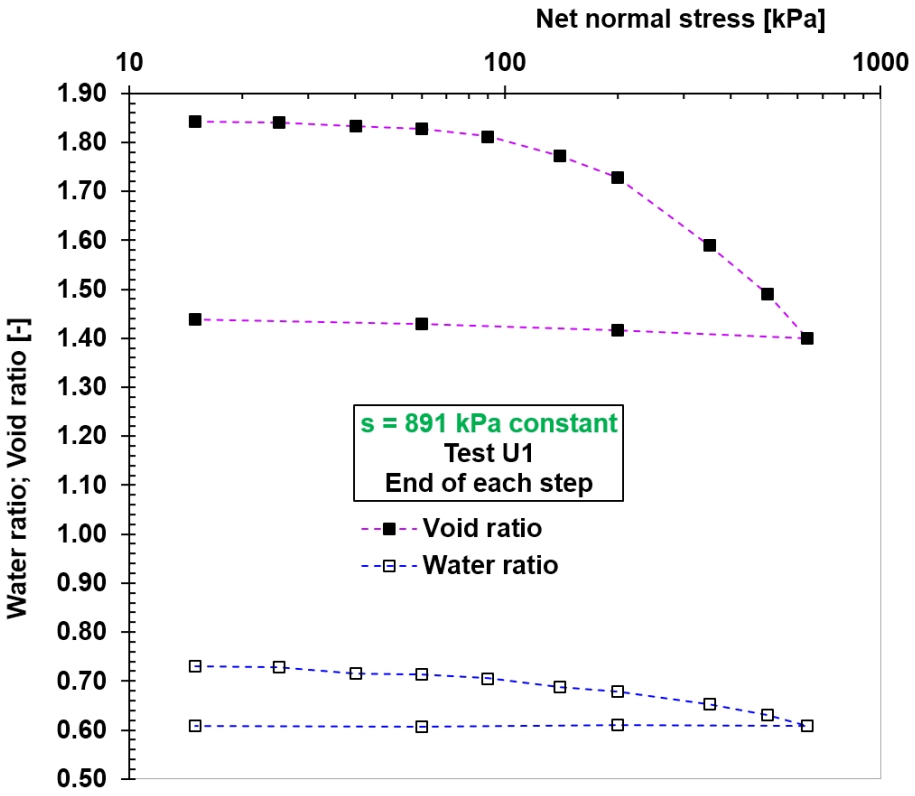

Figure 3.40. Variations of the water ratio (e_w) and the void ratio (e) with net normal stress, at a constant matric suction (s) for the suction-controlled oedometer test U1 (unsaturated soil sample).

Figure 3.41 presents the variations of the linear ($\varepsilon_w^{(\mathrm{lin})}$) and the momentary ($\varepsilon_w^m$) water volume change with net normal stress, at a constant matric suction of 891 kPa for the end of each step of the suction-controlled oedometer test U1. When the overall volume is decreasing, the slopes of the momentary water volume change (versus net normal stress or matric suction) are always greater than the slopes of the linear water volume change, because: $V_{\mathrm{current}} \leq V_0$. As can be seen in this figure, the unloading branch of the "linear water volume change" curve and the unloading branch of the "momentary water volume change" curve show different behaviours. The linear water volume change continues to increase with decreasing net normal stress, whereas the momentary water volume change decreases with decreasing net normal stress. This behaviour can also be seen for the unloading branch in Test U2 at a constant matric suction of 290 kPa (Figure 3.54). However, in Test U3, at a constant matric suction of 92 kPa (i.e., the lowest constant matric suction in this study), the behaviours of the two unloading branches are similar (Figure 3.67). Therefore, it can be concluded that, when the constant matric suction is high, the water volume change continues to increase during unloading of net normal stress. In other words, when the constant matric suction is high, decreasing net normal stress does not increase the water volume of the soil sample (see also Figure 3.32 for Test U1 and Figure 3.45 for Test U2). However, under this condition, the degree of saturation decreases due to the increasing overall volume of the soil sample (see Figure 3.33 for Test U1 and Figure 3.46 for Test U2).

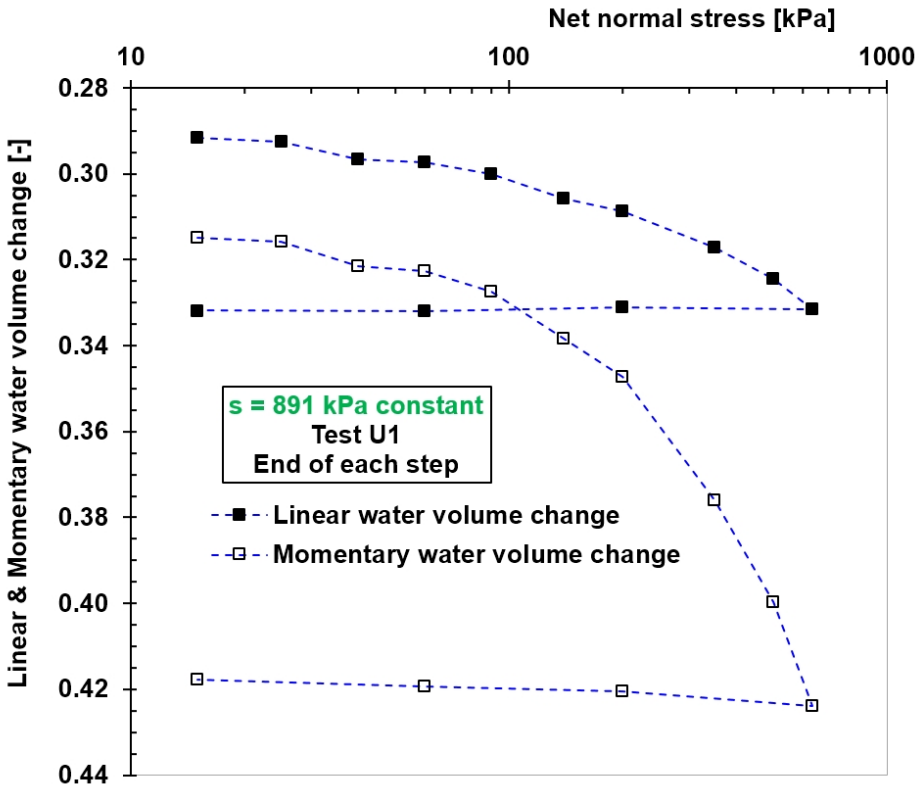

Figure 3.41. Variations of the linear ($\varepsilon_w^{(\mathrm{lin})}$) and the momentary ($\varepsilon_w^m$) water volume change with net normal stress, at a constant matric suction (*s*) for the suction-controlled oedometer test U1 (unsaturated soil sample).

Figure 3.42 shows the relationship between the water ratio (e_w) and the void ratio (e) during the suction-controlled oedometer test U1 under increasing matric suction and net normal stress. Unloading of net normal stress and decreasing matric suction are not included in this figure. The slope of the water ratio versus the void ratio in this figure changes significantly on the left side of point L.

Airò Farulla (2008) studied the $\Delta e_w/\Delta e$ ratios (change in water ratio divided by change in void ratio) for "a compacted scaly clay stressed by wetting and drying cycles in suction-controlled oedometer tests" and he detected that "the $\Delta e_w/\Delta e$ ratios were almost constant as the cycles accumulated" in the reversible condition (p. 323).

The $\Delta e_w/\Delta e$ ratios proposed by Airò Farulla (2008) for the compacted organic soil shows that the average value of $\Delta e_w/\Delta e$ on the right side of point L (Figure 3.42) is about 5.6, whereas this value immediately reduces to about 0.2 on the left side of this point. Point L represents the minimum degree of saturation ($Sr = e_w/e$) during the entire test period (see also Figure 3.33).

The presentation method used in Figure 3.42 (as well as in Figures 3.55 and 3.68 for Tests U2 and U3) is somewhat similar to that used by Airò Farulla, Battiato, and Ferrari (2011, p. 421, fig. 4).

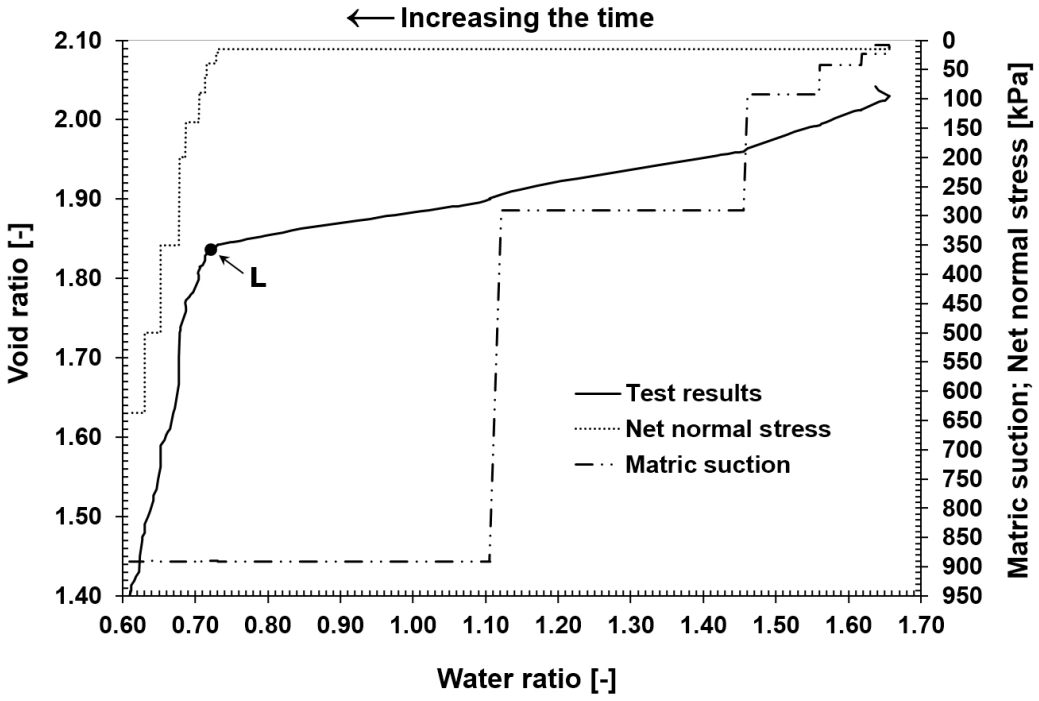

Figure 3.42. Relationship between the water ratio (e_w) and the void ratio (e) for increasing matric suction and net normal stress during the suction-controlled oedometer test U1 (unsaturated soil sample).

3.5.4.2 Test U2

In Test U2, the matric suction was increased incrementally up to 290 kPa at a constant net normal stress of 5 kPa. Then the net normal stress was increased incrementally up to 496 kPa at a constant matric suction of 290 kPa.

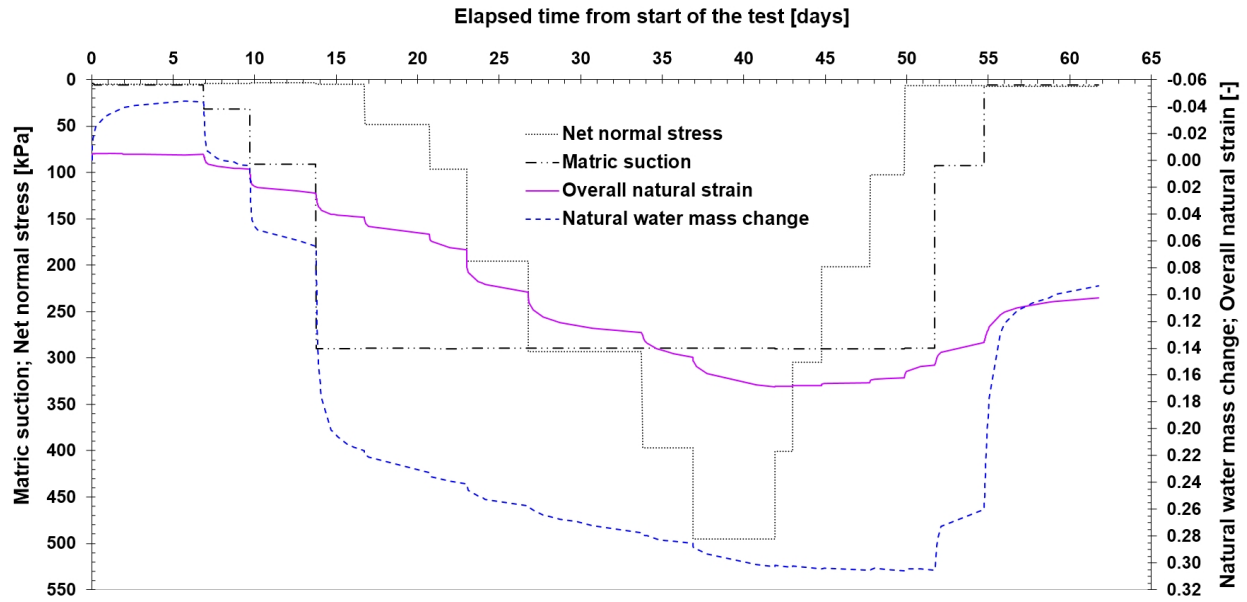

Figure 3.43. Continuous monitoring of the natural water mass change (ε_w^H) and the overall natural strain (ε_v^H) for the suction-controlled oedometer test U2 (unsaturated soil sample).

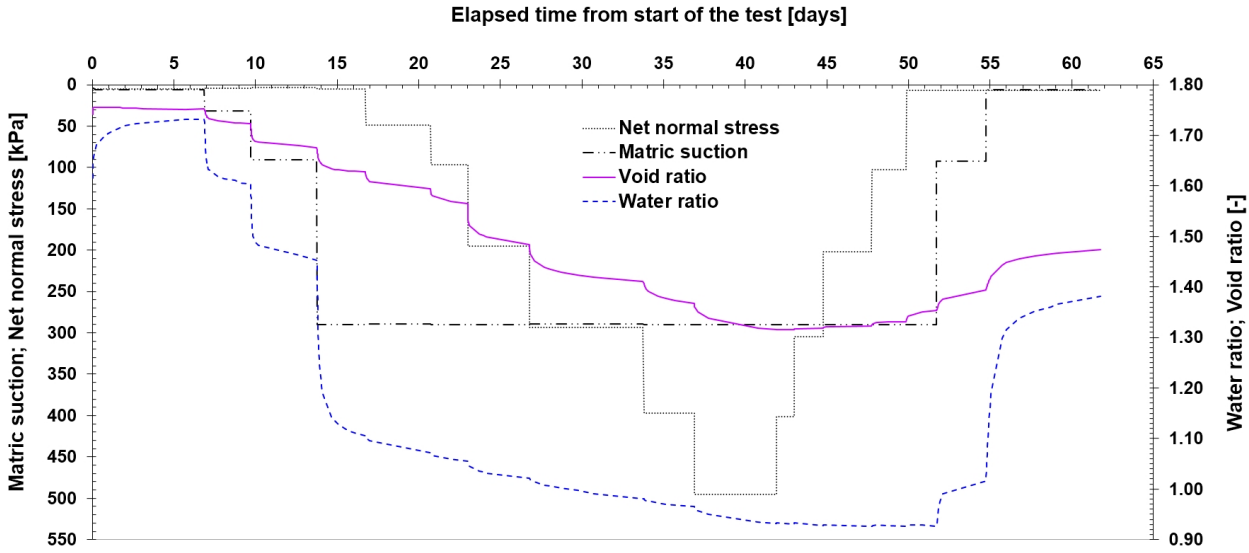

Figure 3.44. Continuous monitoring of the water ratio (e_w) and the void ratio (e) for the suction-controlled oedometer test U2 (unsaturated soil sample).

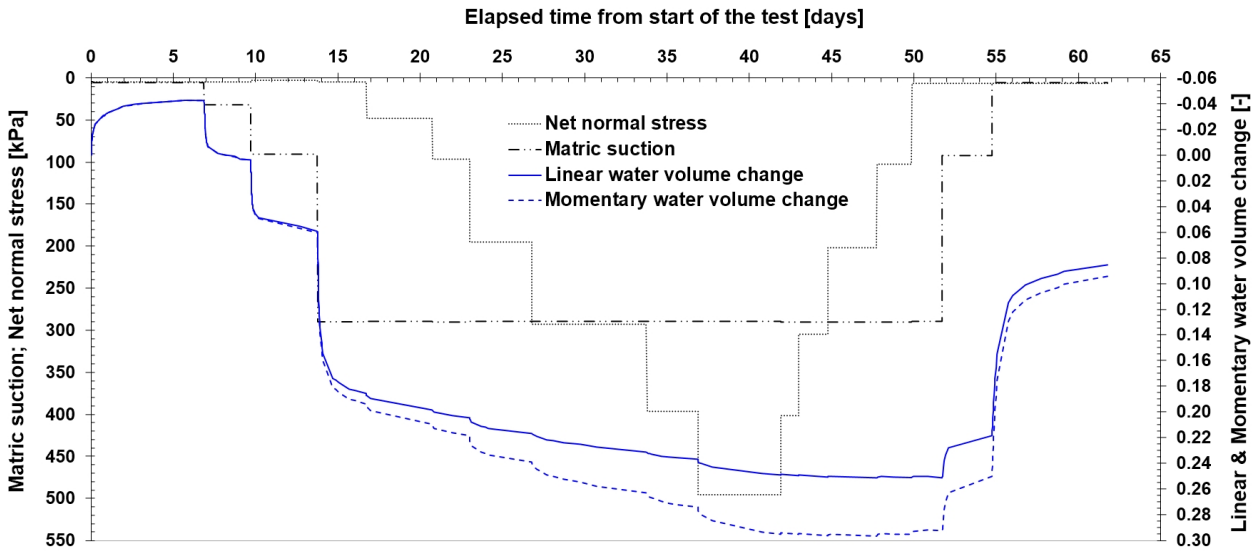

Figure 3.45. Continuous monitoring of the linear ($\varepsilon_w^{(\mathrm{lin})}$) and the momentary ($\varepsilon_w^m$) water volume change for the suction-controlled oedometer test U2 (unsaturated soil sample).

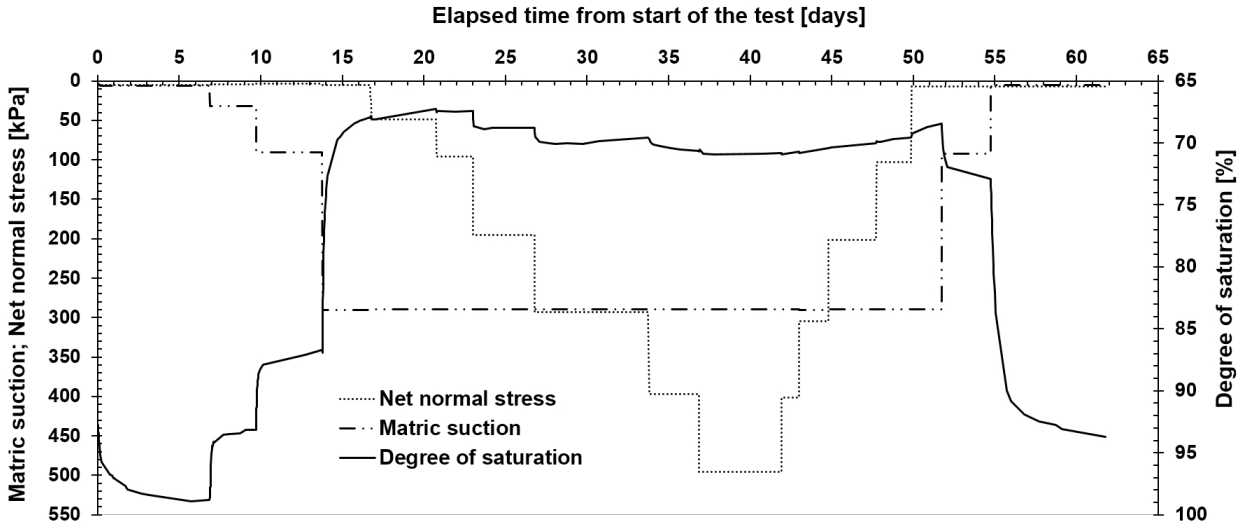

Figure 3.46. Continuous monitoring of the degree of saturation for the suction-controlled oedometer test U2 (unsaturated soil sample).

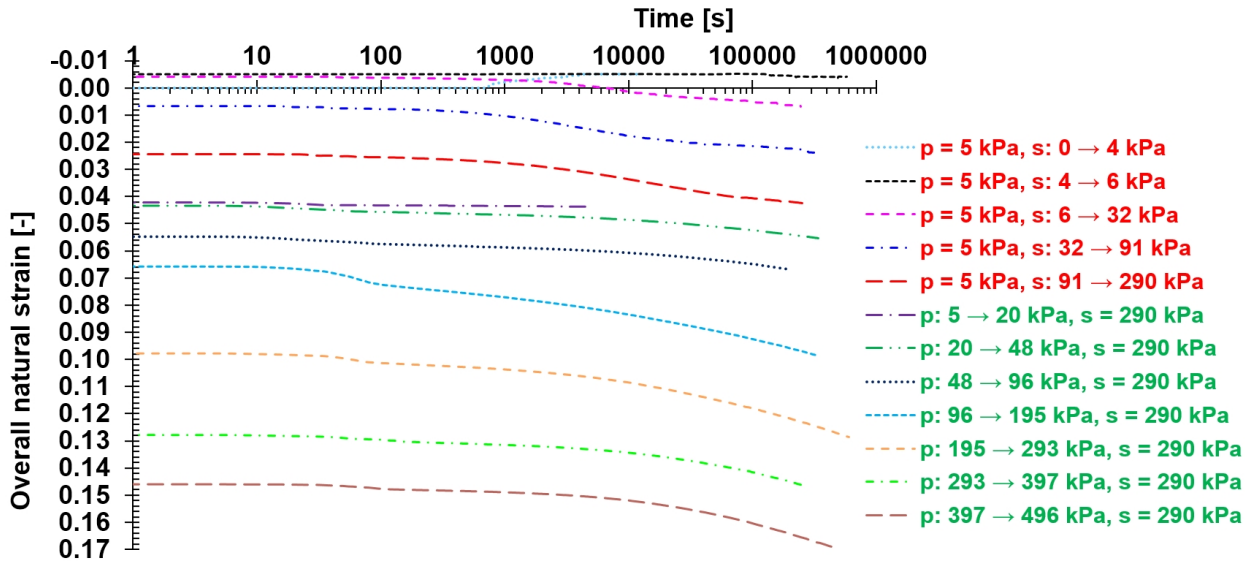

Figure 3.47. Isobars of the soil structure for the suction-controlled oedometer test U2 (unsaturated soil sample).

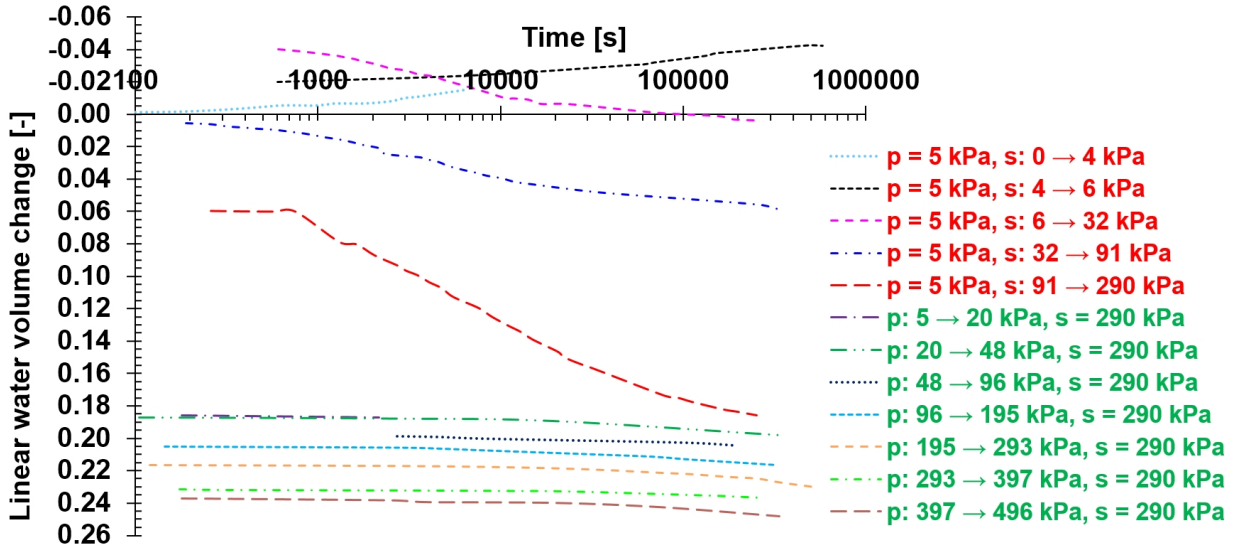

Figure 3.48. Isobars of the water phase for the suction-controlled oedometer test U2 (unsaturated soil sample).

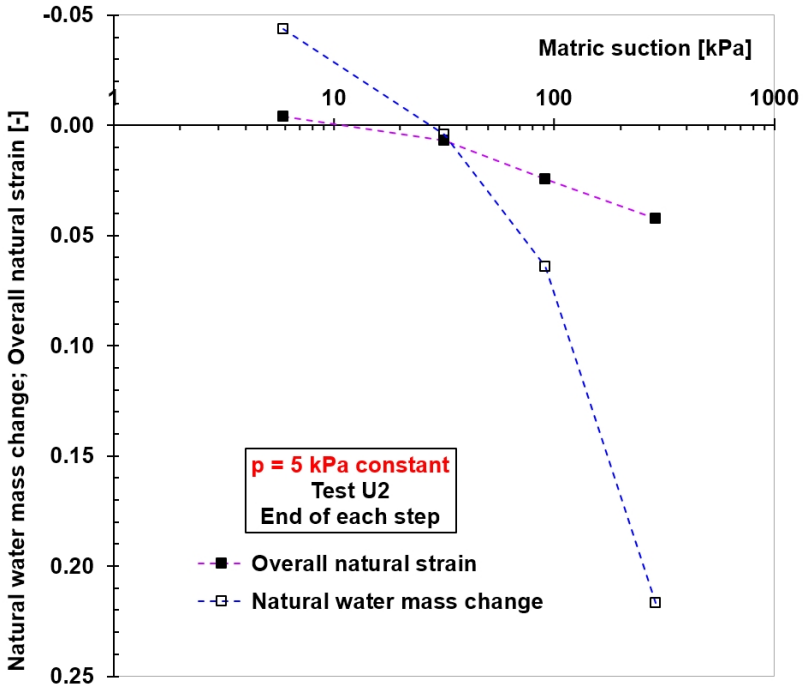

Figure 3.49. Variations of the natural water mass change (ε_w^H) and the overall natural strain (ε_v^H) with matric suction, at a constant net normal stress (p) for the suction-controlled oedometer test U2 (unsaturated soil sample).

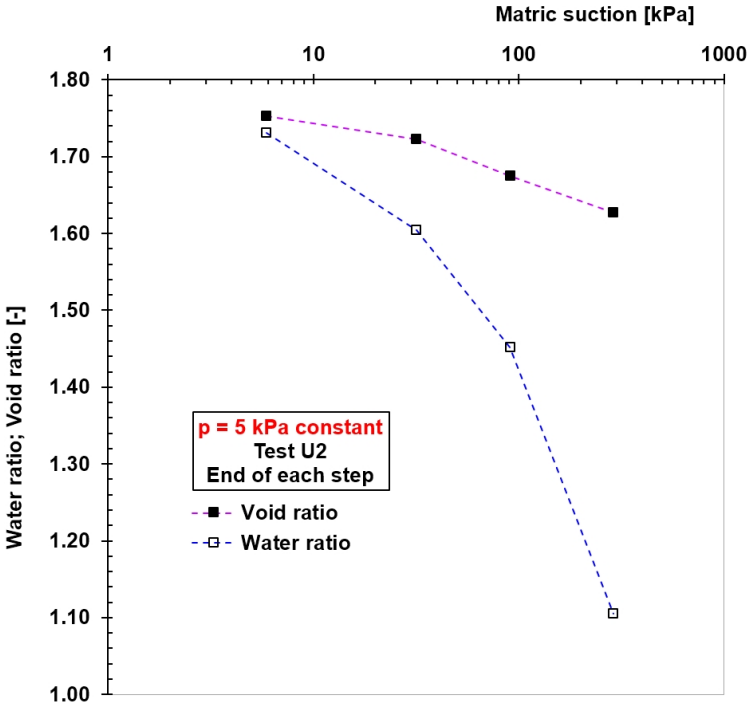

Figure 3.50. Variations of the water ratio (e_w) and the void ratio (e) with matric suction, at a constant net normal stress (p) for the suction-controlled oedometer test U2 (unsaturated soil sample).

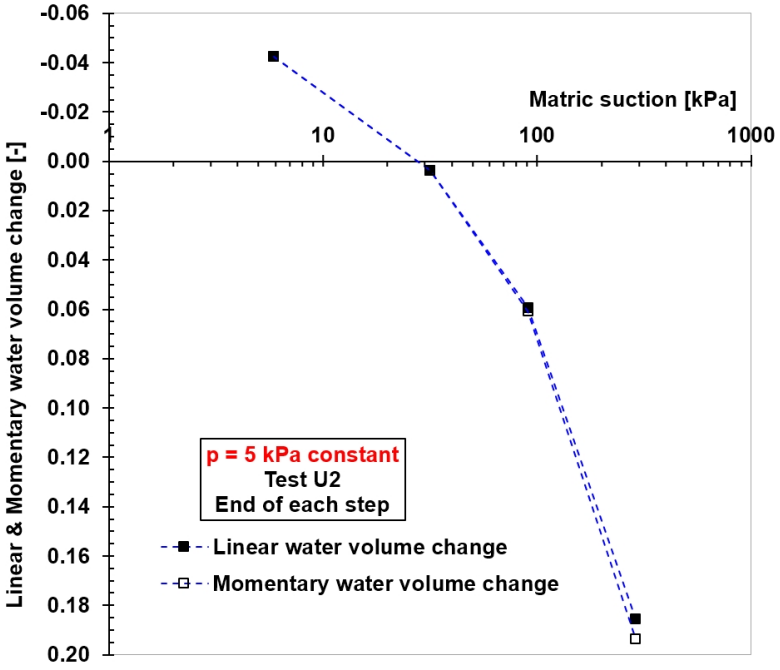

Figure 3.51. Variations of the linear ($\varepsilon_w^{(\mathrm{lin})}$) and the momentary ($\varepsilon_w^m$) water volume change with matric suction, at a constant net normal stress (*p*) for the suction-controlled oedometer test U2 (unsaturated soil sample).

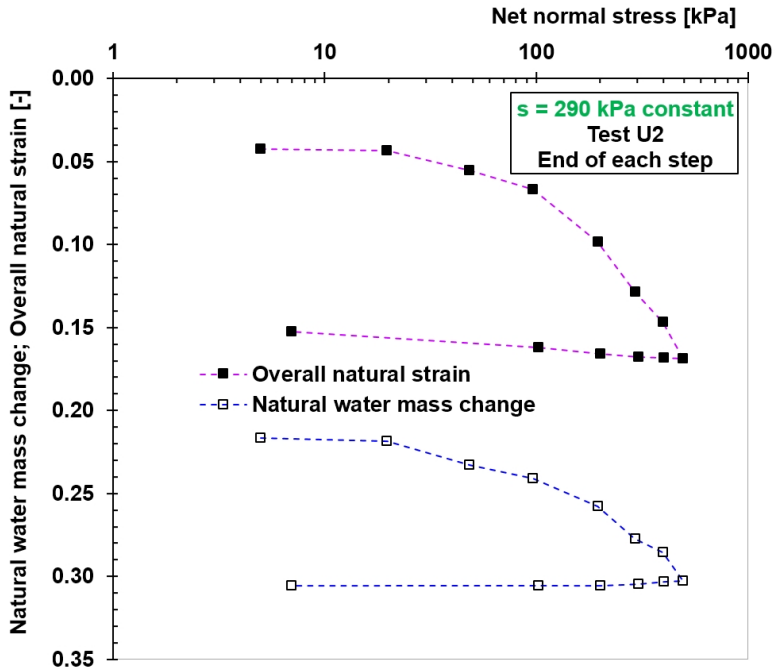

Figure 3.52. Variations of the natural water mass change (ε_w^H) and the overall natural strain (ε_v^H) with net normal stress, at a constant matric suction (*s*) for the suction-controlled oedometer test U2 (unsaturated soil sample).

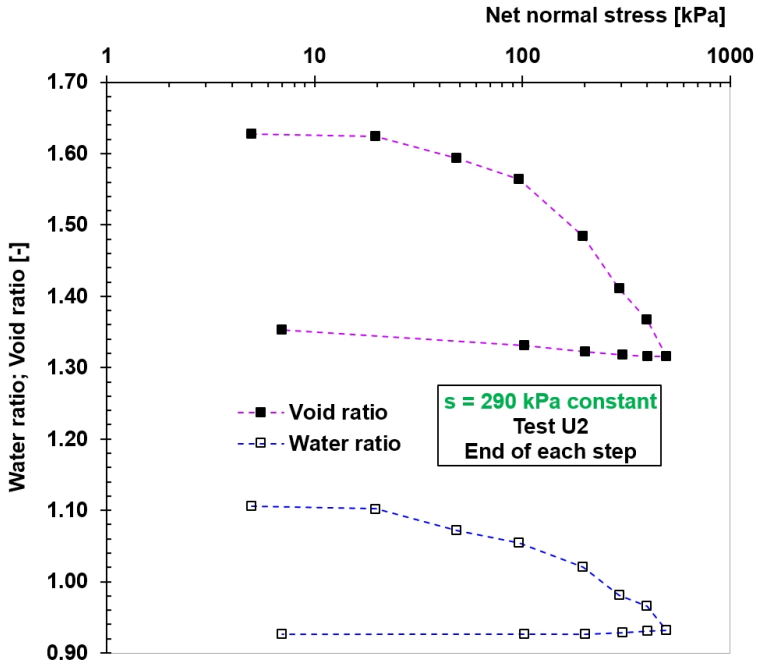

Figure 3.53. Variations of the water ratio (e_w) and the void ratio (e) with net normal stress, at a constant matric suction (s) for the suction-controlled oedometer test U2 (unsaturated soil sample).

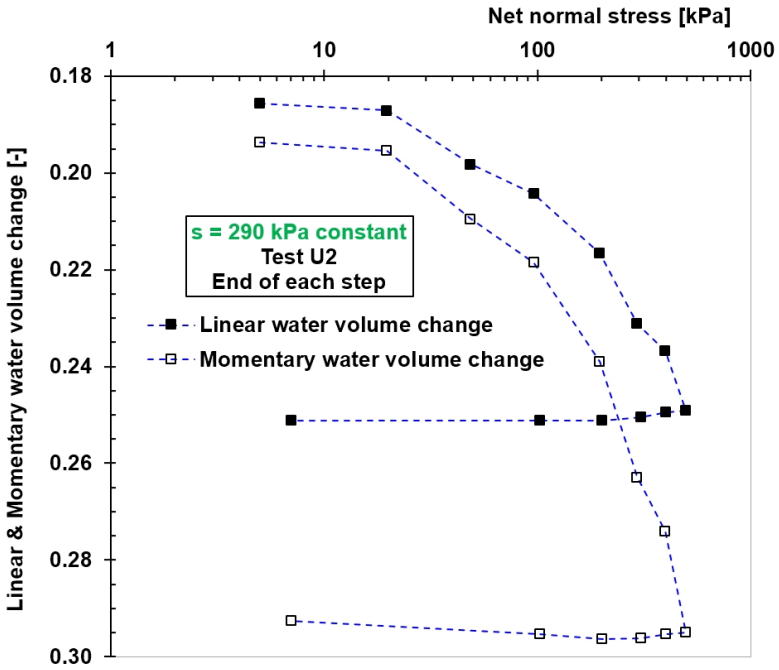

Figure 3.54. Variations of the linear ($\varepsilon_w^{(\mathrm{lin})}$) and the momentary ($\varepsilon_w^m$) water volume change with net normal stress, at a constant matric suction (s) for the suction-controlled oedometer test U2 (unsaturated soil sample).

Figure 3.55 shows the relationship between the water ratio (e_w) and the void ratio (e) during the suction-controlled oedometer test U2 under increasing matric suction and net normal stress. Unloading of net normal stress and decreasing matric suction are not included in this figure. The slope of the water ratio versus the void ratio in this figure changes significantly on the left side of point L, which is similar to the results of Test U1. An average value of $\Delta e_w/\Delta e$ (change in water ratio divided by change in void ratio) on the right side of this point is about 6.7, whereas this value immediately reduces to about 0.5 on the left side of this point. Point L represents the minimum degree of saturation ($Sr = e_w/e$) during the entire test period (see also Figure 3.46).

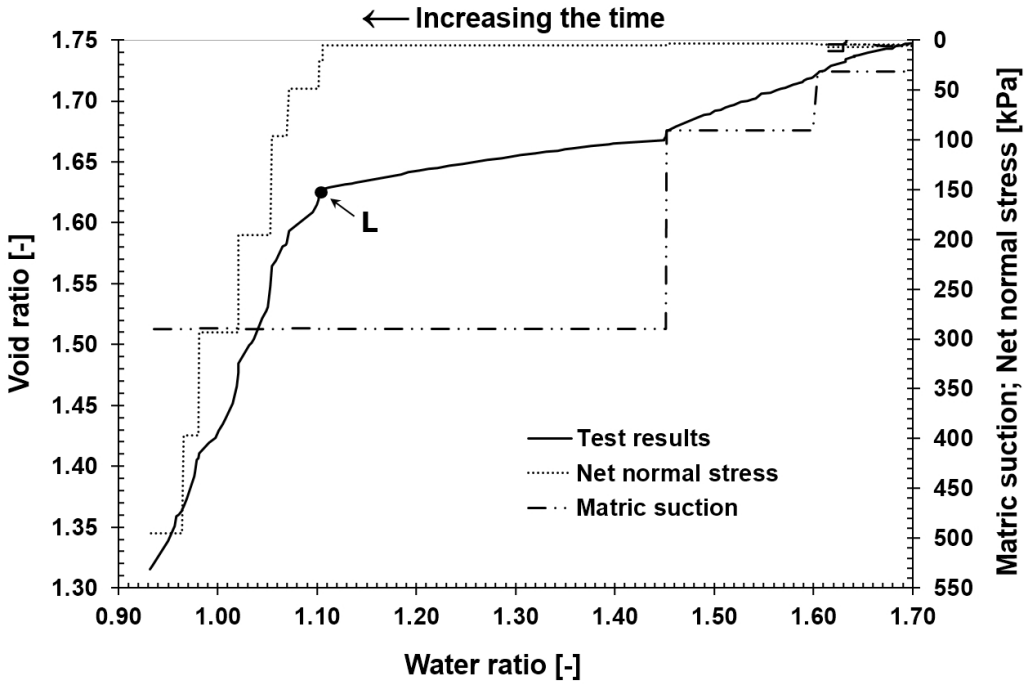

Figure 3.55. Relationship between the water ratio (e_w) and the void ratio (e) for increasing matric suction and net normal stress during the suction-controlled oedometer test U2 (unsaturated soil sample).

3.5.4.3 Test U3

In Test U3, the matric suction was increased incrementally up to 92 kPa at a constant net normal stress of 15 kPa. Then the net normal stress was increased incrementally up to 499 kPa at a constant matric suction of 92 kPa.

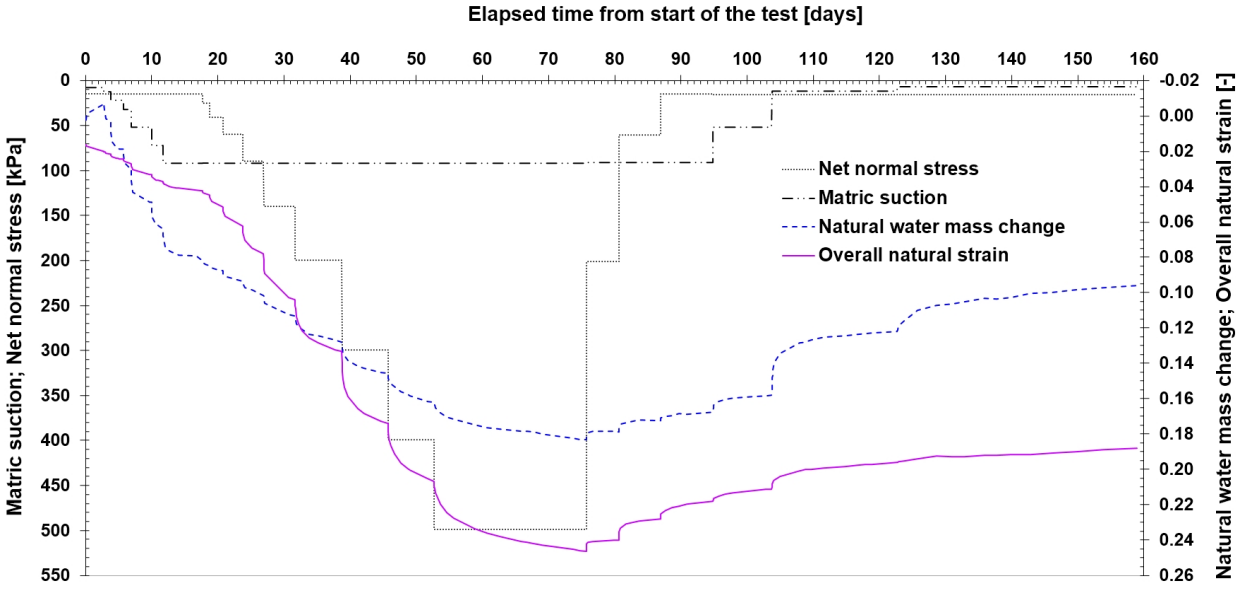

Figure 3.56. Continuous monitoring of the natural water mass change (ε_w^H) and the overall natural strain (ε_v^H) for the suction-controlled oedometer test U3 (unsaturated soil sample).

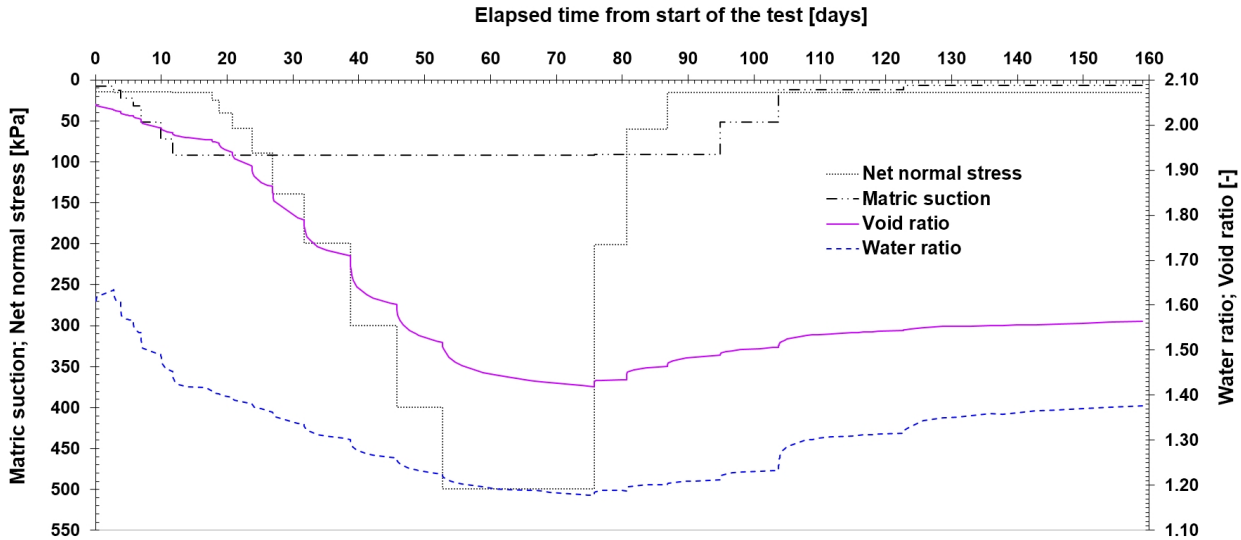

Figure 3.57. Continuous monitoring of the water ratio (e_w) and the void ratio (e) for the suction-controlled oedometer test U3 (unsaturated soil sample).

Figure 3.58 compares the linear ($\varepsilon_w^{(\mathrm{lin})}$) and the momentary ($\varepsilon_w^m$) water volume change for the suction-controlled oedometer test U3 on the unsaturated soil sample. In contrast to Tests U1 and U2 (see Figures 3.32 and 3.45), the water volume of the soil sample in test U3 increased during unloading of net normal stress because the constant matric suction was lower in this test.

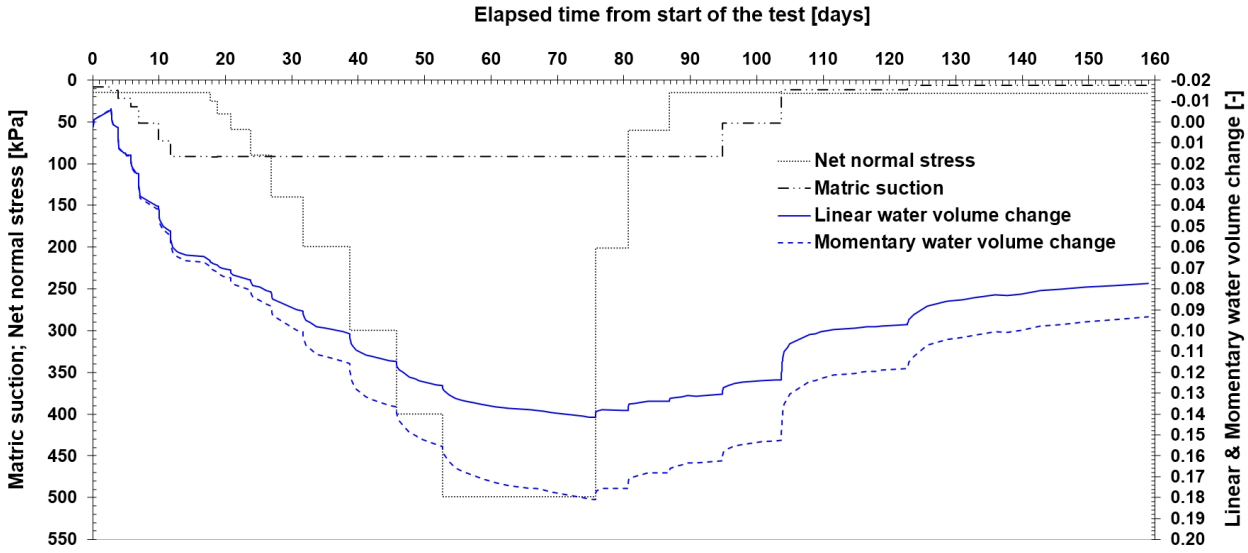

Figure 3.58. Continuous monitoring of the linear ($\varepsilon_w^{(\mathrm{lin})}$) and the momentary ($\varepsilon_w^m$) water volume change for the suction-controlled oedometer test U3 (unsaturated soil sample).

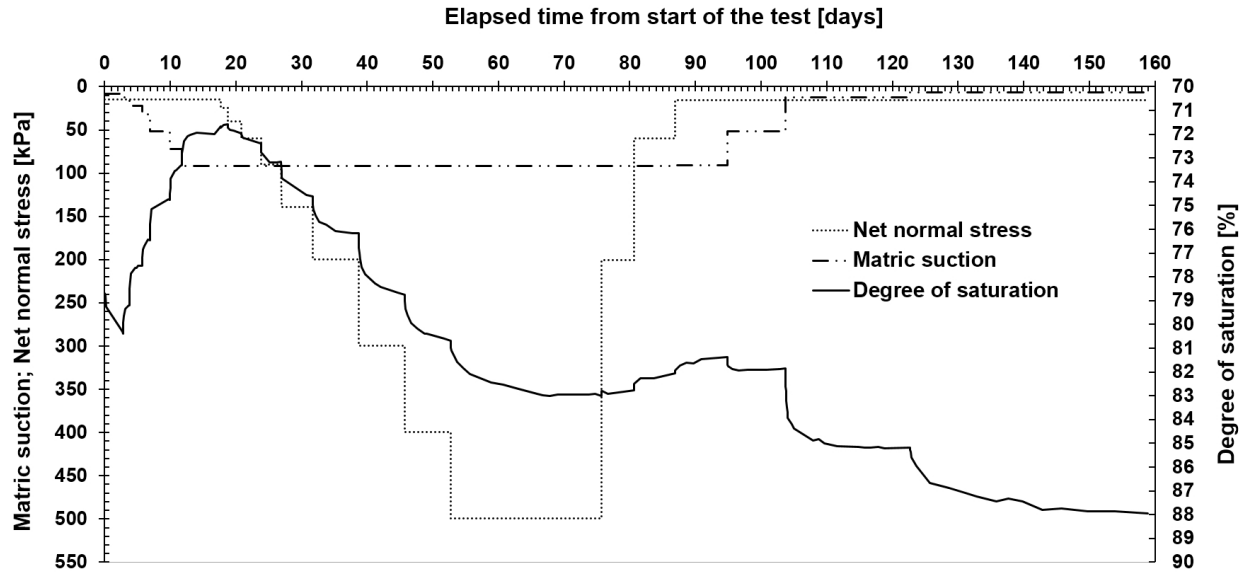

Figure 3.59. Continuous monitoring of the degree of saturation for the suction-controlled oedometer test U3 (unsaturated soil sample).

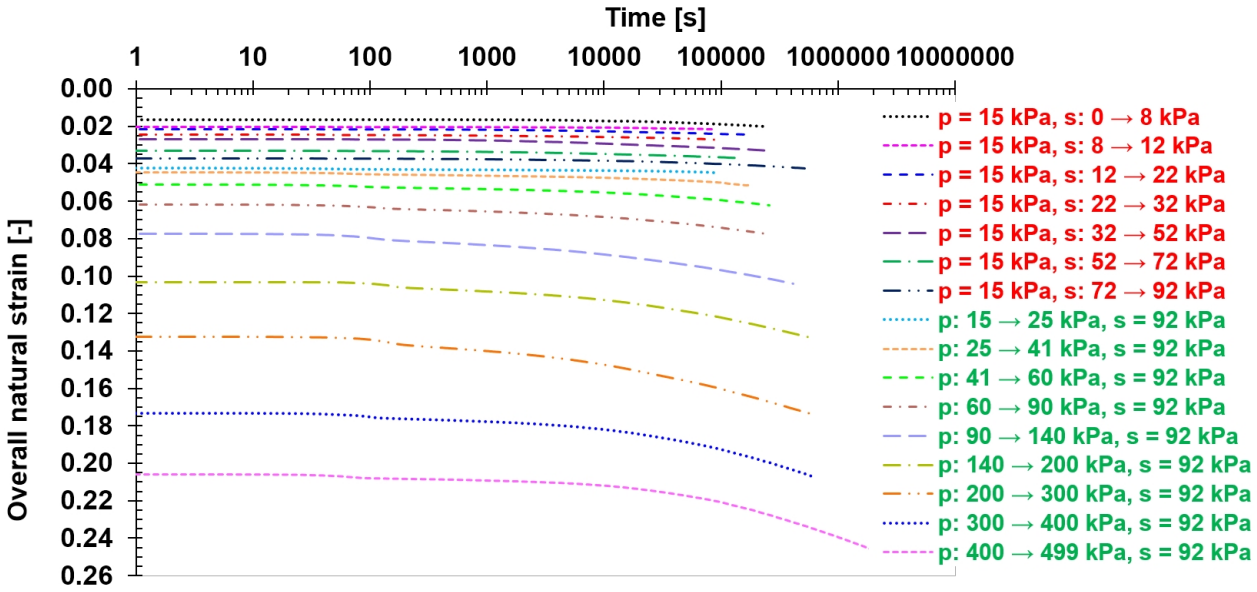

Figure 3.60. Isobars of the soil structure for the suction-controlled oedometer test U3 (unsaturated soil sample).

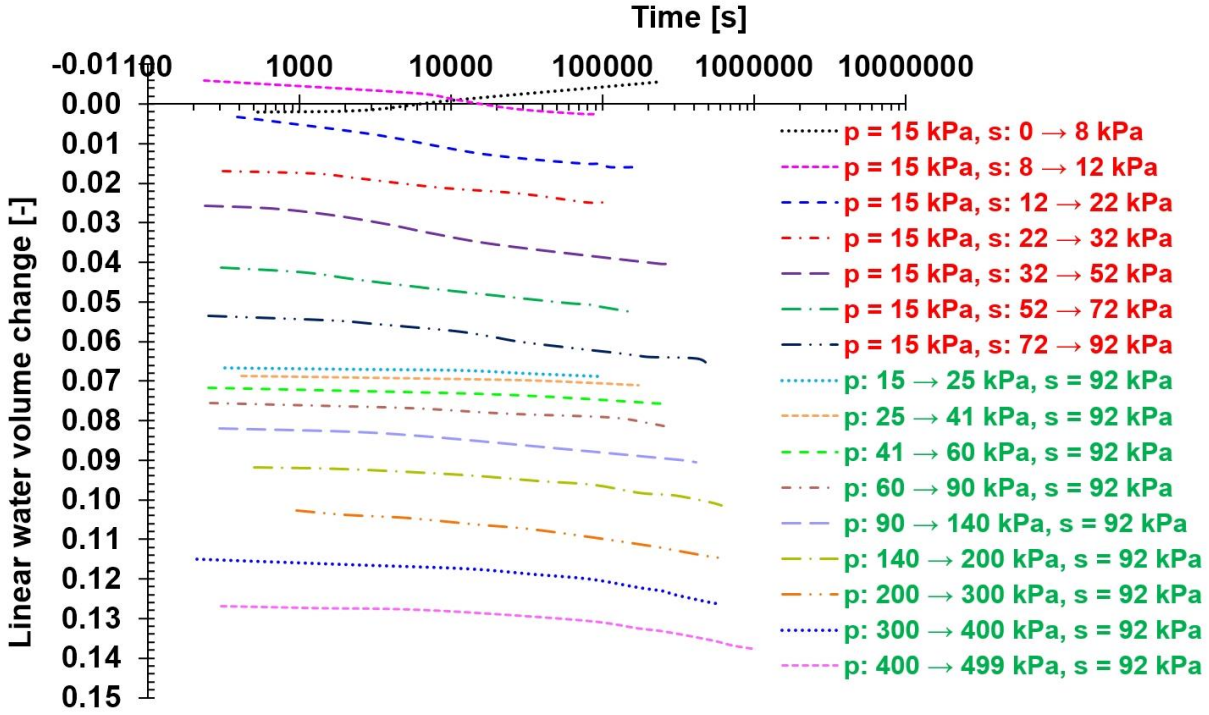

Figure 3.61. Isobars of the water phase for the suction-controlled oedometer test U3 (unsaturated soil sample).

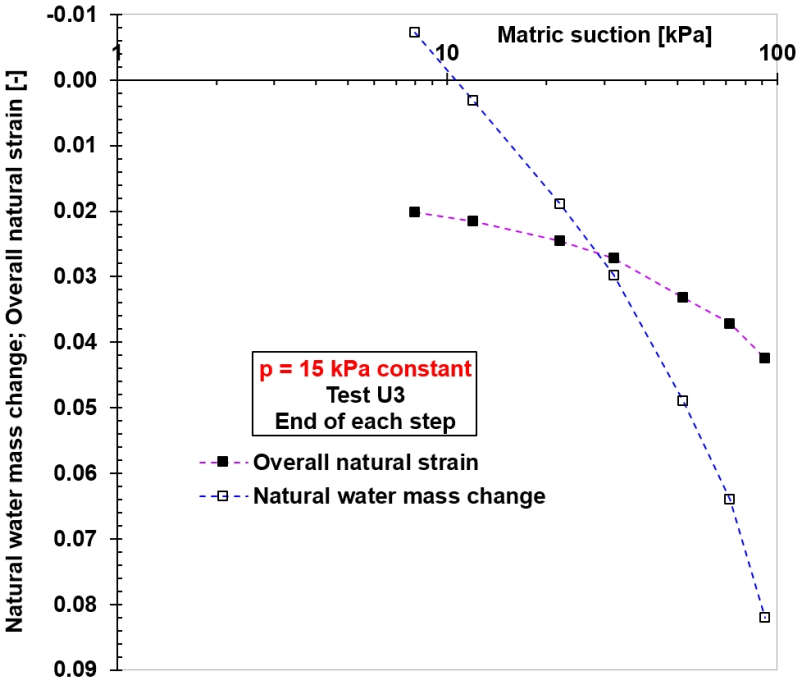

Figure 3.62. Variations of the natural water mass change (ε_w^H) and the overall natural strain (ε_v^H) with matric suction, at a constant net normal stress (p) for the suction-controlled oedometer test U3 (unsaturated soil sample).

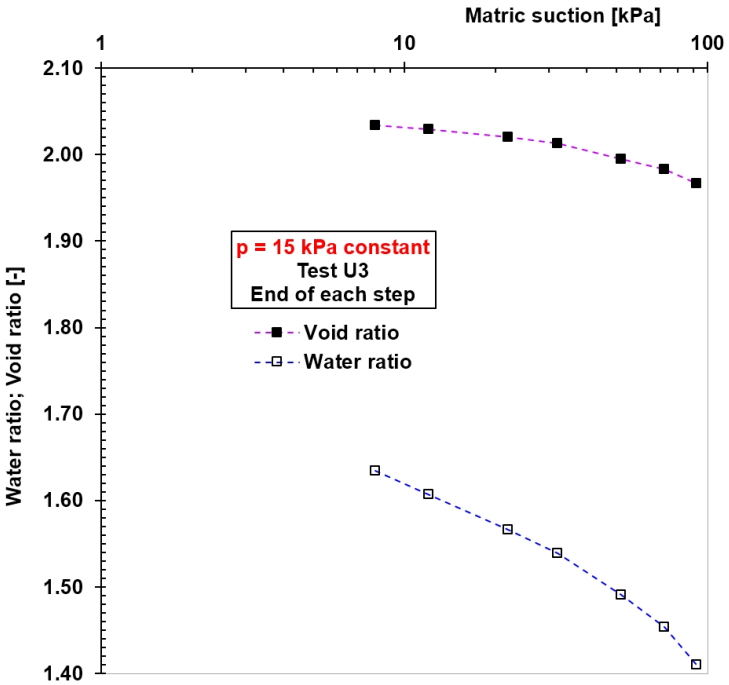

Figure 3.63. Variations of the water ratio (e_w) and the void ratio (e) with matric suction, at a constant net normal stress (p) for the suction-controlled oedometer test U3 (unsaturated soil sample).

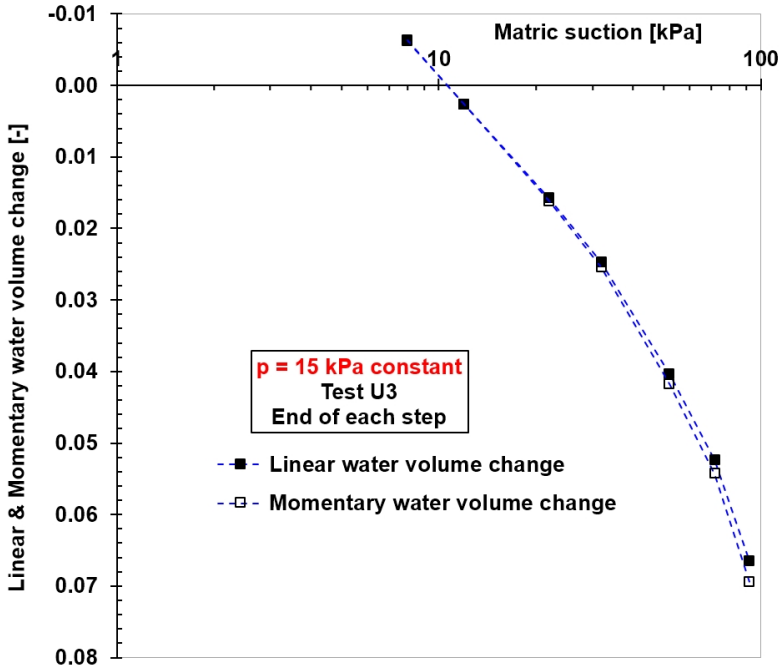

Figure 3.64. Variations of the linear ($\varepsilon_w^{(\mathrm{lin})}$) and the momentary ($\varepsilon_w^m$) water volume change with matric suction, at a constant net normal stress (p) for the suction-controlled oedometer test U3 (unsaturated soil sample).

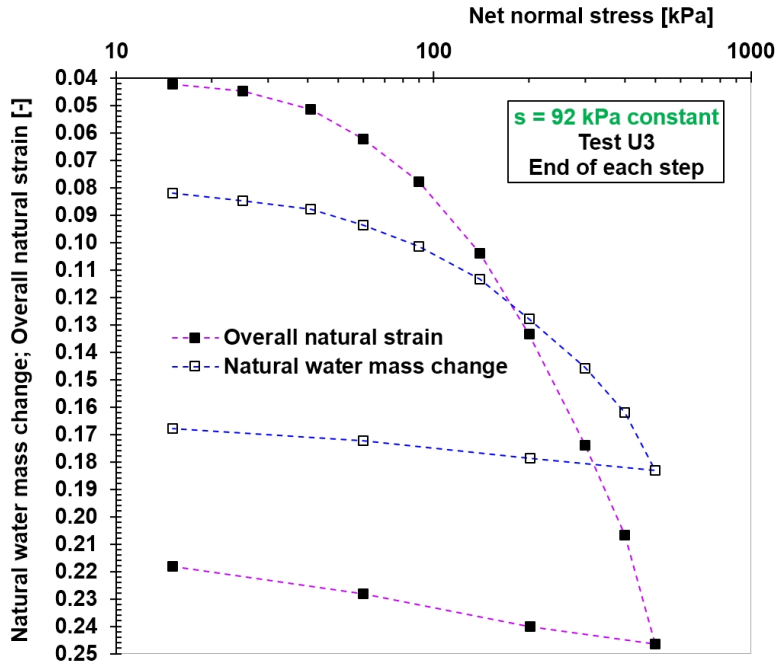

Figure 3.65. Variations of the natural water mass change (ε_w^H) and the overall natural strain (ε_v^H) with net normal stress, at a constant matric suction (s) for the suction-controlled oedometer test U3 (unsaturated soil sample).

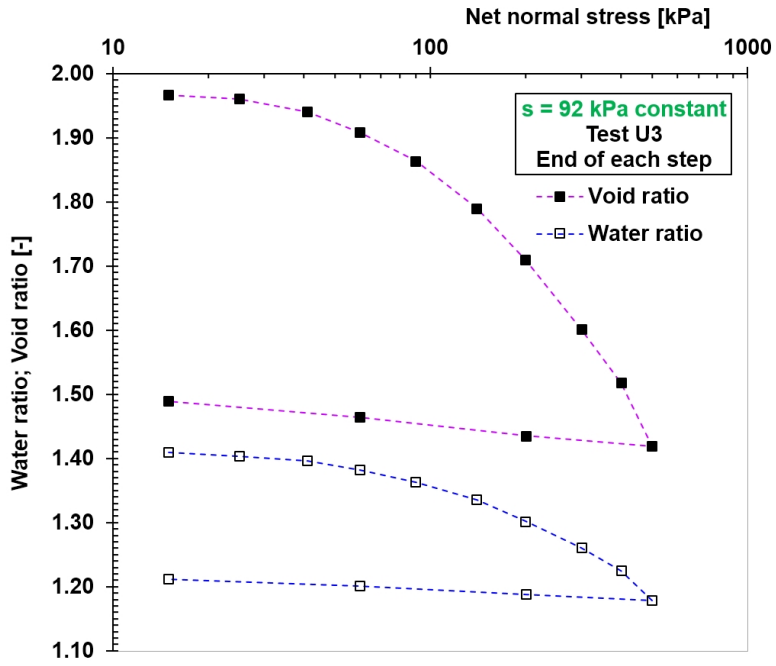

Figure 3.66. Variations of the water ratio (e_w) and the void ratio (e) with net normal stress, at a constant matric suction (s) for the suction-controlled oedometer test U3 (unsaturated soil sample).

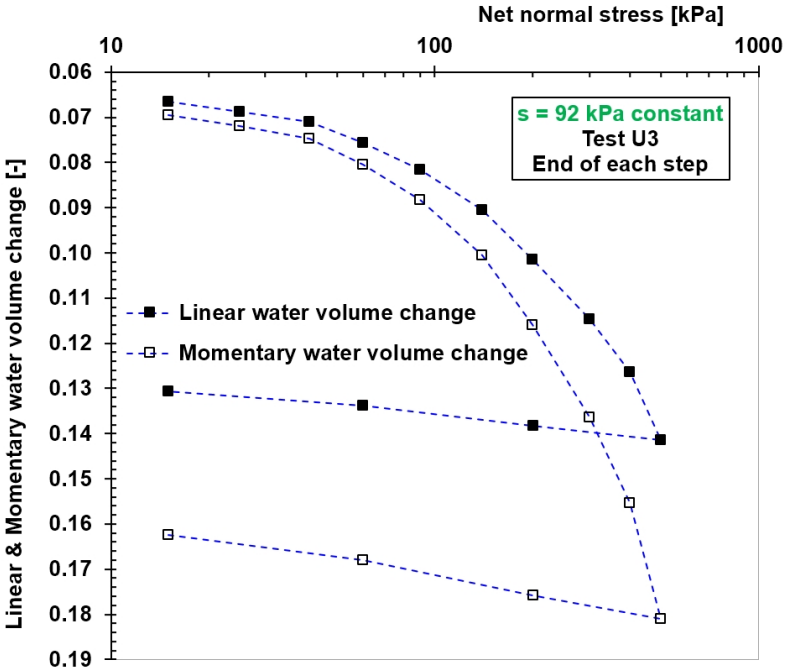

Figure 3.67. Variations of the linear ($\varepsilon_w^{(\mathrm{lin})}$) and the momentary ($\varepsilon_w^m$) water volume change with net normal stress, at a constant matric suction (s) for the suction-controlled oedometer test U3 (unsaturated soil sample).

Figure 3.68 shows the relationship between the water ratio (e_w) and the void ratio (e) during the suction-controlled oedometer test U3 under increasing matric suction and net normal stress. Unloading of net normal stress and decreasing matric suction are not included in this figure. The slope of the water ratio versus the void ratio in this figure changes significantly on the left side of point L, which is similar to the results of Tests U1 and U2. An average value of $\Delta e_w/\Delta e$ (change in water ratio divided by change in void ratio) on the right side of this point is about 3.1, whereas this value immediately reduces to about 0.4 on the left side of this point. Point L represents the minimum degree of saturation ($Sr = e_w/e$) during the entire test period (see also Figure 3.59).

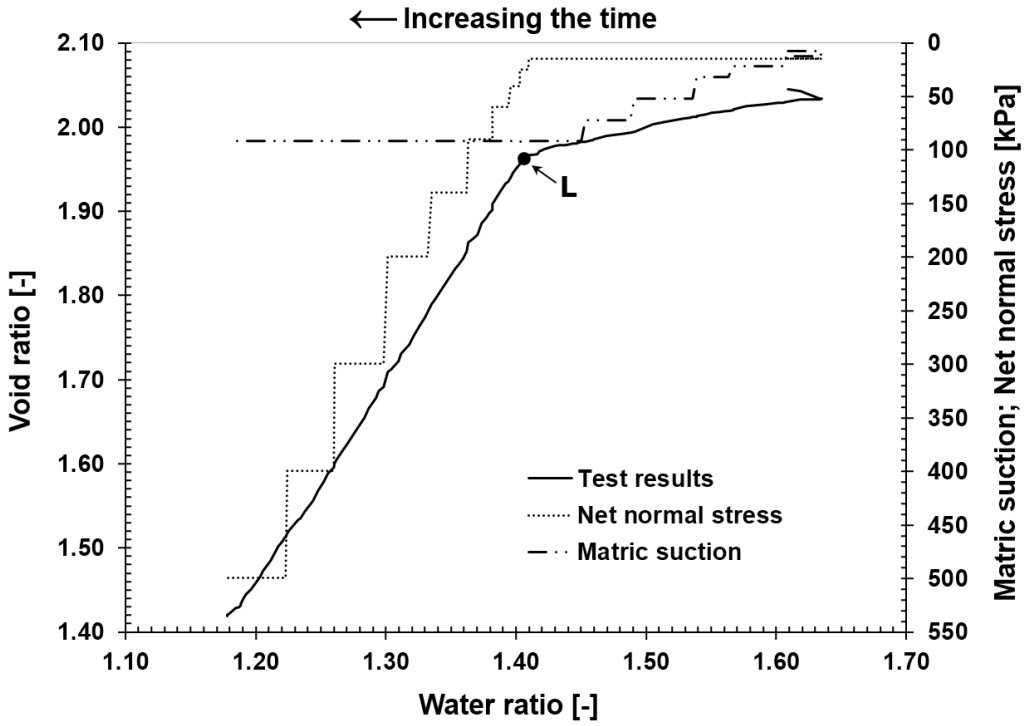

Figure 3.68. Relationship between the water ratio (e_w) and the void ratio (e) for increasing matric suction and net normal stress during the suction-controlled oedometer test U3 (unsaturated soil sample).

Figure 3.69 (based on Figures 3.42, 3.55 and 3.68) compares the relationship between the maximum matric suction and the average value of $\Delta e_w/\Delta e$ (change in water ratio divided by change in void ratio, from Airò Farulla, 2008) for all suction-controlled oedometer tests under two conditions: (i) decreasing Sr *before* reaching point L and (ii) increasing Sr *after* reaching point L. Figure 3.69 shows that, *before* reaching the minimum of Sr (i.e., the upper curve in the figure), $\Delta e_w/\Delta e$ increases to a maximum value as matric suction is increased from 92 to 290 kPa, and it decreases once matric suction is increased from 290 to 891 kPa. In contrast, *after* reaching the minimum of Sr (i.e., the lower curve in the figure), matric suction has no significant effect on the value of $\Delta e_w/\Delta e$. The value of 290 kPa matric suction (in test U2) seems to have a critical role in increasing $\Delta e_w/\Delta e$, *before* reaching the minimum of Sr, for this soil. However, more testing is needed to gain a deeper understanding of the relationship between the maximum matric suction and $\Delta e_w/\Delta e$.

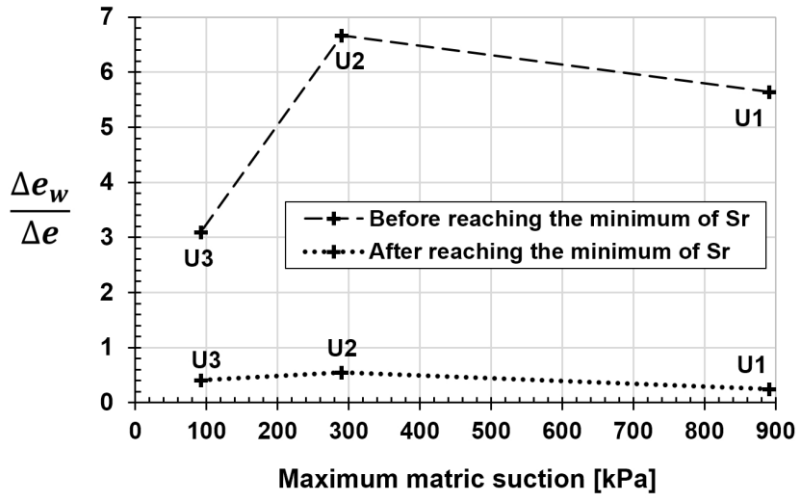

Figure 3.69. Relationship between the maximum matric suction and the average value of $\Delta e_w/\Delta e$ for all suction-controlled oedometer tests on the compacted organic soil.

The schematic in Figure 3.70 shows the effects of two main stress paths on the water volume and air volume changes of the unsaturated soil samples in suction-controlled oedometer tests. The laboratory results show that in the first part of the tests, where the matric suction was increased under a constant net normal stress, the volume of water outflow was higher than the volume of air outflow (schematic drawing 1 in Figure 3.70). This is visible in Figures 3.37, 3.50 and 3.63 for Tests U1, U2 and U3, respectively, where the air ratio (e_a) increases with increasing matric suction. In contrast, when the net normal stress was increased under a constant matric suction, the volume of air outflow was higher than the volume of water outflow (schematic drawing 2 in Figure 3.70). This is visible in Figures 3.40, 3.53 and 3.66 for Tests U1, U2 and U3, respectively, where the air ratio (e_a) decreases with increasing net normal stress.

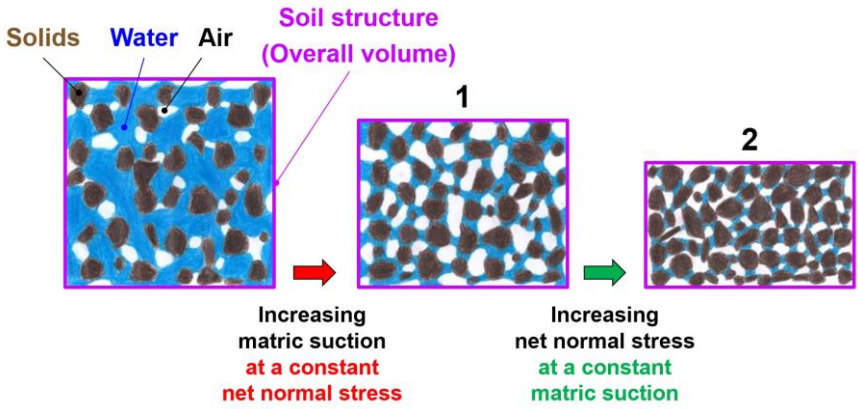

Figure 3.70. Schematic showing the effects of two main stress paths on the water volume and air volume changes of the unsaturated soil samples in suction-controlled oedometer tests.

These results are in line with Fredlund and Rahardjo (1993) who explain that “an increase in matric suction causes a greater change in the volume of water in the soil than the overall volume change of the soil element.” In addition, an increase in “net normal stress produces a greater change in the overall volume of the soil element than it produces for the change in water volume in the element” (p. 422).

3.6 The Dependency of Volume Change Behaviour on Time

In the following two sections, the dependency of volume change behaviour on time in the compacted organic soil is demonstrated by analysing the experimental test results.

3.6.1 The Dependency of Volume Change Behaviour on Time in Saturated Soil Samples

Figures 3.71 and 3.72 demonstrate the dependency of volume change behaviour on time in saturated soil samples. For example, Figure 3.72 shows that the secondary compression index (C_α) continues to increase even after 16 days for the saturated soil sample at the loading step of 639 kPa in the oedometer test S3. As a result, C_α in saturated conditions is not unique and is a function of time. Therefore, applying the classical method to study volume changes of saturated compacted organic soils using C_α (on a plot of void ratio versus logarithmic scale of time) leads to inaccurate results. This problem can be solved by applying the isotache approach.

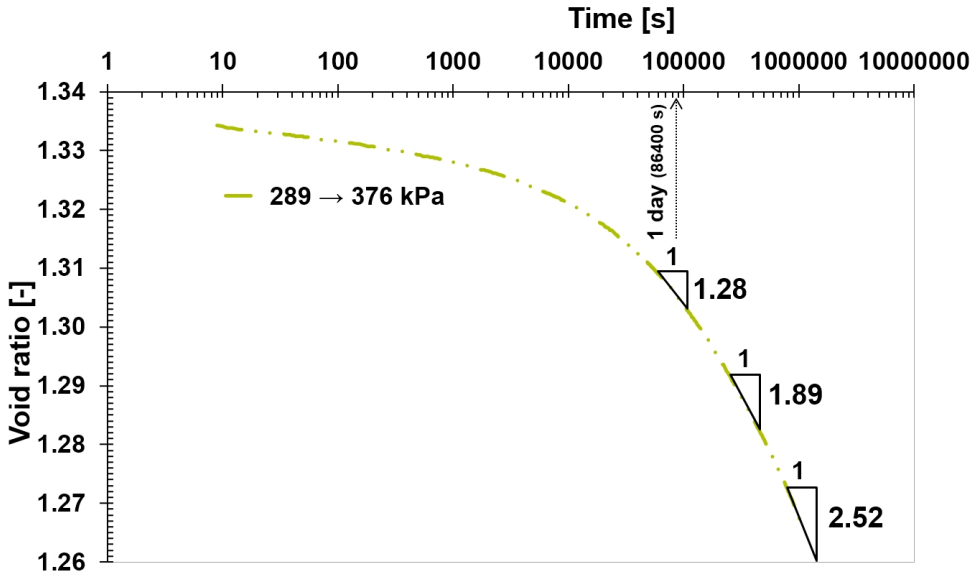

Figure 3.71. The dependency of volume change behaviour on time in the saturated soil sample at the loading step of 376 kPa in oedometer test S3.

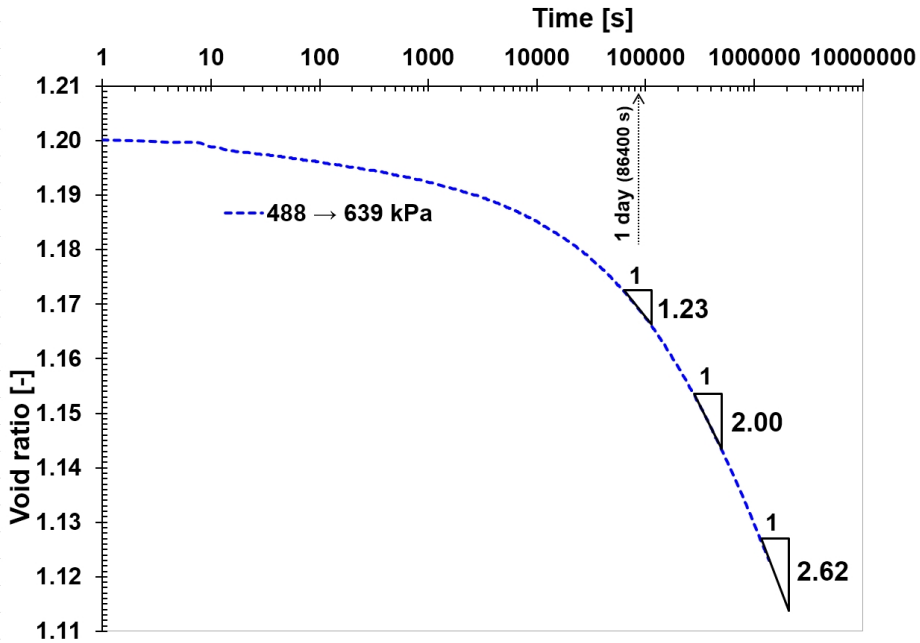

Figure 3.72. The dependency of volume change behaviour on time in the saturated soil sample at the loading step of 639 kPa in oedometer test S3.

3.6.2 The Dependency of Volume Change Behaviour on Time in Unsaturated Soil Samples

Figure 3.73 shows that, for test U3, the secondary compression index (C_α) continues to increase even after 6 days in the soil structure of the unsaturated soil sample under increasing matric suction, 72 → 92 kPa, and a constant net normal stress of 15 kPa.

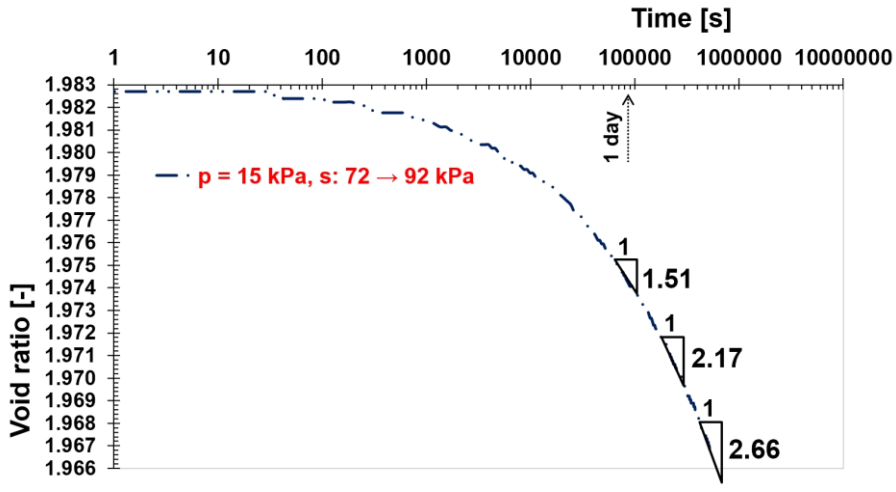

Figure 3.73. The dependency of volume change behaviour on time in the soil structure of the unsaturated soil sample under increasing matric suction, 72 → 92 kPa, and a constant net normal stress of 15 kPa for the suction-controlled oedometer test U3.

Figure 3.74 shows that, for test U3, the secondary compression index (C_α) continues to increase even after 23 days in the soil structure of the unsaturated soil sample under increasing net normal stress, 400 → 499 kPa, and a constant matric suction of 92 kPa.

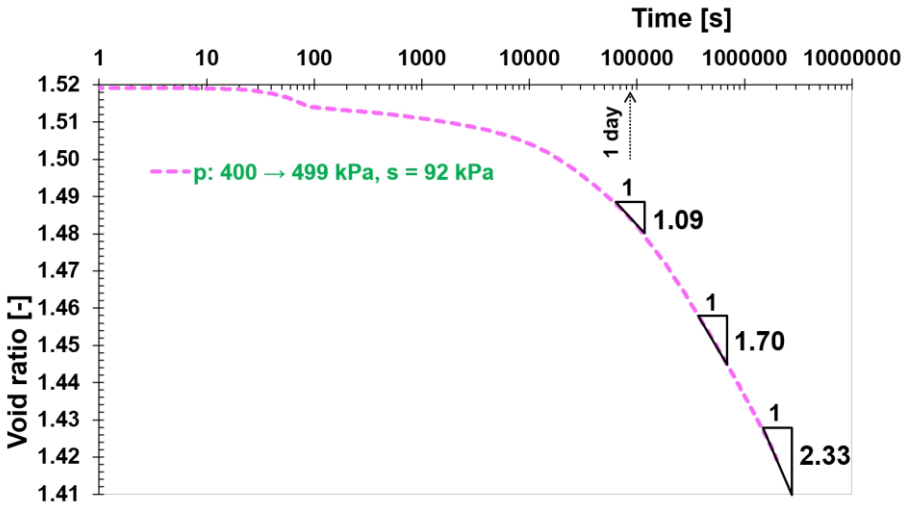

Figure 3.74. The dependency of volume change behaviour on time in the soil structure of the unsaturated soil sample under increasing net normal stress, 400 → 499 kPa, and a constant matric suction of 92 kPa for the suction-controlled oedometer test U3.

3.7 The Dependency of Volume Change Behaviour on Stress and Matric Suction

In the following three sections, the dependency of volume change behaviour on stress and matric suction in the compacted organic soil is demonstrated by analysing the experimental test results.

3.7.1 The Dependency of Volume Change Behaviour on Stress in Saturated Soil Samples

Figure 3.75 shows the dependency of volume change behaviour on stress in the saturated soil sample of oedometer test S3. The figure demonstrates that the slopes of the loading isobars increase with increasing vertical stress for equal elapsed times (e.g., 1 day). As a result, the secondary compression index (see Figure 2.1) in saturated conditions is not unique because it is a function of vertical stress. Therefore, applying the classical method to study volume changes of saturated compacted organic soils using C_α (on a plot of void ratio versus logarithmic scale of time) leads to inaccurate results. This problem can be solved by applying the isotache approach.

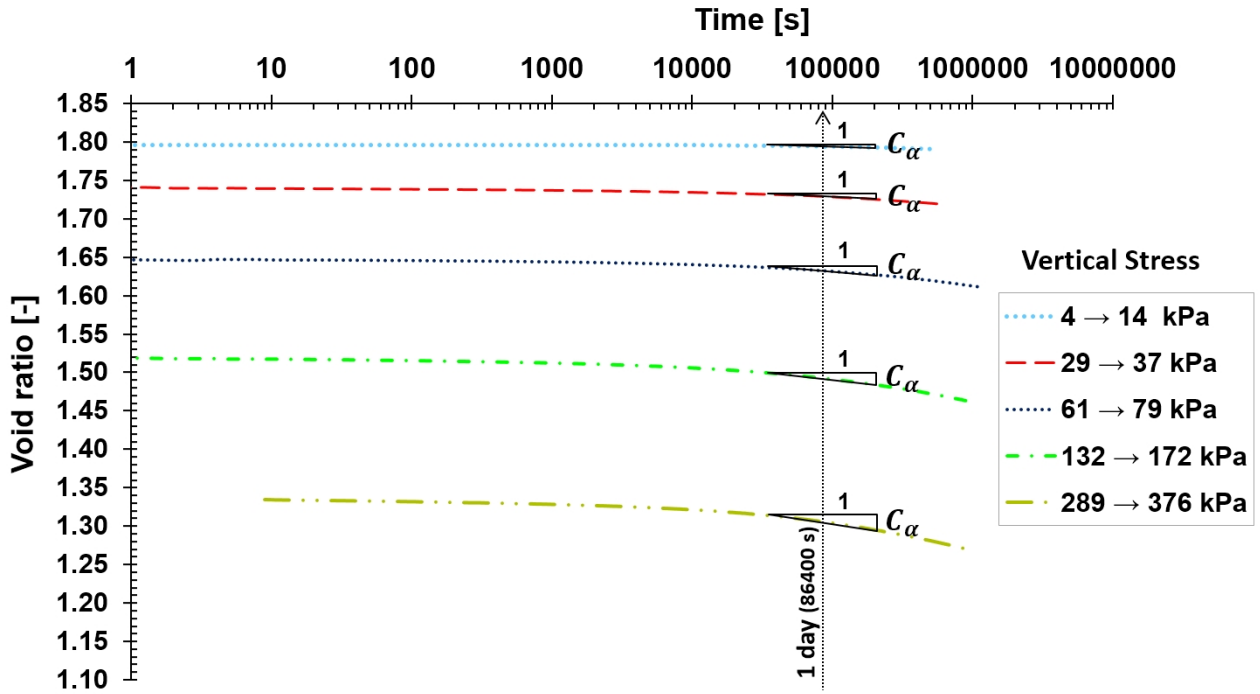

Figure 3.75. The dependency of volume change behaviour on stress in the saturated soil sample of oedometer test S3.

3.7.2 The Dependency of Volume Change Behaviour on Matric Suction in Unsaturated Soil Samples

Figure 3.76 shows the dependency of volume change behaviour on matric suction in the soil structure of the unsaturated soil sample at a constant net normal stress of 15 kPa for the suction-controlled oedometer test U1. The figure demonstrates that the slopes of the curves increase with increasing matric suction at a constant net normal stress for equal elapsed times.

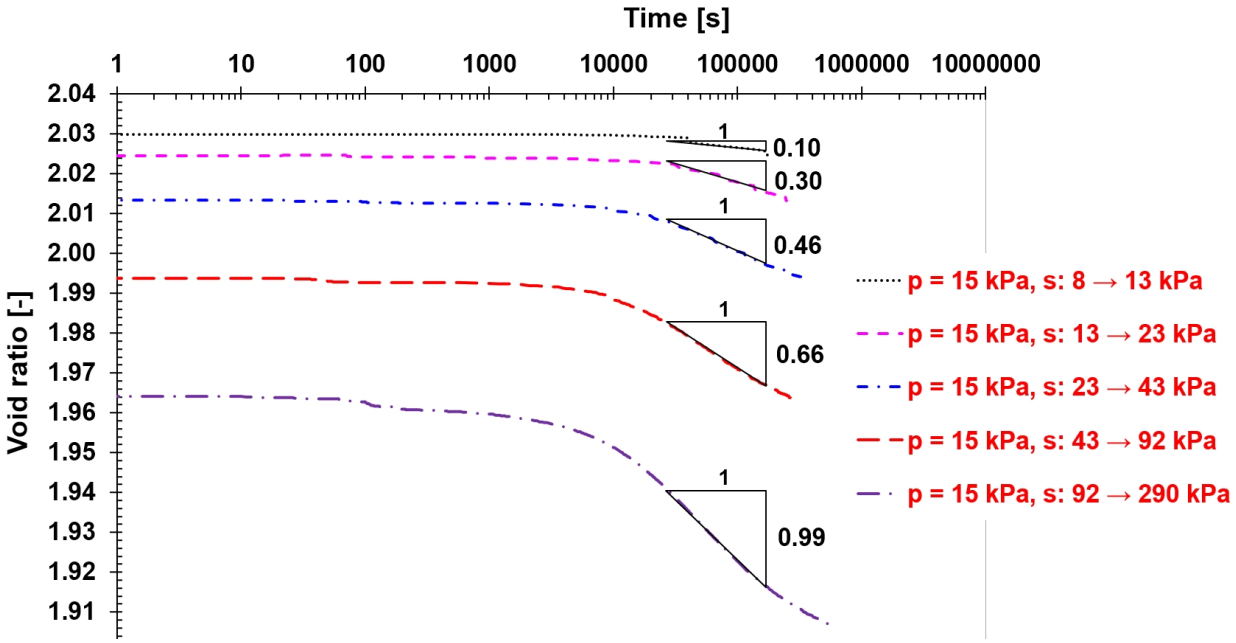

Figure 3.76. The dependency of volume change behaviour on matric suction in the soil structure of the unsaturated soil sample at a constant net normal stress of 15 kPa for the suction-controlled oedometer test U1.

3.7.3 The Dependency of Volume Change Behaviour on Stress in Unsaturated Soil Samples

Figure 3.77 shows the dependency of volume change behaviour on stress in the soil structure of the unsaturated soil sample at a constant matric suction of 891 kPa for the suction-controlled oedometer test U1. The figure demonstrates that the slopes of the curves increase with increasing net normal stress at a constant matric suction for equal elapsed times.

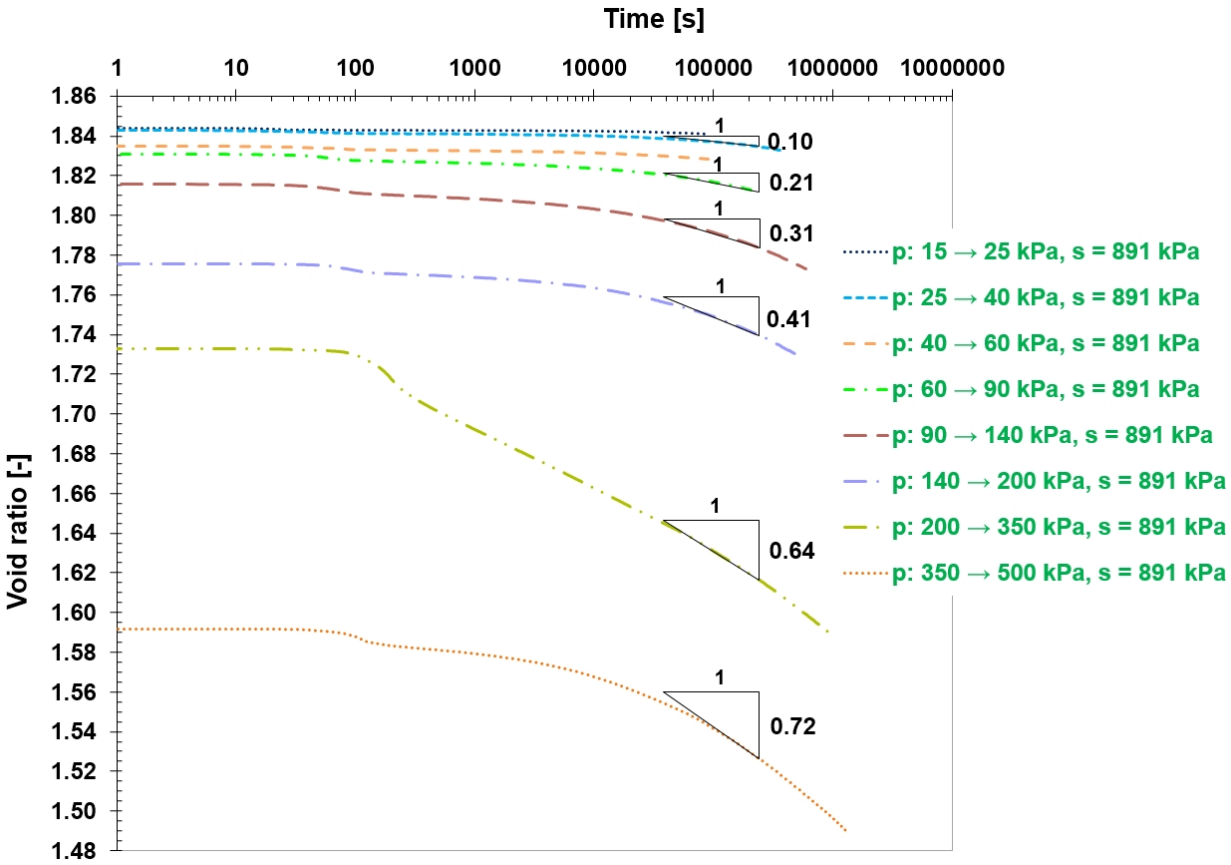

Figure 3.77. The dependency of volume change behaviour on stress in the soil structure of the unsaturated soil sample at a constant matric suction of 891 kPa for the suction-controlled oedometer test U1.

The dependency of water volume change behaviour on time and matric suction in unsaturated soil samples at a constant net normal stress can also be demonstrated in a way similar to that for soil structure. For example, the isobars of the water phase in Figures 3.35 and 3.48 (for Tests U1 and U2) show the dependency of water volume change behaviour on time and matric suction in unsaturated soil samples at a constant net normal stress. However, in the second part of these tests (i.e., increasing net normal stress at a constant matric suction), the water content of the soil samples is very low due to the high values of matric suction. As a result, increasing net normal stress has no significant role in decreasing water content.

Chapter 4: The Isotaches and the Model Parameters

4.1 Introduction

In this chapter, the sensitivity of isotache pattern to the LIR is examined utilising the results of conventional oedometer tests. In addition, using the results of suction-controlled oedometer tests, the a,b,c isotache model is adapted for unsaturated conditions based on the theory of overall volume and water volume changes of unsaturated soils (Fredlund & Morgenstern, 1976), and the isotache patterns are studied. The procedure to determine model parameters from suction-controlled oedometer tests on unsaturated soil samples is introduced. Moreover, the required parameters for the adapted a,b,c isotache model are obtained from the suction-controlled oedometer tests and conventional oedometer tests on the compacted organic soil. Then, the equations for selected parameters of the adapted a,b,c isotache model are suggested as a function of matric suction for the unsaturated compacted organic soil.

4.2 The Isotaches and the Model Parameters of Saturated Soil Samples

The theoretical aspects of the a,b,c isotache model were thoroughly described in *Section 2.1.6*. Figures 4.1, 4.2 and 4.3 present the loading isotaches of the oedometer tests with different Load Increment Ratio (LIR) on saturated soil samples. In all isotache patterns in this study, the same marker symbols are used for each natural strain rate of isotache to make it easy to distinguish the rates and compare them.

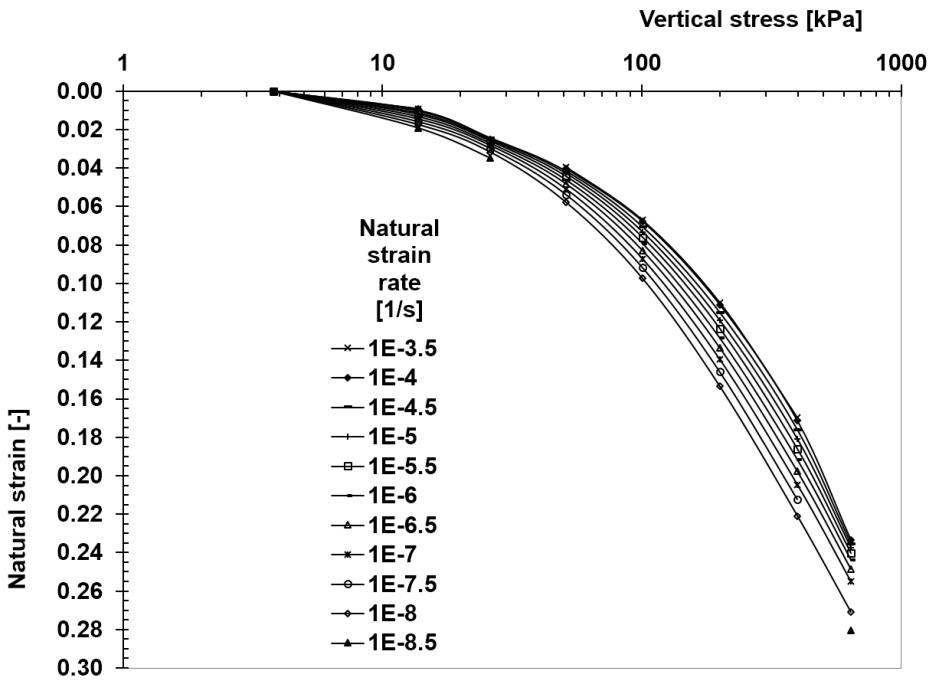

Figure 4.1. Loading isotaches of the oedometer test S1 (LIR = 1.0) on the saturated soil sample.

Figures 4.1, 4.2 and 4.3 indicate that the high rate of natural strain cannot be distinguished at a small value of LIR compared to a large value of LIR. It seems that the rate of elastic strains decreases very fast in small LIR, which is logical when a large load is divided into small parts.

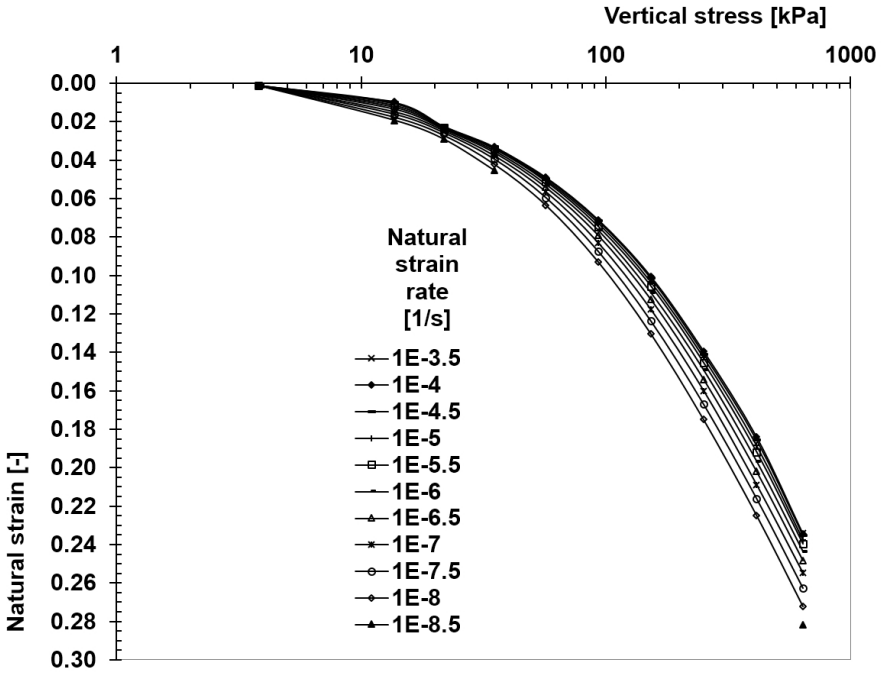

Figure 4.2. Loading isotaches of the oedometer test S2 (LIR = 0.65) on the saturated soil sample.

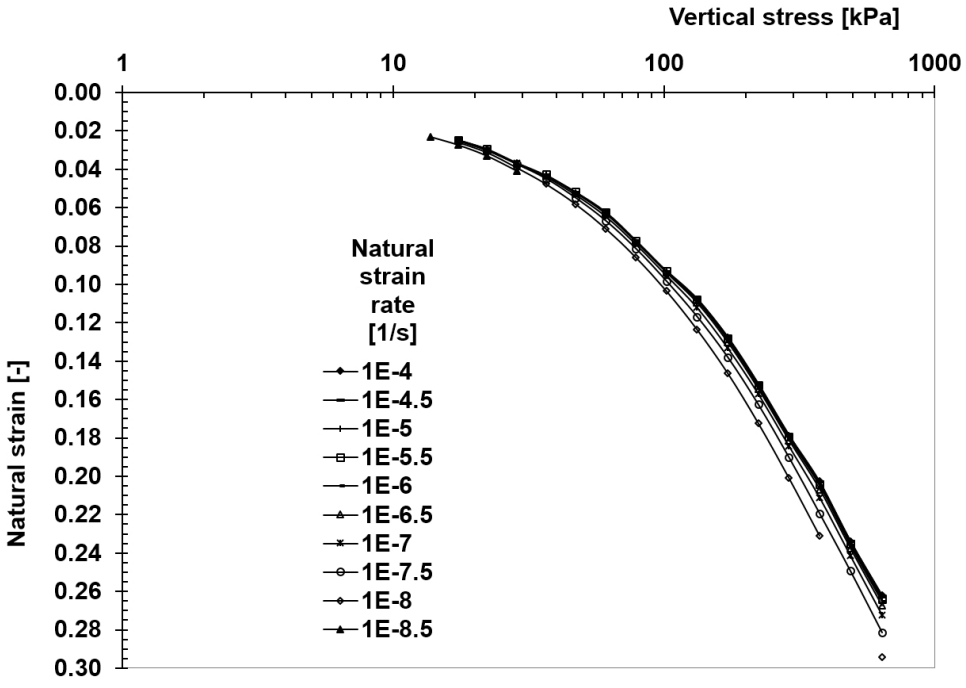

Figure 4.3. Loading isotaches of the oedometer test S3 (LIR = 0.3) on the saturated soil sample.

Based on these figures, the parameters a, b, c and the pre-consolidation stress at zero total strain (p_g) can be obtained as follows:

Test S1

a = 0.0129, b = 0.1016, c = 0.0081, p_g = 52.3 [kPa]

Test S2

a = 0.0126, b = 0.1034, c = 0.0079, p_g = 54.7 [kPa]

Test S3

a = 0.0127, b = 0.1151, c = 0.0098, p_g = 75.3 [kPa]

The above results show that the isotache parameters of Tests S1 (LIR = 1.0) and S2 (LIR = 0.65) are very similar. However, for Test S3, with a very low LIR of 0.3, the parameters b, c and p_g are slightly different. Parameter “a” is similar for all tests. For more information, see Table 4.2.

For a better comparison between the isotaches of the conventional oedometer tests S1, S2 and S3, three isotaches with the natural strain rates of 1E-6, 1E-7, and 1E-8 [1/s] were chosen. As can be seen in Figures 4.4, 4.5 and 4.6, these isotaches for Tests S1 (LIR = 1.0) and S2 (LIR = 0.65) are very similar. For Test S3 (LIR = 0.3), the beginning point of its isotaches is different from other tests which is probably due to the difference in sample properties and/or performance of devices. If for this test, its isotaches shifted to the same beginning point of other tests, a difference would still exist for vertical stresses higher than 500 kPa. Based on Figures 4.4, 4.5 and 4.6, it can be concluded that the decrease of LIR from 1.0 to 0.65 has no effect on the isotache pattern and the values of the parameters a, b, c and p_g of the model. However, the decrease of LIR from 0.65 to 0.3 increases the strain, especially at vertical stresses higher than 500 kPa.

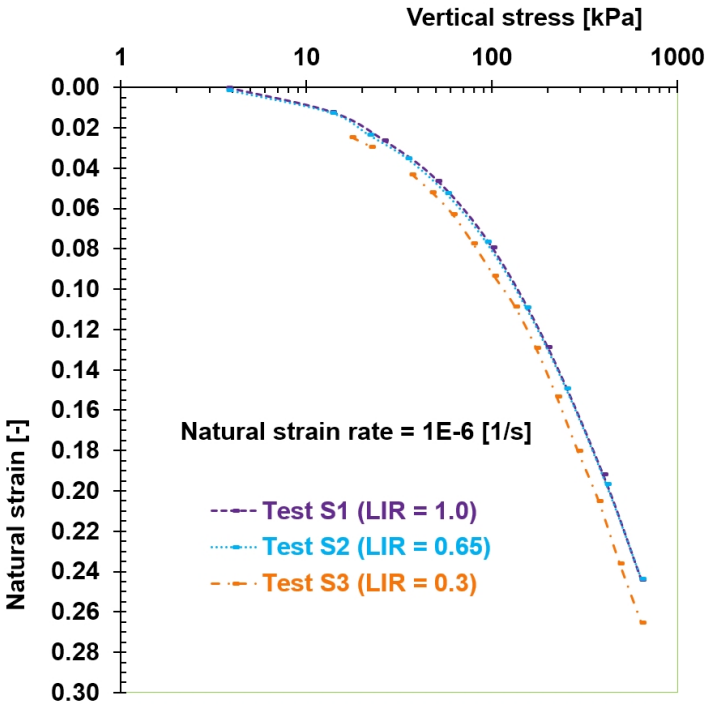

Figure 4.4. The isotaches with a natural strain rate of 1E-6 [1/s] for three tests with different LIR (saturated soil samples).

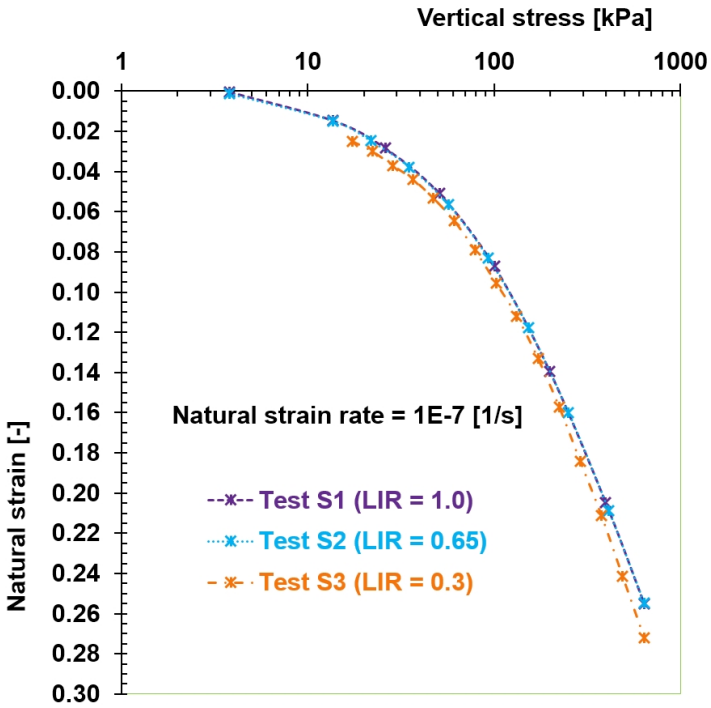

Figure 4.5. The isotaches with a natural strain rate of 1E-7 [1/s] for three tests with different LIR (saturated soil samples).

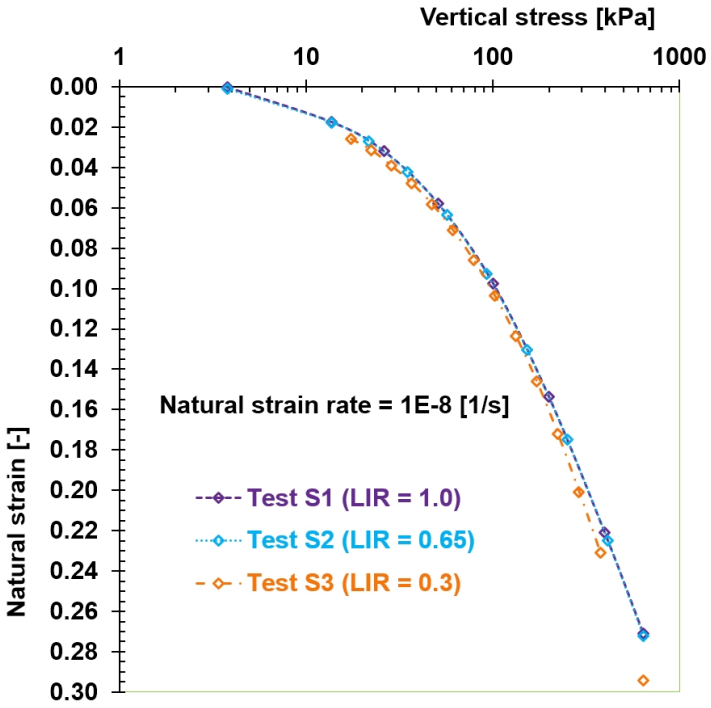

Figure 4.6. The isotaches with a natural strain rate of 1E-8 [1/s] for three tests with different LIR (saturated soil samples).

4.3 The Isotaches of Unsaturated Soil Samples

In this section, the isotaches for the soil structure and water phase of the unsaturated compacted organic soil are plotted using the results of three suction-controlled oedometer tests. Afterwards, the required parameters for the adapted a,b,c isotache model (for unsaturated soil) are determined.

4.3.1 Test U1

Figure 4.7 presents the soil structure isotaches at a constant net normal stress (p) for the suction-controlled oedometer test U1 (unsaturated soil). This figure, along with Figures 4.11 and 4.15 (for Tests U2 and U3), indicates that at a constant net normal stress, the isotache pattern exists for the soil structure of the unsaturated soil when the matric suction increases. Although some isotaches are not parallel and equidistant, these patterns demonstrate that creep in the soil structure of unsaturated soils occurs due to increasing matric suction.

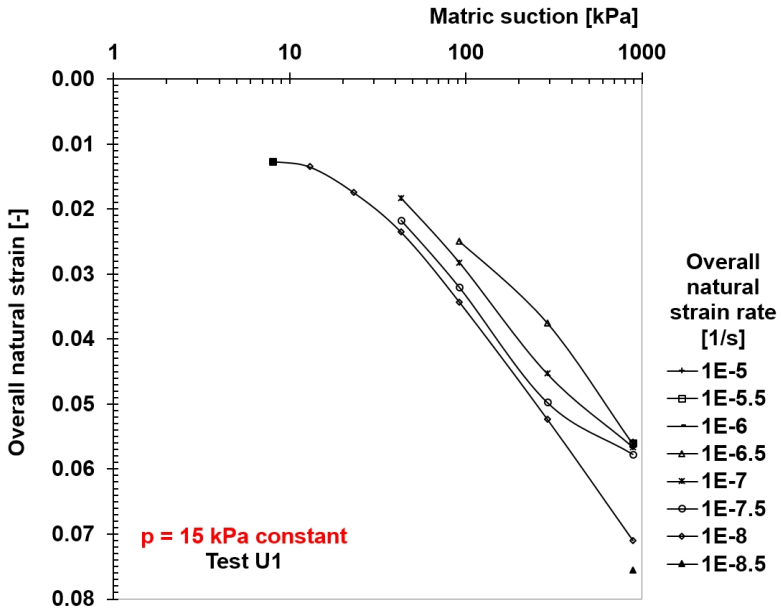

Figure 4.7. Soil structure isotaches at a constant net normal stress (*p*) for the suction-controlled oedometer test U1 (unsaturated soil).

Figure 4.8 presents the soil structure isotaches at a constant matric suction (*s*) for the suction-controlled oedometer test U1 (unsaturated soil). This figure, along with Figures 4.12 and 4.16 (for Tests U2 and U3), indicates that at a constant matric suction, the isotache pattern exists for the soil structure of the unsaturated soil when the net normal stress increases. In other words, these patterns demonstrate that creep in the soil structure of unsaturated soils occurs due to increasing net normal stress.

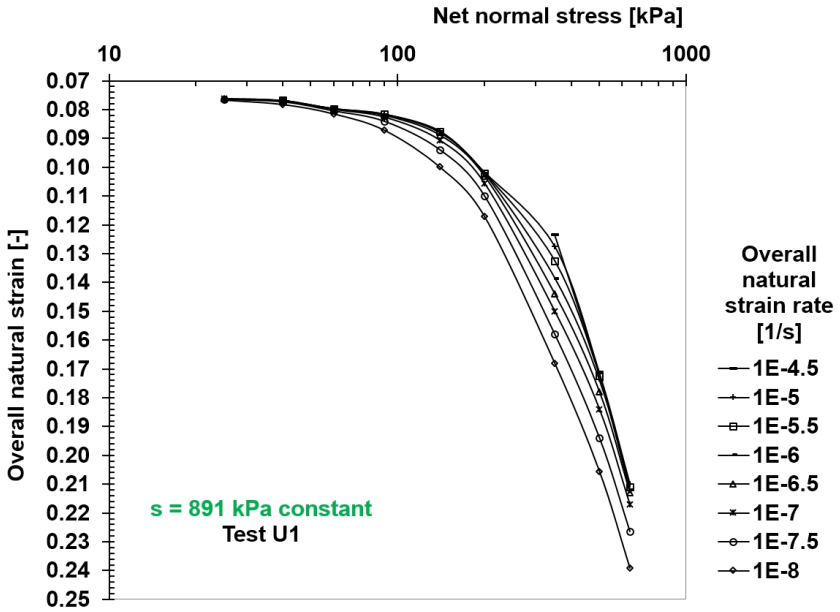

Figure 4.8. Soil structure isotaches at a constant matric suction (*s*) for the suction-controlled oedometer test U1 (unsaturated soil).

Figure 4.9 presents the water phase isotaches at a constant net normal stress (*p*) for the suction-controlled oedometer test U1 (unsaturated soil). This figure, along with Figures 4.13 and 4.17 (for Tests U2 and U3), indicates that at a constant net normal stress, the isotache pattern exists for the water phase of the unsaturated soil when the matric suction increases.

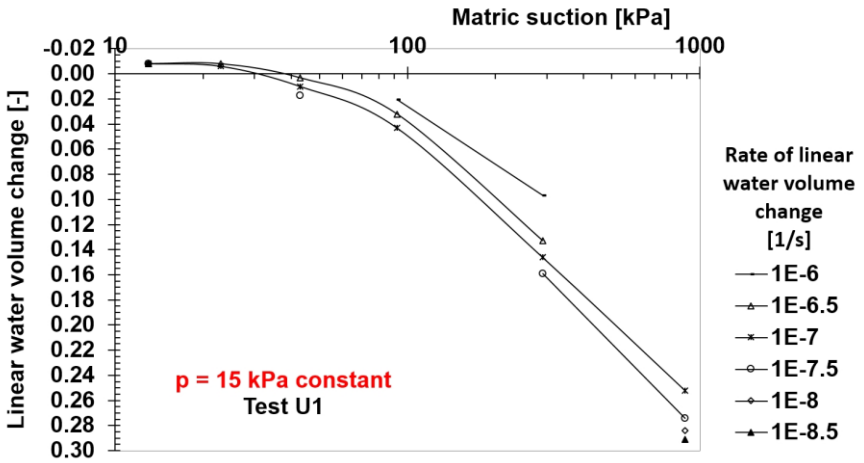

Figure 4.9. Water phase isotaches at a constant net normal stress (*p*) for the suction-controlled oedometer test U1 (unsaturated soil).

Figure 4.10 presents the water phase isotaches at a constant matric suction (*s*) for the suction-controlled oedometer test U1 (unsaturated soil). Due to the high value of matric suction in the second part of this test (s = 891 kPa), the water content of the soil sample is very low. As a result, increasing net normal stress has no significant effect in decreasing water content. Under this condition, the isotache pattern could not be plotted completely (Figure 4.10), because measuring very small changes in the water volume is difficult. Similar behaviour can also be observed for the second part of Test U2 (s = 290 kPa) in Figure 4.14.

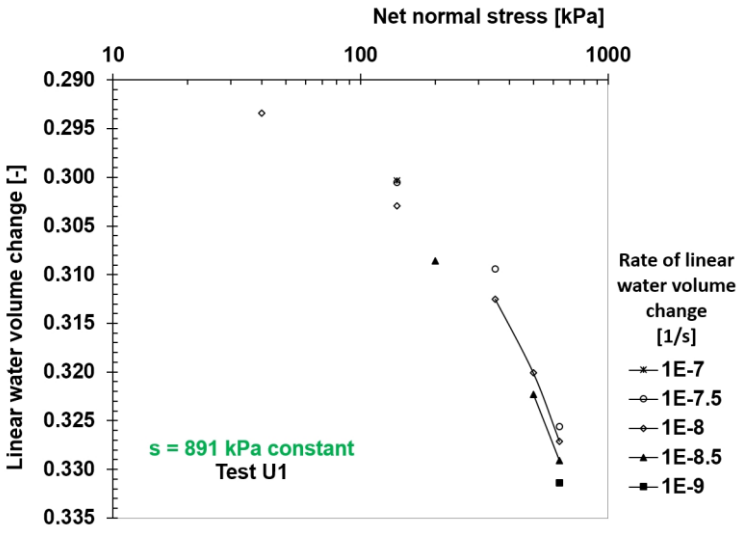

Figure 4.10. Water phase isotaches at a constant matric suction (*s*) for the suction-controlled oedometer test U1 (unsaturated soil).

4.3.2 Test U2

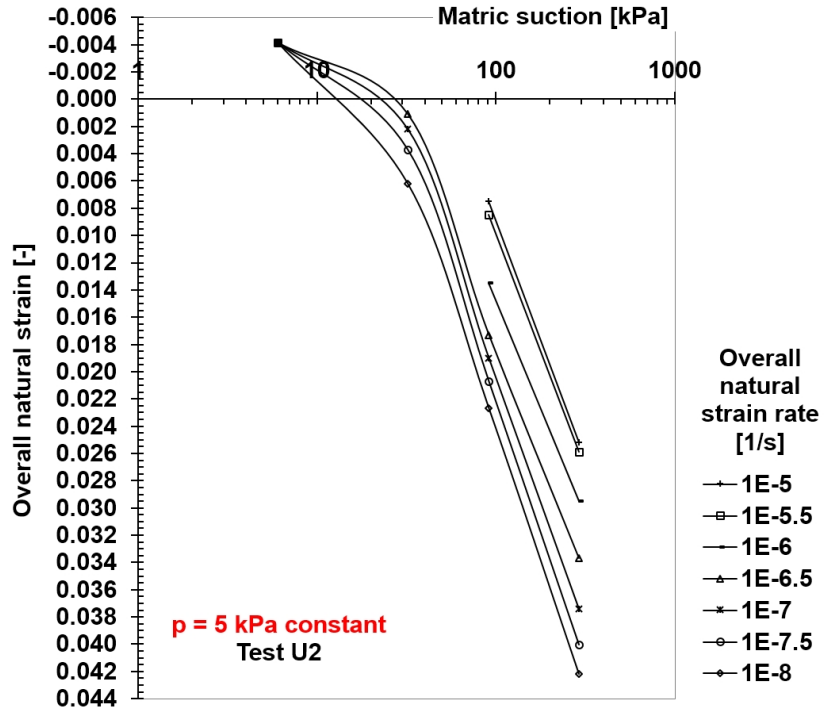

Figure 4.11. Soil structure isotaches at a constant net normal stress (*p*) for the suction-controlled oedometer test U2 (unsaturated soil).

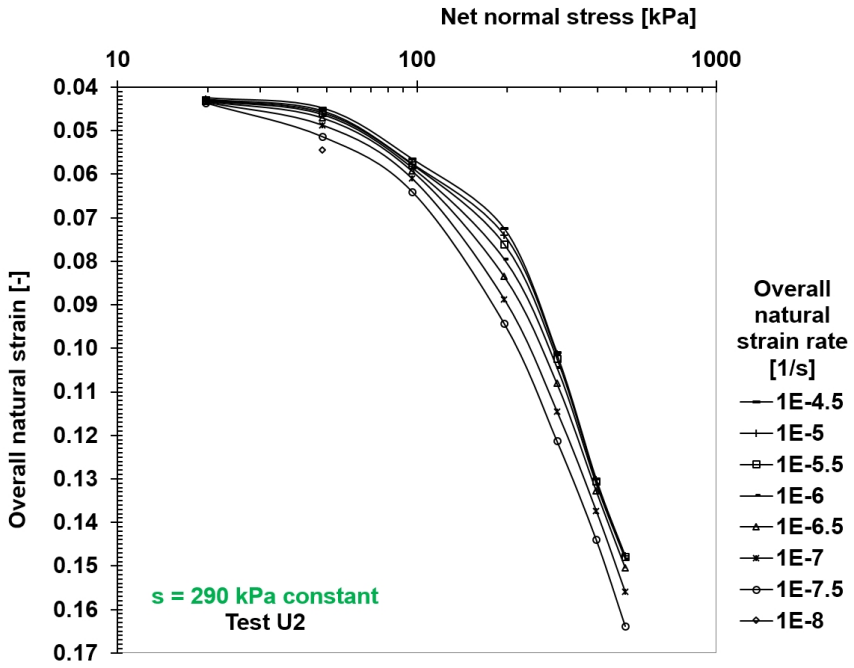

Figure 4.12. Soil structure isotaches at a constant matric suction (*s*) for the suction-controlled oedometer test U2 (unsaturated soil).

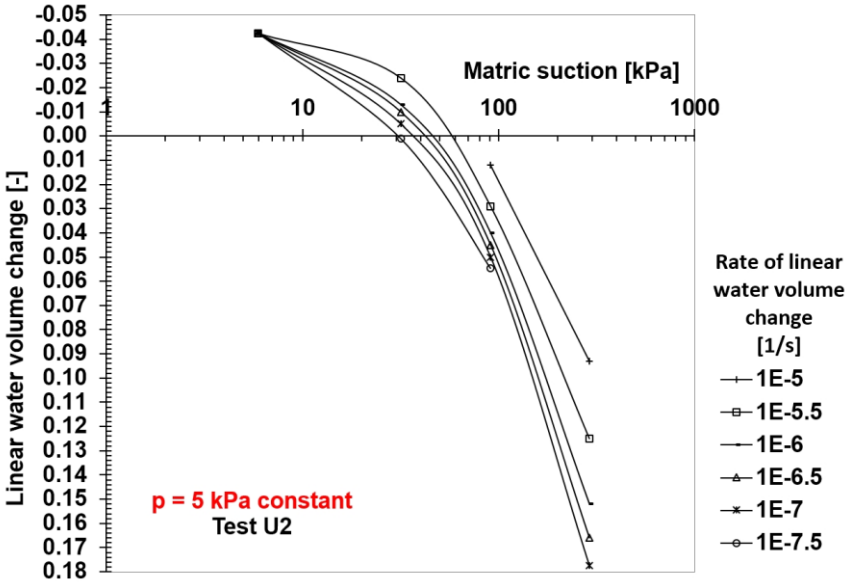

Figure 4.13. Water phase isotaches at a constant net normal stress (*p*) for the suction-controlled oedometer test U2 (unsaturated soil).

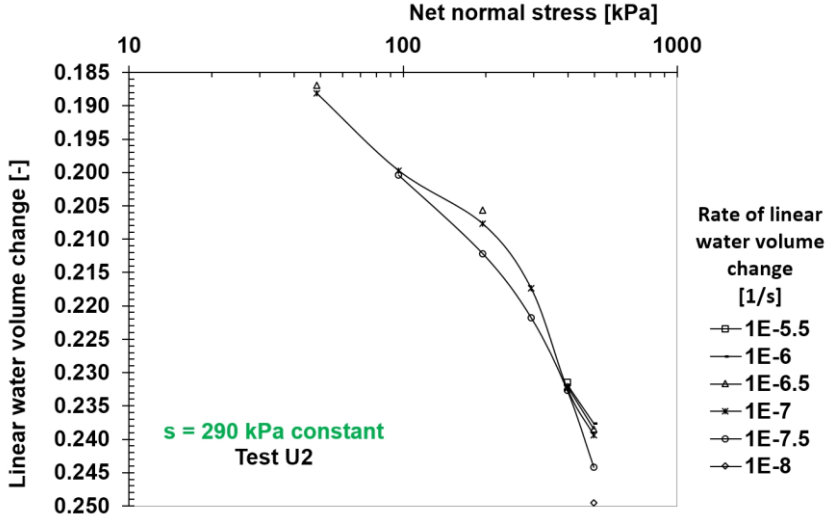

Figure 4.14. Water phase isotaches at a constant matric suction (*s*) for the suction-controlled oedometer test U2 (unsaturated soil).

4.3.3 Test U3

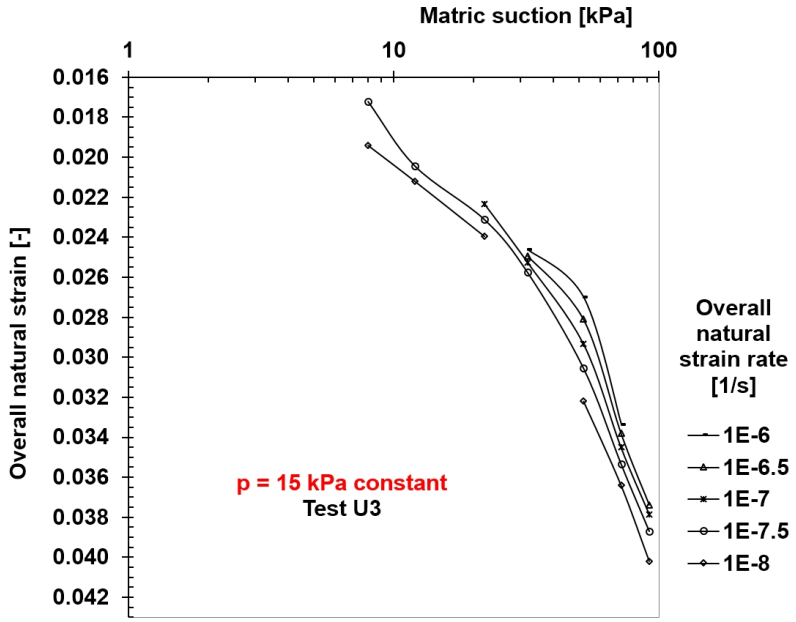

Figure 4.15. Soil structure isotaches at a constant net normal stress (*p*) for the suction-controlled oedometer test U3 (unsaturated soil).

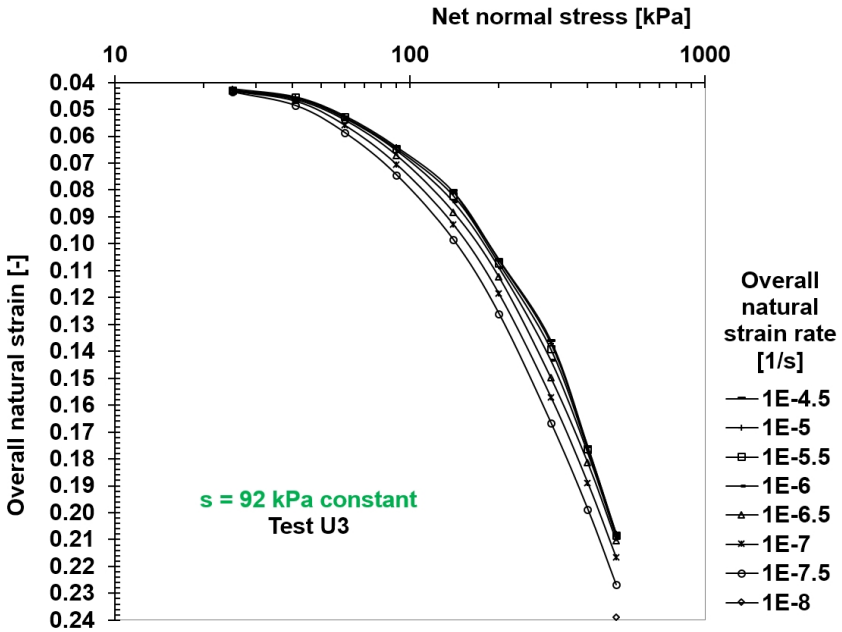

Figure 4.16. Soil structure isotaches at a constant matric suction (*s*) for the suction-controlled oedometer test U3 (unsaturated soil).

Figure 4.17 presents the water phase isotaches at a constant net normal stress (*p*) for the suction-controlled oedometer test U3 (unsaturated soil). It seems that the maximum matric suction was not high enough to reach the yield matric suction of the soil sample.

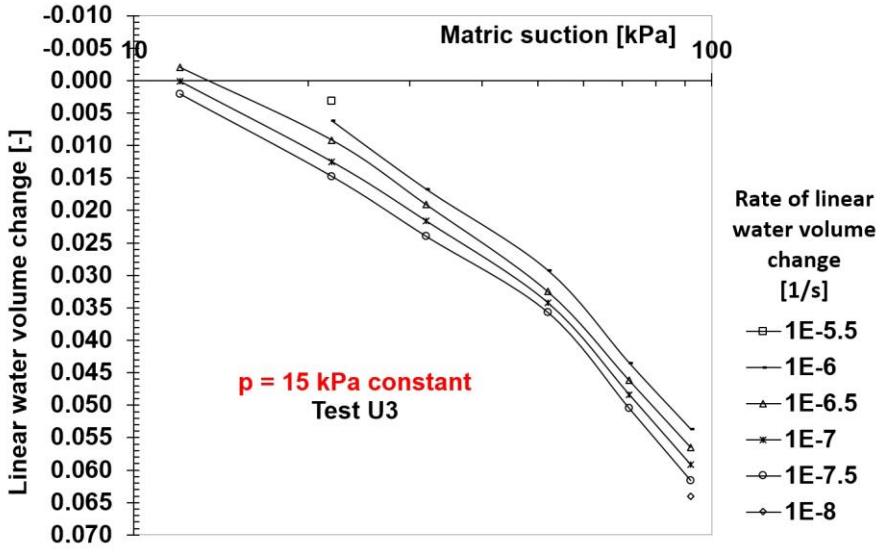

Figure 4.17. Water phase isotaches at a constant net normal stress (*p*) for the suction-controlled oedometer test U3 (unsaturated soil).

Figure 4.18 presents the water phase isotaches at a constant matric suction (*s*) for the suction-controlled oedometer test U3 (unsaturated soil). This figure indicates that at a constant matric suction, the isotache pattern exists for the water phase of the unsaturated soil when the net normal stress increases.

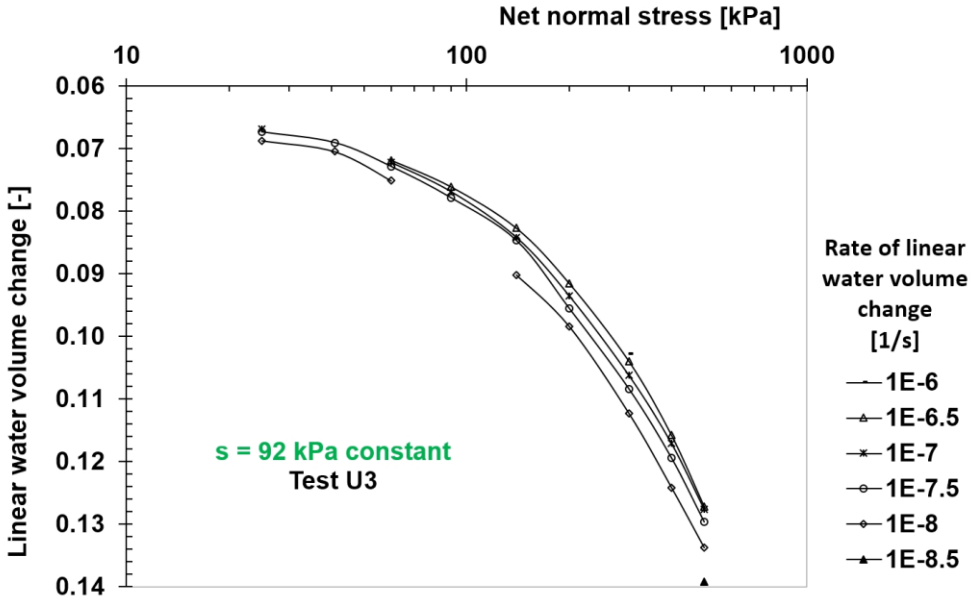

Figure 4.18. Water phase isotaches at a constant matric suction (*s*) for the suction-controlled oedometer test U3 (unsaturated soil).

Figure 4.18, along with Figures 4.9, 4.13 and 4.17 for Tests U1, U2 and U3, respectively, demonstrates that a phenomenon similar to creep in the soil structure exists for the water phase of

the unsaturated soil. This phenomenon, which acts as a delay in the outflow of water from the soil sample, will be called *water-phase creep*. However, further research is needed to gain insight into the isotache patterns of unsaturated soils, especially for the water phase.

Water Phase Isotaches of Test U3 Using the "Natural Water Mass Change" Equation:

As an alternative method, the water phase isotaches of Test U3 are presented here using the "natural water mass change" equation (i.e., $\varepsilon_w^H = -\ln[(1+e_w)/(1+e_{w_0})]$). A detailed description of this equation was given in *Section 3.5.3.3*.

Figure 4.19 presents the water phase isotaches of the unsaturated soil at a constant net normal stress (p) for the suction-controlled oedometer test U3 using the "natural water mass change" equation. Comparison of Figures 4.17 and 4.19 indicates that the isotache patterns for the water phase of Test U3 are more or less similar using either the equation of linear water volume change ($\varepsilon_w^{(\mathrm{lin})}$) or the equation of natural water mass change (ε_w^H).

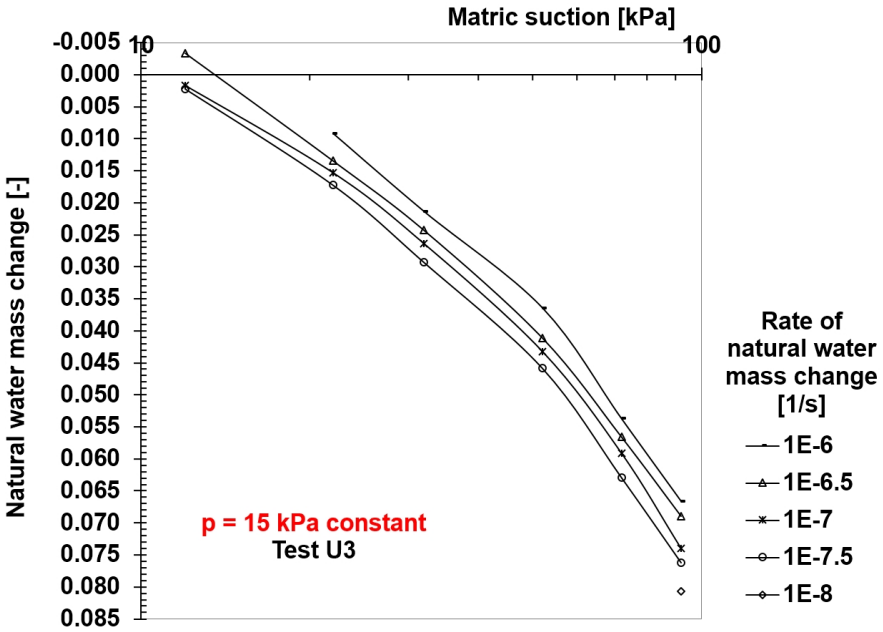

Figure 4.19. Water phase isotaches of the unsaturated soil at a constant net normal stress (p) for the suction-controlled oedometer test U3 using the "natural water mass change" equation.

Figure 4.20 presents the water phase isotaches of the unsaturated soil at a constant matric suction (s) for the suction-controlled oedometer test U3 using the "natural water mass change" equation. Comparison of Figures 4.18 and 4.20 indicates that the isotache patterns for the water phase of Test U3 are more or less similar using either the equation of linear water volume change ($\varepsilon_w^{(\mathrm{lin})}$) or the equation of natural water mass change (ε_w^H).

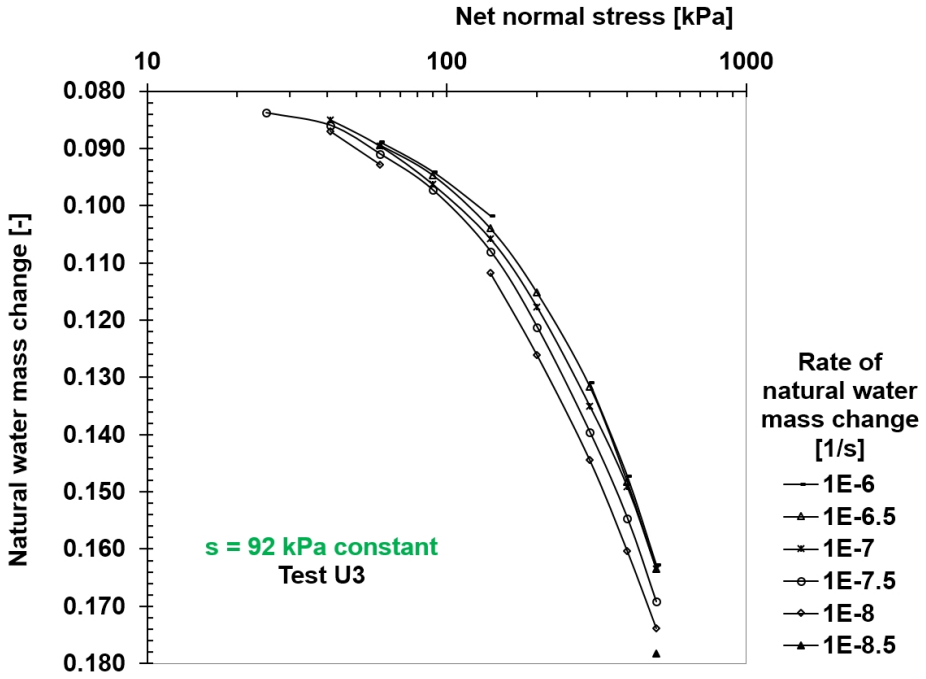

Figure 4.20. Water phase isotaches of the unsaturated soil at a constant matric suction (*s*) for the suction-controlled oedometer test U3 using the "natural water mass change" equation.

4.4 Comparison of the Volume Change Behaviour during Increasing Net Normal Stress

In this study, the model parameters b and c were determined within the range of 300 to 500 kPa net normal stress at different values of constant matric suction. In this range of net normal stress, the approximate averages of Load Increment Ratio (LIR) for Tests U1, U2 and U3 are 0.54, 0.37 and 0.36, respectively. Therefore, the approximate average of LIR across all tests is 0.42. This was the reason for choosing oedometer test S3 (which was performed on the saturated soil sample) for comparison with the suction-controlled oedometer tests on unsaturated soil samples. Oedometer test S3 was conducted at an LIR value closer to 0.42 (i.e., 0.3) compared to Tests S1 and S2 with LIRs of 1.0 and 0.65, respectively.

The initial values on the vertical axes in Figures 4.21, 4.22, 4.23 and 4.24 were adjusted to zero in order to have the same initial state to improve visual clarity for comparing the behaviour during increasing net normal stress.

Figure 4.21 compares the overall natural strain (ε_v^H) versus net normal stress for the end of each step of Tests U1, U2, U3 and S3 under different values of constant matric suction. In addition, Figure 4.22 compares the soil structure isotaches at an overall natural strain rate of 1E-7.5 [1/s] for Tests U1, U2, U3 and S3 under different values of constant matric suction. As shown in Figures 4.21 and 4.22, a greater increase in matric suction shifts the curves toward the upper right side of the diagrams. A detailed comparison of selected parameters is presented in *Section 4.6*.

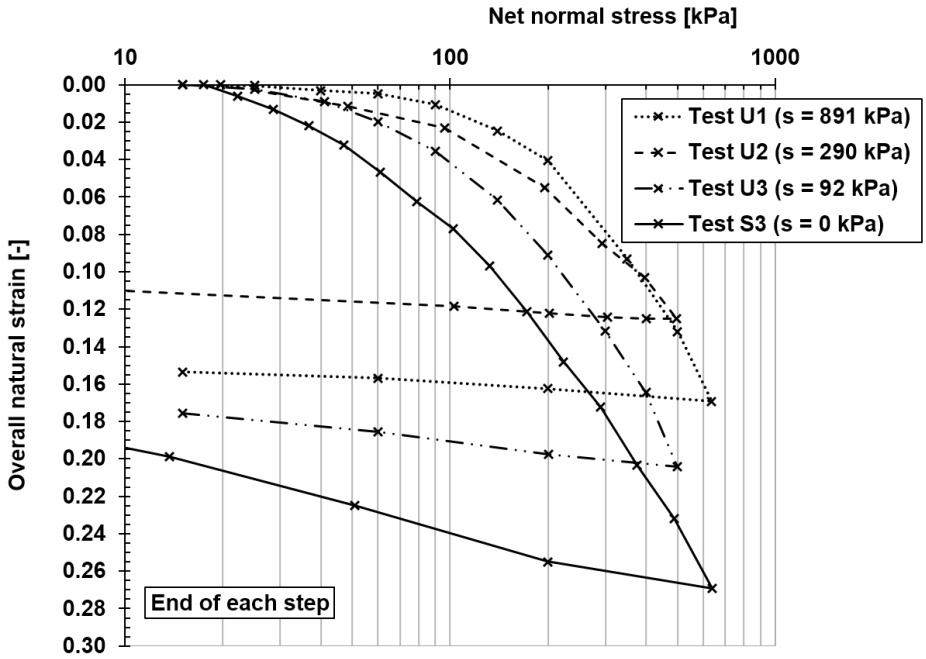

Figure 4.21. Comparison of the overall natural strains (ε_v^H) for the end of each step of Tests U1, U2, U3 and S3 under different values of constant matric suction.

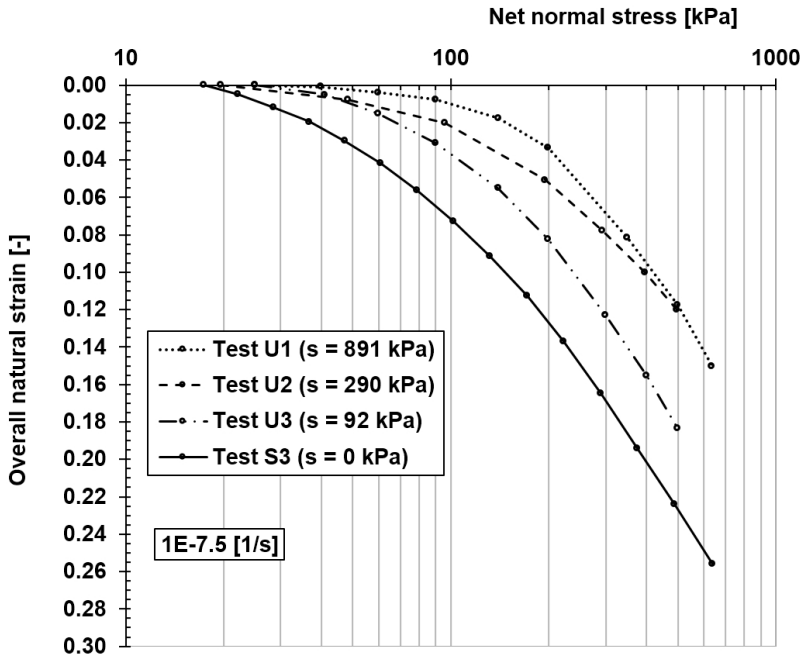

Figure 4.22. Comparison of the soil structure isotaches at an overall natural strain rate of 1E-7.5 [1/s] for Tests U1, U2, U3 and S3 under different values of constant matric suction.

Figure 4.23 compares the linear water volume change ($\varepsilon_w^{(\mathrm{lin})}$) versus net normal stress for the end of each step of Tests U1, U2 and U3 under different values of constant matric suction. In addition, Figure

4.24 compares the water phase isotaches at a “linear water volume change” rate of 1E-7.5 [1/s] for Tests U1, U2 and U3 under different values of constant matric suction.

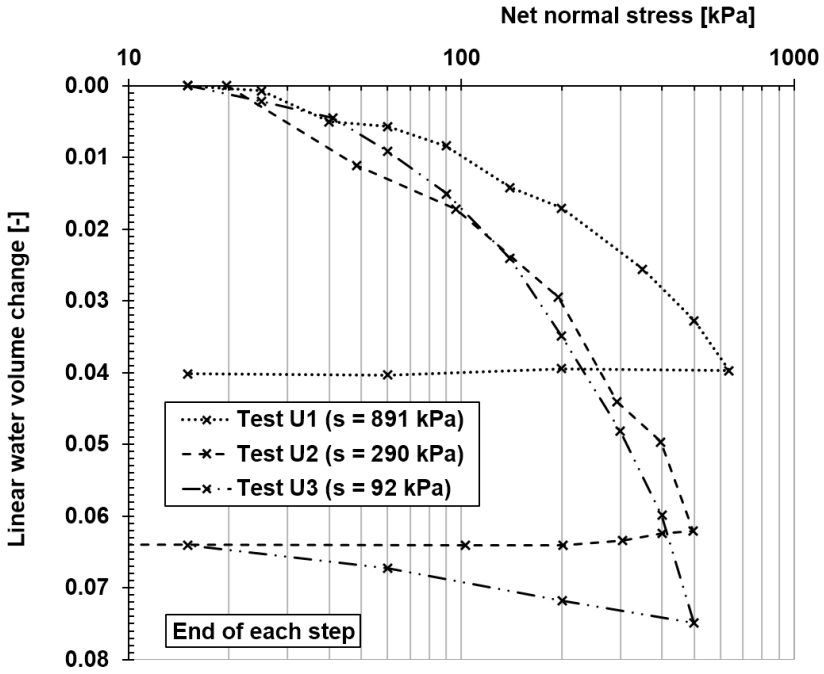

Figure 4.23. Comparison of the linear water volume changes ($\varepsilon_w^{(\mathrm{lin})}$) for the end of each step of Tests U1, U2 and U3 under different values of constant matric suction.

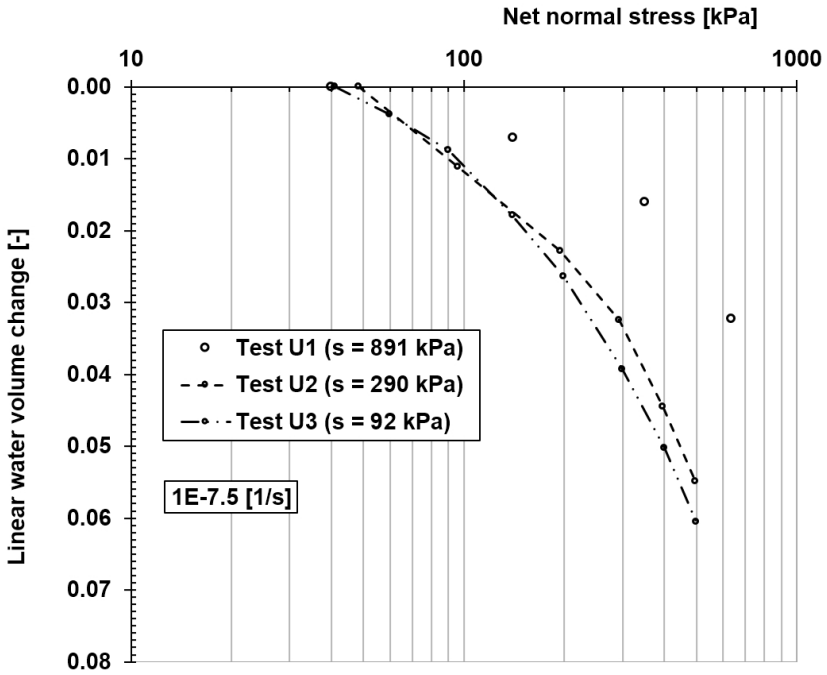

Figure 4.24. Comparison of the water phase isotaches at a “linear water volume change” rate of 1E-7.5 [1/s] for Tests U1, U2 and U3 under different values of constant matric suction.

As shown in Figures 4.23 and 4.24, in the virgin range of stresses, a greater increase in matric suction shifts the curves toward the upper right side of the diagrams. A detailed comparison of selected parameters is presented in *Section 4.6*.

4.5 Determination of Parameters for the Adapted a,b,c Isotache Model (Unsaturated soils)

The test results of this study indicate that the parameters a, b and c in unsaturated conditions depend on the amount of matric suction. Therefore, unlike in the saturated condition, these parameters are not the material parameters, since they are not constant for all situations of a soil. This section introduces the procedure to determine model parameters from suction-controlled oedometer tests on unsaturated soil samples.

4.5.1 Determination of Parameters for the Adapted a,b,c Isotache Model, when Matric Suction Increases at Constant Net Normal Stress (*p*)

In order to determine the parameters of the adapted a,b,c isotache model for increasing matric suction at a constant net normal stress (*p*), the following steps should be taken:

1. Construct the isotaches on a plot of the overall natural strain (i.e., $\varepsilon_v^{H^p}$ for soil structure) or natural water mass change (i.e., $\varepsilon_w^{H^p}$ for water phase) versus matric suction (log scale) as shown in Figures 4.25 and 4.26 (for example, see the results of Test U3 in Figures 4.15 and 4.19).

The overall natural strain rate (for soil structure) and the rate of natural water mass change (for water phase) can be calculated by using equation 2.31 (in *Section 2.1.6.9*) in order to draw the isotaches.

2. Locate the position of 1-day reference isotache. For this aim, the overall natural strain rate (for soil structure), and the rate of natural water mass change (for water phase) should be formatted as 1×10^{-n} (see the example in *Section 2.1.6.9* for saturated soils).

3. Plot the 1-day reference isotache passing from the position that was found in the last step, parallel to the lowest isotache at the highest matric suction level. The parameters b_v^p (for soil structure) and b_w^p (for water phase) are the slopes of these lines and can be calculated as:

$$b_v^p = \frac{\Delta \varepsilon_v^{H^p}{}_{(b)}}{\Delta \ln s_{(b)}} \quad \text{: For soil structure; (Figure 4.25)} \tag{4.1}$$

$$b_w^p = \frac{\Delta \varepsilon_w^{H^p}{}_{(b)}}{\Delta \ln s_{(b)}} \quad \text{: For water phase; (Figure 4.26)} \tag{4.2}$$

4. For soil structure (Figure 4.25), the abscissa of the intersection of the 1-day reference isotache (slope b_v^p) with a horizontal line originating from the initial condition ($s = s_0$, $\varepsilon_v^{H^p} = 0$) represents

the yield matric suction for the soil structure at zero overall total natural strain when the net normal stress is constant ($s_{g\ v}^{p}$). This value is defined as the maximum past matric suction that the soil structure has ever experienced.

In a similar way for the water phase (Figure 4.26), the abscissa of the intersection of the 1-day reference isotache (slope b_w^p) with a horizontal line originating from the initial condition ($s = s_0$, $\varepsilon_w^{H\,p} = 0$) represents the yield matric suction for the water phase at zero total natural water mass change when the net normal stress is constant ($s_{g\ w}^{p}$). This value is defined as the maximum past matric suction that the water phase has ever experienced.

5. Find the minimum slope of an uppermost isotache by visual inspection of the non-virgin part of the isotaches. The parameters a_v^p (for soil structure) and a_w^p (for water phase), which are equal to these minimum slopes, can be calculated as:

$$a_v^p = \frac{\Delta\varepsilon_v^{H\,p}{}_{(a)}}{\Delta \ln s_{(a)}} \quad \text{: For soil structure; (Figure 4.25)} \tag{4.3}$$

$$a_w^p = \frac{\Delta\varepsilon_w^{H\,p}{}_{(a)}}{\Delta \ln s_{(a)}} \quad \text{: For water phase; (Figure 4.26)} \tag{4.4}$$

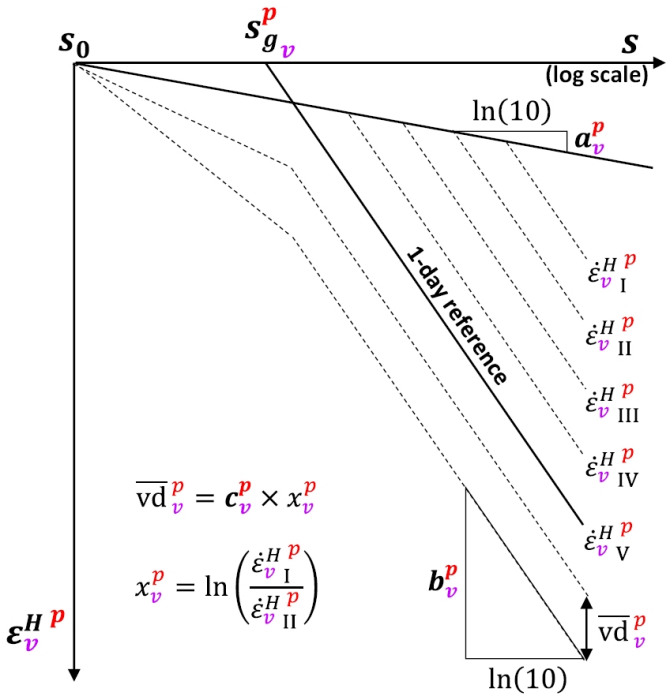

Figure 4.25. Determination of the soil structure parameters of the adapted a,b,c isotache model for increasing matric suction at a constant net normal stress (p).

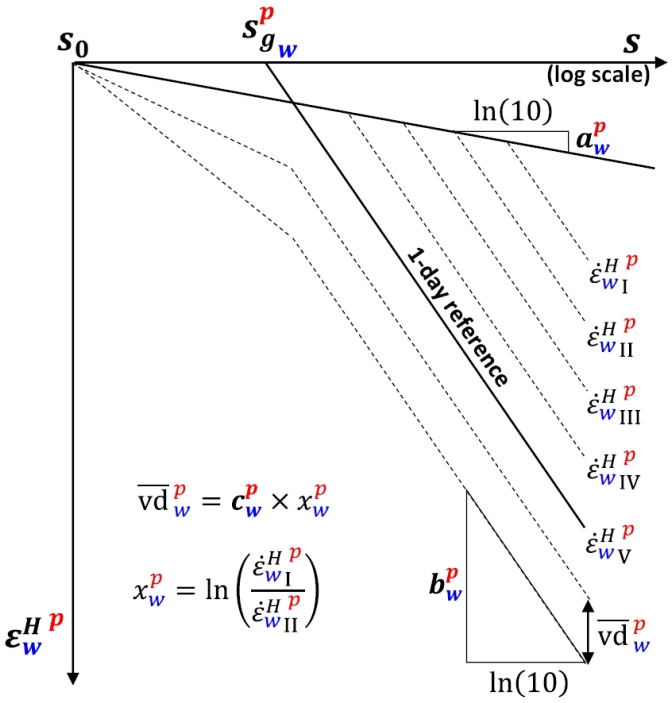

Figure 4.26. Determination of the water phase parameters of the adapted a,b,c isotache model for increasing matric suction at a constant net normal stress (p).

According to Visschedijk and Trompille (2009), as discussed for saturated conditions in *Section 2.1.6.3*, it is recommended that the parameters a_v^p (for soil structure) and a_w^p (for water phase) also be obtained from the matric suction-decreasing path (i.e., wetting) where the creep rates are low, rather than the matric suction-increasing path (i.e., drying prior to reaching the yield matric suction).

6. The parameters c_v^p (for soil structure) and c_w^p (for water phase) can be calculated as:

$$c_v^p = \frac{\overline{\mathrm{vd}}_v^p}{x_v^p} \quad \text{: For soil structure; (Figure 4.25)} \tag{4.5}$$

$$x_v^p = \ln\left(\frac{\dot{\varepsilon}_{v\,\mathrm{I}}^{H\,p}}{\dot{\varepsilon}_{v\,\mathrm{II}}^{H\,p}}\right) \quad \text{: For soil structure; (Figure 4.25)} \tag{4.6}$$

and,

$$c_w^p = \frac{\overline{\mathrm{vd}}_w^p}{x_w^p} \quad \text{: For water phase; (Figure 4.26)} \tag{4.7}$$

$$x_w^p = \ln\left(\frac{\dot{\varepsilon}_{w\,\mathrm{I}}^{H\,p}}{\dot{\varepsilon}_{w\,\mathrm{II}}^{H\,p}}\right) \quad \text{: For water phase; (Figure 4.26)} \tag{4.8}$$

where:

$\overline{\mathrm{vd}}_{v}^{p}$ is an average of the vertical distance between the soil structure isotaches in a region where they lie more straight, parallel, and equidistant, at the highest matric suction level and the lowest overall natural strain rate, when the net normal stress (*p*) is constant.

$\overline{\mathrm{vd}}_{w}^{p}$ is an average of the vertical distance between the water phase isotaches in a region where they lie more straight, parallel, and equidistant, at the highest matric suction level and the lowest rate of natural water mass change, when the net normal stress (*p*) is constant.

x_{v}^{p} and x_{w}^{p} are the parameters which depend on the interval of isotaches (for more information, see Figures 2.7, 2.8 and 2.9 in *Section 2.1.6.2*).

4.5.2 Determination of Parameters for the Adapted a,b,c Isotache Model, when Net Normal Stress Increases at Constant Matric Suction (*s*)

In order to determine the parameters of the adapted a,b,c isotache model for increasing net normal stress at a constant matric suction (*s*), the following steps should be taken:

1. Construct the isotaches on a plot of the overall natural strain (i.e., $\varepsilon_{v}^{H^{s}}$ for soil structure) or natural water mass change (i.e., $\varepsilon_{w}^{H^{s}}$ for water phase) versus net normal stress (log scale) as shown in Figures 4.27 and 4.28 (for example, see the results of Test U3 in Figures 4.16 and 4.20).

The overall natural strain rate (for soil structure) and the rate of natural water mass change (for water phase) can be calculated by using equation 2.31 (in *Section 2.1.6.9*) in order to draw the isotaches.

2. Locate the position of 1-day reference isotache. For this aim, the overall natural strain rate (for soil structure), and the rate of natural water mass change (for water phase) should be formatted as 1×10^{-n} (see the example in *Section 2.1.6.9* for saturated soils).

3. Plot the 1-day reference isotache passing from the position that was found in the last step, parallel to the lowest isotache at the highest net normal stress level. The parameters b_{v}^{s} (for soil structure) and b_{w}^{s} (for water phase) are the slopes of these lines and can be calculated as:

$$b_{v}^{s} = \frac{\Delta\varepsilon_{v}^{H^{s}}{}_{(b)}}{\Delta \ln p_{(b)}} \quad \text{: For soil structure; (Figure 4.27)} \tag{4.9}$$

$$b_{w}^{s} = \frac{\Delta\varepsilon_{w}^{H^{s}}{}_{(b)}}{\Delta \ln p_{(b)}} \quad \text{: For water phase; (Figure 4.28)} \tag{4.10}$$

4. For soil structure (Figure 4.27), the abscissa of the intersection of the 1-day reference isotache (slope b_{v}^{s}) with a horizontal line originating from the initial condition ($p = p_0$, $\varepsilon_{v}^{H^{s}} = 0$) represents

the pre-consolidation net normal stress for the soil structure at zero overall total natural strain when the matric suction is constant ($p^s_{g\,v}$).

In a similar way for the water phase (Figure 4.28), the abscissa of the intersection of the 1-day reference isotache (slope b^s_w) with a horizontal line originating from the initial condition ($p = p_0$, $\varepsilon^{H\,s}_w = 0$), represents the pre-consolidation net normal stress for the water phase at zero total natural water mass change when the matric suction is constant ($p^s_{g\,w}$).

5. Find the minimum slope of an uppermost isotache by visual inspection of the non-virgin part of the isotaches. The parameters a^s_v (for soil structure) and a^s_w (for water phase), which are equal to these minimum slopes, can be calculated as:

$$a^s_v = \frac{\Delta\varepsilon^{H\,s}_{v\ (a)}}{\Delta \ln p_{\ (a)}} \quad \text{: For soil structure; (Figure 4.27)} \tag{4.11}$$

$$a^s_w = \frac{\Delta\varepsilon^{H\,s}_{w\ (a)}}{\Delta \ln p_{\ (a)}} \quad \text{: For water phase; (Figure 4.28)} \tag{4.12}$$

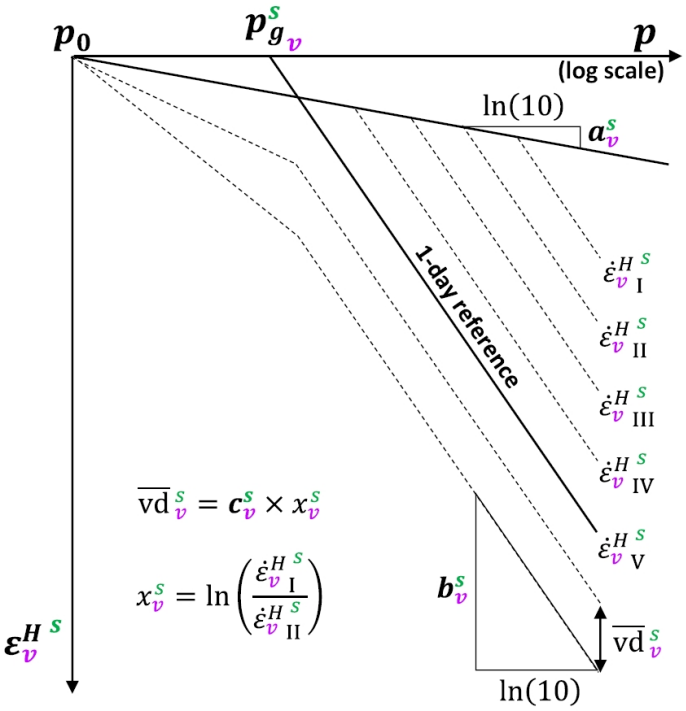

Figure 4.27. Determination of the soil structure parameters of the adapted a,b,c isotache model for increasing net normal stress at a constant matric suction (s).

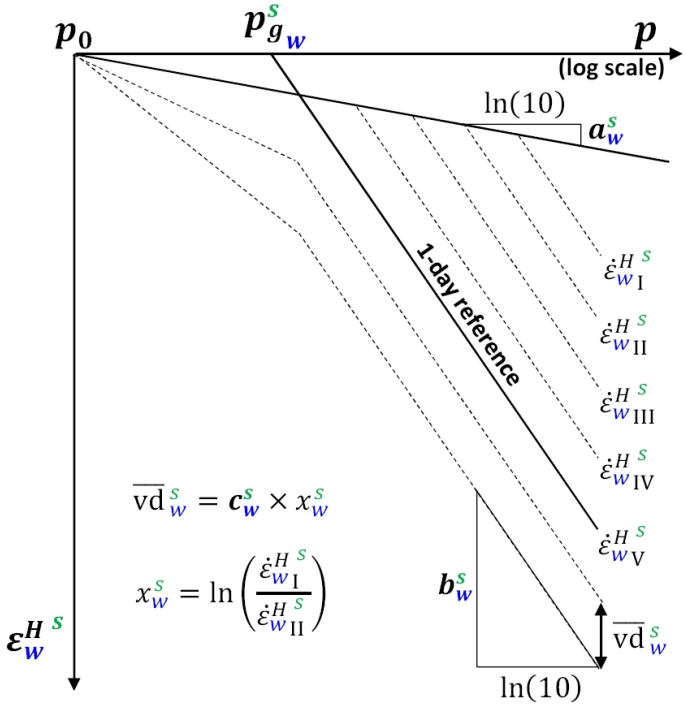

Figure 4.28. Determination of the water phase parameters of the adapted a,b,c isotache model for increasing net normal stress at a constant matric suction (*s*).

According to Visschedijk and Trompille (2009), as discussed for saturated conditions in *Section 2.1.6.3*, it is recommended that the parameters a^s_v (for soil structure) and a^s_w (for water phase) also be obtained from unloading curves, where creep rates are low.

6. The parameters c^s_v (for soil structure) and c^s_w (for water phase) can be calculated as:

$$c^s_v = \frac{\overline{\mathrm{vd}}^{\,s}_{v}}{x^s_v} \qquad \text{: For soil structure; (Figure 4.27)} \qquad (4.13)$$

$$x^s_v = \ln\left(\frac{\dot{\varepsilon}^{H\,s}_{v\,\mathrm{I}}}{\dot{\varepsilon}^{H\,s}_{v\,\mathrm{II}}}\right) \qquad \text{: For soil structure; (Figure 4.27)} \qquad (4.14)$$

and,

$$c^s_w = \frac{\overline{\mathrm{vd}}^{\,s}_{w}}{x^s_w} \qquad \text{: For water phase; (Figure 4.28)} \qquad (4.15)$$

$$x^s_w = \ln\left(\frac{\dot{\varepsilon}^{H\,s}_{w\,\mathrm{I}}}{\dot{\varepsilon}^{H\,s}_{w\,\mathrm{II}}}\right) \qquad \text{: For water phase; (Figure 4.28)} \qquad (4.16)$$

where:

$\overline{\mathrm{vd}}^{\,s}_{v}$ is an average of the vertical distance between the soil structure isotaches in a region where they lie more straight, parallel, and equidistant, at the highest net normal stress level and the lowest overall natural strain rate, when the matric suction (*s*) is constant.

$\overline{\mathrm{vd}}\,{}^{s}_{w}$ is an average of the vertical distance between the water phase isotaches in a region where they lie more straight, parallel, and equidistant, at the highest net normal stress level and the lowest rate of natural water mass change, when the matric suction (*s*) is constant.

x_v^s and x_w^s are the parameters which depend on the interval of isotaches (for more information, see Figures 2.7, 2.8 and 2.9 in *Section 2.1.6.2*).

4.6 Parameters Obtained from the Test Results to Use in the Adapted a,b,c Isotache Model

Based on the method mentioned above, the parameters of the adapted a,b,c isotache model were obtained from the suction-controlled oedometer tests and conventional oedometer tests on the compacted organic soil and are summarised in Tables 4.1 and 4.2. In the next chapter, these parameters will be used in the adapted a,b,c isotache model to simulate the overall volume and water volume changes of the soil. Various parameters in Tables 4.1 and 4.2 are defined as follows:

a_v^p, b_v^p, c_v^p : Isotache parameters for the soil structure of unsaturated soils at a constant net normal stress

$s_{g\,v}^{p}$: Yield matric suction for the soil structure (i.e., the maximum past matric suction that the soil structure has ever experienced) at zero overall total natural strain when the net normal stress is constant

a_v^s, b_v^s, c_v^s: Isotache parameters for the soil structure of unsaturated soils at a constant matric suction

$p_{g\,v}^{s}$: Pre-consolidation net normal stress for the soil structure at zero overall total natural strain when the matric suction is constant

$a_w^{(\mathrm{lin})^p}, b_w^{(\mathrm{lin})^p}, c_w^{(\mathrm{lin})^p}$: Isotache parameters for the water phase (linear water volume change) of unsaturated soils at a constant net normal stress

$a_w^{(\mathrm{lin})^s}, b_w^{(\mathrm{lin})^s}, c_w^{(\mathrm{lin})^s}$: Isotache parameters for the water phase (linear water volume change) of unsaturated soils at a constant matric suction

$s_{g\,w}^{(\mathrm{lin})^p}$: Yield matric suction for the water phase (i.e., the maximum past matric suction that the water phase has ever experienced) at zero total linear water volume change when the net normal stress is constant

$p_{g\,w}^{(\mathrm{lin})^s}$: Pre-consolidation net normal stress for the water phase at zero total linear water volume change when the matric suction is constant

Table 4.1

Parameters Obtained from the Suction-Controlled Oedometer Tests at a Constant Net Normal Stress (on the Unsaturated Compacted Organic Soil)

		s Variable		Soil structure (overall volume)						Water phase					
Test	p Constant	s_0	s	$s_{g_v}^{p}$	a_v^p	b_v^p	c_v^p	c_v^p/b_v^p	a_v^p/b_v^p	$s_{g\ w}^{(\mathrm{lin})p}$	$a_w^{(\mathrm{lin})p}$	$b_w^{(\mathrm{lin})p}$	$c_w^{(\mathrm{lin})p}$	$c_w^{(\mathrm{lin})p}/b_w^{(\mathrm{lin})p}$	$a_w^{(\mathrm{lin})p}/b_w^{(\mathrm{lin})p}$
-	kPa	kPa	kPa	kPa	-	-	-	-	-	kPa	-	-	-	-	-
U1	15	8	891	28.6	0.0045	0.0167	0.0020	0.12	0.27	73.9	0.0200	0.1025	0.0173	0.17	0.19
U2	5	6	290	20.0	0.0031	0.0167	0.0020	0.12	0.19	37.9	0.0107	0.1099	0.0091	0.08	0.10
U3	15	8	92	27.3		0.0157					0.0204				

Note. Parameters *b* and *c* were determined from the final steps of increasing matric suction.

Table 4.2

Parameters Obtained from the Suction-Controlled Oedometer Tests at a Constant Matric Suction and Conventional Oedometer Tests (on the Compacted Organic Soil)

		p Variable		Soil structure (overall volume)						Water phase					
Test	s Constant	p_0	p	$p_{g_v}^{s}$	a_v^s	b_v^s	c_v^s	c_v^s/b_v^s	a_v^s/b_v^s	$p_{g\ w}^{(\mathrm{lin})s}$	$a_w^{(\mathrm{lin})s}$	$b_w^{(\mathrm{lin})s}$	$c_w^{(\mathrm{lin})s}$	$c_w^{(\mathrm{lin})s}/b_w^{(\mathrm{lin})s}$	$a_w^{(\mathrm{lin})s}/b_w^{(\mathrm{lin})s}$
-	kPa	kPa	kPa	kPa	-	-	-	-	-	kPa	-	-	-	-	-
U1	891	15	637	173.8	0.0059	0.1031	0.0087	0.08	0.06	144.8		0.0212	0.0020	0.09	
U2	290	5	496	118.0	0.0018	0.0802	0.0060	0.07	0.02	125.5		0.0429			
U3	92	15	499	112.1	0.0067	0.1162	0.0084	0.07	0.06	112.8	0.0030	0.0416	0.0040	0.10	0.07
S1	0	1	639	52.3	0.0129	0.1016	0.0081	0.08	0.13						
S2	0	1	639	54.7	0.0126	0.1034	0.0079	0.08	0.12						
S3	0	1	639	75.3	0.0127	0.1151	0.0098	0.08	0.11						

Note. Parameters *b* and *c* were determined within the range of 300 to 500 kPa net normal stress.

Figure 4.29 presents the relationship between the value of constant matric suction (s) and the apparent pre-consolidation net normal stress for the soil structure at zero overall total natural strain when the matric suction is constant ($p_{g_v}^{s}$). This figure, which is drawn based on the data in Table 4.2, shows that the value of $p_{g_v}^{s}$ increases with increasing matric suction. These results are in line with most test results for other types of soils available in the literature. A curve, with the following equation, was fitted to the test results:

$$p_{g_v}^{s} = 78.56 + 0.001296 \cdot s + 1.571 \cdot s^{0.6} \qquad R^2 = 0.97 \qquad (4.17)$$

where the units of both $p_{g_v}^{s}$ and s are kPa.

This yield curve is conceptually similar to the loading-collapse (LC) of the Barcelona Basic Model.

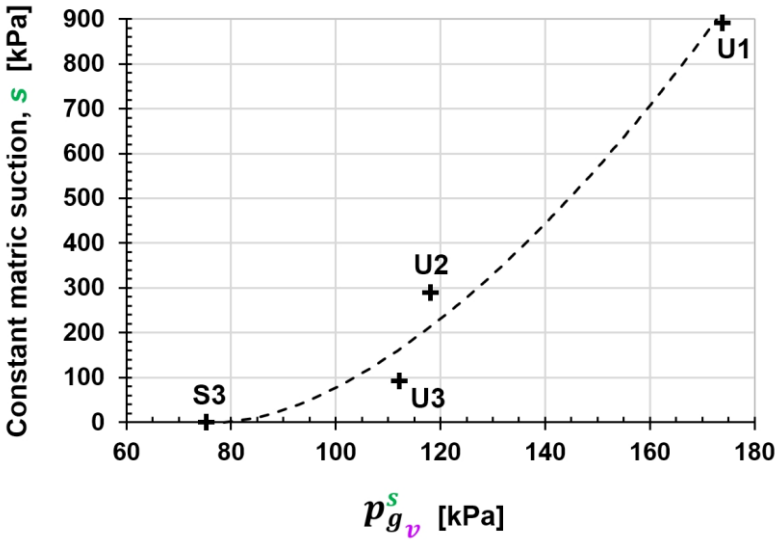

Figure 4.29. Relationship between the value of constant matric suction and the apparent pre-consolidation net normal stress for the soil structure at zero overall total natural strain when the matric suction is constant.

Figure 4.30 presents the relationship between the value of constant matric suction (s) and the apparent pre-consolidation net normal stress for the water phase at zero total linear water volume change when the matric suction is constant ($p_{g}^{(\mathrm{lin})^{s}}{}_{w}$). This figure, which is drawn based on the data in Table 4.2, shows that the value of $p_{g}^{(\mathrm{lin})^{s}}{}_{w}$ increases with increasing matric suction. A curve, with the following equation, was fitted to the test results:

$$p_{g}^{(\mathrm{lin})^{s}}{}_{w} = 97.34 - 0.02414 \cdot s + 1.172 \cdot s^{0.6} \qquad R^2 = 1 \qquad (4.18)$$

where the units of both $p_{g}^{(\mathrm{lin})^{s}}{}_{w}$ and s are kPa.

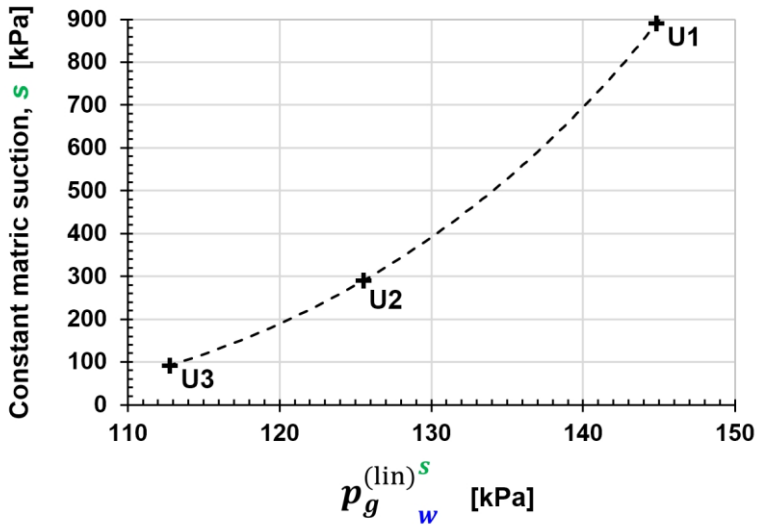

Figure 4.30. Relationship between the value of constant matric suction and the apparent pre-consolidation net normal stress for the water phase at zero total linear water volume change when the matric suction is constant.

Figure 4.31 presents the relationship between the value of constant matric suction (s) and the isotache parameter "a" for the soil structure at a constant matric suction (a_v^s), based on the data in Table 4.2. A curve, with the following equation, was fitted to the test results:

$$a_v^s = 0.01301 + 3.672 \times 10^{-6} \cdot s^{1.3} - 0.0005491 \cdot s^{0.6} \qquad R^2 = 0.99 \qquad (4.19)$$

where the unit of s is kPa.

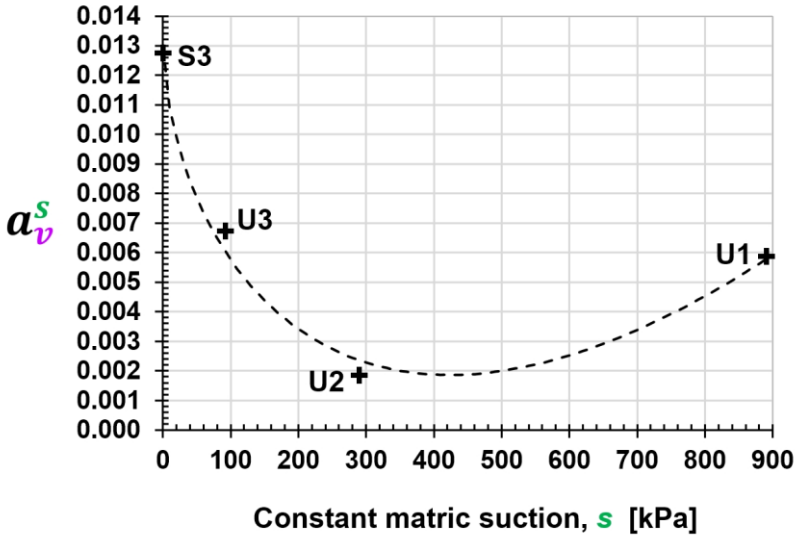

Figure 4.31. Relationship between the value of constant matric suction and the isotache parameter "a" for the soil structure at a constant matric suction (a_v^s).

Figure 4.32 presents the relationship between the value of constant matric suction (s) and the isotache parameter b for the soil structure at a constant matric suction (b_v^s), based on the data in Table 4.2. A curve, with the following equation, was fitted to the test results:

$$b_v^s = 0.1214 - 0.0002308 \cdot s + 3.561 \times 10^{-6} \cdot s^{1.6} \qquad R^2 = 0.77 \qquad (4.20)$$

where the unit of s is kPa.

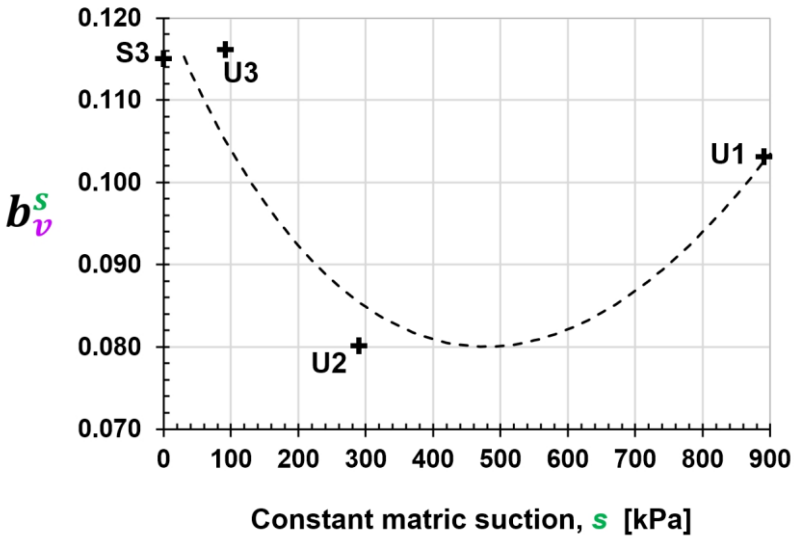

Figure 4.32. Relationship between the value of constant matric suction and the isotache parameter b for the soil structure at a constant matric suction (b_v^s).

Figure 4.33 presents the relationship between the value of constant matric suction (s) and the isotache parameter c for the soil structure at a constant matric suction (c_v^s), based on the data in Table 4.2. A curve, with the following equation, was fitted to the test results:

$$c_v^s = 0.01 - 5.869 \times 10^{-5} \cdot s + 1.469 \times 10^{-5} \cdot s^{1.2} \qquad R^2 = 0.96 \qquad (4.21)$$

where the unit of s is kPa.

Figures 4.31, 4.32 and 4.33 demonstrate that the isotache parameters of the soil structure at a constant matric suction (a_v^s, b_v^s and c_v^s) decrease to the minimum values as matric suction is increased from zero to 290 kPa for this compacted organic soil. Then, these parameters increase once the soil reaches 891 kPa matric suction. Increasing these parameters beyond a certain matric suction value could be interpreted as resulting from a new geometrical arrangement of the soil fabric when the matric suction approaches a very high value. In addition, the brittleness of organic particles may increase significantly beyond a certain matric suction value due to decreasing water content, and as a result, the organic particles may start to break (i.e., collapse) under the applied net normal

stress. However, further research is needed to better understand the dependency of the isotache parameters on matric suction.

This behaviour is more or less similar to the observations of Rampino et al. (2000, p. 758) on the value of κ for a silty sand, as illustrated in Figure 2.27b in *Section 2.2.5*.

Increasing these parameters beyond a certain matric suction value is also in line with the observation of Koliji (2008, p. 134) on the reconstituted samples of a clay with low plasticity. As illustrated in Figure 2.29 in *Section 2.2.5*, his test results show that the tangential compressibility index (i.e., the slope of the normal consolidation part of the oedometer curve) increases significantly when the condition of soil samples changes from saturated to unsaturated.

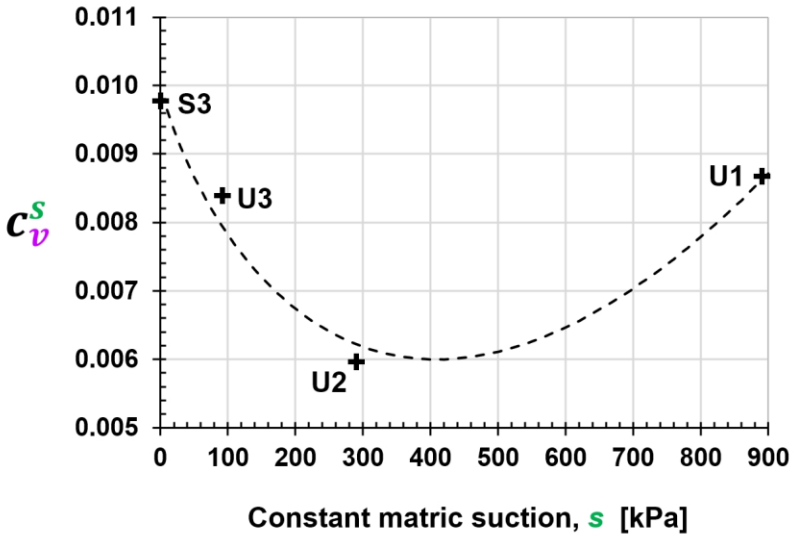

Figure 4.33. Relationship between the value of constant matric suction and the isotache parameter c for the soil structure at a constant matric suction (c_v^s).

4.7 Values of c/b and a/b for Unsaturated Conditions

The "C_α/C_C concept" proposed by Mesri and Godlewski (1977) for saturated soils, is also observed here for the unsaturated compacted organic soil. Based on the test results, the range of c/b and a/b for the soil structure are summarised below.

At a constant matric suction ($0 \leq s \leq 891$ kPa), when the net normal stress increases:

$$\frac{c_v^s}{b_v^s} = 0.07 - 0.08$$

$$\frac{a_v^s}{b_v^s} = 0.02 - 0.13$$

For more information, see Table 4.2.

The values of c_v^s/b_v^s seem to be independent of the matric suction and are within the range of 0.025-0.10 reported by Mesri and Godlewski (1977) for C_α/C_C in saturated soils. The values of c_v^s/b_v^s are also within the range of 0.04-0.1 reported by Den Haan (1996) for c/b in saturated soils.

In addition, the test results show that the values of a_v^s/b_v^s for saturated conditions are within the range of 0.11-0.13, which is in line with Den Haan and Sellmeijer (2000), who report that a/b is approximately 0.1-0.2 in saturated soils. For unsaturated soil samples, the values of a_v^s/b_v^s are within the range of 0.02-0.06. Therefore, the values of a_v^s/b_v^s in unsaturated conditions are smaller than these values in saturated conditions.

At a constant net normal stress ($5 \leq p \leq 15$ kPa), when the matric suction increases:

$$\frac{c_v^p}{b_v^p} = 0.12$$

$$\frac{a_v^p}{b_v^p} = 0.19 - 0.27$$

For more information, see Table 4.1.

Chapter 5: Modelling and Simulation

5.1 Introduction

In this chapter, the framework and equations of the adapted a,b,c isotache model are presented for the overall volume and water volume changes of unsaturated soils. Afterwards, the suction-controlled oedometer tests were simulated using the adapted model and compared with the test results of overall volume and water volume changes.

5.2 Equations of the Adapted a,b,c Isotache Model for Unsaturated Soils when the Net Normal Stress is Constant

In the following two sections, the incremental form of the a,b,c isotache model for saturated soils (Den Haan, 1994, 1996, 2008; see also Leoni et al., 2008), which was reviewed in *Section 2.1.6.8*, is adapted for unsaturated conditions based on the volume change theory for unsaturated soils (Fredlund & Morgenstern, 1976), at a constant net normal stress. In the equations, subscripts I and II denote the first and the last creep isotache in a step, respectively, and the subscript 1 stands for 1-day (for more information, see Figures 2.21 and 2.22 in *Section 2.1.6.8*). The reference intrinsic time is equal to one day ($\tau^{p}_{v\,1}$ & $\tau^{p}_{w\,1} = 1$ day) in all relevant calculations.

5.2.1 Overall Natural Strain at a Constant Net Normal Stress

The overall natural strain of an unsaturated soil at a constant net normal stress (*p*) can be calculated by using the following incremental form of the adapted a,b,c isotache model. Figure 5.1 helps to understand the definition of the parameters used in the equations.

$$s^{p}_{g\,v\,vp} = \left[\left(s^{p}_{g\,v}\right)^{b^{p}_{v}} \cdot (s_0)^{-a^{p}_{v}}\right]^{\left(\frac{1}{b^{p}_{v}-a^{p}_{v}}\right)} \tag{5.1}$$

$$s^{p}_{g\,v\,vp_{(\text{update})_i}} = s^{p}_{g\,v\,vp} \cdot \text{EXP}\left(\frac{\varepsilon^{H\,p}_{v\,vp\,i-1}}{b^{p}_{v} - a^{p}_{v}}\right) \tag{5.2}$$

$$OCR^{p}_{v\,vp\,\text{I}\,i} = \left(\frac{s^{p}_{g\,v\,vp_{(\text{update})_i}}}{s_i}\right) \tag{5.3}$$

$$\tau^{p}_{v\,\text{I}\,i} = \tau^{p}_{v\,1} \cdot OCR^{p}_{v\,vp\,\text{I}\,i}{}^{\left(\frac{b^{p}_{v}-a^{p}_{v}}{c^{p}_{v}}\right)} \tag{5.4}$$

$$\tau^{p}_{v\,\text{II}\,i} = \tau^{p}_{v\,\text{I}\,i} + \Delta t^{p}_{i} \tag{5.5}$$

$$\varepsilon_{v}^{H\,p}{}_{vp\,i} = c_{v}^{p} \cdot \ln\left(\frac{\tau_{v}^{p}{}_{\mathrm{II}\,i}}{\tau_{v}^{p}{}_{\mathrm{I}\,i}}\right) \tag{5.6}$$

$$\varepsilon_{v}^{H\,p}{}_{e\,i} = a_{v}^{p} \cdot \ln\left(\frac{s_i}{s_0}\right) \tag{5.7}$$

$$\varepsilon_{v}^{H\,p}{}_{i} = \varepsilon_{v}^{H\,p}{}_{e\,i} + \sum_{0}^{i} \varepsilon_{v}^{H\,p}{}_{vp\,i} \tag{5.8}$$

$$\varepsilon_{v}^{(\mathrm{lin})p}{}_{i} = 1 - \mathrm{EXP}(-\varepsilon_{v}^{H\,p}{}_{i}) \tag{5.9}$$

where

$a_{v}^{p}, b_{v}^{p}, c_{v}^{p}$: Isotache parameters for the soil structure of unsaturated soils at a constant net normal stress

$\varepsilon_{v}^{H\,p}{}_{vp\,i}$: Visco-plastic part of the overall natural strain at a constant net normal stress (step i)

$\sum_{0}^{i} \varepsilon_{v}^{H\,p}{}_{vp\,i}$: All the visco-plastic parts of the overall natural strain accumulated up to the current step i, at a constant net normal stress

$\varepsilon_{v}^{H\,p}{}_{e\,i}$: Elastic part of the overall natural strain at a constant net normal stress (step i)

$\varepsilon_{v}^{H\,p}{}_{i}$: Overall total natural strain at a constant net normal stress (step i)

$\varepsilon_{v}^{(\mathrm{lin})p}{}_{i}$: Overall total linear strain at a constant net normal stress (step i)

$s_{g}^{p}{}_{v}$: Yield matric suction for the soil structure (i.e., the maximum past matric suction that the soil structure has ever experienced) at zero overall total natural strain when the net normal stress is constant

$s_{g}^{p}{}_{v\,vp}$: Yield matric suction for the soil structure at zero overall visco-plastic natural strain when the net normal stress is constant

$s_{g}^{p}{}_{v\,vp_{(\mathrm{update})_i}}$: Updated yield matric suction for the soil structure in an overall visco-plastic natural strain coordinate at a constant net normal stress (step i)

s_0: Initial matric suction when the net normal stress is constant

s_i: Desired matric suction when the net normal stress is constant (step i)

$OCR_{v}^{p}{}_{vp\,\mathrm{I}\,i}$: Over-consolidation ratio for the isotache I; in an overall visco-plastic natural strain coordinate at a constant net normal stress (step i)

Δt_{i}^{p}: Duration of creep (in days) for step i at a constant net normal stress

$\tau^{p}_{v\,\mathrm{I}\,i}$: Intrinsic time (in days) for the isotache I of the soil structure at a constant net normal stress (step i)

$\tau^{p}_{v\,\mathrm{II}\,i}$: Intrinsic time (in days) for the isotache II of the soil structure at a constant net normal stress (step i). For more information about isotache I (τ_{I}) and isotache II (τ_{II}), see Figures 2.21 and 2.22 in *Section 2.1.6.8*.

$\tau^{p}_{v\,1}$: Reference intrinsic time (in days) for the soil structure at a constant net normal stress

$\tau^{p}_{v\,i} = c^{p}_{v} / \dot{\varepsilon}^{H\,p}_{v\,vp\,i}$ (Based on equation 2.15)

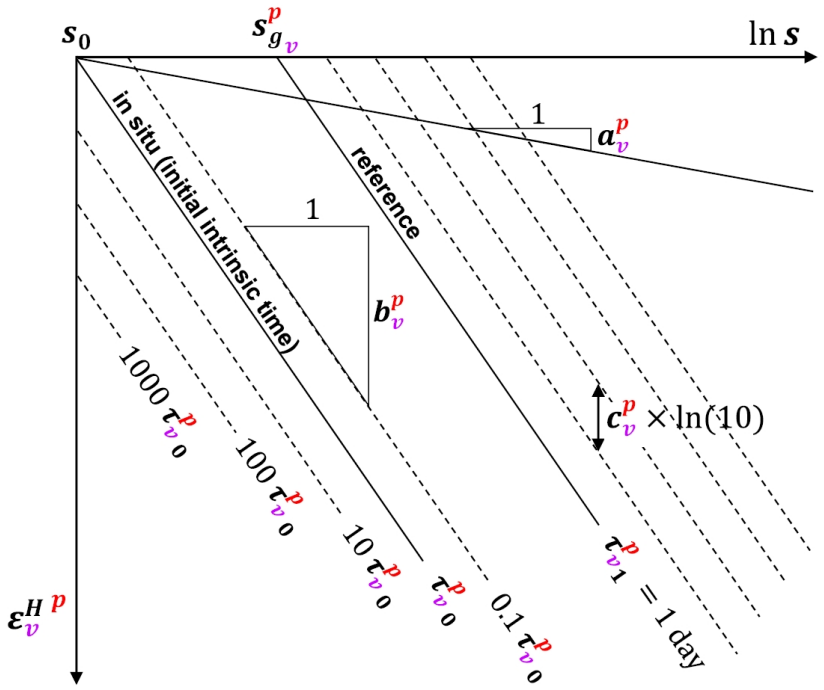

Figure 5.1. The adapted a,b,c isotache model for the soil structure of unsaturated soils at a constant net normal stress.

5.2.2 Natural Water Mass Change at a Constant Net Normal Stress

The natural water mass change of an unsaturated soil at a constant net normal stress (p) can be calculated by using the following incremental form of the adapted a,b,c isotache model. Figure 5.2 helps to understand the definition of the parameters used in the equations.

$$s^{p}_{g\,w\,vp} = \left[\left(s^{p}_{g\,w}\right)^{b^{p}_{w}} \cdot (s_0)^{-a^{p}_{w}}\right]^{\left(\frac{1}{b^{p}_{w} - a^{p}_{w}}\right)} \tag{5.10}$$

$$s_{g\,{}^{p}_{w\ vp\,(\mathrm{update})_i}} = s_{g\,{}^{p}_{w\ vp}} \cdot \mathrm{EXP}\left(\frac{\varepsilon^{H\ p}_{w\,vp\ i-1}}{b^{p}_{w} - a^{p}_{w}}\right) \tag{5.11}$$

$$OCR^{p}_{w\ vp\ \mathrm{I}\ i} = \left(\frac{s_{g\,{}^{p}_{w\ vp\,(\mathrm{update})_i}}}{s_i}\right) \tag{5.12}$$

$$\tau^{p}_{w_{\mathrm{I}\ i}} = \tau^{p}_{w_1} \cdot OCR^{p}_{w\ vp\ \mathrm{I}\ i}{}^{\left(\frac{b^{p}_{w} - a^{p}_{w}}{c^{p}_{w}}\right)} \tag{5.13}$$

$$\tau^{p}_{w_{\mathrm{II}\ i}} = \tau^{p}_{w_{\mathrm{I}\ i}} + \Delta t^{p}_{i} \tag{5.14}$$

$$\varepsilon^{H\ p}_{w\,vp\ i} = c^{p}_{w} \cdot \ln\left(\frac{\tau^{p}_{w_{\mathrm{II}\ i}}}{\tau^{p}_{w_{\mathrm{I}\ i}}}\right) \tag{5.15}$$

$$\varepsilon^{H\ p}_{w\,e\ i} = a^{p}_{w} \cdot \ln\left(\frac{s_i}{s_0}\right) \tag{5.16}$$

$$\varepsilon^{H\ p}_{w\,i} = \varepsilon^{H\ p}_{w\,e\ i} + \sum_{0}^{i} \varepsilon^{H\ p}_{w\,vp\ i} \tag{5.17}$$

$$\varepsilon^{(\mathrm{lin})\,p}_{w\ \ i} = \frac{m_d \cdot (1 + e_{w_0}) \cdot \left[1 - \exp\left(-\varepsilon^{H\ p}_{w\,i}\right)\right]}{\rho_s \cdot V_0} \tag{5.18}$$

where

$a^{p}_{w}, b^{p}_{w}, c^{p}_{w}$: Isotache parameters for the water phase (natural water mass change) of unsaturated soils at a constant net normal stress

$\varepsilon^{H\ p}_{w\,vp\ i}$: Visco-plastic part of the natural water mass change at a constant net normal stress (step i)

$\sum_{0}^{i} \varepsilon^{H\ p}_{w\,vp\ i}$: All the visco-plastic parts of the natural water mass change accumulated up to the current step i, at a constant net normal stress

$\varepsilon^{H\ p}_{w\,e\ i}$: Elastic part of the natural water mass change at a constant net normal stress (step i)

$\varepsilon^{H\ p}_{w\,i}$: Total natural water mass change at a constant net normal stress (step i)

$\varepsilon^{(\mathrm{lin})\,p}_{w\ \ i}$: Total linear water volume change at a constant net normal stress (step i). For more information, see equation 3.28.

$s_{g\ w}^{p}$: Yield matric suction for the water phase (i.e., the maximum past matric suction that the water phase has ever experienced) at zero total natural water mass change when the net normal stress is constant

$s_{g\ w\ vp}^{p}$: Yield matric suction for the water phase at zero visco-plastic natural water mass change when the net normal stress is constant

$s_{g\ w\ vp_{(\mathrm{update})_i}}^{p}$: Updated yield matric suction for the water phase in a visco-plastic natural water mass change coordinate at a constant net normal stress (step i)

s_0: Initial matric suction when the net normal stress is constant

s_i: Desired matric suction when the net normal stress is constant (step i)

$OCR_{w\ vp\ \mathrm{I}\ i}^{p}$: Over-consolidation ratio for the isotache I; in a visco-plastic natural water mass change coordinate at a constant net normal stress (step i)

Δt_i^p: Duration of creep (in days) for step i at a constant net normal stress

$\tau_{w_{\mathrm{I}\ i}}^{p}$: Intrinsic time (in days) for the isotache I of the water phase (natural water mass change) at a constant net normal stress (step i)

$\tau_{w_{\mathrm{II}\ i}}^{p}$: Intrinsic time (in days) for the isotache II of the water phase (natural water mass change) at a constant net normal stress (step i). For more information about isotache I (τ_{I}) and isotache II (τ_{II}), see Figures 2.21 and 2.22 in *Section 2.1.6.8*.

$\tau_{w_1}^{p}$: Reference intrinsic time (in days) for the water phase (natural water mass change) at a constant net normal stress

$\tau_{w\ i}^{p} = c_w^p / \dot{\varepsilon}_{w\ vp\ i}^{H\ p}$ (Based on equation 2.15)

m_d: Dry mass of the soil element

e_{w_0}: Initial water ratio

ρ_s: Density of soil solids

V_0: Initial overall volume of the soil element

When the net normal stress is constant, the distinction between equation 5.18 for the water phase and equation 5.9 for the soil structure should be carefully considered.

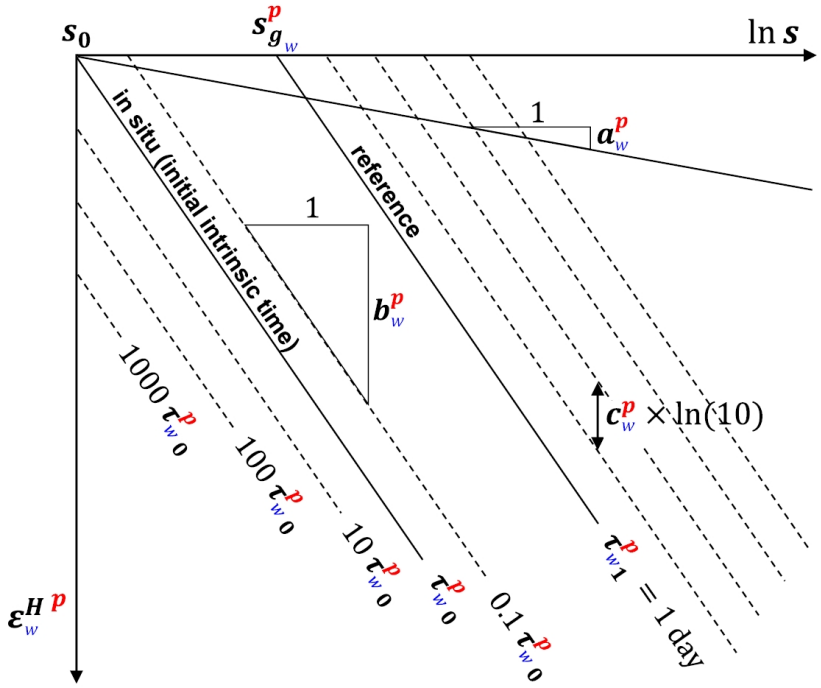

Figure 5.2. The adapted a,b,c isotache model for the water phase of unsaturated soils at a constant net normal stress.

5.3 Equations of the Adapted a,b,c Isotache Model for Unsaturated Soils when the Matric Suction is Constant

In the following two sections, the incremental form of the a,b,c isotache model for saturated soils (Den Haan, 1994, 1996, 2008; see also Leoni et al., 2008), which was reviewed in *Section 2.1.6.8*, is adapted for unsaturated conditions based on the volume change theory for unsaturated soils (Fredlund & Morgenstern, 1976), at a constant matric suction. In the equations, subscripts I and II denote the first and the last creep isotache in a step, respectively, and the subscript 1 stands for 1-day (for more information, see Figures 2.21 and 2.22 in *Section 2.1.6.8*). The reference intrinsic time is equal to one day ($\tau^s_{v_1}$ & $\tau^s_{w_1} = 1$ day) in all relevant calculations.

5.3.1 Overall Natural Strain at a Constant Matric Suction

The overall natural strain of an unsaturated soil at a constant matric suction (s) can be calculated by using the following incremental form of the adapted a,b,c isotache model. Figure 5.3 helps to understand the definition of the parameters used in the equations.

$$p^s_{g_{v\,vp}} = \left[\left(p^s_{g_v}\right)^{b^s_v} \cdot (p_0)^{-a^s_v}\right]^{\left(\frac{1}{b^s_v - a^s_v}\right)} \tag{5.19}$$

$$p_{g\,v\,vp(\text{update})_i}^{s} = p_{g\,v\,vp}^{s} \cdot \text{EXP}\left(\frac{\varepsilon_{v\,vp\,i-1}^{H\,s}}{b_v^s - a_v^s}\right) \tag{5.20}$$

$$OCR_{v\,vp\,\text{I}\,i}^{s} = \left(\frac{p_{g\,v\,vp(\text{update})_i}^{s}}{p_i}\right) \tag{5.21}$$

$$\tau_{v\,\text{I}\,i}^{s} = \tau_{v\,1}^{s} \cdot OCR_{v\,vp\,\text{I}\,i}^{s\,\left(\frac{b_v^s - a_v^s}{c_v^s}\right)} \tag{5.22}$$

$$\tau_{v\,\text{II}\,i}^{s} = \tau_{v\,\text{I}\,i}^{s} + \Delta t_i^s \tag{5.23}$$

$$\varepsilon_{v\,vp\,i}^{H\,s} = c_v^s \cdot \ln\left(\frac{\tau_{v\,\text{II}\,i}^{s}}{\tau_{v\,\text{I}\,i}^{s}}\right) \tag{5.24}$$

$$\varepsilon_{v\,e\,i}^{H\,s} = a_v^s \cdot \ln\left(\frac{p_i}{p_0}\right) \tag{5.25}$$

$$\varepsilon_{v\,i}^{H\,s} = \varepsilon_{v\,e\,i}^{H\,s} + \sum_0^i \varepsilon_{v\,vp\,i}^{H\,s} \tag{5.26}$$

$$\varepsilon_{v\,i}^{(\text{lin})\,s} = 1 - \text{EXP}(-\varepsilon_{v\,i}^{H\,s}) \tag{5.27}$$

where

a_v^s, b_v^s, c_v^s: Isotache parameters for the soil structure of unsaturated soils at a constant matric suction

$\varepsilon_{v\,vp\,i}^{H\,s}$: Visco-plastic part of the overall natural strain at a constant matric suction (step i)

$\sum_0^i \varepsilon_{v\,vp\,i}^{H\,s}$: All the visco-plastic parts of the overall natural strain accumulated up to the current step i, at a constant matric suction

$\varepsilon_{v\,e\,i}^{H\,s}$: Elastic part of the overall natural strain at a constant matric suction (step i)

$\varepsilon_{v\,i}^{H\,s}$: Overall total natural strain at a constant matric suction (step i)

$\varepsilon_{v\,i}^{(\text{lin})\,s}$: Overall total linear strain at a constant matric suction (step i)

$p_{g\,v}^{s}$: Pre-consolidation net normal stress for the soil structure at zero overall total natural strain when the matric suction is constant

$p_{g\,v\,vp}^{s}$: Pre-consolidation net normal stress for the soil structure at zero overall visco-plastic natural strain when the matric suction is constant

$p^{s}_{g_{v\ vp_{(\text{update})}}}{}_{i}$: Updated pre-consolidation net normal stress for the soil structure in an overall visco-plastic natural strain coordinate at a constant matric suction (step i)

p_0: Initial net normal stress when the matric suction is constant

p_i: Desired net normal stress when the matric suction is constant (step i)

$OCR^{s}_{v\ vp_{\mathrm{I}\ i}}$: Over-consolidation ratio for the isotache I; in an overall visco-plastic natural strain coordinate at a constant matric suction (step i)

Δt^{s}_{i}: Duration of creep (in days) for step i at a constant matric suction

$\tau^{s}_{v_{\mathrm{I}\ i}}$: Intrinsic time (in days) for the isotache I of the soil structure at a constant matric suction (step i)

$\tau^{s}_{v_{\mathrm{II}\ i}}$: Intrinsic time (in days) for the isotache II of the soil structure at a constant matric suction (step i). For more information about isotache I (τ_{I}) and isotache II (τ_{II}), see Figures 2.21 and 2.22 in *Section 2.1.6.8*.

$\tau^{s}_{v_1}$: Reference intrinsic time (in days) for the soil structure at a constant matric suction

$\tau^{s}_{v\ i} = c^{s}_{v} / \dot{\varepsilon}^{H\ s}_{v\ vp\ i}$ (Based on equation 2.15)

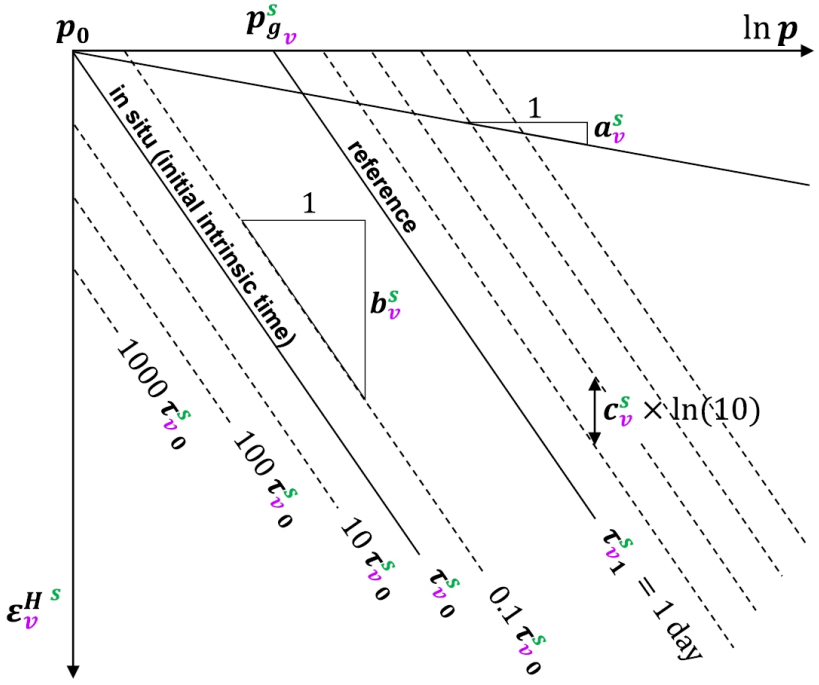

Figure 5.3. The adapted a,b,c isotache model for the soil structure of unsaturated soils at a constant matric suction.

5.3.2 Natural Water Mass Change at a Constant Matric Suction

The natural water mass change of an unsaturated soil at a constant matric suction (*s*) can be calculated by using the following incremental form of the adapted a,b,c isotache model. Figure 5.4 helps to understand the definition of the parameters used in the equations.

$$p^{s}_{g\,w\,vp} = \left[\left(p^{s}_{g\,w}\right)^{b^{s}_{w}} \cdot (p_0)^{-a^{s}_{w}}\right]^{\left(\frac{1}{b^{s}_{w}-a^{s}_{w}}\right)} \tag{5.28}$$

$$p^{s}_{g\,w\,vp_{(\mathrm{update})_i}} = p^{s}_{g\,w\,vp} \cdot \mathrm{EXP}\left(\frac{\varepsilon^{H\,s}_{w\,vp\;i-1}}{b^{s}_{w}-a^{s}_{w}}\right) \tag{5.29}$$

$$OCR^{s}_{w\,vp\,\mathrm{I}\,i} = \left(\frac{p^{s}_{g\,w\,vp_{(\mathrm{update})_i}}}{p_i}\right) \tag{5.30}$$

$$\tau^{s}_{w\,\mathrm{I}\,i} = \tau^{s}_{w\,1} \cdot OCR^{s}_{w\,vp\,\mathrm{I}\,i}{}^{\left(\frac{b^{s}_{w}-a^{s}_{w}}{c^{s}_{w}}\right)} \tag{5.31}$$

$$\tau^{s}_{w\,\mathrm{II}\,i} = \tau^{s}_{w\,\mathrm{I}\,i} + \Delta t^{s}_{i} \tag{5.32}$$

$$\varepsilon^{H\,s}_{w\,vp\;i} = c^{s}_{w} \cdot \ln\left(\frac{\tau^{s}_{w\,\mathrm{II}\,i}}{\tau^{s}_{w\,\mathrm{I}\,i}}\right) \tag{5.33}$$

$$\varepsilon^{H\,s}_{w\,e\;i} = a^{s}_{w} \cdot \ln\left(\frac{p_i}{p_0}\right) \tag{5.34}$$

$$\varepsilon^{H\,s}_{w\,i} = \varepsilon^{H\,s}_{w\,e\;i} + \sum_{0}^{i} \varepsilon^{H\,s}_{w\,vp\;i} \tag{5.35}$$

$$\varepsilon^{(\mathrm{lin})\,s}_{w\;\;i} = \frac{m_d \cdot (1+e_{w_0}) \cdot \left[1-\exp\left(-\varepsilon^{H\,s}_{w\,i}\right)\right]}{\rho_s \cdot V_0} \tag{5.36}$$

where

$a^{s}_{w}, b^{s}_{w}, c^{s}_{w}$: Isotache parameters for the water phase (natural water mass change) of unsaturated soils at a constant matric suction

$\varepsilon^{H\,s}_{w\,vp\;i}$: Visco-plastic part of the natural water mass change at a constant matric suction (step i)

$\sum_{0}^{i} \varepsilon^{H\,s}_{w\,vp\;i}$: All the visco-plastic parts of the natural water mass change accumulated up to the current step i, at a constant matric suction

$\varepsilon_{w\,e\,i}^{H\,s}$: Elastic part of the natural water mass change at a constant matric suction (step i)

$\varepsilon_{w\,i}^{H\,s}$: Total natural water mass change at a constant matric suction (step i)

$\varepsilon_{w\,\;i}^{(\mathrm{lin})\,s}$: Total linear water volume change at a constant matric suction (step i). For more information, see equation 3.28.

$p_{g\,w}^{s}$: Pre-consolidation net normal stress for the water phase at zero total natural water mass change when the matric suction is constant

$p_{g\,w\;vp}^{s}$: Pre-consolidation net normal stress for the water phase at zero visco-plastic natural water mass change when the matric suction is constant

$p_{g\,w\;vp_{(\mathrm{update})\,i}}^{s}$: Updated pre-consolidation net normal stress for the water phase in a visco-plastic natural water mass change coordinate at a constant matric suction (step i)

p_0: Initial net normal stress when the matric suction is constant

p_i: Desired net normal stress when the matric suction is constant (step i)

$OCR_{w\;vp\;\mathrm{I}\;i}^{s}$: Over-consolidation ratio for the isotache I; in a visco-plastic natural water mass change coordinate at a constant matric suction (step i)

Δt_i^s: Duration of creep (in days) for step i at a constant matric suction

$\tau_{w\,\mathrm{I}\;i}^{s}$: Intrinsic time (in days) for the isotache I of the water phase (natural water mass change) at a constant matric suction (step i)

$\tau_{w\,\mathrm{II}\;i}^{s}$: Intrinsic time (in days) for the isotache II of the water phase (natural water mass change) at a constant matric suction (step i). For more information about isotache I (τ_{I}) and isotache II (τ_{II}), see Figures 2.21 and 2.22 in *Section 2.1.6.8*.

$\tau_{w\,1}^{s}$: Reference intrinsic time (in days) for the water phase (natural water mass change) at a constant matric suction

$\tau_{w\,i}^{s} = c_w^s / \dot{\varepsilon}_{w\,vp\;i}^{H\,s}$ (Based on equation 2.15)

m_d: Dry mass of the soil element

e_{w_0}: Initial water ratio

ρ_s: Density of soil solids

V_0: Initial overall volume of the soil element

Here also when the matric suction is constant, the distinction between equation 5.36 for the water phase and equation 5.27 for the soil structure should be carefully considered.

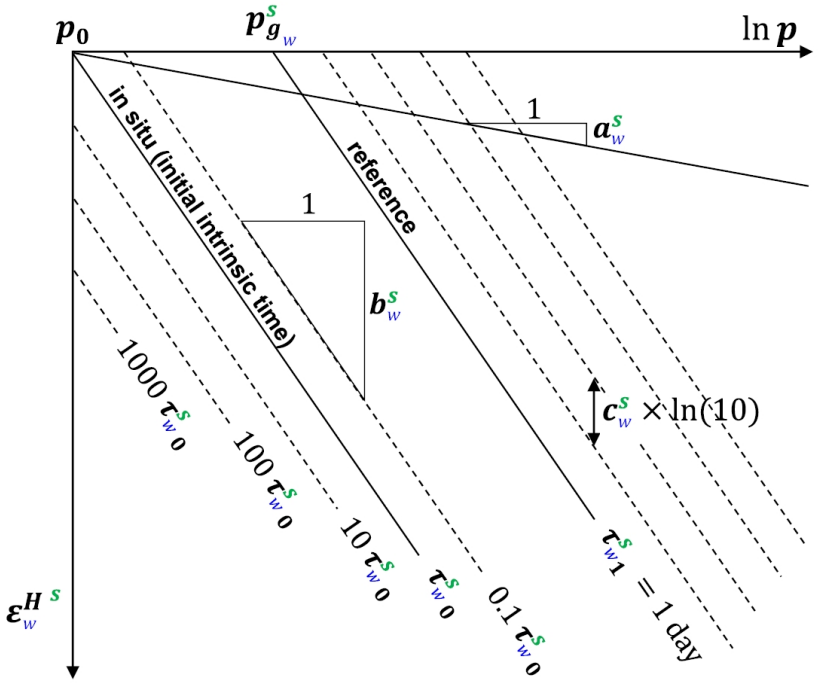

Figure 5.4. The adapted a,b,c isotache model for the water phase of unsaturated soils at a constant matric suction.

5.4 Simulation

5.4.1 Simulation of the Conventional Oedometer Test

This section describes the simulation of the conventional oedometer test S1 on the saturated compacted organic soil. The over-consolidation ratio in a total natural strain coordinate at the end of a loading step (OCR_{II}) can be obtained by using the following procedure. In the equations, subscripts I and II denote the first and the last creep isotache in a step, respectively, and the subscript 1 stands for 1-day (for more information, see Figures 2.21 and 2.22 in *Section 2.1.6.8*). The reference intrinsic time is equal to one day ($\tau_1 = 1$ day) in all relevant calculations.

$$p_{g_{vp}} = \left[(p_g)^b \cdot (\acute{\sigma}_{v_0})^{-a}\right]^{\left(\frac{1}{b-a}\right)} \qquad \text{Equation 2.17}$$

where the calculated value of $p_{g\ vp}$ should be updated at each step.

Equation 2.19 can be written as:

$$OCR = OCR_{vp}^{\left(\frac{b-a}{b}\right)} \tag{5.37}$$

Equations 2.18 and 2.20 are redefined for the first creep isotache of a loading step in a visco-plastic natural strain coordinate as:

$$OCR_{vp\ \mathrm{I}} = \left(\frac{p_{g\ vp}}{\acute{\sigma}_v}\right) \tag{5.38}$$

$$\tau_{\mathrm{I}} = \tau_1 \cdot OCR_{vp\ \mathrm{I}}^{\left(\frac{b-a}{c}\right)} \tag{5.39}$$

At the end of a loading step:

$$\tau_{\mathrm{II}} = \tau_{\mathrm{I}} + \Delta t \qquad \text{Equation 2.26}$$

Equation 5.39 can be written for the end of a loading step as:

$$\tau_{\mathrm{II}} = \tau_1 \cdot OCR_{vp\ \mathrm{II}}^{\left(\frac{b-a}{c}\right)} \tag{5.40}$$

or,

$$OCR_{vp\ \mathrm{II}} = \left(\frac{\tau_{\mathrm{II}}}{\tau_1}\right)^{\left(\frac{c}{b-a}\right)} \tag{5.41}$$

In addition, equation 5.37 can also be expressed for the end of a loading step as:

$$OCR_{\mathrm{II}} = OCR_{vp\ \mathrm{II}}^{\left(\frac{b-a}{b}\right)} \tag{5.42}$$

By combining the equations 5.41 and 5.42, the over-consolidation ratio in a total natural strain coordinate at the end of a loading step can be obtained as follows:

$$OCR_{\mathrm{II}} = \left[\left(\frac{\tau_{\mathrm{II}}}{\tau_1}\right)^{\left(\frac{c}{b-a}\right)}\right]^{\left(\frac{b-a}{b}\right)} = \left(\frac{\tau_{\mathrm{II}}}{\tau_1}\right)^{\left(\frac{c}{b}\right)} \tag{5.43}$$

This equation represents a link between τ_{II} and OCR_{II} which is a fundamental aspect of the a,b,c isotache model.

Figure 5.5 presents the simulation of the conventional oedometer test S1 on the saturated compacted organic soil. Two aspects of this figure can be explained as follows:

1. The pattern of isotaches was simulated using the a,b,c isotache model on a plot of natural strain versus vertical stress (log scale). The average of the visco-plastic part of the natural strain rate

($\dot{\varepsilon}_{vp}^{H}$) at the end of the last three steps and the average of the over-consolidation ratio in a total natural strain coordinate (OCR_{II} based on equation 5.43) at the end of the last three steps were calculated for each isotache line.

2. The conventional oedometer test S1 was simulated utilising the a,b,c isotache model, at the end of each step (●) by using the isotache parameters (a, b, c and p_g) of Test S2. The isotache parameters of Test S2 were used for simulation of saturated soil samples, because the LIR of this test is a middle value (LIR = 0.65). The results of this simulation (●) are compared with the laboratory results (×) at the end of each step. The values on the graph indicate the duration of each step of the oedometer test S1 (in days).

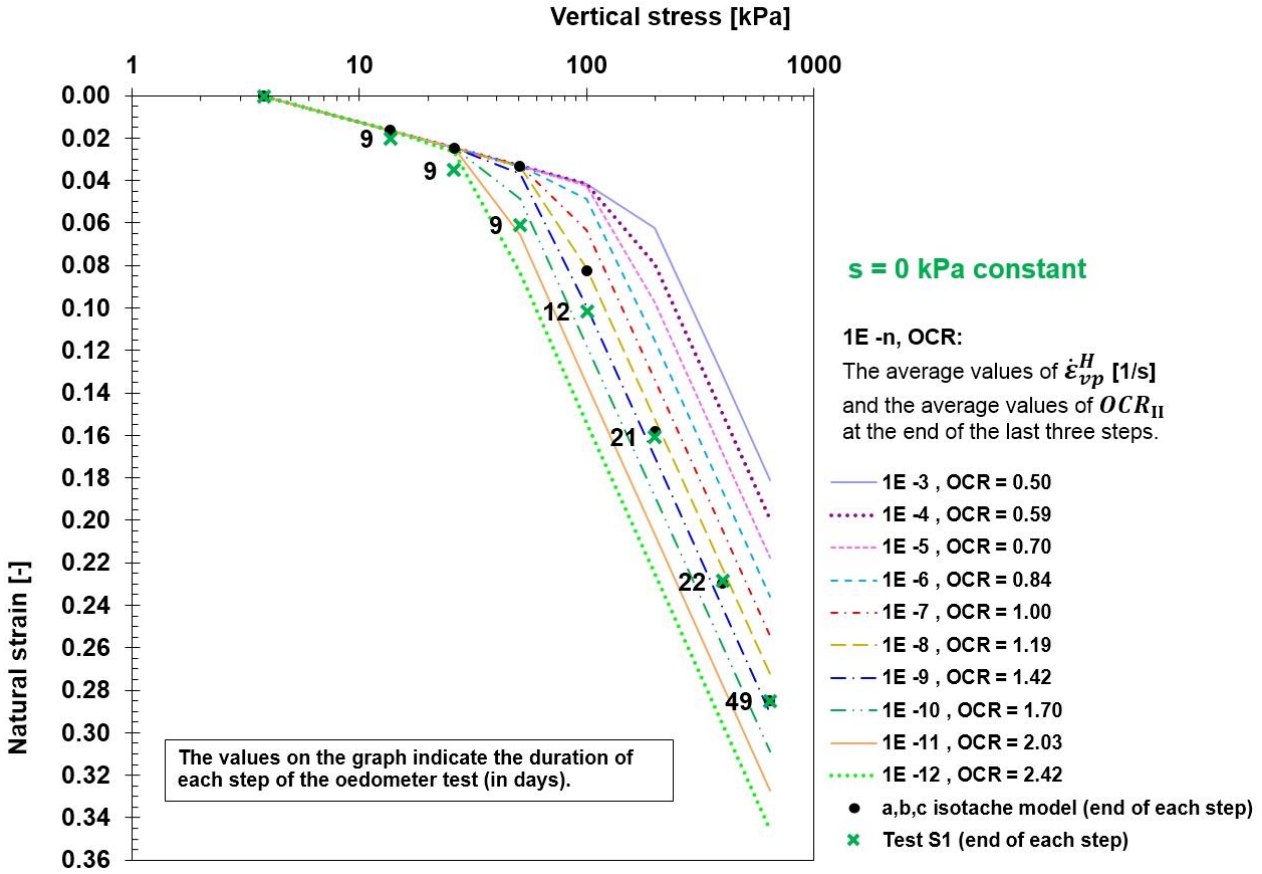

Figure 5.5. Simulation of the conventional oedometer test S1 (saturated compacted organic soil).

As can be seen in Figure 5.5, the comparison between the model and the test results shows that the a,b,c isotache model can predict deformations of the saturated soil sample with high accuracy.

The simulation can also be applied “as a back analysis” as Abed (2008) explains “where the available field data is used to calibrated [*sic*] the missing parameters of the model” (p. 166).

5.4.2 Simulation of the Suction-Controlled Oedometer Tests for the Soil Structure

This section describes the simulation of the suction-controlled oedometer tests for the soil structure of the unsaturated compacted organic soil. The over-consolidation ratios in an overall total natural strain coordinate at the end of a loading step when the net normal stress is constant ($OCR^{p}_{v\,\mathrm{II}}$) or when the matric suction is constant ($OCR^{s}_{v\,\mathrm{II}}$) were calculated by using equations 5.44 and 5.45 and are presented for each isotache. These equations were obtained by a procedure similar to that in *Section 5.4.1*.

Figure 5.6 presents the simulation of the suction-controlled oedometer test U1 for the soil structure of the unsaturated compacted organic soil at a constant net normal stress of 15 kPa.

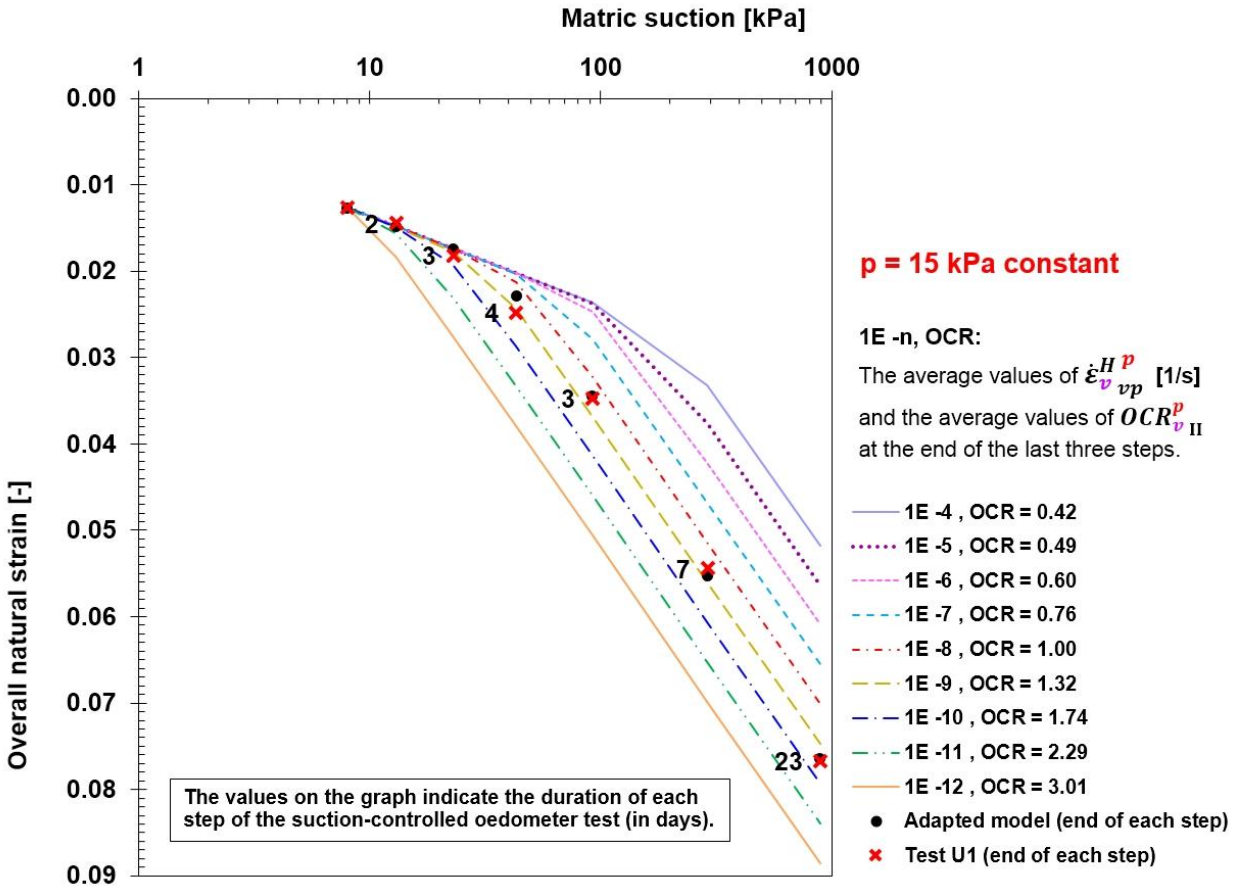

Figure 5.6. Simulation of the suction-controlled oedometer test U1 for the soil structure at a constant net normal stress of 15 kPa (unsaturated compacted organic soil).

Two aspects of Figure 5.6 can be explained as follows:

1. The pattern of isotaches was simulated using the adapted model on a plot of overall natural strain versus matric suction (log scale). The average of the visco-plastic part of the overall natural strain

rate ($\dot{\varepsilon}_{v}^{H}{}_{vp}^{p}$) at the end of the last three steps and the average of the over-consolidation ratio in an overall total natural strain coordinate ($OCR_{v}^{p}{}_{\text{II}}$ based on equation 5.44) at the end of the last three steps were calculated for each isotache line, when the net normal stress was kept 15 kPa constant.

$$OCR_{v}^{p}{}_{\text{II}} = \left(\frac{\tau_{v}^{p}{}_{\text{II}}}{\tau_{v}^{p}{}_{1}}\right)^{\left(\frac{c_{v}^{p}}{b_{v}^{p}}\right)} \tag{5.44}$$

2. The suction-controlled oedometer test U1 was simulated using the adapted model, at the end of each step. The results of this simulation (●) are compared with the laboratory results (×) at the end of each step. The values on the graph indicate the duration of each step of the suction-controlled oedometer test U1 (in days).

As can be seen in Figure 5.6, the comparison between the adapted a,b,c isotache model and the test results shows that the adapted model can predict deformations of the soil structure with high accuracy at a constant net normal stress.

Figure 5.7 presents the simulation of the suction-controlled oedometer test U1 for the soil structure of the unsaturated compacted organic soil at a constant matric suction of 891 kPa. Two aspects of this figure can be explained as follows:

1. The pattern of isotaches was simulated using the adapted model on a plot of overall natural strain versus net normal stress (log scale). The average of the visco-plastic part of the overall natural strain rate ($\dot{\varepsilon}_{v}^{H}{}_{vp}^{s}$) at the end of the last three steps and the average of the over-consolidation ratio in an overall total natural strain coordinate ($OCR_{v}^{s}{}_{\text{II}}$ based on equation 5.45) at the end of the last three steps were calculated for each isotache line, when the matric suction was kept 891 kPa constant.

$$OCR_{v}^{s}{}_{\text{II}} = \left(\frac{\tau_{v}^{s}{}_{\text{II}}}{\tau_{v}^{s}{}_{1}}\right)^{\left(\frac{c_{v}^{s}}{b_{v}^{s}}\right)} \tag{5.45}$$

2. The suction-controlled oedometer test U1 was simulated using the adapted model, at the end of each step. The results of this simulation (●) are compared with the laboratory results (×) at the end of each step. The values on the graph indicate the duration of each step of the suction-controlled oedometer test U1 (in days).

As can be seen in Figure 5.7, the comparison between the adapted a,b,c isotache model and the test results shows that the adapted model can predict deformations of the soil structure with high accuracy at a constant matric suction.

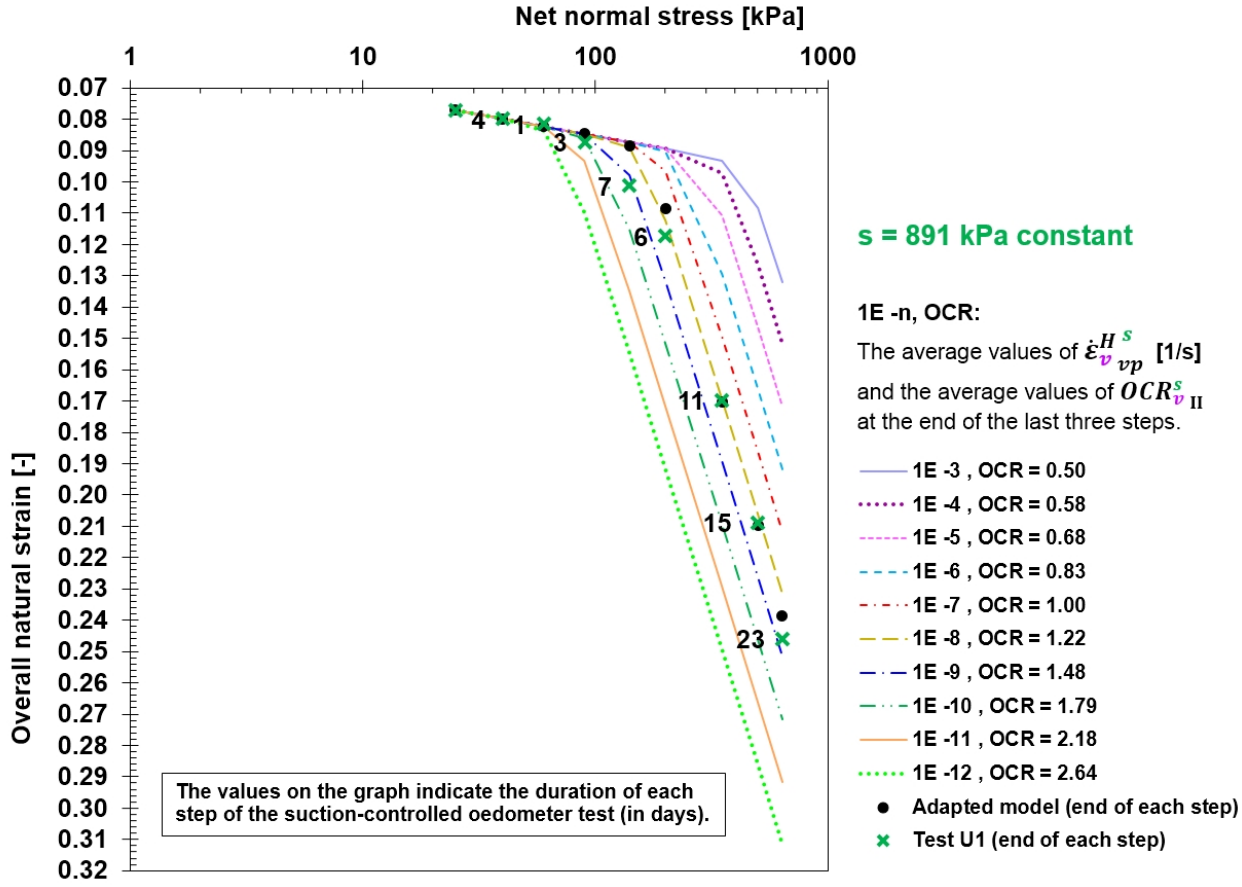

Figure 5.7. Simulation of the suction-controlled oedometer test U1 for the soil structure at a constant matric suction of 891 kPa (unsaturated compacted organic soil).

Figure 5.8 is created by combining the Figures 5.6 and 5.7. This figure presents the simulation of the suction-controlled oedometer test U1 for the soil structure of the unsaturated compacted organic soil under two conditions: (1) increasing matric suction when net normal stress was 15 kPa constant, (2) increasing net normal stress when matric suction was 891 kPa constant. The average of the visco-plastic part of the overall natural strain rate at the end of the last three steps when the net normal stress is constant ($\dot{\varepsilon}_{v\,vp}^{H\,p}$) as well as when the matric suction is constant ($\dot{\varepsilon}_{v\,vp}^{H\,s}$) are presented for each isotache. Furthermore, the average of the over-consolidation ratios at the end of the last three steps in an overall total natural strain coordinate when the net normal stress is constant ($OCR_{v\,\mathrm{II}}^{p}$) as well as when the matric suction is constant ($OCR_{v\,\mathrm{II}}^{s}$) are presented for each isotache, based on equations 5.44 and 5.45.

Figure 5.8 shows that for an equal increase in the stress-state variables (i.e., *s* or *p*), the magnitude of overall natural strain for the first stress path of Test U1 (i.e., increasing *s* at a constant *p*) is much less than that of the second stress path of the test (i.e., increasing *p* at a constant *s*).

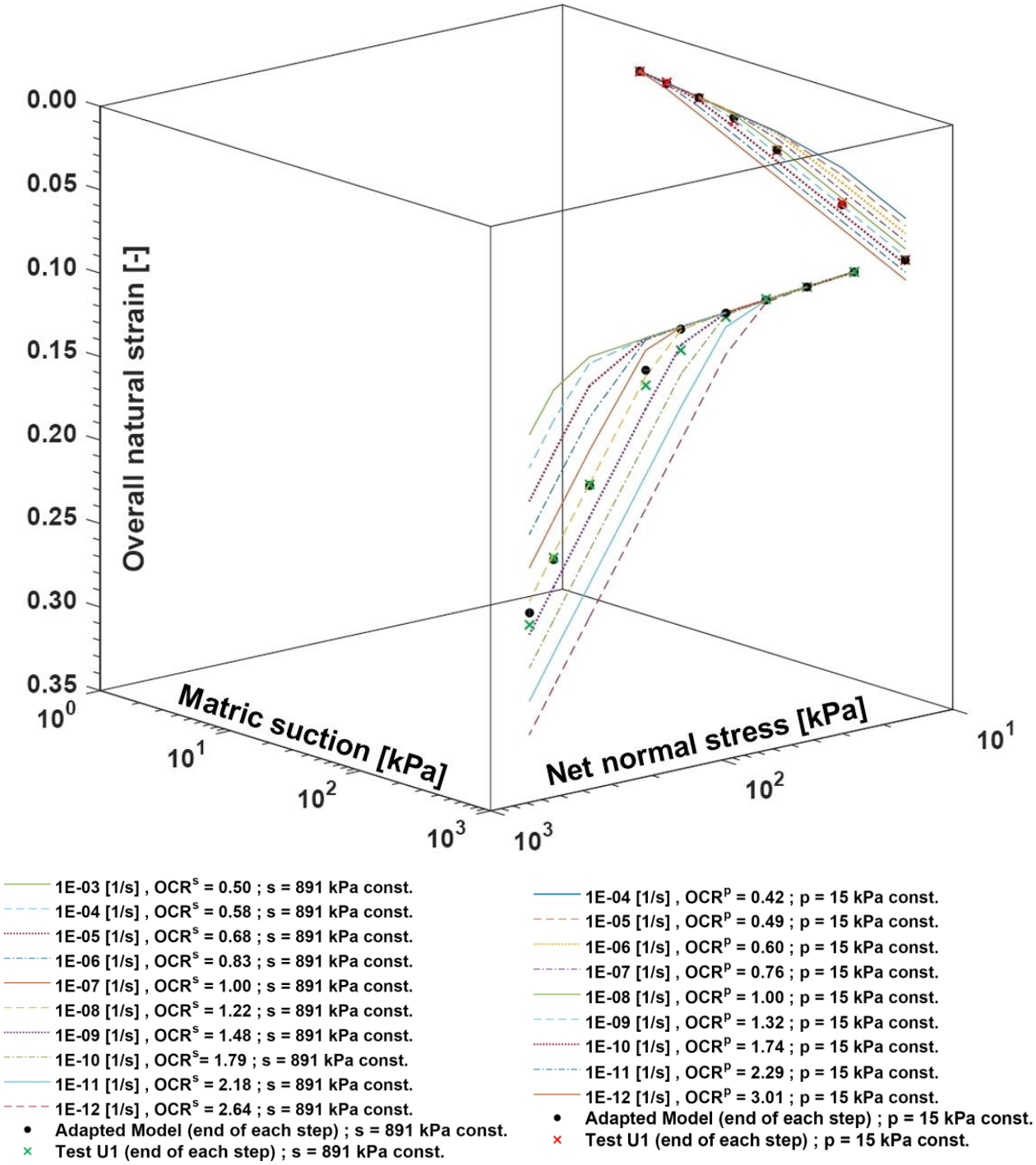

Figure 5.8. Three-dimensional simulation of the suction-controlled oedometer test U1 for the soil structure (unsaturated compacted organic soil).

5.4.3 Simulation of the Suction-Controlled Oedometer Tests for the Water Phase

This section describes the simulation of the suction-controlled oedometer tests for the water phase of the unsaturated compacted organic soil.

The over-consolidation ratios in a total linear water volume change coordinate at the end of a loading step when the net normal stress is constant ($OCR_{w}^{(\mathrm{lin})^{p}}{}_{\mathrm{II}}$) or when the matric suction is constant ($OCR_{w}^{(\mathrm{lin})^{s}}{}_{\mathrm{II}}$) were calculated by using equations 5.46 and 5.47 and are presented for each isotache. These equations were obtained by a procedure similar to that in *Section 5.4.1*.

Figure 5.9 presents the simulation of the suction-controlled oedometer test U1 for the water phase of the unsaturated compacted organic soil at a constant net normal stress of 15 kPa. Two aspects of this figure can be explained as follows:

1. The pattern of isotaches was simulated using the adapted model on a plot of linear water volume change (see equation 3.11) versus matric suction (log scale). The average of the visco-plastic part of the rate of linear water volume change ($\dot{\varepsilon}_{w}^{(\mathrm{lin})^{p}}{}_{vp}$) at the end of the last two steps were calculated for each isotache line, when the net normal stress was kept 15 kPa constant. Furthermore, the average of the over-consolidation ratio in a total linear water volume change coordinate ($OCR_{w}^{(\mathrm{lin})^{p}}{}_{\mathrm{II}}$) at the end of the last two steps were calculated based on equation 5.46 for each isotache line, when the net normal stress was kept 15 kPa constant.

$$OCR_{w}^{(\mathrm{lin})^{p}}{}_{\mathrm{II}} = \left(\frac{\tau_{w}^{(\mathrm{lin})^{p}}{}_{\mathrm{II}}}{\tau_{w}^{(\mathrm{lin})^{p}}{}_{1}} \right)^{\left(\frac{c_{w}^{(\mathrm{lin})^{p}}}{b_{w}^{(\mathrm{lin})^{p}}} \right)} \tag{5.46}$$

where

$\tau_{w}^{(\mathrm{lin})^{p}}{}_{\mathrm{II}}$: Intrinsic time (in days) for the isotache II of the water phase (linear water volume change) at a constant net normal stress

$\tau_{w}^{(\mathrm{lin})^{p}}{}_{1}$: Reference intrinsic time (in days) for the water phase (linear water volume change) at a constant net normal stress

2. The suction-controlled oedometer test U1 was simulated using the adapted model, at the end of each step. The results of this simulation (●) are compared with the laboratory results (×) at the end of each step. The values on the graph indicate the duration of each step of the suction-controlled oedometer test U1 (in days).

As can be seen in Figure 5.9, the comparison between the adapted a,b,c isotache model and the test results shows that the adapted model can predict water volume changes of the unsaturated soil sample with high accuracy at a constant net normal stress.

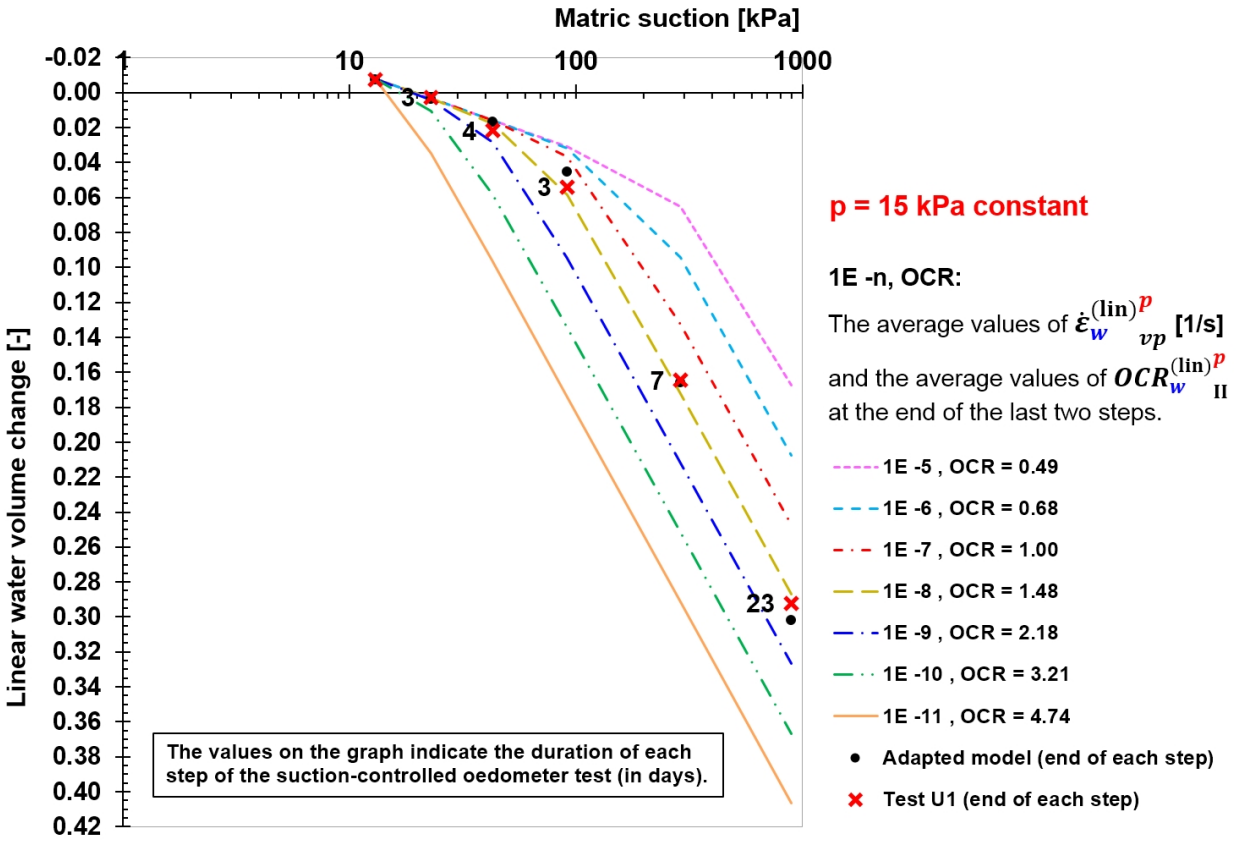

Figure 5.9. Simulation of the suction-controlled oedometer test U1 for the water phase at a constant net normal stress of 15 kPa (unsaturated compacted organic soil).

Figure 5.10 presents the simulation of the suction-controlled oedometer test U3 for the water phase of the unsaturated compacted organic soil at a constant matric suction of 92 kPa. Two aspects of this figure can be explained as follows:

1. The pattern of isotaches was simulated using the adapted model on a plot of linear water volume change (see equation 3.11) versus net normal stress (log scale). The average of the visco-plastic part of the rate of linear water volume change ($\dot{\varepsilon}_w^{(\mathrm{lin})^s}{}_{vp}$) at the end of the last three steps were calculated for each isotache line, when the matric suction was kept 92 kPa constant. Furthermore, the average of the over-consolidation ratio in a total linear water volume change coordinate ($OCR_w^{(\mathrm{lin})^s}{}_{\mathrm{II}}$) at the end of the last three steps were calculated based on equation 5.47 for each isotache line, when the matric suction was kept 92 kPa constant.

$$OCR_w^{(\mathrm{lin})^s}{}_{\mathrm{II}} = \left(\frac{\tau_w^{(\mathrm{lin})^s}{}_{\mathrm{II}}}{\tau_w^{(\mathrm{lin})^s}{}_{1}} \right)^{\left(\frac{c_w^{(\mathrm{lin})^s}}{b_w^{(\mathrm{lin})^s}} \right)} \tag{5.47}$$

where

$\tau_{w\ \mathrm{II}}^{(\mathrm{lin})^{s}}$: Intrinsic time (in days) for the isotache II of the water phase (linear water volume change) at a constant matric suction

$\tau_{w\ 1}^{(\mathrm{lin})^{s}}$: Reference intrinsic time (in days) for the water phase (linear water volume change) at a constant matric suction

2. The suction-controlled oedometer test U3 was simulated using the adapted model, at the end of each step. The results of this simulation (●) are compared with the laboratory results (×) at the end of each step. The values on the graph indicate the duration of each step of the suction-controlled oedometer test U3 (in days).

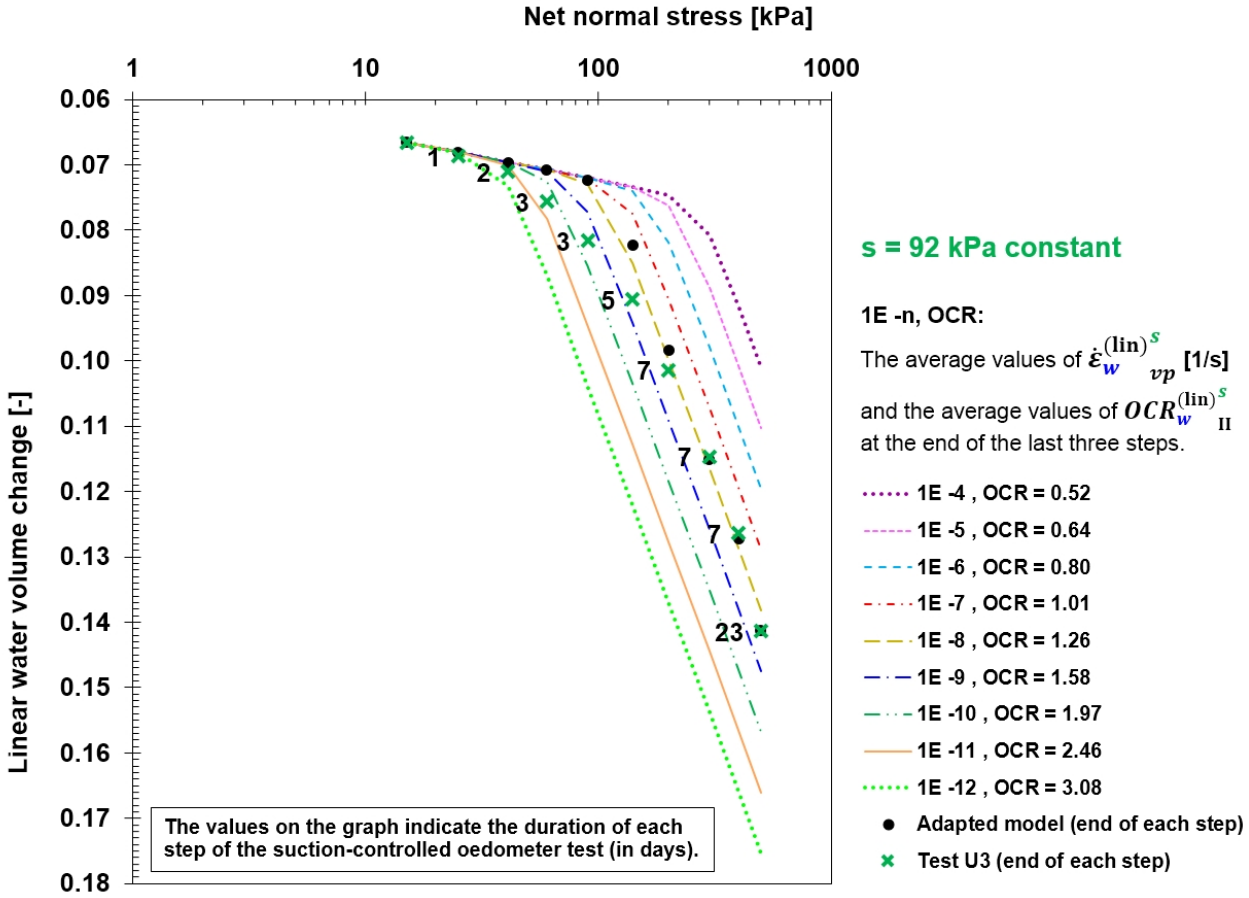

Figure 5.10. Simulation of the suction-controlled oedometer test U3 for the water phase at a constant matric suction of 92 kPa (unsaturated compacted organic soil).

As can be seen in Figure 5.10, the comparison between the adapted a,b,c isotache model and the test results shows that the adapted model can predict water volume changes of the unsaturated soil sample with high accuracy at a constant matric suction.

Chapter 6: Conclusion

6.1 Summary and Conclusions

In this research, three conventional oedometer tests were performed on saturated soil samples at various Load Increment Ratios (LIR), and three suction-controlled oedometer tests were conducted on unsaturated soil samples. All six samples were prepared from a Sandy Organic Silt (OH) by using static compaction at the wet side of the Proctor optimum. At the beginning of each test, the water content and dry density of all samples were very similar.

The long-term volume change behaviour of the unsaturated compacted organic soil was studied in terms of the overall natural strain (ε_v^H) and natural water mass change (ε_w^H), void ratio (e) and water ratio (e_w), linear ($\varepsilon_w^{(\mathrm{lin})}$) and momentary ($\varepsilon_w^m$) water volume change, as well as in terms of the degree of saturation (Sr).

In this study, the overall volume and water volume changes were monitored during testing. To increase the accuracy of water volume measurement during the long duration tests, an additional standpipe was added to each suction-controlled oedometer apparatus as a benchmark (for more information, see *Appendix D*).

The suction-controlled oedometer test results show that significant overall volume and water volume changes occur when the unsaturated soil sample is subjected to a matric suction greater than the yield matric suction. This finding agrees with Rahardjo and Fredlund (1996). Similarly, significant overall volume and water volume changes occur when the unsaturated soil sample is subjected to a net normal stress greater than the pre-consolidation net normal stress.

The suction-controlled oedometer test results show that, at a constant net normal stress when the applied matric suction is greater than the yield value, the slope of the natural water mass change curve is significantly steeper than the slope of the overall natural strain curve. Therefore, parameter b for the water phase is much larger than b for the soil structure at a constant net normal stress. In contrast, at a constant matric suction when the applied net normal stress is greater than the pre-consolidation value, the slope of the overall natural strain curve is significantly steeper than the slope of the natural water mass change curve. Therefore, parameter b for the soil structure is much larger than b for the water phase at a constant matric suction.

The suction-controlled oedometer test results indicate that, at a constant net normal stress, the air ratio ($e_a = V_a/V_s \;\&\; e_a = e - e_w$) increases as matric suction increases. In contrast, at a constant matric suction, the air ratio decreases as net normal stress increases.

Comparison between the linear water volume change ($\varepsilon_w^{(\mathrm{lin})}$) and the natural water mass change (ε_w^H) indicates that when the amount of water volume change is high, the difference between the linear water volume change and the natural water mass change is significant (see Figure 3.28).

When the overall volume is decreasing, the value of the momentary water volume change (ε_w^m) is greater than the value of the linear water volume change ($\varepsilon_w^{(\mathrm{lin})}$), because: $V_{\mathrm{current}} \leq V_0$. Under this condition, the slopes of the momentary water volume change (versus net normal stress or matric suction) are always greater than the slopes of the linear water volume change. Therefore, the volume

changes in each step due to the applied net normal stress or matric suction can be much better distinguished for the momentary water volume change.

Based on the suction-controlled oedometer test results, when the constant matric suction is high, the water volume change continues to increase during unloading of net normal stress. In other words, when the constant matric suction is high, decreasing net normal stress does not increase the water volume of the soil sample. However, under this condition, the degree of saturation decreases due to the increasing overall volume of the soil sample.

Two approximately constant values for $\Delta e_w/\Delta e$ (change in water ratio divided by change in void ratio, from Airò Farulla, 2008) were distinguished in each suction-controlled oedometer test on the compacted organic soil, under increasing matric suction and net normal stress. The larger value of $\Delta e_w/\Delta e$ belongs to the path of decreasing degree of saturation, and the smaller one belongs to the path of increasing degree of saturation. The transition between these two paths represents the minimum degree of saturation during the entire test period.

Based on the experimental test results, the volume change behaviour of the saturated compacted organic soil is dependent on time and stress. In addition, the dependency of volume change behaviour on time, stress and matric suction was observed in the soil structure of the unsaturated compacted organic soil. The findings demonstrate that the secondary compression index (C_α) of the compacted organic soil in unsaturated conditions is not unique and is a function of time and net normal stress, similar to its saturated condition. Furthermore, C_α for this soil is a function of matric suction as well. Therefore, applying the classical method to study volume changes of unsaturated compacted organic soils using C_α (on a plot of void ratio versus logarithmic scale of time) leads to inaccurate results. This problem is solved by applying the isotache approach.

In addition, it was observed that in the water phase of this unsaturated soil, at a constant net normal stress, the water volume change behaviour was dependent on time and matric suction.

The conventional oedometer test results on the saturated compacted organic soil show that the decrease of Load Increment Ratio (LIR) from 1.0 to 0.65 has no effect on the isotache pattern and the values of the parameters a, b, c and p_g of the model. However, the decrease of LIR from 0.65 to 0.3 increases the strain, especially at vertical stresses higher than 500 kPa. Therefore as a preliminary conclusion: in order to obtain reliable parameters via the isotache approach, a constant LIR should be maintained during tests. However, more testing is needed to better understand the sensitivity of the isotache pattern to LIR.

A necessary condition for a parameter to be used for studying the water phase of unsaturated soils via the isotache approach is that it be independent of the overall volume change of the soil sample. This study recommends using the “natural water mass change” (ε_w^H), especially when the water volume change is high.

This research highlights that the volume change of an unsaturated compacted organic soil can also be predicted by the isotache approach used for saturated soils. Utilising the results of suction-controlled oedometer tests, the a,b,c isotache model was adapted for unsaturated conditions based

on the theory of overall volume and water volume changes of unsaturated soils (Fredlund & Morgenstern, 1976), and the isotache patterns were studied.

The test results demonstrate that a phenomenon similar to creep in the soil structure exists for the water phase of the unsaturated soil. This phenomenon, which acts as a delay in the outflow of water from the soil sample, will be called *water-phase creep*. However, further research is needed to gain insight into the isotache patterns of unsaturated soils, especially for the water phase.

At a constant net normal stress, isotache patterns exist for the soil structure when the matric suction increases. These patterns demonstrate that creep in the soil structure of unsaturated soils occurs due to increasing matric suction. In addition, at a constant net normal stress, isotache patterns exist for the water phase when the matric suction increases. Although some isotaches are not parallel and equidistant **when the net normal stress is constant** and the matric suction increases, it could be concluded that:

- During creep in the **soil structure**, there is a strong possibility that a unique relationship exists between the matric suction (*s*), the overall *total* natural strain ($\varepsilon_v^{H\,p}$), and the *visco-plastic* part of the overall natural strain rate ($\dot{\varepsilon}_{v\,vp}^{H\,p}$).
- During **water-phase** creep, there is a strong possibility that a unique relationship exists between the matric suction (*s*), the *total* natural water mass change ($\varepsilon_w^{H\,p}$), and the *visco-plastic* part of the rate of natural water mass change ($\dot{\varepsilon}_{w\,vp}^{H\,p}$).

Moreover, at a constant matric suction, isotache patterns exist for the soil structure when the net normal stress increases. These patterns demonstrate that creep in the soil structure of unsaturated soils occurs due to increasing net normal stress. In addition, at a constant matric suction, isotache patterns exist for the water phase when the net normal stress increases. Although some isotaches are not parallel and equidistant **when the matric suction is constant** and the net normal stress increases, it could be concluded that:

- During creep in the **soil structure**, there is a strong possibility that a unique relationship exists between the net normal stress (*p*), the overall *total* natural strain ($\varepsilon_v^{H\,s}$), and the *visco-plastic* part of the overall natural strain rate ($\dot{\varepsilon}_{v\,vp}^{H\,s}$).
- During **water-phase** creep, there is a strong possibility that a unique relationship exists between the net normal stress (*p*), the *total* natural water mass change ($\varepsilon_w^{H\,s}$), and the *visco-plastic* part of the rate of natural water mass change ($\dot{\varepsilon}_{w\,vp}^{H\,s}$).

In this study, the procedure to determine model parameters from suction-controlled oedometer tests on unsaturated soil samples was introduced. Afterwards, the required parameters for the adapted a,b,c isotache model were obtained from the suction-controlled oedometer tests and conventional oedometer tests on the compacted organic soil.

The test results indicate that the matric suction has very important effects on the volume change behaviour of the unsaturated compacted organic soil. The parameters a, b and c in unsaturated conditions depend on the amount of matric suction. Therefore, unlike in the saturated condition, these

parameters are not the “material parameters”, since they are not constant for all situations of a soil. The effects of matric suction on the volume change behaviour were discussed and the equations for selected parameters of the adapted a,b,c isotache model were suggested as a function of matric suction for the unsaturated compacted organic soil. Based on the test results, both the apparent pre-consolidation net normal stress for the soil structure at zero overall total natural strain ($p_{g\,v}^{s}$), and the apparent pre-consolidation net normal stress for the water phase at zero total linear water volume change ($p_{g\,w}^{(\mathrm{lin})\,s}$) increase with increasing the value of constant matric suction (s).

The test results demonstrate that the isotache parameters of the soil structure at a constant matric suction (a_v^s, b_v^s and c_v^s) decrease to the minimum values as matric suction is increased from zero to 290 kPa for this compacted organic soil. Then, these parameters increase once the soil reaches 891 kPa matric suction. Increasing these parameters beyond a certain matric suction value could be interpreted as resulting from a new geometrical arrangement of the soil fabric when the matric suction approaches a very high value. In addition, the brittleness of organic particles may increase significantly beyond a certain matric suction value due to decreasing water content, and as a result, the organic particles may start to break (i.e., collapse) under the applied net normal stress. However, further research is needed to better understand the dependency of the isotache parameters on matric suction.

The “C_α/C_C concept” proposed by Mesri and Godlewski (1977) for saturated soils, is also observed here for the unsaturated compacted organic soil. The values of c_v^s/b_v^s seem to be independent of the matric suction and are within the range of 0.025-0.10 reported by Mesri and Godlewski (1977) for C_α/C_C in saturated soils. The values of c_v^s/b_v^s are also within the range of 0.04-0.1 reported by Den Haan (1996) for c/b in saturated soils.

In addition, the test results show that the values of a_v^s/b_v^s for saturated conditions are within the range of 0.11-0.13, which is in line with Den Haan and Sellmeijer (2000), who report that a/b is approximately 0.1-0.2 in saturated soils. For unsaturated soil samples, the values of a_v^s/b_v^s are within the range of 0.02-0.06. Therefore, the values of a_v^s/b_v^s in unsaturated conditions are smaller than these values in saturated conditions.

The framework and equations of the adapted a,b,c isotache model were presented for the overall volume and water volume changes of unsaturated soils. Afterwards, the suction-controlled oedometer tests were simulated using the adapted model and compared with the test results of overall volume and water volume changes. The comparison between the adapted a,b,c isotache model and the test results shows that the adapted model can simulate and predict the overall volume and water volume changes of this soil with high accuracy.

The straightforward approach presented in this research could encourage engineers to use compacted organic soils in geotechnical practice.

6.2 Recommendations for Future Research

It is not possible to answer all of the questions concerning the volume change behaviour of compacted organic soils through only six laboratory tests. This research has focused on the volume change behaviour due to increasing net normal stress for different values of constant matric suction. In the future, this study could be extended to increasing matric suction for different values of constant net normal stress. In other words, more suction-controlled oedometer tests should be performed to obtain a complete set of results.

The classical S-shape isobars were not observed in this research. A maximum LIR value of 1 was chosen in this research, but the S-shape isobars might be observed with higher values of LIR. Therefore, an experimental study of the relationship between the shape of isobars and the values of LIR and OCR is recommended for both saturated and unsaturated compacted organic soils.

In this research, only the volume change behaviour of the loading steps was studied by using the isotache approach. Further studies could also be performed on the volume change behaviour during the unloading and reloading steps at a constant matric suction. Such studies would examine the influence of stress history on the volume change behaviour of soil samples. In addition, further research can be performed to study the influence of drying and wetting history on the volume change behaviour of soil samples at a constant net normal stress.

References

Airò Farulla, C. (2008). Stress path dependence of hydromechanical behaviour of compacted scaly clay in wetting and drying suction controlled oedometer tests at constant vertical net stress. *Unsaturated Soils: Advances in Geo-Engineering, Proceedings of the First European Conference on Unsaturated Soils, E-Unsat 2008, Durham, United Kingdom, July 2–4 2008,* CRC Press, (pp. 321-326).

Airò Farulla, C., Battiato, A., & Ferrari, A. (2011). The void ratio dependency of the retention behaviour for a compacted clay. In *Unsaturated Soils: Proceedings of the Fifth International Conference on Unsaturated Soils, Barcelona, Spain.* Taylor & Francis Group (pp. 417-422).

Abed, A. A. (2008). *Numerical modeling of expansive soil behavior* (Doctoral dissertation). Universität Stuttgart. Retrieved from http://www.uni-stuttgart.de/igs/content/publications/IGS_Dissertationen/Diss_Abed_Online.pdf

Alonso, E. E., Gens, A., & Josa, A. (1990). A constitutive model for partially saturated soils. *Géotechnique, 40*(3), 405-430.

Alonso, E. E., Pinyol, N. M., & Puzrin, A. M. (2010). Collapse of Compacted Soil: Girona Road Embankments, Spain. In *Geomechanics of Failures. Advanced Topics* (pp. 85-127). Springer Netherlands.

ASTM D698-00a, (2000). *Standard test methods for laboratory compaction characteristics of soil using standard effort (12,400 ft-lbf/ft^3 (600 kN-m/m^3)). ASTM International.* www.astm.org

ASTM D1557-12, (2012). *Standard test methods for laboratory compaction characteristics of soil using modified effort (56,000 ft-lbf/ft^3 (2,700 kN-m/m^3)). ASTM International.* www.astm.org

ASTM D2216-10, (2010). *Standard test methods for laboratory determination of water (moisture) content of soil and rock by mass. ASTM International.* www.astm.org

ASTM D2435/D2435M – 11, (2011). *Standard test methods for one-dimensional consolidation properties of soils using incremental loading. ASTM International.* www.astm.org

ASTM D2487 – 06, (2006). *Standard practice for classification of soils for engineering purposes (Unified Soil Classification System). ASTM International.* www.astm.org

ASTM D2974 – 00, (2000). *Standard test methods for moisture, ash, and organic matter of peat and other organic soils. ASTM International.* www.astm.org

ASTM D4186-06, (2006). *Standard test method for one-dimensional consolidation properties of saturated cohesive soils using controlled-strain loading. ASTM International.* www.astm.org

Atkinson, J. (2007). *The mechanics of soils and foundations.* CRC Press.

Barends, F. B. J. (1992). *Theory of consolidation. Lecture Notes.* Delft University of Technology.

Birle, E., Heyer, D., & Vogt, N. (2008). Influence of the initial water content and dry density on the soil–water retention curve and the shrinkage behavior of a compacted clay. *Acta Geotechnica, 3*(3), 191-200.

Birle, E. (2011). *Geohydraulische Eigenschaften verdichteter Tone unter besonderer Berücksichtigung des ungesättigten Zustandes* (Doctoral dissertation). Technische Universität München, (in German). Retrieved from http://mediatum.ub.tum.de/download/1084296/1084296.pdf

Birle, E. (2012). Effect of initial water content and dry density on the pore structure and the soil-water retention curve of compacted clay. In *Unsaturated Soils: Research and Applications* (pp. 145-152). Springer Berlin Heidelberg.

Bjerrum, L. (1967). Engineering geology of Norwegian normally-consolidated marine clays as related to settlements of buildings. *Géotechnique, 17*(2), 83-118.

Bowles, J. E. (1997). *Foundation analysis and design.* McGraw-Hill.

Chen, Z. H., Fredlund, D. G., & Gan, J. K. (1999). Overall volume change, water volume change, and yield associated with an unsaturated compacted loess. *Canadian geotechnical journal, 36*(2), 321-329.

Colleselli, F., Cortellazzo, G., & Cola, S. (2000). Laboratory testing of Italian peaty soils. In T. B. Edil, & P. J. Fox, (Eds.), *Geotechnics of High Water Content Materials, ASTM STP 1374*, (pp. 226-240).

Cui, K., Défossez, P., Cui, Y. J., & Richard, G. (2010). Quantifying the effect of matric suction on the compressive properties of two agricultural soils using an osmotic oedometer. *Geoderma, 156*(3-4), 337-345.

Das, B. M., & Sobhan, K. (2014). *Principles of geotechnical engineering.* Cengage Learning.

Degago, S. A., Grimstad, G., Jostad, H. P., Nordal, S., & Olsson, M. (2011). Use and misuse of the isotache concept with respect to creep hypotheses A and B. *Géotechnique, 61*(10), 897-908.

Degago, S. A. (2015, January). *Evaluation of creep hypotheses A and B.* Presented at the Workshop: Creep Behaviour of Soils – Focus on Practical Applications. Norwegian Geotechnical Institute, Oslo, Norway. Retrieved from http://www.ntnu.edu/documents/11435961/0/NGI_WS_CREEP_Presentations_red-5QjEmrcd.pdf/e84610df-7e52-4d1f-b811-1788d5c6a260

Den Haan, E. J., & Edil, T. B. (1994). Secondary and tertiary compression of peat. *Proceedings of the International Workshop on Advances in Understanding and Modelling the Mechanical Behaviour of Peat, Delft, Netherlands, 16-18 June 1993.* Rotterdam: A.A. Balkema, 49-60.

Den Haan, E. J. (1994). *Vertical compression of soils* (Doctoral dissertation). Delft University Press. Retrieved from http://repository.tudelft.nl/assets/uuid:b8dc88e0-f400-4d86-9a2e-4e00b68d0472/ceg_haan_19941128.PDF

Den Haan, E. J. (1996). A compression model for non-brittle soft clays and peat. *Géotechnique, 46,* No 1, 1-16.

Den Haan, E. J., & Sellmeijer, H. J. B. (2000). Calculation of soft ground settlement with an isotache model. *Soft Ground Technology, A.S.C.E. Geotechnical Special Publication Number 112, Proceedings Soft Ground Technology Conference, Noordwijkerhout,* 94-104.

Den Haan, E. J., & Van den Berg, P. (2001). *Evaluation of creep models for soft soils (under axially symmetric conditions)*. Delft Cluster.

Den Haan, E. J., & Kamao, S. (2003). Obtaining isotache parameters from a C.R.S. K_o-oedometer. *Soils and Foundations, 43*(4)*,* 203-214.

Den Haan, E. J., & Kruse, G. A. M. (2007). Characterisation and engineering properties of Dutch peats. *Proceedings of the Characterisation and Engineering Properties of Natural Soils,* Taylor & Francis Group, London, UK, 2101-2133.

Den Haan, E. J. (2008). De intrinsieke tijd in het Isotachenmodel. *GEOtechniek.* (in Dutch), 34-38.

DIN 18135:2012-04, (2012). *Baugrund – Untersuchung von Bodenproben – Eindimensionaler Kompressionsversuch. Deutsches Institut für Normung e. V.*

Fredlund, D. G., & Morgenstern, N. R. (1976). Constitutive relations for volume change in unsaturated soils. *Canadian Geotechnical Journal, 13*(3), 261-276.

Fredlund, D. G., & Rahardjo, H. (1986). Unsaturated soil consolidation theory and laboratory experimental data. *Consolidation of Soils: Testing and Evaluation, ASTM STP 892,* 154-169.

Fredlund, D. G., & Rahardjo, H. (1993). *Soil mechanics for unsaturated soils.* John Wiley & Sons.

Fredlund, D. G., Rahardjo, H., & Fredlund, M. D. (2012). *Unsaturated soil mechanics in engineering practice.* John Wiley & Sons.

Ho, D. Y. F., Fredlund, D. G., & Rahardjo, H. (1992). Volume change indices during loading and unloading of an unsaturated soil. *Canadian Geotechnical Journal, 29*(2), 195-207.

Hobbs, N. B. (1986). Mire morphology and the properties and behaviour of some British and foreign peats. *Quarterly Journal of Engineering Geology and Hydrogeology, v.19*, 7-80.

Holtz, R. D., & Kovacs, W. D. (1981). *An introduction to geotechnical engineering.* Prentice-Hall.

Honda, M., Iizuka, A., Ohno, S., Kawai, K., & Wang, W. (2006). An evaluation method for the volume change characteristics of compacted soil. *Unsaturated Soils 2006* (pp. 837-848). ASCE.

Jommi, C., & Romero, E. (2008). Mixed isotropic-rotational hardening to model the deformational response of unsaturated compacted soils. *Unsaturated Soils: Advances in Geo-Engineering, Proceedings of the First European Conference on Unsaturated Soils, E-Unsat 2008, Durham, United Kingdom, July 2–4 2008,* CRC Press, (pp. 617-623).

Jommi, C., & Della Vecchia, G. (2010). Geomechanical analysis of river embankments. In L. Laloui (Ed.), *Mechanics of unsaturated geomaterials* (pp. 353-374). ISTE Ltd and John Wiley & Sons, Inc.

Kayadelen, C. (2008). The consolidation characteristics of an unsaturated compacted soil. *Environmental geology, 54*(2), 325-334.

Kim, Y. T., & Leroueil, S. (2001). Modeling the viscoplastic behaviour of clays during consolidation: application to Berthierville clay in both laboratory and field conditions. *Canadian Geotechnical Journal, 38*(3), 484-497.

Knappett, J. A., & Craig, R. F. (2012). *Craig's soil mechanics.* Spon Press.

Koliji, A. (2008). *Mechanical behaviour of unsaturated aggregated soils* (Doctoral dissertation). ÉCOLE POLYTECHNIQUE FÉDÉRALE DE LAUSANNE.
Retrieved from http://infoscience.epfl.ch/record/114779/files/EPFL_TH4011.pdf

Krieg, S. (2000). *Viskoses Bodenverhalten von Mudden, Seeton und Klei* (Doctoral dissertation). Universität Fridericiana in Karlsruhe, Heft 150, (in German).

Lai, X. L., Wang, S. M., Ye, W. M., & Cui, Y. J. (2014). Experimental investigation on the creep behavior of an unsaturated clay. *Canadian Geotechnical Journal, 51*(6), 621-628.

Lambe, T. W., & Whitman, R. W. (1969). *Soil mechanics.* John Wiley & Sons.

Landva, A. O., & La Rochelle, P. (1983). Compressibility and shear characteristics of Radforth peats. *Testing of peats and organic soils, ASTM STP 820*, 157-191.

Leoni, M., Karstunen, M., & Vermeer, P. A. (2008). Anisotropic creep model for soft soils. *Géotechnique, 58,* No 3, 215–226.

Leroueil, S., & Hight, D. W. (2013). Compacted soils: From physics to hydraulic and mechanical behaviour. *Proceedings of the First Pan-American Conference on Unsaturated Soils, Advances in Unsaturated Soils, Colombia, 20–22 February 2013*, CRC Press, Taylor & Francis Group (pp. 41-59).

Limsiri, C. (2008). *Very soft organic clay applied for road embankment: Modelling and optimisation approach* (Doctoral dissertation). Leiden, Netherlands: Taylor & Francis/Balkema.

Lloret, A., & Alonso, E. E. (1980). Consolidation of unsaturated soils including swelling and collapse behaviour. *Géotechnique, 30*(4), 449-477.

Mesri, G., & Godlewski, P. M. (1977). Time- and stress-compressibility interrelationship. *Journal of the Geotechnical Engineering Division, 103*(5), 417-430.

Mesri, G., & Castro, A. (1987). C_α/C_C concept and K_0 during secondary compression. *Journal of Geotechnical Engineering, 113*(3), 230-247.

Mesri, G., & Ajlouni, M. (2007). Engineering properties of fibrous peats. *Journal of Geotechnical and Geoenvironmental Engineering, 133*(7), 850-866.

Murray, E. J., & Sivakumar, V. (2010). *Unsaturated soils: a fundamental interpretation of soil behaviour.* John Wiley & Sons.

Nash, D., & Brown, M. (2014). Influence of destructuration of soft clay on time-dependent settlements: comparison of some elastic viscoplastic models. *International Journal of Geomechanics, ASCE,* A4014004.

Nowamooz, H., Mrad, M., Abdallah, A., & Masrouri, F. (2009). Experimental and numerical studies of the hydromechanical behaviour of a natural unsaturated swelling soil. *Canadian Geotechnical Journal, 46*(4), 393-410.

Papadaki, E. (2013). *Modelling of peat compressed under sand bodies: experimental and numerical approach* (Master's thesis), Faculty of Civil Engineering and Geosciences, Technical University of Delft. Retrieved from http://repository.tudelft.nl/assets/uuid:faf79020-4c07-4931-9bf6-dcdbe491bca8/MSc_thesis-Eirini_Papadaki.pdf

Qin, P. J., Ye, W. M., Chen, Y. G., Chen, B., & Cui, Y. J. (2015). Influence of strain-rate on hydromechanical behavior of highly compacted GMZ01 bentonite. *Engineering Geology, 195,* 85-92.

Rackwitz, F., Schüßler, M., Savidis, S. A., & Ney, M. (2011). Bodenmechanische Eigenschaften organischer Ablagerungen der brandenburgischen Niederungs- und Luchgebiete. *geotechnik, 34*(2), 97-107, (in German).

Rahardjo, H., & Fredlund, D. G. (1995). Experimental verification of the theory of consolidation for unsaturated soils. *Canadian Geotechnical Journal, 32*(5), 749-766.

Rahardjo, H., & Fredlund, D. G. (1996). Consolidation apparatus for testing unsaturated soils. *Geotechnical Testing Journal, 19*(4), 341-353.

Rampino, C., Mancuso, C., & Vinale, F. (2000). Experimental behaviour and modelling of an unsaturated compacted soil. *Canadian Geotechnical Journal, 37*(4), 748-763.

Romero, E. (1999). *Characterisation and thermo-hydro-mechanical behaviour of unsaturated Boom clay: An experimental study* (Doctoral dissertation). Universitat Politècnica de Catalunya, Barcelona, Spain.

Romero, E., Della Vecchia, G., & Jommi, C. (2011). An insight into the water retention properties of compacted clayey soils. *Géotechnique, 61*(4), 313-328.

Samson, L. (1985). Postconstruction settlement of an expressway built on peat by precompression. *Canadian Geotechnical Journal, 22*(3), 308-312.

Savidis, S. A., Rackwitz, F., & Schüßler, M. (2008). Design and construction of granular soil columns for ground improvement of very soft soils for road embankments. Proc. 6th International Conference on Case Histories in Geotechnical Engineering, Arlington, VA. Retrieved from http://scholarsmine.mst.edu/cgi/viewcontent.cgi?article=2862&context=icchge

Sipkema, D. (2006). *a,b,c-Isotachenmodel van a,b,c tot zetting* (Master's thesis). TU Delft, (in Dutch), Retrieved from http://repository.tudelft.nl/assets/uuid:93945e99-10dc-4e9b-9658-3c467e819c3f/01b_eindrapport_Dylan_Sipkema.pdf

Sridharan, A., & Prakash, K. (1985). Improved rectangular hyperbola method for the determination of coefficient of consolidation. *Geotechnical Testing Journal, 8*(1), 37-40.

Šuklje, L. (1957). The analysis of the consolidation process by the isotache method. *Proceedings of the 4th International Conference on Soil Mechanics and Foundation Engineering, London, Vol. 1,* pp. 200-206.

Taciroglu, E. (1998). *Constitutive modeling of the resilient response of granular solids* (Doctoral dissertation). University of Illinois at Urbana – Champaign, Urbana, Illinois. Retrieved from http://www.seas.ucla.edu/~etacir/ftp/Thesis.dir/TacirogluThesis.pdf

Taylor, D. W. (1948). *Fundamentals of soil mechanics.* John Wiley & Sons, New York.

Terzaghi, K., Peck, R. B., & Mesri, G. (1996). *Soil mechanics in engineering practice.* John Wiley & Sons.

Toll, D. G. (1995). A conceptual model for the drying and wetting of soil. *Proceedings of the First International Conference on Unsaturated Soils, Paris*, (pp. 805-810).

Vermeer, P. A. & Neher, H. P. (1999). A soft soil model that accounts for creep. *Proceedings of the international symposium "Beyond 2000 in Computational Geotechnics"*, (pp. 249-261).

Verruijt, A. (2001). *Soil mechanics.* Delft University of Technology. Retrieved from http://ocw.tudelft.nl/fileadmin/ocw/courses/DredgingProcesses/res00020/embedded/SoilMechBook.pdf

Visschedijk, M. A. T., & Trompille, V. (2009). MSettle version 8.2 - Embankment Design and Soil Settlement Prediction. Deltares, Delft, the Netherlands: Delft Cluster. Retrieved from http://repository.tudelft.nl/assets/uuid:88aa11df-55a9-4266-89f1-aefb5568dca2/MSettle-Manual_op__Delft_GeoSystems_site.pdf

Watabe, Y. & Leroueil, S. (2012). Modeling and implementation of the isotache concept for long-term consolidation behavior. *International Journal of Geomechanics, ASCE,* A4014006.

Wesley, L. D. (2010). *Geotechnical engineering in residual soils.* John Wiley & Sons.

Ye, W. M., Lai, X. L., Wang, Q., Chen, Y. G., Chen, B., & Cui, Y. J. (2014). An experimental investigation on the secondary compression of unsaturated GMZ01 bentonite. *Applied Clay Science, 97-98,* pp. 104-109.

Appendices

Appendix A: Details of the Laboratory Tests

A.1 Laboratory Tests to Determine Soil Properties

Wet and dry sieve analysis was performed on the soil. An unusual light brown foam was observed during the wet sieving (Figure A.1).

Figure A.1. Appearance of a light brown foam during the wet sieving (Zentrum Geotechnik, Technische Universität München).

The maximum particle size found in the natural soil was 14 mm. As Figure A.2a shows, the coarse grain particles have nearly rounded corners and edges.

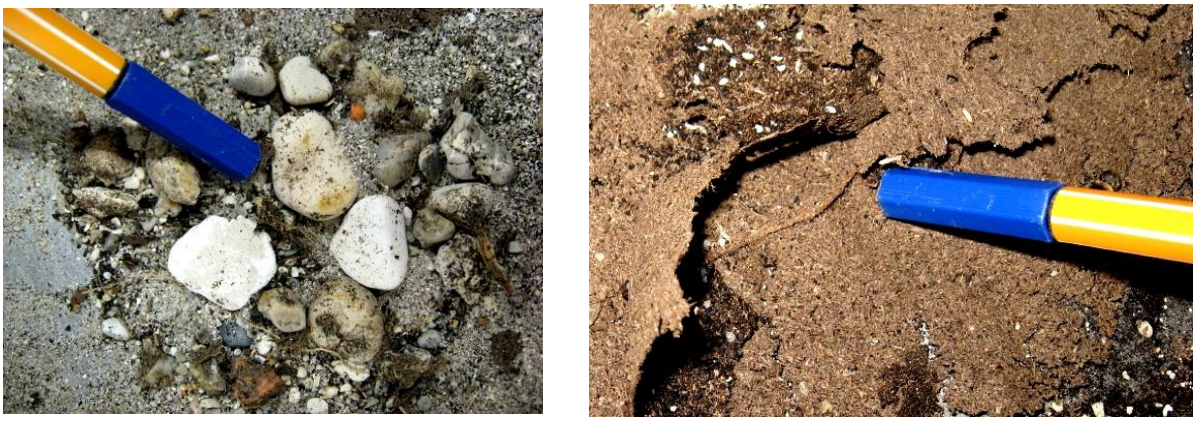

(a) (b)

Figure A.2. Appearances of: (a) the coarse grains and (b) the fibrous particles - remaining on a 0.125 mm sieve, after washing the soil sample (Zentrum Geotechnik, Technische Universität München).

The colour of the soil in its natural condition ranges from dark brown to black but changed to light brown after oven drying at 105° C for 24 hours (Figure A.3). After high-temperature heating, at 440 °C for 5 hours, the colour changes to very light brown (Figure A.4b).

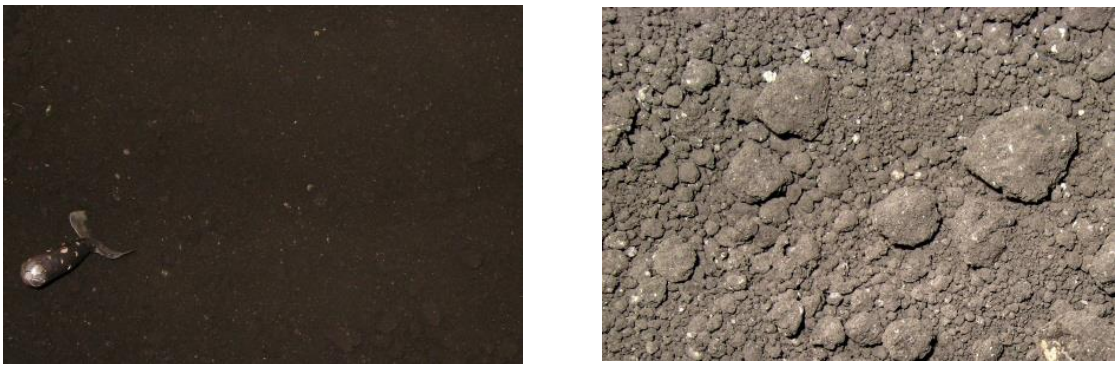

(a) (b)

Figure A.3. (a) Appearance of the soil colour in the natural condition and (b) after oven drying at 105° C for 24 hours (Zentrum Geotechnik, Technische Universität München).

(a) (b)

Figure A.4. Determination of soil organic matter. (a) The high-temperature oven used in this study and (b) appearance of the soil after high-temperature heating at 440 °C for 5 hours (Zentrum Geotechnik, Technische Universität München).

The soil in the natural condition (Figure A.3a) has an odour of decaying vegetation due to a significant amount of organic matter. The odour of the soil is very unpleasant if a mixture of the soil and water is kept for 24 hours at 60 °C. After oven drying at 105 °C for 24 hours (Figure A.3b) the odour significantly reduces. The odour of the soil completely disappears after high-temperature heating at 440 °C for 5 hours (Figure A.4b).

(a) (b)

Figure A.5. (a) Liquid limit test and (b) plastic limit test (Zentrum Geotechnik, Technische Universität München).

A.2 Conventional Oedometer Tests on Saturated Soil Samples

(a) (b)

Figure A.6. (a) The mould used for static compaction of the soil samples and (b) inserting a soil sample from the mould into the ring of the oedometer apparatus (Zentrum Geotechnik, Technische Universität München).

Figure A.7. Conventional oedometer apparatus used in this study for Tests S1, S2 and S3 on saturated soil samples (Zentrum Geotechnik, Technische Universität München).

(a) (b)

Figure A.8. A soil sample and ring from a conventional oedometer test; (a) immediately after the test and (b) after oven drying at 60 ^{o}C (Zentrum Geotechnik, Technische Universität München).

Appendix B: Analytical Solution of the Primary Consolidation

This appendix presents two Visual Basic for Applications (VBA) scripts, which are an adapted form of the BASIC computer programs written by Verruijt (2001).

Script 1

Script 1 (adapted from Verruijt, 2001, p. 105) is for a program that calculates the amount of excess pore-water pressure (Δu) as a function of depth (z) and a specific time (t) by using the analytical solution of equation 3.6.

```
Sub Isochrones()
' Script 1 (adapted from Verruijt, 2001, p. 105) is for a program that calculates the amount of excess pore-water pressure (∆u) as a function of depth (z) and a specific time (t) by using the analytical solution of equation 3.6.

Worksheets("Isochrones").Range("O8:R108").ClearContents
Dim H As Double ' Hdr: Drainage length
Dim Cv As Double ' Coefficient of consolidation
Dim t As Double ' Value of time
Dim N As Single ' Number of subdivisions
Dim I As Single
Dim Tv As Double ' Time factor
Dim Pi As Double ' 3.14
Dim m As Single
Dim MM As Double
Dim L As Double
Dim zH As Double ' z/Hdr
Dim uu0 As Double ' u/u0

H = Worksheets("Isochrones").Cells(18, 5) ' Hdr: Drainage length
Cv = Worksheets("Isochrones").Cells(19, 5) ' Coefficient of consolidation
t = Worksheets("Isochrones").Cells(20, 5) ' Value of time
N = 100 ' Number of subdivisions
Pi = 4 * Atn(1) ' 3.14
Tv = Cv * t / (H ^ 2) ' Time factor
Worksheets("Isochrones").Cells(I + 8, 15) = t ' Time
Worksheets("Isochrones").Cells(I + 8, 16) = Tv ' Time factor
For I = 0 To N
zH = I / N
Worksheets("Isochrones").Cells(I + 8, 17) = zH ' z/Hdr
m = 0
uu0 = 0
label2:
MM = Pi * 0.5 * ((2 * m) + 1)
L = (MM ^ 2) * Tv
uu0 = uu0 + ((2 / MM) * (Sin(MM * zH)) * Exp(-L))
m = m + 1
If L < 20 Then GoTo label2
Worksheets("Isochrones").Cells(I + 8, 18) = uu0 ' u/u0
Next I
End Sub
```

Script 2

Script 2 (adapted from Verruijt, 2001, p. 108) is for a program that calculates the average degree of consolidation (U_{avg}) as a function of time (t) by using the analytical solution of equation 3.8.

```
Sub Uav()
' Script 2 (adapted from Verruijt, 2001, p. 108) is for a program that calculates the average degree of consolidation (Uavg) as a function of time (t) by using the analytical solution of equation 3.8.

Worksheets("Uav").Range("O8:Q1000").ClearContents
Dim H As Double ' Hdr: Drainage length
Dim Cv As Double ' Coefficient of consolidation
Dim t As Double ' Value of time
Dim Tv As Double ' Time factor
Dim Pi As Double ' 3.14
Dim m As Single
Dim MM As Double
Dim L As Double
Dim U As Double
Dim Uav As Double ' Average degree of consolidation (Uavg)
Dim I As Single
H = Worksheets("Uav").Cells(18, 5) ' Hdr: Drainage length
Cv = Worksheets("Uav").Cells(19, 5) ' Coefficient of consolidation
Pi = 4 * Atn(1) ' 3.14
t = 0.0000001 ' Initial time (Note: Due to the logarithmic scale of the x-axis, t must be > 0)
I = 0
label1:
I = I + 1
t = t * (I ^ 0.05)
Tv = Cv * t / (H ^ 2) ' Time factor
Worksheets("Uav").Cells(I + 7, 15) = t ' Time
Worksheets("Uav").Cells(I + 7, 16) = Tv ' Time factor
m = 0
U = 0
label2:
MM = Pi * 0.5 * ((2 * m) + 1)
L = (MM ^ 2) * Tv
U = U + ((2 / (MM ^ 2)) * Exp(-L))
m = m + 1
If L < 20 Then GoTo label2
Uav = 1 - U
Worksheets("Uav").Cells(I + 7, 17) = Uav ' Average degree of consolidation (Uavg)
If Uav < 1 Then GoTo label1
End Sub
```

Appendix C: Calibration of the Suction-Controlled Oedometers

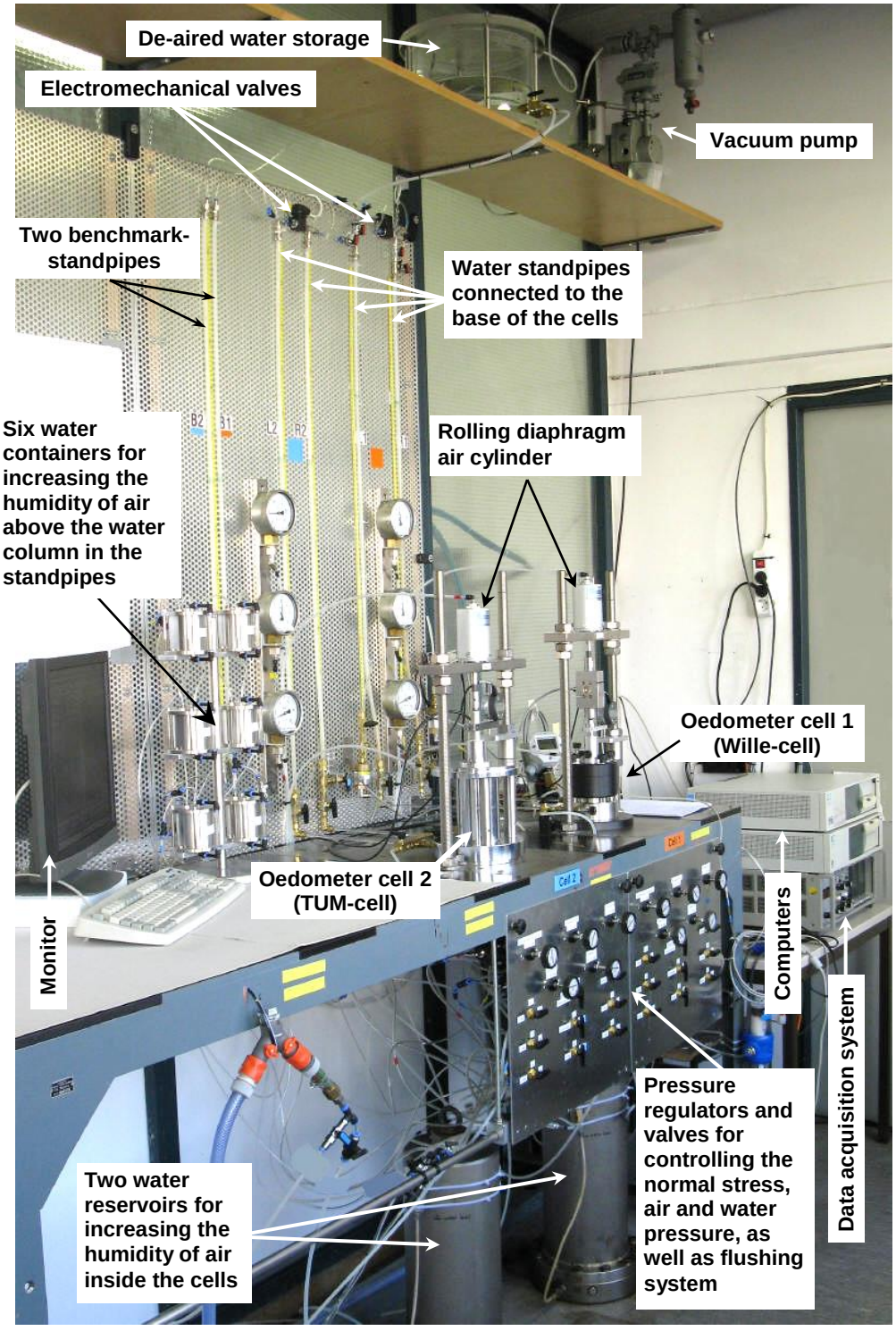

Figure C.1. Components of the suction-controlled oedometer apparatus (Zentrum Geotechnik, Technische Universität München).

Deformations of the oedometers under vertical stresses and air pressures were measured by replacing the soil sample with a hard steel disk. The calibration values were deducted from the measured vertical deformation of the soil samples.

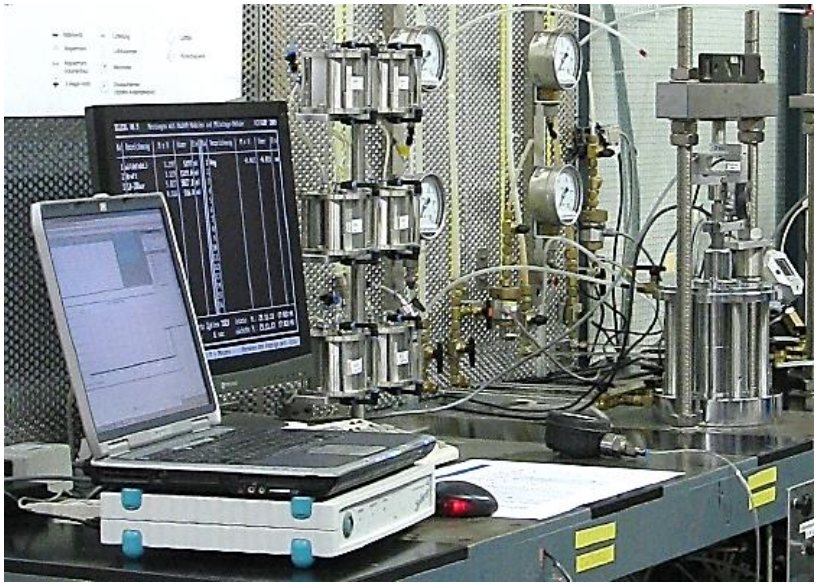

(a)

(b)

Figure C.2. (a) The electronic measuring system for calibration of the exact net normal stresses, and (b) the digital manometer for measuring the air and water pressures (Zentrum Geotechnik, Technische Universität München).

(a)

(b)

Figure C.3. Calibration of the force transducer by using another pre-calibrated force transducer. (a) Cell 2, (b) Cell 1 (Zentrum Geotechnik, Technische Universität München).

Appendix D: Benchmark-Standpipe

To increase the accuracy of water volume measurement during the long duration tests, an additional standpipe was added to each suction-controlled oedometer apparatus as a benchmark (see figures C.1 and D.1). A valve was installed at the lower part of each benchmark-standpipe, and was kept closed during tests. The upper part of each benchmark-standpipe was connected to the upper part of the cell-standpipes.

Utilising the benchmark-standpipe during the suction-controlled oedometer test has the following advantages:

- Evaporation in standpipes is easily measured and therefore the exact water mass of the soil sample can be determined at any time.
- Any unusual changes in the water level of cell-standpipes can be compared with the benchmark-standpipe. For example, decreases in the water level inside the cell-standpipes immediately after applying the water pressure, which occur due to the increasing volume of all plastic standpipes, can be easily determined by using the benchmark-standpipe.

For instance, in Test U3, the comparison between the water mass measured by using the benchmark-standpipe and the water mass calculated after drying the soil sample is as follows:

Duration of Test U3: 159 [days]

Water mass measured (at the end of the test) by using the benchmark-standpipe = 32.8 [g]

Water mass calculated by drying the soil sample (in oven) after the test = 32.1 [g]

Difference = 0.7 [g]

The small difference indicates that the results of water volume change in this study are very reliable.

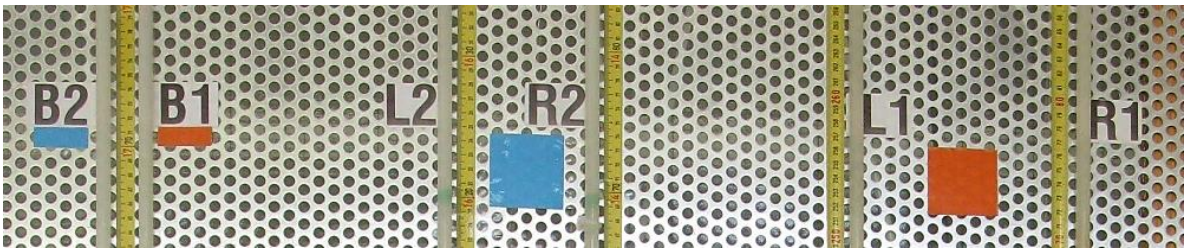

Figure D.1. All standpipes of the suction-controlled oedometers. From left to right: the benchmark-standpipes (B2 & B1); cell-standpipes connected to the underside of the high air entry disk of Cell 2 (L2 & R2); and cell-standpipes connected to the underside of the high air entry disk of Cell 1 (L1 & R1) (Zentrum Geotechnik, Technische Universität München).